BIOMECHANICS OF THE EQUINE TARSAL JOINT

By

Siriporn Khumsap

A DISSERTATION

Submitted to
Michigan State University
in partial fulfillment of the requirements
for the degree of

DOCTOR OF PHILOSOPHY

Department of Large Animal Clinical Sciences

2002

ABSTRACT

BIOMECHANICS OF THE EQUINE TARSAL JOINT

By

Siriporn Khumsap

This study was performed to test whether two-dimensional (2D) and three-dimensional (3D) kinematic, ground reaction force (GRF) and 2D inverse dynamic analysis could identify differences between sound horses and horses with mild tarsal joint lameness. Hypotheses tested were that kinematic and kinetic profiles of horses with distal tarsal synovitis differ from those of sound horses, and that the tarsal joint complex undergoes 3D motion. Four sound horses were selected on the basis of clinical evaluation, radiography and nuclear scintigraphy. Gait analysis was performed for the sound condition, after which synovitis was induced by injecting endotoxin into the right distal intertarsal and tarsometatarsal joints. Gait analysis was repeated 24-30 hours later for the lame condition. Independent t-tests were performed to identify differences between the variables in the two conditions. In the sound condition, tarsal joint ranges of motion were 12.12° ± 0.96 and 44.67° ± 1.90 during stance and swing, respectively. The peak vertical force on the hind limb was 9.05 ± 0.40 N/kg. During stance, the tarsal joint power profile showed two cycles of elastic energy storage and release on the extensor aspect, which was a mechanism for minimizing energy expenditure at the trot. During swing, the tarsal joint power profiles showed two bursts of energy generation, on the flexor aspect in early swing then on the extensor aspect in late swing. After synovitis induction, tarsal joint range of motion during stance decreased by 2.20° ± 1.28. Peak

vertical force and vertical impulse decreased by 0.31 ± 0.18 N/kg and 0.05 ± 0.03 Ns/kg. The mechanical deficits at the tarsal joint included a trend toward a decrease in energy absorption during early stance, and a decrease in energy generation during push off. During swing, there was a trend toward a decrease in tarsal positive net joint energy. There was no compensatory increase in energy generation from the other joints within the lame hind limb. The contralateral hind limb showed a trend toward an increase in peak vertical force of 0.17 ± 0.13 N/kg and increase in positive power at the coxofemoral joint during early swing. Vertical impulse in the contralateral forelimb decreased by 0.05 ± 0.02 Ns/kg. It was found that the tarsal joint complex showed 3D rotational and translational motions. In the sound condition, the tarsal joint complex was flexed, abducted and internally rotated, and translated in cranial, lateral and proximal directions during stance. The motions during swing were similar to those during stance, except that the joint externally rotated. Skin-based markers could estimate those motions fairly accurately, except for internal/external rotation and medial/lateral translation. Synovitis resulted in decreases in range of tarsal joint flexion of 2.5° ± 1.4, cranial translation of 4.2 ± 2.5 mm during stance and proximal translation of 2.4 ± 1.4 mm during swing. It is concluded that the tarsal joint is an important source of mechanical energy generation throughout the stride, and that mechanical deficiencies due to distal tarsal synovitis were mainly present during stance. Compensation by the other limbs included load shifting to the contralateral hind limb and unloading of the diagonal lame limb pair. The decrease in tarsal joint translation during stance due to synovitis might lead to stationary articular cartilage of the distal tarsal joints. High intensity loading on the cartilage may lead to cartilage necrosis, which may explain pathogenesis of bone spavin.

ACKNOWLEDGMENTS

First, I would like to extend my appreciation for all the advice, support and kindly understanding from my guidance committee: Dr. John Stick, Dr. Steven Arnoczky, Dr. Frank Nickels and Dr. Diana Rosenstein. A sincerely grateful appreciation to my major professor and advisor, Dr. Hilary Clayton. Being a graduate student is a hard work. It is even harder to be an international graduate student. With her knowledge, generous understanding and good humor, she is the best advisor ever and will be the goal standard for me in the future.

I would like to thank Dr. Christopher Byron who help me performed the clinical procedures in this study, all the graduate students in the Mary Anne McPhail Equine Performance Center and Carissa Wickens for assistance during data collection. A special thank to Joel Lanovaz for his expertise, friendship and advice.

This study supported by the Mary Anne McPhail endowment and the Department of Large Animal Clinical Sciences. Thanks to those horses whom 'volunteered' to participate in my study: Apollo, Homer, Pulga, Athena and Trouble.

Finally, I would like to thank my parents who always support my will for education and my husband who always makes me smile and happy.

TABLE OF CONTENTS

LIST OF TABLES

LIST OF FIGURES

INTRODUCTION

RATIONALE

Horses have played an important role in the development of human civilization (van Weeren, 2001). Unlike most of the other domesticated species, horses were used to transport people, to work the land and as vehicles in wartime. These uses developed due to the horse's outstanding locomotor capabilies. Today, some horses are still used for transportation but their primary use is in equestrian sports, such as racing, dressage, jumping, polo and rodeo.

In sporting horses, lameness in either the forelimb or the hind limb will limit the horse's ability to perform to a greater or lesser degree. Lameness can be observed while the horse is in motion. Characteristics of the stride, such as the stance and swing phases, the arc of foot flight, how the foot lands, joint flexion angles and symmetry of head and hip motion, are used for identifying the lame limb (Stashak, 1987). However, human eyes have limited temporal resolution, subclinical lameness is difficult to detect because the asymmetries are subtle and the evaluation is considered subjective. In an attempt to enhance the ability to evaluate lameness in horses, gait analysis has been used to quantify gait asymmetries.

Biomechanics is the application of mechanical laws to living structures. For several decades, biomechanical principles have been applied in human locomotion, both for studying clinical aspects of gait and for exploring methods of improving performance in sport. Recently, the techniques for biomechanical analysis have been adapted to study locomotion in horses. The technique of gait analysis includes analysis of movement

(kinematics) and the forces responsible for movement (kinetics). A further step in the procedure, inverse dynamic analysis, combines kinematic and kinetic measurements with inertial properties of the limb segment to analyze the mechanical work performed across the joint. The advantage of inverse dynamic analysis is that it calculates variables that cannot be measured directly, including net joint moments, net joint powers and net joint energies. The net joint moment represents the net torque produced by the action of soft tissues (muscles, tendons and ligaments) around the representative center of rotation of the joint. Net joint power is the rate of net mechanical work done by the soft tissues around the joint. Net joint energy is the amount of mechanical work done across a joint during a period of time. Similar patterns of limb movement may be the result of different combinations of muscular activity and these are demonstrated by inverse dynamic analysis. It gives information describing the amount of energy each joint absorbs (negative work), and the amount of energy each joint generates (positive work) to move the limb and body. The ability to calculate kinetic variables around a joint enhances the ability to detect abnormal patterns of these variables in response to pain and thus facilitates our understanding of the underlying mechanisms of locomotor compensation for lameness.

PROBLEM STATEMENT

Osteoarthritis of the distal intertarsal and tarsometatarsal joints (bone spavin) is one of the common causes of hind limb lameness in the horse. Estimates of prevalence of bone spavin range from 27% (Gabel, 1983) to more than one-third (Gough and Munroe, 1998) of cases with hind limb lameness. The prevalence of radiographic signs of bone

spavin in Icelandic horses was found to be 23% in Sweden (Eksell, et al., 1998) and 30.3% in Iceland (Bjornsdottir, et al., 2000). It is regarded as one of the most important diseases in sport horses (Willms, et al., 1996) as well as in racehorses (Moyer, et al., 1983). The problem is usually subtle and it may be difficult to identify the improvement after diagnostic local anesthesia (Moyer, et al., 1993). There are different levels of correlation between clinical evaluation and radiographic findings, from poor correlation (Gough and Munroe, 1998) up to 73% agreement (Axelsson, et al., 1998). It would be useful to have a more reliable modality to diagnose osteoarthritis in the distal intertarsal and tarsometatarsal joints. High detail radiography has been used to detect subchondral bone plate irregularities, joint margin changes and sclerosis in the distal tarsal joints of weanling, young and adult horses. High detail radiography may enhance the ability to find radiographic changes that could not be detected by clinical radiography, especially subchondral bone plate irregularities and joint margin changes (Laverty, et al., 1991). Nevertheless the evaluation should be supplemented with other ancillary aids. Nuclear scintigraphy is probably the most accurate modality to detect active turnover of subchondral bone. The ability of cartilage to attenuate and transfer loading forces to subchondral bone alters with degeneration. As a result, subchondral bony structures are subjected to more load, resulting in microfracture. In an attempt to repair the microfracture, metabolic activity increases shortly after injury, and long before the sclerotic change detected by radiography. Therefore, nuclear scintigraphy is a promising modality to evaluate the early stage of distal tarsal osteoarthritis. The effects of multiple injections of radiopharmaceutical agent on the horse's long-term health have not yet been identified, so repeated evaluation in horses suspected to have osteoarthritis may be a

concern. Gait analysis, which requires markers attached on the skin and force plate evaluation, is a non-invasive technique and it can be used as frequently as needed. The kinematic and kinetic analysis of the tarsal joint may be useful for detection early signs of disease and for monitoring the response to treatment.

To date, there has been a limited number of publications describing net joint moments, net joint powers and net joint energies in horses. In the hind limb, the only reports of inverse dynamic analysis have described normal horses at the walk (Clayton, et al., 2001; Khumsap, et al., 2001a). Before using this technique as a clinical tool, however, kinematic and kinetic data describing the normal function of the tarsal joint must be known. The gait used in lameness evaluation is the trot, which implies a need for establishing normative profiles at the trot. Once the information from normal tarsal joints has been obtained, it can be used as a basis for evaluating deviations from the normal pattern in specific types of lameness, such as pain due to osteoarthritis of the distal intertarsal and tarsometatarsal joints.

Movements of the limb joints distal to the shoulder and hip in normal horses are primarily those of flexion and extension, and consequently, the published kinematic studies have focused on two-dimensional analysis in the sagittal plane. However, complex joints, such as the tarsal joint, may not function simply as a hinge joint. Measurable amounts of motion from percutaneous pins inserted into the tibia and metatarsus have shown that tarsal joint motion occurs in the frontal (abduction and adduction) and transverse (axial rotation) planes. Motion also appears to occur outside the tarsocrural joint (Lanovaz, et al., 2002). The reference bone data have been used to

develop skin correction algorithms (Appendix A) to increase the accuracy of skin marker based data describing three-dimensional motion of the normal equine tarsal joint.

OBJECTIVES

A pre-requisite to the use of gait analysis as a clinical tool, normative values for the kinematics, ground reaction forces, net joint moment, net joint power and net joint energy profiles in sound horses should be established. Once the normative profiles have been identified, they can be used as a basis to evaluate the effects of a specific type of lameness. The establishment of non-invasive techniques to evaluate the motion of the tarsal joint complex outside the sagittal plane will be useful in the evaluation of sport horses. The objectives of the study were to:

1. Study the two-dimensional kinematic and kinetic analysis of the equine hind limb in sound trotting horses.
2. Study the effect on locomotion of unilateral synovitis in the distal intertarsal and tarsometatarsal joints, including compensations within the lame limb (intra-limb) and between different limbs (inter-limb).
3. Study the three-dimensional kinematic analysis of the tarsal joint complex in sound trotting horses and the effect of distal tarsal synovitis on three-dimensional kinematics of the lame tarsal joint.

HYPOTHESES

1. Kinematic and kinetic variables of the hind limbs in sound horses have a similar pattern in different horses after adjustment for the effect of subject velocity and body

mass.

2. Kinematic and kinetic profiles of horses affected with distal tarsal synovitis differ from the profiles obtained from sound horses.

3. Tarsal joint complex has the motion outside the sagittal plane which can be identified using skin markers.

OVERVIEW

In this dissertation, the primary interest was to further knowledge of tarsal joint function in sound horses and in horses with pathological conditions of the distal intertarsal and tarsometatarsal joints. Data were obtained from a group of normal horses using retro-reflective markers attached to the skin. The effects of unilateral lameness located at the distal intertarsal and tarsometatarsal joints were studied by the induction of synovitis in these joints in one hind limb. Chapter 1 describes a literature review of the clinical applications of gait analysis. Chapter 2 describes the materials and methods, including the kinematic and force plate techniques, and the establishment of segmental coordinate systems for three-dimensional analysis of the equine tarsal joint complex. Chapter 3 addresses Hypothesis 1, by reporting the two-dimensional kinematics, ground reaction forces, net joint moments, net joint powers and net joint energies of the equine hind limbs in sound trotting horses. Chapter 4 addresses Hypothesis 2, by reporting the biomechanical profiles in horses affected with distal intertarsal and tarsometatarsal synovitis and identifies differences from sound horses. This chapter includes a description of the compensatory effects found within the limb and between the limbs. Chapter 5 addresses Hypothesis 3, by reporting three-dimensional kinematics of the

equine tarsal joint complex in sound horses. This chapter also includes an evaluation of a 3D skin marker set to obtain 3D tarsal joint motion and effect of the distal intertarsal and tarsometatarsal synovitis on 3D motion. The last section of this dissertation is a conclusion of the results.

CHAPTER 1

EQUINE GAIT ANALYSIS: REVIEW OF CLINICAL APPLICATIONS

This chapter includes five main sections of the literature review. The first section is the brief history of gait analysis in horses, including the development of equipment and techniques for gait analysis in horses. The second section is a review of gait analysis in sound horses, including the characteristics of normal kinematic and ground reaction forces in trotting horses. The third section reviews the application of gait analysis in varying aspects, including the use of motion analysis and a force plate to evaluate abnormalities in locomotion and to monitor the effect of treatment. The fourth section is a review of the inverse dynamic technique and its application in normal and lame horses. The last section reviews three-dimensional kinematic analysis in horses.

HISTORY OF GAIT ANALYSIS IN HORSES

The early work in this modern era on gait analysis in horses began in the late 1800s. A major contribution was Muybridge's work in 1877 using a battery of still cameras to capture the horse in different gaits and activities. His work triggered the interest of many researchers to further analyse locomotion using photographic techniques. When Leach and Dagg (1983) reviewed the research on equine locomotion and biomechanics, it was stated that the understanding of locomotion and structure and function of the musculoskeletal system was far from complete. The techniques of lameness diagnosis had not really improved since the 17th century, and the concepts of

how a horse adapted to lameness in one or more limbs was limited. They stated three areas of concern to the veterinarian; 1. research must be directed at understanding and distinguishing the factors influencing locomotion; 2. clinical evaluation of lameness must be based on scientifically validated information; and 3. the effects of treatment on locomotion must be more thoroughly documented. Leach and Crawford (1983) proposed six major research areas for equine locomotion: 1. characteristics of normal locomotion; 2. factors influencing locomotion; 3. factors that can be used to predict performance and thereby aid in the selection of a prospective athlete; 4. factors predisposing to injury; 5. epidemiology and economics of lameness; and 6. clinical identification and management of lameness. To facilitate gait studies, a standard terminology for analysis of equine locomotion was suggested by Leach, et al. (1984) and revised in the First International Workshop on Animal Locomotion (Leach, 1993).

A review by Dalin and Jeffcott (1985) stated the limitations of kinematic and kinetic analysis as a routine clinical tool. The availability of high-speed cinematography brought many advances in kinematic analysis, particularly in measuring temporal variables. The delay from recording to analysis was a major limiting factor in the practical application of this technique. Video analysis allowed immediate play back, but it gave poor spatial and temporal resolution, which caused problems when measuring small distances, small angular movements or short duration events. There have been marked improvements in temporal resolution and some improvement in spatial resolution of video systems in recent years but, high-speed video systems are expensive.

In the 1980s, automatic motion analysis systems became available for kinematic measurement and analysis (Leach, 1987). Most of these systems used infrared light,

either reflected from passive markers, or emitted by light emitting diodes attached to the limbs. Due to their sensitivity to light, most of these systems could not be used in daylight. Digital infrared cameras with excellent spatial and temporal resolution are now available for incorporation into fully automated gait analysis systems that offer real time digitizing and three-dimensional display of markers.

The requirement that markers be attached to the skin gives rise to measurement error because of skin movement relative to the underlying bony structures (Leach, 1987). In an attempt to reduce the errors due to skin displacement, van Weeren (1989) developed models to correct for two-dimensional skin displacement in common marker locations. His thesis reported skin correction algorithms for the fore and hind limbs at walk and trot, which have been used in several studies to improve the accuracy of data describing the motion of limb segments from skin markers.

Force plate analysis is the method of choice for rapid and accurate measurement of ground reaction forces (GRFs). Data collection requires a single hoof to hit the force plate at a time. The early force plates were small, and it many runs were usually required to obtain one successful hoof hit at the trot, which greatly limited its use. Recently, larger force plates have been marketed, enabling a reduction in the ratio of unsuccessful to successful trials (Clayton, 1996). A good force plate hit was obtained every five passes at the trot on a force plate measuring 60 x 60 cm (Merkens, et al., 1993).

The availability of video-based motion analysis and large force plates, in combination with advanced computer technology has greatly facilitated progress in equine gait analysis. Several studies have been performed to identify normal kinematic and kinetic patterns, and to study pathological patterns obtained from lame horses. The

most ambitious aim of clinical biomechanics in horses is computer diagnosis of gait deficits. Analysis of multiple kinematic or kinetic characteristics might allow early and objective diagnosis of a lameness (Buchner, 2001a).

GAIT ANALYSIS IN SOUND HORSES

One of the major research areas for equine locomotion according to Leach and Crawford (1983) is the characteristics of normal locomotion. In sound horses, gait analysis techniques have been used to obtain quantitative measurements of kinematic and kinetic data, as an aid to increase the understanding animal movement patterns and force generation to move the limb. In a clinical setting, the goal is to use this information as normative data for comparison it with data from different types of lameness.

Kinematic analysis. Kinematic analysis is a tool for quantifying movements. The output is in the form of temporal, linear, and angular measurements that describe the movements of the body segments and joint angles (Clayton, 1996). Patterns of limb motion have been quantified and described. For purposes of lameness evaluation, the trot is the gait of choice, so this section will focus on the trot. In trotting horses, the forelimb and hind limb rotate like pendulum around rotation point, at the proximal part of scapula and at the acetabulum (Back, et al., 1995a; Back, et al., 1995b). During the stance phase, the limb shortens as it accepts load. In the forelimb, the shortening in early stance was due to hyperextension of the carpal joint and shortening of distance from the cubital joint to the hoof (Hjerten and Drevemo, 1993). In the hind limb, shortening was due to the

flexion of the femorotibial, tarsal and distal interphalangeal joints and extension of the metatarsophalangeal joint (Hjerten, et al., 1994).

Clinical evaluation is based on observation of abnormal or asymmetrical motion between left and right forelimb or hind limb pairs at the trot. It is important, therefore, to evaluate the degree of symmetry using kinematic analysis in trotting horses. In assessment of locomotion symmetry (Pourcelot, et al., 1997a; Pourcelot, et al., 1997b), skin markers were attached over anatomical landmarks of the forelimb and hind limb pairs of sound horses. Joint angle motion was found to be more symmetrical than vertical displacement of the markers overlying the joint centers of rotation. Furthermore, vertical displacement of the proximal markers at the trunk was less symmetrical than that of the markers overlying the distal limb joints. Comparing the symmetry of proximal markers between forelimbs and hind limbs, the hind limbs had a lower level of vertical displacement symmetry than the forelimbs. The asymmetry in vertical displacement of the tuber coxae can be detected in sound trotting horses (Buchner, et al., 1996c). This is probably due to the ability to move the vertebral column in flexion/extension, rotation and lateral bending. Since the forces generated by muscles are used to accelerate the body, the symmetry can be assessed by comparing acceleration of the point of interest on the left and right sides of the body, such as the acceleration quotient of the tuber coxae (Buchner, et al., 1993). Perfect symmetry in sound horses should yield a quotient of 1. That study reported a range of acceleration quotients from 1.03 to 1.54 in sound horses. This supported the idea that asymmetrical motion of the tuber coxae occurred in sound trotting horses, which is due to the different swinging characteristics of the coxofemoral joints and the flexibility of the vertebral column of the individual horses.

Movement of body center of mass (BCM) in sound horses has been studied (Buchner, et al., 2000). BCM is defined as the centroid of all mass elements of an object. The position of BCM changes according to the orientation of all body segments. A knowledge of BCM position can be used to study the load distribution on the limbs and the external work of locomotion. At the trot, observation from the side of the horse showed that the BCM moves down and slightly cranially at the beginning of stance, then caudally and down until the middle of stance. After that, it started to move upward and cranially to the end of stance. When observed in a frontal view, the BCM has a slight medio-lateral movement toward the weight bearing forelimb during the first half of stance and then moves back toward the midline in terminal stance. The displacement magnitude of the BCM is significantly smaller than the externally visible trunk movements, which contributes to the high locomotor efficiency of horses.

The characteristics of hoof landing were studied and indicated differences between the fore and hind hooves. Fore hooves had higher vertical hoof velocity and acceleration at impact than hind hooves, while hind hooves had higher horizontal velocity and acceleration than fore hooves (Back, et al., 1995c; Johnston, et al., 1996). Therefore, the fore hoof bounces more at impact, whereas the hind hoof slides into the ground.

Several factors may influence the kinematic variables, notably subject velocity. At the walk, increasing velocity was associated with increasing frequency and constant stride length. At the trot, increasing velocity was associated with variable alterations in stride length and stride frequency (Rooney, et al., 1991). As velocity increases, there are increases in retraction-protraction range of motion, tarsal joint flexion and tarsal and coxofemoral joint ranges of motion (Galisteo, et al., 1998). Training also affects the

kinematic variables. Elite trained horses showed different kinematics compared to untrained horses, including a decrease in percent stance duration, and several differences in forelimb joint angle variables, but minimal differences in hind limb joint angle variables (Morales, et al., 1998). Kinematics also changes with farriery modifications. Horses with acute angulation of the hind hooves had increases in breakover time, overreach distance and overreach duration (Clayton, 1990). Each horse from a homogenous population adopts a constant angular pattern that is very close to that of other horses (Degueurce, et al., 1997). Variation can be reduced by comparing horses from a homogeneous population under similar conditions.

Kinetic analysis. The force plate is an accurate tool to evaluate ground reaction forces (GRFs). The ground reaction forces are recorded and resolved into three orthogonal components: vertical, longitudinal and transverse. The point of force application to the hoof (center of pressure) is also recorded. The vertical force component represents the force of the body mass that loads the limb. The longitudinal component may be positive or negative, representing propulsion and braking forces, respectively. During the first half of stance, the negative longitudinal force decelerates the forward motion. In the second half of stance, the positive longitudinal force acts to propel the body forward. The transverse component represents the force that turns the body to left or right. When the horses move in straight line, this force component is very small. The variables obtained from force plate analysis are peak forces and times of their occurrences. Force impulses, calculated by time integration of the areas underneath the force curves, represent the total amount of force applied over a period of time.

The advantage of force plate analysis is the relatively easy instrumental set up and data collection procedures. The limitation is the need for several trials to collect sufficient good hits. Probably due to the relatively small force plate, which required a large number of attempts to obtain one successive trial, the early studies that established the standard GRF of normal horses was performed in walking horses (Merkens, et al., 1985; Merkens, et al., 1988; Merkens and Schamhardt, 1988). At the walk, the magnitudes of vertical peak forces were higher in the forelimbs than the hind limbs. The magnitudes of the longitudinal force peaks and impulses were similar in the forelimbs and hind limbs, indicating an equal contribution to deceleration and acceleration of each of the four limbs during walking. At the trot, the mean vertical forces were highly correlated with the body weight (Barr, et al., 1995). The peak longitudinal force is around 1/10 of the peak vertical force and the peak transverse force is very small, about 1/100 of the peak vertical force (Seeherman, et al., 1987). The magnitudes of peak vertical force, vertical impulse and peak braking force were greater in the forelimbs than in the hind limbs, but the peak propulsive force was higher in the hind limbs (Morris and Seeherman, 1987). In the forelimb, peak force and impulse were higher for the braking component than the propulsive component, whereas the opposite was found in the hind limbs (Merkens, et al., 1993). This indicates the important role of the forelimb to decelerate the body, and the hind limb to accelerate and propel the body forward at the trot. Transverse forces were inconsistent and corresponding within-subject variation was considered too high for a meaningful further analysis. The GRF variables are consistent and show little variation within horses when data are collected on different days (Seeherman, et al., 1987).

In the analysis of equine locomotion, identification of the times of hoof impact and lift off are require to calculate temporal stride variables, such as stance duration, swing duration and stride duration. Force plate analysis proved to be an accurate method to identify the time when the hoof was on the ground (Schamhardt and Merkens, 1994). In the laboratories that do not have a force plate, an alternative method is to use accelerometer attached to the hoof. At impact, the sudden change of hoof acceleration is fairly easy to detect but at the lift off hoof acceleration is less abrupt, so the accelerometer may not determine lift off time correctly. Recently, a new method has been reported (Peham, et al., 1999b) in which stance duration at the walk obtained from high speed (240 frames/s) kinematic analysis was highly correlated with that obtained from a force plate.

Subject velocity influences the magnitude of the GRF. When walking velocity increases, there is an increase in peak vertical force but a decrease in vertical impulse on the hind limb (Khumsap, et al., 2001b). In the forelimb, an increase in walking velocity results in an increase in peak vertical force and decreases in vertical impulse and braking impulse (Khumsap, et al., 2002). In the forelimbs, higher trotting speed may be associated with greater vertical (Barr, et al., 1995) and braking (McLaughlin, et al., 1996) forces. Therefore, when comparing information among different horses or assessing the effect of different conditions, subject velocity is an important factor that needs to be controlled.

GAIT ANALYSIS IN LAME HORSES

One of the goals of studying gait analysis in horses is to apply the technique as a research or clinical tool to evaluate lameness. After the normal patterns of gait have been identified, they can be used as a standard for comparison with pathological patterns obtained from lame horses. Comparison of normal and abnormal functions of selected joints and limb segments enhances the understanding of gait pathology and offers a method of monitoring the outcome of treatment. Gait analysis principles have been applied to evaluate lameness in a variety of disciplines. The studies on lameness in horses have been performed either on naturally occurring lameness or, more often, on induced-lameness. The induced-lameness provides less variability of the site and degree of lameness in the limb, which facilitates comparisons of gait variables between lame and sound horses, and may be able to assess specific lame patterns or to compare between lamenesses at the different sites in the limb.

Kinematic analysis in lame horses. Mild lameness at the trot may be difficult to assess subjectively. A study comparing subjective evaluation and kinematic analysis of mild lameness at the trot before and after palmar digital nerve block showed that experienced clinicians had higher within-observer agreement of lameness improvement than interns or residents, but they still had more difficulty detecting the true state of lameness than kinematic analysis (Keegan, et al., 1998b). Another study indicated similar findings in assessment of mild forelimb lameness. A clinician and a motion analysis system assigned the lameness to the same limb in all cases but grading of the lameness

differed in 6 out of 29 cases (Peham, et al., 1999a). Therefore, kinematic analysis can be used as an informative tool supporting subjective veterinary judgment.

A kinematic symmetry index has been developed to evaluate the magnitude of motion of the forelimb and hind limb pairs in horses. In lame horses, vertical displacement indices of anatomical landmarks generally have lower symmetry but are more sensitive to lameness than the joint angle indices (Pourcelot, et al., 1997a). In a group of horses with unilateral fore or hind limb lameness, the most sensitive lameness indicators were the symmetry indices of the vertical displacement of the proximal markers of the limbs (Audigie, et al., 2001). Asymmetry in proximal marker displacement might reflect supporting limb lameness, while asymmetry in distal marker displacement might reflect swinging limb lameness. A limitation to the use of symmetry indices is that they do not determine the lame side and are unable to detect bilateral lameness (Pourcelot, et al., 1997a).

Each lame horse has an optimum trotting speed that reveals the maximum asymmetrical movement (Peham, et al, 1998). In the forelimb, lameness assessed by asymmetry of vertical head motion increased significantly with trotting speed in moderately lame horses, while there was no significant correlation between speed and asymmetrical motion in mild or subclinical forelimb lameness (Peham, et al., 2000). Therefore, moderate forelimb lameness measured as head motion asymmetry depends on the speed at which the measurements are taken. Measurements taken at two trotting speeds can be used to construct an individual regression calculation to standardize the magnitude of head motion at any speed within the trotting range.

A group of horses with fore or hind limb lameness was observed kinematically before and after diagnostic blocks to assess the compensatory movement patterns (Uhlir, et al., 1997). Asymmetrical acceleration of the head and sacrum indicates that horses with a unilateral supporting forelimb lameness showed a false supporting lameness in the contralateral hind limb, while horses with a true hind limb lameness showed a false lameness in the ipsilateral forelimb. It was suggested that a horse that appears to have ipsilateral fore and hind limb lameness is likely to have a true hind limb lameness, and a horse that appears to have a forelimb and contralateral hind limb lameness is likely to have a true forelimb lameness. This may be useful for planning diagnostic blocks in lameness evaluation.

Horses with induced fore or hind hoof lameness had compensatory patterns both within and between the limbs (Buchner, et al., 1996b). When lameness presented at the hoof, there were decreases in joint extension of the metacarpophalangeal/metatarsophalangeal joint and in joint flexion of the distal interphalangeal joint on the lame limb at the trot during stance. The contralateral limbs had compensatory increases in metacarpophalangeal/metatarsophalangeal joint extension and distal interphalangeal joint flexion. In the proximal joints, such as scapulohumeral and tarsal joints, there were increases in joint flexion with increasing lameness degree, indicating that these joints were acting as load dampers when there was a pain in the hoof. Vertical motion of the trunk, represented by the withers for forelimb lameness and the tuber sacrale/tuber coxae for hind limb lameness was smaller during stance of the lame limb in the lame condition than in the sound condition (Buchner, et al., 1996c). The

trunk was supported earlier at the start of the lame limb stance phase to reduce peak loading and save the horse energy to lift the body mass into swing.

Front hoof lameness induced by pressure on the frog area was associated with a decrease in peak metacarpophalangeal joint extension during stance, and increases in head vertical displacement and asymmetrical head movement at the trot. A similar lameness model using pressure at the toe area resulted in similar changes in metacarpophalangeal kinematics and head movement, together with the earlier occurrence of peak metacarpophalangeal joint extension, maximum hoof height near mid swing and an increase in maximum limb protraction (Keegan, et al., 2000). Kinematic analysis may enable differentiation between lameness at the heel and toe.

Evaluation of horses at the trot with amphotericin-induced carpal synovitis at 9, 16 and 23 days after induction, indicated that stride length, stance duration and forelimb abduction were not changed. Carpal joint range of motion on the sound limb and asymmetrical motion of the withers during stance phases of sound and lame forelimbs significantly decreased only at 9 days after the induction. The metacarpophalangeal joint range of motion in the lame limb and asymmetrical head excursion during stance phases of sound and lame forelimbs significantly decreased at all measurement times compared to baseline data before lameness induction (Peloso, et al., 1993b). Head excursion was the most consistent variable for assessment of carpal lameness in the horse.

Another aspect of kinematic analysis assesses the compensatory movement patterns of the body center of mass (BCM). Lameness induction by pressure-induced mild or moderate pain on the sole of the fore hoof has been used to study the movement of BCM (Buchner, et al., 2001). During the stance phase of a moderate forelimb

lameness, the magnitude of vertical BCM movement decreased by 34% and vertical BCM acceleration decreased by 21% compared with the sound condition. During the stance phase of the contralateral forelimb, vertical BCM movement increased by 9%. In the medio-lateral direction, there was a mean shift of BCM motion toward the sound forelimb. The caudal movement of the BCM during the lame diagonal stance was only 9 mm, representing a minor compensatory effect. Marked changes in vertical acceleration of BCM during the lame diagonal stance resulted from adjustment of head and neck movement, which creates a torque on the trunk that changes its momentum (Vorstenbosch, et al., 1997). The effect is an increase in loading of the sound forelimb and unloading of the diagonal hind limb. In the lame diagonal stance, the forelimb was unloaded and the load shifted to the diagonal hind limb without changing the BCM position.

Horses with various hind limb lamenesses of different degrees had increased vertical displacement of the tuber coxae in the lame hind limb compared to the contralateral hind limb, and this is probably the best criterion for the diagnosis of hind limb lameness (May and Wyn-Jones, 1987). Since the same amount of vertical displacement can be achieved with different vertical velocities, vertical acceleration of the tuber coxae may represent the effects of lameness in a more suitable way (Buchner, et al., 1993). The maximum and minimum peaks of the coxofemoral acceleration were used to calculate the coxofemoral acceleration quotient. In the lame horses the acceleration quotient ranged from 1.32 to 2.96, which overlapped the value of 1.03 to 1.54 in sound horses. It has been stated that horses with an acceleration quotient greater than 1.61 can be assessed as lame with 95% confidence (Buchner, et al., 1993).

The effects of unilateral lameness induction in the distal intertarsal and tarsometatarsal joints, and the improvement after intra-articular anesthesia were evaluated kinematically. After lameness induction, tarsal joint flexion during stance increased, while metatarsophalangeal joint extension during stance and the limb protraction distance decreased (Kramer, et al., 2000). Vertical excursion of the tuber coxae became more asymmetric than in the sound condition. After intra-articular anesthesia, limb protraction returned to pre-lameness values, and vertical excursion of tuber coxae became more symmetric than in the lame condition. Hind limb protracting distance may be one of the more sensitive indicators of the severity of tarsal joint lameness. Evaluation of limb protraction is assessed when observing the horse from the side.

Kinetic analysis in lame horses. Force plate analysis is a non-invasive tool for measuring GRFs, which can be used to aid in the localization of a subtle lameness to a particular limb and to evaluate the effect of diagnostic regional anesthesia, particularly in proximal limb lameness where regional anesthesia is rarely 100% effective and small improvements in weight bearing are considered a positive response (Seeherman, et al., 1987).

In a study comparing clinical examination with force plate analysis to evaluate horses with mild lameness, in 15 out of 22 cases the same limb was identified but there was no correlation between the degree of lameness assigned by the two methods (Weishaupt, et al., 2001). Therefore, assessment of asymmetry in peaks force or impulses in fore or hind limb pairs may complement the clinical evaluation in difficult or mild cases.

Perineural and intra-articular anesthesia are useful diagnostic aids to localize the site of lameness within a limb. The method is based on the assumption that the technique itself does not change the movement pattern. Force plate analysis of normal horses after palmar digital nerve block, abaxial sesamoid nerve block and high palmar nerve block did not change the clinical score or the GRF variables (Keg, et al., 1996). This confirms that local anesthesia does not alter the loading pattern in healthy horses.

At the trot, horses with an induced full-thickness articular cartilage defect in the carpal joint had decreases in peak vertical force, peak braking force and the corresponding impulses in the lame forelimb compared to the values obtained before the operation. The contralateral forelimb had no change in peak vertical force, but there were increases in peak braking force and impulse. The peak vertical force, peak propulsive force and corresponding impulses in the ipsilateral hind limb also decreased. The stance time on all four limbs did not change (Morris and Seeherman, 1987). Changes in GRF variables within the lame limb and redistribution of forces between the other limbs indicates the potential for secondary injury resulting from compensation for a specific type of lameness.

Measurement of the repeatable peaks of vertical and longitudinal forces and the slope between the peaks has been used to assess subclinical tendon injury (Dow, et al., 1991). GRF measurements collected from 24 Thoroughbred horses at the trot over a period of two years were repeatable with low variation within horses, between sessions within horses and between horses. A characteristic increase in first slope measurement, which corresponded to a reduced rate of limb loading during early stance, became apparent in the force patterns before the horse exhibited clinical lameness due to

tendinitis. Thus GRF analysis provided an objective means of detecting tendon injury at an early stage.

The GRF abnormalities may be described by a single value, such as asymmetry in peak vertical force during mid stance, or by an evaluation of characteristic changes in the selected points on the force curve. Principal component analysis has been applied to evaluate the characteristic points on the vertical GRF trace of the equine forelimbs at the trot. Four points at the beginning of stance and four points at the end of stance on vertical force curve were obtained (Williams, et al., 1999) in three groups of horses: sound, horses with superficial digital flexor (SDF) tendinitis and horses with navicular disease. Principal component analysis could identify differences in early stance between sound and SDF tendinitis horses and in late stance between sound and navicular disease horses, while asymmetry of peak vertical force could not be detected between the three groups. Evaluation of peak vertical force alone may be misleading, whereas asymmetries at the other specific points on the force curve may be more useful diagnostically. Further analysis by principal component analysis between sound horses and horses affected with navicular disease showed significant differences in component values during early and late stance. After palmar digital nerve block, the locomotion pattern in late stance returned to similar values as in sound horses, but the pattern during early stance did not change (Williams, 2001). This indicated that horses with navicular disease have an abnormal limb loading pattern during early stance, that is not due to pain in the navicular area. This may have prognostic value in horses susceptible to development of navicular disease.

Shoeing with a medial or lateral 3.7-degree wedge on the fore hooves resulted in displacement of the point of force application by approximately 10 mm in the direction of the wedge throughout stance. Even 24 hours after shoeing, the horses could not compensate for an acute hoof imbalance by redistributing the load under the hoof (Wilson, et al., 1998)

To assess the differentiation between flexor tendon lameness and suspensory ligament lameness using high plantar nerve block, force plate analysis has been used as an objective evaluation tool (Keg, et al., 1994). Tendinitis of the superficial or deep digital flexor tendon, or desmitis of the suspensory ligament were induced by collagenase injection of the hind limb. The affected horses showed decreases in peak force values and impulses of the vertical, braking and propulsive forces. The braking impulse was highly correlated with clinical lameness score. High plantar nerve block alleviated lameness due to flexor tendinitis, with less consistent alleviation of lameness due to suspensory desmitis. Since this block relieved lameness due to flexor tendinitis and suspensory desmitis, it cannot distinguish between them.

Combined kinematic and kinetic analyses. No single method of gait analysis can evaluate every parameter of locomotion. Kinematic analysis of lame horses describes changes in movement patterns due to lameness but does not explain the relationship between kinematic changes and the changes in force generation. Force plate analysis alone provides meaningful information of changes in vertical, longitudinal and transverse components of the GRF due to lameness, but it measures one limb at a time and does not indicate how changes in forces affect movement profiles. Ideally, a method of gait

analysis should include both kinematic and kinetic measurements, but to date only a few studies have reported complete sets of data.

Horses with induced SDF tendinitis in one forelimb were evaluated by comparison between the lame forelimb and the contralateral compensating forelimb. The lame limbs had lower peak vertical GRF, less flexion of the distal interphalangeal joint and less extension of the metacarpophalangeal joint, compared with compensating limbs. Compensating limbs had a more protracted orientation throughout the stance, and higher peak braking force and impulse (Clayton, et al., 2000b). Protracted orientation of the compensating limb at initial ground contact facilitated support of the trunk in a less elevated position, allowing the horse to transfer its weight from the lame to the compensating forelimb without raising the body mass into a suspension phase.

After immobilization of the normal metacarpophalangeal joint in a fiberglass cast for 7 weeks, followed by cast removal, resulted in all horses being lame on the cast limb. An exercise program, beginning with hand-walking and ending with treadmill exercise for 8 weeks, slightly improved lameness but did not restore the normal joint function. There were significant decreases in the metacarpophalangeal joint range of motion and asymmetrical GRF peaks between the lame and contralateral forelimbs (Harreveld, et al., 2002).

Effects of treatment regimes. Both kinematic and force plate analysis can be used to monitor the outcome of specific treatment objectively.

The effect of electroacupuncture in horses suffering from chronic laminitis or navicular disease (Steiss, et al., 1989) was evaluated using a force plate to measure load

distribution before and after four consecutive weeks of treatment. Even though the horses seemed to improve clinically, the objective evaluation did not show significant differences between control and treatment groups. The use of line firing and tendon splitting to treat collagenase-induced SDF tendinitis showed progressive changes of GRF variables up to 11 months post treatment, compared to the pre-induction variables. The horses that were treated with rest alone showed a progressive return to the pre-induction state (Goodship, et al., 1987).

The effect of a modified hyaluronan on amphotericin-induced carpal synovitis was studied using computerized motion analysis to evaluate the horses' motion before lameness induction, after lameness induction but before the hyaluronan administration, and after intra-articular hyaluronan administration. After lameness induction, there were increases in asymmetrical head and withers excursions during the sound and lame forelimb stance phases. The hyaluronan did not significantly improve the symmetry of head and withers excursions. It was concluded that intra-articular administration of hyaluronan was not effective in reducing lameness associated with amphotericin-induced synovitis (Peloso, et al., 1993a).

In horses, synovectomy is used as palliative therapy for traumatic and septic arthritis. Gait analysis was used for objective evaluation of gait changes associated with carpal synovectomy and a subsequent exercise program (Clayton, et al., 1998). Video recording was made in three sessions: before the operation, two days after the operation and four months after the operation following two months rest and two months of a progressive exercise program. There was no significant difference in clinical lameness score, vertical head displacement, peak metacarpophalangeal joint extension, peak carpal

joint flexion and peak carpal joint extension between the surgical limb and contralateral forelimb on any of the three evaluation sessions. Therefore, synovectomy in sound horses did not cause lameness in the initial post operative period and horses can safely return to work two months after carpal synovectomy.

The effect of oral administration of propentofylline on the treatment of navicular disease was evaluated using force plate analysis (Kirker-Head, et al., 1993). The vertical GRFs were measured for all four limbs to quantify the weight bearing profile prior to and following treatment with 7.5 mg/kg propentofylline twice a day for 6 weeks. The proportion of the total mass normalized force born by the forelimbs increased significantly following treatment, although more of the horses returned to complete soundness. The force plate analysis provided an objective means of assessing effectiveness of treatment and was more sensitive in assessing drug efficacy than clinical examination.

Several types of lameness are treated by alterations in hoof balance and application of orthopedic shoes. In horses with navicular disease, kinematic studies showed that application of either flat bar stock with rolled-toe or caudally extending branches/egg-bar shoes for three weeks did not significantly reduce the asymmetrical head movement. During the swing phase, carpal joint flexion and maximum hoof height increased, but these changes were not solely the result of a reduction in the level of lameness (Keegan, et al., 1998a). The balance and shoeing could be performed concurrently with other treatments without interfering with the evaluation of the outcome of the other treatments.

INVERSE DYNAMIC ANALYSIS: CLINICAL APPLICATION

In the early computer era, kinematic and GRF data were reported and analyzed separately. The resulting information gave some useful criteria to quantify abnormalities in movement and force patterns due to lameness, but was not useful for discriminating between lameness at different sites within the limb. For example, lameness induced by pressure on the hoof sole of the forelimb (Buchner, et al., 1996b; Galisteo, et al., 1997; Keegan, et al., 2000) produced similar kinematic changes to an induced lameness of the carpal joint (Back, et al., 1993; Peloso, et al., 1993b). These changes included a decrease in maximal metacarpophalangeal joint extension during lame limb stance and an increase in asymmetry of head excursion during left and right stance phases. Most horses also showed a decrease in carpal joint range of motion. The use of a force plate to measure changes in GRF due to carpal lameness (Morris and Seeherman, 1987) and SDF tendinitis (Clayton, 2000b) reported similar findings, most notably a decrease in peak vertical GRF, vertical impulse, peak braking GRF and braking impulse. If the objective is to use gait analysis as a diagnostic tool, kinematic and kinetic data should be combined to provide more information about the underlying mechanisms.

Inverse dynamic analysis is a technique that estimates the forces that cause an observed motion. It offers a method of calculating variables that cannot be measured directly. The technique treats the body as a system of rigid, linked segments connected at the joints. The net joint moment, or joint torque, is calculated. It represents the action of soft tissues around the joint. By combining net joint moment data with joint angular velocity, net joint power can be calculated, which measures the rate of mechanical work done around the joint. Integration of the area under the net joint power curve yields net

joint energy, which measures the amount of mechanical work done across a joint over a period of time. Negative net joint power indicates negative work is being performed (eccentric muscular contraction, or elastic stretching of ligaments or tendons) that absorbs mechanical energy and controls joint movement. Positive net joint power indicates positive work is being performed (concentric muscular contraction, or release of stored elastic energy) to generate mechanical energy to move the joint. Inverse dynamic analysis allows the evaluation of the sources of mechanical power for movement. In human studies, it has been shown that mechanical power is the most informative variable for evaluation of pathological gait (Winter, 1990).

The first reports of equine inverse dynamic analysis were based on the concept of quasistatic equilibrium. The problem with this approach is that only the external force taken into account is the GRF, which ignores the effect of inertial and gravitational forces acting on individual limb segments. In humans, most of the joint moments in the lower extremity during stance can reasonably be approximated by the quasistatic approach (Wu and Ladin, 1996). Therefore, the early equine studies, which described joint moments at the distal interphalangeal and metacarpophalangeal joints were reasonable and acceptable. It was impossible to calculate net joint moments in the more proximal parts of the equine limb with reasonable accuracy until the complete inertial properties of equine body segments had been identified (Buchner, et al., 1997). Furthermore, inverse dynamic analysis during the swing phase requires knowledge of the inertial properties. Descriptions of inverse dynamics that take account of inertial properties of the limb segments to analyze equine locomotion have been published, both during stance and swing phases.

Inverse dynamics in sound horses. The technique has been used to identify the kinetic pattern of the limb joints at walk and trot. Information has been reported for the forelimb of normal horses at the walk (Colborne, et al., 1997a; Colborne, et al., 1998; Clayton, et al., 2000a), and the mechanical function of each joint has been described. During stance, the distal interphalangeal and scapulohumeral joints act as energy dampers, as shown by a power profile dominated by energy absorption. The metacarpophalangeal joint functions elastically to store and release strain energy. The carpal joint acts like a strut as the body rolls over the grounded limb and does not appear to play an important role in energy absorption or generation. The cubital joint is the only joint that shows net joint energy generation at the walk. During the braking phase, energy generated at the cubital joint maintains the extended position of the limb. Later in the stance phase, energy generation at this joint provides forward propulsion. During the swing phase, the cubital joint is, again, the only joint that provides energy generation to protract and retract the entire limb, while the more distal joints are driven by inertial forces, with their movements being controlled by negative work around each joint. The main sources of energy absorption during swing are the scapulohumeral and carpal joints.

The net joint moment and power profiles of the normal forelimbs at the trot showed consistent and repeatable patterns in each joint (Clayton, et al., 1998; Lanovaz, et al., 1999). During stance, the distal interphalangeal and metacarpophalangeal joints perform similar functions to the walk, except that the magnitudes of net joint energy absorption and elastic energy release are greater at the trot than at the walk. The metacarpophalangeal joint acts as an elastic spring, absorbing then releasing elastic energy to bounce the limb upward into the swing phase. The net joint power profile at the

carpal joint shows two small cycles of elastic energy storage and release. The cubital and scapulohumeral joints also appear to work elastically in the first half of stance. The scapulohumeral joint plays an important role in energy generation to propel the body forward during the second half of stance. The function of forelimb joints during the swing phase of the trot is similar to their functions at the walk.

In the hind limb, inverse dynamic analysis has been applied to analyze net joint mechanical work at the walk (Clayton, et al., 2001). During stance, the distal interphalangeal and metatarsophalangeal joints perform similar functions to those joints in the forelimbs. The tarsal joint performs mostly positive work to move the limb throughout stance, whereas the femorotibial joint performs mostly negative work to control the joint motion. The coxofemoral joint is the main source of energy generation to propel the body forward. During swing, the coxofemoral joint is again the main source of positive work, acting to protract and retract the entire limb. It is assisted by positive work at the tarsal joint that raises and lowers the distal limb. The femorotibial joint performs negative work to control flexion and extension of this joint. The metatarsophalangeal and distal interphalangeal joints are driven by inertial forces under the influence of the proximal limb joints' motion.

The effects of an increase in walking velocity on net mechanical work have been studied in the hind limb during stance phase (Khumsap, et al., 2001a). An increase in walking velocity requires an increase in net joint energy generation at the coxofemoral and tarsal joints, which confirms the important role of these two joints in performing positive work during locomotion. The mechanical work patterns of the equine hind limb at the trot have not yet been described.

Inverse dynamic analysis has been applied to study the effects of different types of shoes. The application of normal shoes in sound horses did not effect the net joint moments of the metacarpophalangeal or distal interphalangeal joints during the stance phase. Shoeing improves the quality of the trot in sound horses because the increased inertia of the lower limb produces an increase in swing phase retraction and animation of the trot (Willemen, et al., 1997). Rocker-toed shoes are used to facilitate breakover, but analysis of the net joint moment in the distal interphalangeal joint did not reveal any benefits associated with this type of shoe (Willemen, et al., 1996). The duration of breakover time and distal interphalangeal net joint moment did not differ between rocker-toed shoes and standard flat shoes in healthy Dutch warmblood horses.

A study that applied inverse dynamic analysis to study the landing in jumping horses showed that the highest vertical GRF occurred in the trailing forelimb at landing. The tendon forces calculated using inverse dynamics indicated the relative loading of the tendons increased from deep digital flexor tendon to suspensory ligament, and was highest in SDF tendon (Meershoek, et al., 2001). An increase in fence height from 0.80 m to 1.20 m substantially increased superficial digital flexor tendon forces, whereas it hardly influenced suspensory ligament forces and did not influence distal accessory ligament strain.

Inverse dynamics in lame horses and effects of treatment. Inverse dynamic analysis describing the effects of SDF tendinitis on forelimb locomotion (Clayton, et al., 2000c) showed that the peak value of the net joint moments was lower in the lame limb than in the contralateral forelimb at all joints crossed by the SDF muscle and tendon

(metacarpophalangeal, carpal and cubital joints). There were decreases in energy absorption at the distal interphalangeal joint, in elastic energy absorption and release at the metacarpophalangeal and carpal joints, and in energy generation at the cubital joint. The decrease in net joint energy profiles in all joints indicated that gait was energetically inefficient in horses with SDF tendinitis.

Inverse dynamic analysis has been used to evaluate the effects of desmotomy of the accessory ligament of the deep digital flexor tendon on equine forelimb function (Buchner, et al., 1996a). The net joint moment of the distal interphalangeal joint was significantly decreased 10 days after desmotomy. There was no transfer of load from the operated limb to the contralateral forelimb. The net joint moment at the metacarpophalangeal joint did not change 10 days after operation. Instead, the compensatory response was due to redistribution of force loading in the other structures of the operated limb, with increases in force generation in the suspensory ligament and SDF tendon to maintain the net joint moment at the metacarpophalangeal joint.

Long-term consequences of desmotomy have been observed (Savelberg, et al., 1997; Becker, et al., 1998). Six months later, the peak net joint moment during the second half of stance reached about 80% of its presurgical value, which indicated that function of the deep digital flexor tendon and accessory ligament was not completely recovered after 6 months. There were no changes in joint angle, peak joint moment, or peak loading of suspensory ligament and SDF tendon at the metacarpophalangeal joint. It was concluded that desmotomy of the accessory ligament of the deep digital flexor tendon was not associated with long-term changes that could be considered hazardous for the horses.

The effects of orthopedic shoes on locomotion have also been studied. Horses with SDF tendinitis were shod with flat shoes and 6-degree heel wedges (Clayton, et al., 2000d). After five days adaptation to the wedge shoe, there were decreases in peak net joint moment and energy absorption at the distal interphalangeal joint. The different profiles of the net joint moment between the lame limb and contralateral limb at the distal interphalangeal joints indicated the deep digital flexor muscle in the lame limb was contracting more strongly to compensate for the impaired SDF tendon. Significant findings were confined to the hoof but no advantage could be identified in terms of a decrease in the peak net joint moment at the metacarpophalangeal joint. Therefore, application of heel wedges may not be an effective way to alleviate lameness due to SDF tendinitis.

Horses suffering from navicular disease have been shod with two types of orthopedic shoes. Heel wedges have been used to reduce the tension in the deep digital flexor tendon and egg-bar shoes have been used to correct the weight distribution and reduce the moment of force at the distal interphalangeal joint. Inverse dynamic analysis has been used to evaluate the effect of these shoes on forces exerted on the navicular bone (Willemen, et al., 1999). The maximal force on the navicular bone was reduced by 24% when the horses were shod with heel wedge shoes compared with flat shoes. Egg-bar shoes did not reduce the force on the navicular bone. Therefore, horses suffering from navicular disease may benefit from heel wedge shoes but it is doubtful that egg-bar shoes will be beneficial.

THREE-DIMENSIONAL ANALYSIS IN EQUINE BIOMECHANICS

Most of the measurements of the limb joints in normal horses are primarily those of flexion and extension, and most of the published kinematic studies have been restricted to 2-D analysis in the sagittal plane. However, complex joints, such as the carpus and tarsus, may also show measurable amounts of abduction-adduction and internal-external rotation, which are important components of normal movement and which may change in response to pathological conditions. There have been very few three-dimensional analyses of equine locomotion., though multiple camera techniques have been used synchronously to capture the horse's motion in more than one plane. Images from two or more cameras are combined into one picture, in which the depth of the fields of view and location of skin markers are taken into account. True three-dimensional analysis describes three rotational motions and three translational motions of the joint.

In horses, the concept of a joint coordinate system has been applied in vitro to study the three-dimensional motion of the equine forelimb (Degueurce, et al., 2000). Reflective markers were attached to the metacarpal bone and three phalanges, then the limbs were loaded with a compressive force. During the neutral loading, the metacarpophalangeal joint extended and the proximal phalanx externally rotated relative to the third metacarpal bone, but there was no specific trend in abduction/adduction (Chateau, et al., 2001). Addition of a lateral hoof wedge induced internal rotation and abduction of the proximal phalanx. The opposite phenomenon was observed with a medial wedge (Chateau, et al., 2001). A similar technique was used to study proximal interphalangeal joint motion (Degueurce, et al., 2001). It was found that the joint had low-amplitude of flexion, with the rate of flexion increasing exponentially with load. This

confirms that flexion of the proximal interphalangeal joint is only provoked by rather high loads. The abduction/adduction and axial rotation remained constant during the neutral loading.

Three-dimensional evaluation of limb joints in vivo have been performed on the carpal joint of horses at walk (Nicodemus, 2000). A joint coordinate system was applied to analyze the three-dimensional rotation of the carpal joint. The carpal joint flexed, adducted and internally rotated during mid swing, then approached the standing joint angles in preparation for the start of stance.

Recently, three-dimensional kinematic analysis has been performed on the tarsal joint of sound horses at the trot (Lanovaz, et al., 2002). The motions of the third metatarsal bone relative to tibia were observed via retro-reflective marker triads attached Steinmann pins transcutaneously into the lateral aspects of those bones. It was found that the tarsal joint underwent flexion, abduction and internal rotation during stance, and underwent flexion, abduction and external rotation during swing.

Other studies have used intra-medullary pins driven to the dorsal spinous processes to observe the three-dimensional motion of the vertebral columns of horses at the walk (Faber, et al., 2000), trot (Faber, et al., 2001a) and canter (Faber, et al., 2001b). In a symmetrical gait, such as walk and trot, the vertebral column showed two periods of extension and flexion in each stride, but only one cycle of extension and flexion at canter. At the walk, the lateral bending and axial rotation were characterized by one peak and one trough, whereas one peak and one trough of lateral bending with two cycles of axial rotation were found at the trot.

CONCLUSION

The gait analysis procedures in horses have been developed and improved through time. Advance in computer technology have enhanced the ability to use gait analysis as an aid in clinical evaluation of equine locomotion in variety of disciplines. Techniques used in human locomotion, such as principal component analysis and inverse dynamic analysis, have been adapted to analyze equine locomotion. The joint mechanical energy profiles in horses have been described and it should be possible to apply inverse dynamic analysis for evaluation the effects of specific type of lameness or assessment of treatment regimes.

CHAPTER 2

MATERIALS AND METHODS

The procedures included in this chapter describe the selection of suitable horses, the method of induction of synovitis, and the techniques used for gait analysis (Figure 2-1). The data comprized kinematic variables, ground reaction force variables, net joint moments, net joint powers and net joint energies. Statistical analyses were performed to compare the data before and after lameness induction.

Figure 2-1 Flow chart showing sequence of procedures.

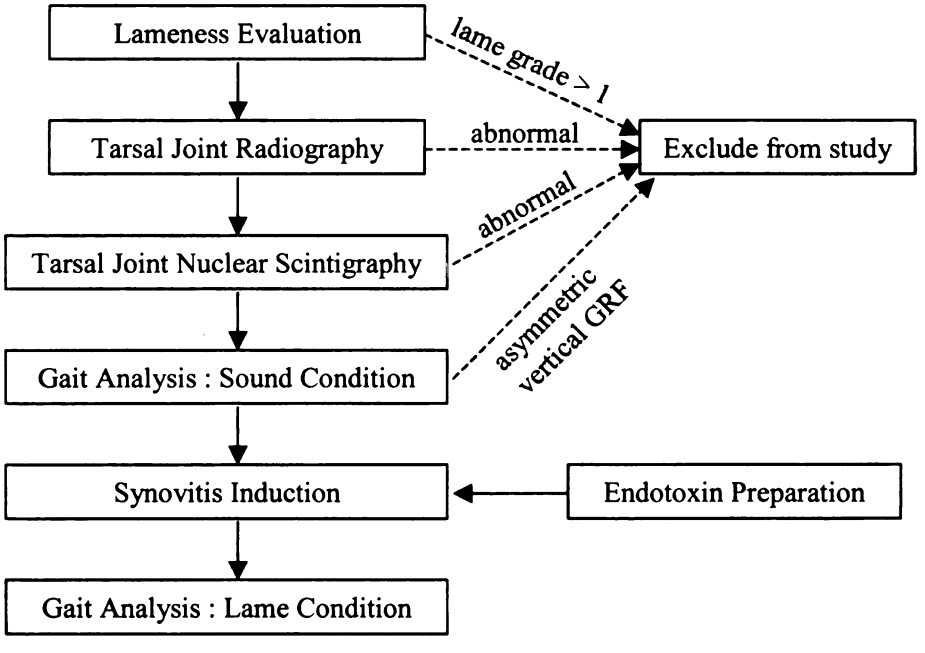

SUBJECT SELECTION

Four horses, aged 2-3 years old, were selected for this study on the basis of the findings from clinical evaluation, radiography, nuclear scintigraphy and ground reaction force (GRF) analysis. The horses' weight and height at the withers ranged from 333-392 kg and 1.43-1.50 m, respectively.

Lameness evaluation. Each horse was evaluated for lameness using the grading system of 0-5 (American Association of Equine Practitioners, 1991). The definition of lameness is a deviation from the normal gait or posture due to pain or a mechanical dysfunction. The classification is as follow,

- Grade 1 : Difficult to observe; not consistently apparent regardless of circumstances (i.e. weight-carrying, circling, inclines, hard surface, etc.)
- Grade 2 : Difficult to observe at a walk or trotting a straight line; consistently apparent under certain circumstances (i.e. weight-carrying, circling, inclines, hard surface, etc.)
- Grade 3 : Consistently observable at a trot under all circumstances
- Grade 4 : Obvious lameness; marked nodding, hitching or shortened stride
- Grade 5 : Minimal weight-bearing in motion and / or at rest; inability to move

The horses used in this study were selected from a groups of 18 horses that had recently completed on exercise study. Each horse was led at the trot on a straight line on a hard surface to evaluate the degree of lameness. After grading the lameness, flexion of the tarsal/stifle joints was performed on both hind limbs of each horse by holding the

fourth metatarsal bone parallel to the ground for 90 seconds, then trotting the horse in a straight line on a hard surface. Lameness after the flexion test was also graded. Eight horses with lameness equal or less than grade 1 before and after the flexion tests proceeded to radiography.

Radiography. Routine radiography of the tarsal joints was performed on both hind limbs. The radiographic views included lateromedial, dorsoplantar, laterodorsal-plantaromedial oblique and mediodorsal-plantarolateral oblique views. Radiographic films from each horse were evaluated by a Board Certified Veterinary Radiologist. Horses with abnormal tarsal bones or arthritic changes in both distal intertarsal and tarsometatarsal joints on the same limb were excluded from the study. Juvenile spavin has been reported in young horses before training (Laverty, et al., 1991; Barneveld and van Weeren, 1999), and this condition has been described as an incidental finding that may not be clinically significant. Therefore, horses with mild osteophytic changes in only one joint (distal intertarsal or tarsometatarsal joint) were not excluded at this stage. The remaining six horses proceeded to nuclear scintigraphy.

Nuclear scintigraphy. Since radiographic changes might not be apparent in the early stage of degenerative joint disease, nuclear scintigraphy, which is more sensitive than radiography for detecting degenerative changes at an early stage, was included in the selection process. A Board Certified Veterinary Radiologist performed the nuclear scintigraphic procedures. Each horse was catheterized intravenously in the jugular vein using a 14 gauge, 13.3 cm catheter (Angiocath, Infusion Therapy Systems Inc., Sandy,

UT) to deliver Technetium-99M bound with methylene diphosphonate at a dosage of 10 mCi per 45.4 kg body weight. The horse was isolated in an equine nuclear medicine stall for at least 2 hours before the bone phase scintillation images were taken. The horse was sedated using detomidine hydrochloride (Dormosedan, Pfizer Animal Health, Exton, PA) approximately 3 mg intravenously then was placed in front of the scintillation detector for nuclear imaging. Two bone phase scintigraphic images, lateral and plantar views, were taken from the tarsal joints of both hind limbs. The images were evaluated for increased radiopharmaceutical uptake. After nuclear scintigraphic images were taken, the jugular catheter was removed and the horse was returned to an equine nuclear medicine stall for 24 hours isolation. Horses with normal or only mildly increased radiopharmaceutical uptake in the tarsal region proceeded to gait analysis.

Ground reaction force analysis. The peak vertical force and vertical impulse are very consistent with mean symmetry of 97±2 % symmetrical values between the left and right sides of the forelimb and hind limb pairs (Merkens, et al., 1993). Therefore, left-right symmetry of vertical ground reaction force (GRF) was used as a selection criterion in this study. Velocities, peak vertical forces and vertical impulses of 5 trials from left and right forelimbs and hind limbs during the sound condition were analyzed. Symmetry values of peak vertical force and vertical impulse were obtained by dividing the values from one limb by the values from the other limb. The numerator was always the lesser value and denominator was always the larger value. The result was as a percentage. Horses with force variables that differed by more than 3 standard deviations from values reported in the literature was considered asymmetrical and was excluded form further

analysis. There were two horses excluded at this stage, one with marked asymmetrical forces in the forelimbs and the other with marked asymmetrical forces in the hind limbs.

TARSAL SYNOVITIS INDUCTION

Endotoxin preparation. The endotoxin injection was prepared in a biological safety cabinet. A 5 mg vial of lipopolysaccharide endotoxin from *Escherichia coli* O55:B5 (L2637, Sigma-Aldrich, Saint Louis, MO) was diluted with 5 ml sterile water and kept as endotoxin stock solution at concentration of 1 mg/ml. The stock solution was diluted ten-fold by adding 9 ml of 6.6 pH diluent (Normosol-R, Abbott Laboratories, North Chicago, IL) to 1 ml of stock solution to obtain a second stock at 100 μg/ml. The same procedure was repeated by mixing 1 ml of the second stock with 9 ml of 6.6 pH diluent to obtain the final endotoxin solution of 10 μg/ml. Five sterile vials (American Pharmaceutical Partners Inc., Los Angeles, CA) were used to keep the final endotoxin solution, with 2 ml in each vial. The solution was stored at 46°F until used.

Intraarticular injection of endotoxin. Non-infectious synovitis was induced in the right tarsal joints of each horse by a clinician from the Large Animal Hospital, Michigan State University. Before induction of synovitis, a physical examination was performed to determine baseline values of rectal temperature, pulse rate, respiratory rate, mucous membrane color, capillary refill time and joint appearance. The horse was sedated by intravenous injection of a mixture of 3 mg detomidine hydrochloride and 3 mg butorphanol tartrate (Torbugesic, Fort Dodge Animal Health, Overland Park, KS). Synovitis was induced in the distal intertarsal and tarsometatarsal joints by injection of 5

μg endotoxin into each joint. The skin over the sites of entry into the tarsometatarsal joint on the lateral side, and the distal intertarsal joint on the medial side of the right hind limb were aseptically prepared by hair clipping and scrubbing with betadine scrub, alcohol and betadine solution. A 20 gauge, 3.8 cm needle used to inject 0.5 ml of 10 μg/ml endotoxin solution into the tarsometatarsal joint, which was approached by inserting the needle over the proximal end of the fourth metatarsal bone. A 22 gauge, 3.8 cm needle was used to inject 0.5 ml of 10 μg/ml endotoxin solution into the distal intertarsal joint, which was entered at the gap between the central tarsal, the third tarsal and the fused first and second tarsal bones.

Care after endotoxin injection. Physical examination of each horse was performed every two hours after injection of endotoxin for the first 12 hours, then at intervals of 6 hours, until 24 hours after induction. The parameters assessed were rectal temperature, pulse rate, respiratory rate, mucous membrane color, capillary refill time, joint appearance and assessment of appetite. Lameness evaluation was performed approximately every 12 hours. If the horse developed a lameness of grade 3 or greater, 0.5-1 g of phenylbutazone (Phenylzone paste, Schering-Plough Animal Health Corp., Union, NJ) was administered orally according to the severity of lameness. When the horse had a mild but consistent lameness (grade 2) at the trot on a hard surface, gait analysis was performed. After gait analysis, each horse was kept in a stall and examined daily until it had no sign of lameness at the walk and minimal lameness at the trot (grade 1 or less). At this time, the horse was returned to pasture.

GAIT ANALYSIS

Gait analysis was performed twice in each horse. After the horse had been selected as suitable for the study, gait analysis was performed to obtain data in the sound condition, from both left and right sides of the horse. After synovitis induction, gait analysis was repeated to obtain data for the lame condition from both left and right sides. A flow chart showing the data collection procedures is shown in Figure 2-2.

Figure 2-2 Flow chart for gait analysis procedures.

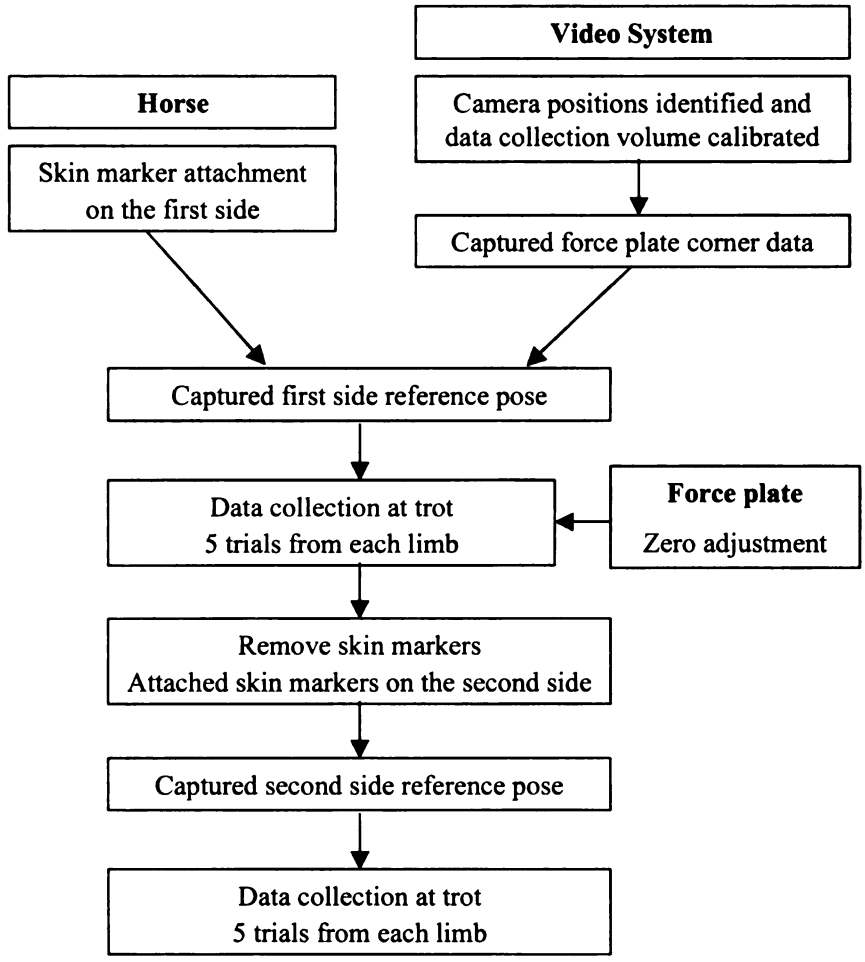

Kinematic data.

The video system (Motion Analysis Corporation, Santa Rosa, CA) consisted of 6 video cameras, a video processor computer (MIDAS), tracking computer, SVGA CRT monitor and multisync digitizing monitor (Figure 2-3). Each camera had a ring light surrounding the camera lens that produced a bright red strobed light to illuminate spherical, retro-reflective markers attached to the horse. The video cameras captured the location of the markers in space. All six cameras were synchronized and the video analog inputs were sent to a video processor computer to be converted to digital image data, then forwarded to a tracking computer via an Ethernet connection. The tracking computer combined the digital input from the six cameras to calculate the location of markers in space relative to the camera locations. At any point in time, each marker had to be seen by at least two cameras in order to identify the marker location. After all the marker locations had been identified, the computer generated a picture of the markers linked according to a predetermined marker template. These pictures were generated in real time as the horse moved across the field of view.

Figure 2-3 Motion analysis video system.

Video system with 6 cameras (1-6) arranged on the far side of the runway. The computer system is located behind camera 5. The runway is in the foreground.

The calibration system Calibration consisted of two steps: identification of the camera locations in space and calibration of the data collection volume. To identify the camera locations, a rigid L-shaped frame with 4 spherical, retro-reflective markers attached at predefined locations was placed in the middle of data collection field. This frame was also used to identify the origin and orientation of the global coordinate system by aligning its two arms with the longitudinal and transverse axes of the force plate (Figure 2-4). All six cameras captured the markers on the L-shaped frame and sent the input to the computer units. Based on the known locations of the markers, the computer inversely calculated the location of each camera, and after this procedure, the cameras were stationary until data collection had been completed.

Figure 2-4 Position of a rigid L-shaped frame in the data collection field.

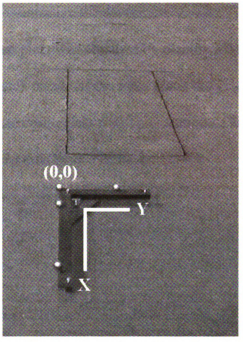

The global coordinate system was identified for the horizontal longitudinal (X) and horizontal transverse (Y) axes. The vertical axis (Z) was perpendicular to the X and Y axes (not shown in this picture). The force plate can be seen above the L-shaped frame. The marker on the left corner of the frame (0,0) was used to identify the origin of the global coordinate system in the X and Y axes. The origin in the Z axis was at ground level directly beneath the (0,0) point.

Calibration of the data collection volume was performed to refine the calculated locations of the cameras and to reduce the effects of lens distortion. It involved the use of a 1000 mm wand calibration stick with three 3.8 cm spherical retro-reflective control markers. All cameras captured the wand moving throughout the data collection volume in directions parallel to each of the three axes (X, Y and Z). The calibrated volume measured approximately $5 \times 2 \times 3$ meters (Figure 2-5). The computer units combined the information from the six cameras. Based on the fact that the wand length was constant at

1000 mm, computer algorithms adjusted each camera view along the three axes using least square residual error to optimize the six camera views.

Location of the force plate was obtained by placing a 2.54 cm diameter, spherical retro-reflective marker at each corner of the force plate, then capturing these markers on all cameras as the force plate corner data file. The location of the force plate within the data collection volume could then be determined.

Figure 2-5 Data collection volume after calibration.

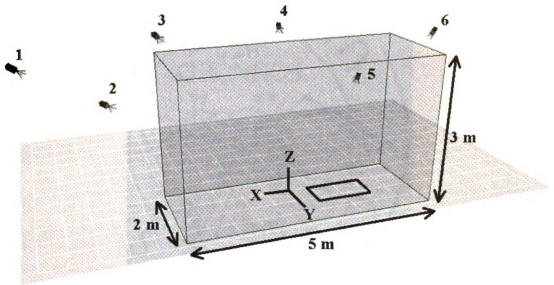

The position of the six cameras (1-6), the orientation and origin of the global coordinate system (X,Y,Z axes) and the location of the force plate on the runway (rectangle) were identified.

Skin marker setup The whole body skin marker setup was used to obtain two-dimensional kinematic data for the forelimb and hind limb, and three-dimensional kinematic data for the tarsal joint.

Figure 2-6 Position of retro-reflective markers on the cranial part of the body.

On the cranial part of the body (Figure 2-6), 2.54 cm spherical, retro-reflective markers were attached to the skin over the following anatomical landmarks: 1. wing of first cervical vertebra; 2. base of the neck; 3. tuberosity of scapular spine; 4. caudal part of greater tubercle of humerus (representing center of rotation of scapulohumeral joint); 5. attachment of lateral collateral ligament of cubital joint on distal humerus (representing center of rotation of cubital joint); 6. distal edge of ulnar carpal bone midway between the

lateral styloid process of radius and proximal third metacarpus (representing center of rotation of carpal joint); 7. distal end of third metacarpus at attachment of the lateral collateral ligament of metacarpophalangeal joint (representing the center of rotation of metacarpophalangeal joint); 8. lateral hoof wall distal to the coronary band; 9. hoof wall at toe and 10. hoof wall at heel.

Figure 2-7 Position of retro-reflective markers on the caudal part of the body.

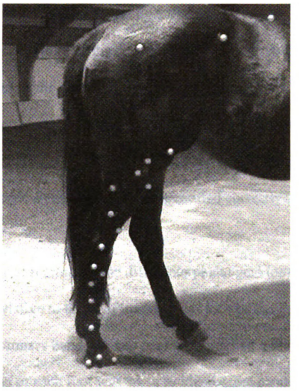

On the caudal part of the body (Figure 2-7), 2.54 cm spherical, retro-reflective markers were attached on the skin over 11. dorsal midline of the trunk; 12. ventral part of the tuber coxae; 13. caudodorsal projection of the greater trochanter; 14. cranial part of distal femur; 15. femoral condyle at the attachment of the lateral collateral ligament of femorotibial joint (representing center of rotation of femorotibial joint); 16. proximal tibia at the attachment of lateral collateral ligament of femorotibial joint; 17. lateral

malleolus of distal tibia; 18. dorsal edge of the head of fourth metatarsus; 19. distal end of third metatarsus at the attachment of the lateral collateral ligament of metatarsophalangeal joint (representing center of rotation of metatarsophalangeal joint); 20. lateral hoof wall distal to the coronary band; 21. hoof wall at toe; and 22. hoof wall at heel. In order to track the three-dimensional motion of tibia and metatarsal segments, additional markers were attached on those two segments: 23. distal edge of tibial tuberosity; 24. midpoint of a line connecting 16 and 17; 25. caudal aspect of the tibia approximately two-third of the distance along a line from 16 to 24; 26. cranial aspect of the tibia approximately one-third of the distance along a line from 24 to 17; 27. approximately one-third of the distance along a line from 18 to 19; 28. approximately two-third of the distance along a line from 18 to 19; 29. dorsal edge of third metatarsus between 18 and 27; and 30. dorsal edge of third metatarsus between 28 and 19. All skin markers could be captured simultaneously and identified correctly by the computer units (Figure 2-8).

Since the center of rotation of the distal interphalangeal joint cannot be directly palpated, its position relative to the hoof markers was located radiographically. The three hoof markers on the coronary band, toe and heel were marked with metal beads. A lateromedial radiograph of each foot was taken to identify the position of the center of rotation of the distal interphalangeal joint relative to the position of the three hoof markers. During post-processing of the data, the positions of the hoof markers were used to determine the distal interphalangeal joint location, as described later.

Figure 2-8 Stick figure of whole body marker setup displayed by the computer monitor.

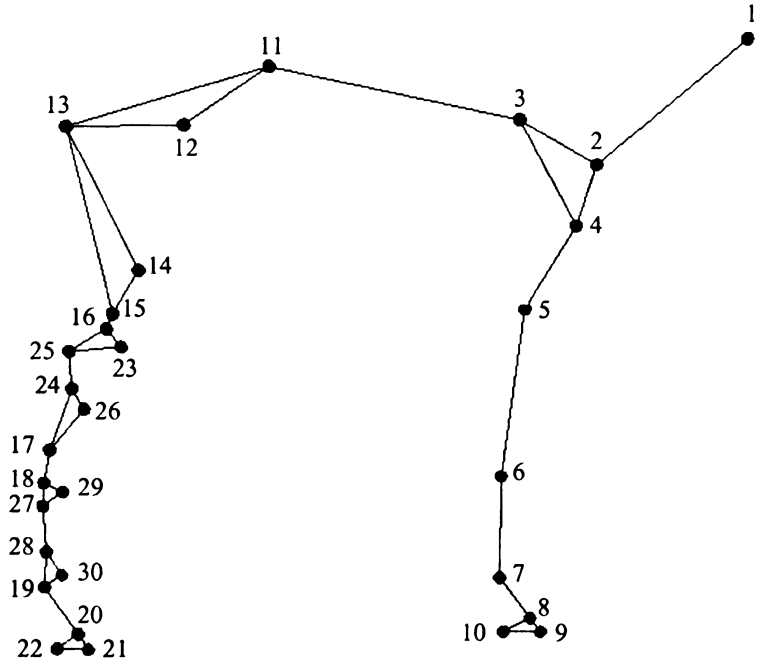

Force plate data. A 60 cm × 120 cm force plate (AMTI LG6, AMTI, Watertown, MA) embedded in the middle of the runway, was used to collect GRF data with a sampling frequency of 1,200 Hz. The force plate reading was adjusted to zero in all three directions before each data collection session. When a horse stepped on the plate, forces in the vertical, horizontal longitudinal and horizontal transverse directions, and the location of the center of pressure were recorded to the same computer units as the video system. The kinematic axes were aligned with the force plate axes using the force plate corner data file. The conventional axes for force plate in this study were defined as vertical (Z), horizontal longitudinal (X) and horizontal transverse (Y) axes. Force data

were synchronized temporally and spatially with the kinematic data within the computer units.

Data collection procedures.

Normalization for horse size Horse height affects stride length, with shorter horses using higher stride frequencies than taller horses at the same velocity, which requires more energy expenditure over the same distance. Comparisons between horses of different sizes are facilitated by scaling the data so that each animal moves at the same velocity relative to its body size. Scaling in human locomotion uses Froude numbers to adjust the velocity of progression using a characteristic length, such as leg length. When people walk with equal Froude numbers, they have dynamic similarity (Zatsiorky, et al., 1994). Scaling can also be used to obtain dynamic similarity in horses. Height at the withers, which is proportional to the segment lengths of the forelimbs and hind limbs (Holmstrom, 1990), is applied in gait analysis to scale the gait variables.

The important GRFs are those used to accelerate/decelerate the body mass and those used to oppose gravitational forces. In order to achieve dynamic similarity, the proportion of acceleration and gravitational forces should be similar for animals of different sizes (Hof, 2001).

$$\frac{m_1 a_1}{m_1 g} = \frac{m_2 a_2}{m_2 g}$$

where m_1 is mass of subject 1, a_1 is the acceleration of subject 1, m_2 is mass of subject 2, and a_2 is the acceleration of subject 2.

From this equation, the scaling for absolute acceleration of any horse should be adjusted for gravitational acceleration ($g = 9.81\ m/s^2$). When analyzing other variables

that relate to change in height at the withers (distance in the direction of gravitational acceleration), they should be scaled to achieve dynamic similarity as well. The equations used to scale time and velocity are as follow :

$$\text{acceleration} = \frac{\text{distance}}{\text{time}^2} \qquad \text{then} \qquad \text{time} = \sqrt{\frac{\text{distance}}{\text{acceleration}}} = \sqrt{\frac{l_0}{g}}$$

$$\text{velocity} = \frac{\text{distance}}{\text{time}} = \frac{\text{distance}}{\sqrt{\frac{\text{distance}}{\text{acceleration}}}} = \sqrt{\text{distance} \times \text{acceleration}} = \sqrt{l_0 \times g}$$

When l_0 is height at the withers in meters, the term used to describe the adjusted variables is *"Dimensionless units"* because the numerator and denominator have the same units. In this study, normalization for velocity was used to select trials for analysis from each horse. The dimensionless units for subject velocity (VDU) were calculated using the following equation :

$$\text{velocity} = \frac{\text{measured velocity (m/s)}}{\sqrt{l_0 \times g}}$$

A previous study (Clayton, et al., 2000b) reported the mean preferred trotting velocity for normal horses was 0.83 VDU and moderate lameness reduced the preferred trotting velocity by approximately 10%. The velocity in dimensionless units in this study was selected in the range of 0.73-0.77 VDU, which was considered to be a reasonable range for achieving comparable velocities before and after synovitis induction.

Data collection The first session for data collection was used to obtain data describing the horse in the sound condition. Video cameras were set to record at a rate of 120 frames per second, with a shutter speed of 1/1000 and f-stop setting around 4. Recordings of the force plate corner data, the rigid L-shaped frame and the wand calibration were used to identify camera locations, force plate location, and global

coordinate system, respectively, and to calibrate the data collection volume. The whole body marker setup was attached to the first side of the horse's body. Two additional 2.54 cm spherical, retro-reflective markers (reference markers) were attached on the medial malleolus of the tibia and the dorsal edge of the head of the second metatarsus. The horse was positioned obliquely to the longitudinal axis of the data collection volume in such a way that all the markers could be seen by at least two cameras. A video recording, named the reference pose, was captured, then the two reference markers were removed.

The handler led the horse at the trot through the data collection volume. A good hit was one in which the horse placed its first side forelimb and/or hind limb on the force plate without any other limb being on the force plate at the same time. Custom software was used to calculate velocity and velocity in dimensionless units (VDU) of the marker overlying the tuberosity of the scapular spine and used as the approximate forward velocity for each trial. The information was instantly available after completion of the trial. Successful trials were selected on the basis of a good hit on the force plate by the first side forelimb and/or hind limb, combined with velocity in the range of 0.73-0.77 VDU. The data collection was continued until 5 successful trials had been obtained from both the forelimb and hind limb. After the data collection on the first side of the horse was completed, the skin around each marker was stained by waterproof ink then the markers were removed. A whole body marker setup was then attached on the second side of the horse's body. Data collection procedures were repeated including attachment of medial reference markers, recording of the reference pose, capture of 5 successful trials from both the forelimb and hind limb, and skin marking with waterproof ink around each marker before removal.

After induction of synovitis, when the horse was assessed as having a grade 2 lameness or less, data were recorded for the lame condition on both left and right sides as described previously. Marker placement could be reproduced from the sound condition by placing markers at the positions indicated by waterproof ink. Data collection procedures were performed including whole body marker set attachment on the first side, attachment of the medial reference markers and recording of the reference pose. After 5 successful trials from the first side forelimb and hind limb had been captured, the markers were removed and a whole body marker setup attached in the positions marked by waterproof ink on the second side of the horse. The data collection procedures were repeated until 5 successful trials from the second side forelimb and hind limb had been obtained.

DATA PROCESSING AND ANALYSIS

Two-dimensional variables. Data from the tracking computer units were transferred to a processing computer to be manipulated before analysis. Kinematic information from successful trials was analyzed on a stride-by-stride basis. For the right side data, a stride started and ended at the instant of ground contact, so the complete stride consisted of a stance phase followed by a swing phase. For the left side data, the stride started and ended at lift off, so each stride consisted of a swing phase followed by a stance phase. This difference between the two sides was necessary because the calibrated volume extended to one side of the force plate. Custom software (MAC Project Organizer, Mary Anne McPhail Equine Performance Center, East Lansing, MI) was used to organize kinematic and force information for each trial in preparation for further

processing. Matlab software (Version 6.1, The Math Works, Inc., Natick, MA) was used for the mathematical calculations. A fourth order Butterworth digital filter was used to filter the raw kinematic data with a cut off frequency of 10 Hz, and to filter the raw force plate data with a cut off frequency of 40 Hz. Skin displacement correction for the trot (van Weeren, 1989) was applied to the kinematic data obtained from markers at the greater tubercle of humerus, proximal radius, distal edge of ulnar carpal bone, caudodorsal projection of the greater trochanter, femoral condyle, proximal tibia, the head of the fourth metatarsus and distal end of the third metatarsus before any further kinematic data analysis.

Kinematic variables Temporal variables were obtained from the time recording of the limb events. Stride duration was determined from the number of frames elapsing between successive ground contacts of each right hoof for the right side data or successive lift offs of each left hoof for the left side data. The force plate is very accurate for identifying the time the hoof was on the ground (Schamhardt and Merkens, 1994) so it was used to detect the ground contact and lift off frames for each limb. The limb patterns from the ground contact and lift off frame were calculated from all markers on the limb and be used as the patterns to identify the successive ground contact frame for the right limbs and former lift off frame for the left limbs. Stance and swing durations were determined from the number of frames elapsing while the limb was on the ground and off the ground, respectively.

Angular displacement, velocity and acceleration were obtained for each joint during the complete stride. The retro-reflective markers over the anatomical landmarks on the fore and hind limbs were used to construct stick figures with the lines representing

segments of the limbs, and the joint angles being formed where the segment lines intersected. The lateral radiograph of the hoof was used to identify the location of the center of rotation of the distal interphalangeal joint relative to the position of the three hoof markers. The center of rotation of the distal interphalangeal joint was determined on the radiograph using a standard method to identify the center of circular object (Figure 2-9). Two straight lines were drawn across the distal articular surface of the second phalanx then a perpendicular was drawn from the middle of each line toward the center of the bone. The intersection of these perpendicular lines was the center of joint rotation.

Figure 2-9 Diagram showing the method used to identify the center of a circular object.

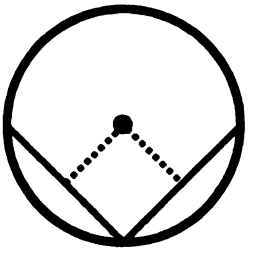

Custom software (Radcof, Mary Anne McPhail Equine Performance Center, East Lansing, MI) was used to identify the center of rotation of the distal interphalangeal joint from the lateromedial radiograph of the hoof (Figure 2-10). The spatial relationship between the hoof markers and the joint center of rotation was then determined. The standard procedure was to use the markers at the coronary band and toe, but other markers combinations could be used if these ones had not been tracked well by the video system. The hoof coordinate system was established using the chosen markers and the reference length was measured between them. The hoof segment was aligned parallel

with the dorsal edge of the third phalanx from the center of the distal interphalangeal joint to the distal hoof wall. Standard two-dimensional transformation (Winter, 1990) was used to locate the distal interphalangeal joint, distal hoof wall and hoof angle with the respect to the hoof coordinate system and reference length. During kinematic analysis, the hoof coordinate system was re-established in each frame, the locations of the distal interphalangeal joint and distal hoof wall were determined in the hoof coordinate system, then the standard two-dimensional transformation and reference length were used to define those locations in the kinematic global coordinate system. This procedure was performed for every frame during the stride.

Figure 2-10 Lateral radiograph of the hoof and hoof coordinate system.

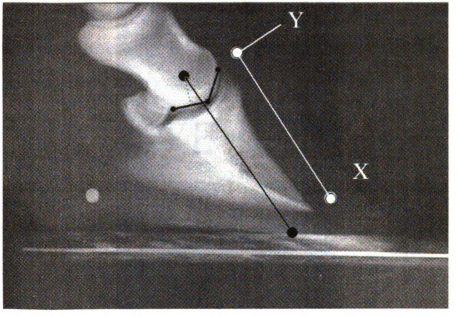

Custom software was used to calculate the location of distal interphalangeal joint center of rotation using two straight lines drawn across the distal arctic surface of the second phalanx (short, dark lines). The joint center of rotation was located at the intersection of lines (dashed lines) drawn perpendicular to their midpoints. Alignment of hoof segment (long black line) relative to the hoof coordinate system (white lines) was determined from retro-reflective markers at the coronary band and toe.

A similar transformation was used to locate the center of rotation of the tarsocrural joint on a lateromedial radiograph. The standard method for identifying the center of a circular object, in this case the tibial tarsal bone, was applied and the tarsal coordinate system was established (Figure 2-11). The reference length was 10 cm long and was drawn distally from the markers on the fourth metatarsal bone, parallel to the long axis of the third metatarsal bone. Standard two-dimensional transformation was used to locate the tarsocrural joint center of rotation in the tarsal coordinate system using the reference length, and was transposed to the kinematic global coordinate system. This procedure was repeated for every frame during the stride.

Figure 2-11 Lateral radiograph of the tarsus and tarsal coordinate system.

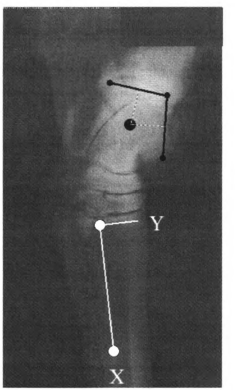

Custom software was used to calculate the location of the tarsocrural joint center of rotation relative to the tarsal coordinate system (white lines) constructed from the retro-reflective marker at the dorsal edge of the head of the fourth metatarsal bone and a reference line parallel to the long axis of the third metatarsal bone.

The coxofemoral joint center of rotation lies medial to the cranial part of the greater trochanter. Its position was calculated from the locations of the skin markers on the femur. The skin marker correction algorithm was applied, then the position of this marker was transformed in the X-Y plane. The reference length for the femoral segment was the distance between the markers on the caudal part of greater trochanter and the femoral condyle. It was used to establish the hip coordinate system (Figure 2-12). Anatomical measurements on the equine femurs showed that the center of the femoral head was cranial and distal to the caudal part of greater trochanter by 7.8% and 17.8%, respectively, of the reference length. Standard two-dimensional transformation was performed to locate the coxofemoral center of rotation in the hip coordinate system. The hip coordinate system was re-established from kinematic data using skin markers on the caudal greater trochanter and femoral condyle. Two-dimensional transformation was performed to define the location of the coxofemoral joint in the global coordinate system.

Figure 2-12 Lateral side of equine femur and hip coordinate system.

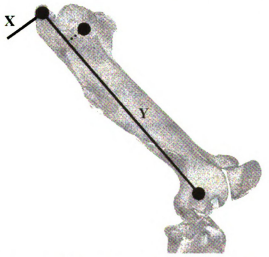

The hip coordinate system established from markers at the caudal part of greater trochanter and femoral condyle. The position of the coxofemoral joint center of rotation relative to these markers was calculated by two-dimensional transformation.

The angle of each joint was measured on its anatomical flexor side. Thus, the angles of the scapulohumeral, carpal, femorotibial, metacarpophalangeal, metatarsophalangeal and distal interphalangeal joints were measured on the caudal or palmar/plantar side of the limb and the angles of the cubital, coxofemoral and tarsal joints were measured on the cranial or dorsal side of the limb. During locomotion, the angle between adjacent segments was measured; flexion was defined as a decrease in the angle and extension occurred when the angle increased. The peak magnitudes of joint flexion and extension and their times of occurrence were obtained. Each trial was standardized to stance or swing duration, and the time of occurrence of each peak was expressed as percent of stance or swing duration. The range of joint motion was the difference between maximal and minimal values of joint angle during stance or swing phases of each trial. The kinematic variables from the sound and lame conditions were obtained for comparison.

Linear variables were calculated from changes in location of digitized markers on anatomical landmarks of interest within the calibrated volume. Stride length was the forward longitudinal displacement of each limb between successive ground contacts or lift offs. Vertical displacements of the tuber coxae, coxofemoral joint, femorotibial joint, tarsal joint, metatarsophalangeal joint, distal interphalangeal joint and distal hoof wall were measured during the stance or swing phases as the differences between the lowest and the highest position of each landmark. After the temporal and linear variables were obtained, the exact velocity in m/s of the limb in each trial was calculated by stride length divided by stride duration. The velocity in dimensionless units then was calculated as described previously.

Force plate variables GRF data from each trial were analyzed to determine the peak magnitudes of the vertical force peak, negative longitudinal or braking force and positive longitudinal or propulsive force and their times of occurrence expressed as percent of stance duration. Impulses were calculated by time integration of the force curves and expressed as vertical impulse, braking impulse and propulsive impulse. Force peaks and impulses were normalized to horse mass and expressed as N/kg and Ns/kg, respectively.

Net joint moment, net joint power and net joint energy The kinematic and GRF data were synchronized in the time domain and combined with inertial parameters of the limb segments (Buchner, et al., 1997). An inverse dynamic analysis (Winter, 1990) was used to calculate the sagittal plane net joint moments for the distal interphalangeal, metacarpophalangeal, metatarsophalangeal, carpal, tarsal, cubital, femorotibial, scapulohumeral and coxofemoral joints. Moments on the anatomical flexor side were assigned a negative value and those on the extensor side were assigned a positive value. Net joint power was calculated as the product of net joint moment and joint angular velocity. The value was positive when the net joint moment and joint angular velocity had the same polarity (concentric muscular action) and negative when they had opposite polarities (eccentric muscular action). The net joint moment and net joint power were normalized to stance or swing duration and to horse mass, and was expressed as moment and power per kg body weight (Nm/kg and W/kg). Maximal moment and power values were determined from the obvious and consistent peaks in the net joint moment and net joint power curve. Bursts of energy absorption and generation were calculated by time integration of the negative and positive parts, respectively, of the net joint power curves.

The area under a positive power curve was net joint energy generation and the area under a negative power curve was net joint energy absorption. The net joint energy variables were measured as Joule/kg (J/kg) body weight. The net joint moment peaks, net joint power peaks, net joint energy absorption and generation, and time of occurrence of each peak expressed in percent of stance or swing duration from sound and lame conditions were obtained for comparison.

Three-dimensional kinematic variables for the tarsal joint. One method of expressing three-dimensional (3D) joint kinematics is to describe the relative movement between two segmental coordinate systems. In this study, segmental coordinate systems were constructed for the tibial and metatarsal segments. Because skin displacement of the marker locations relative to the underlying bones is an important source of errors in kinematic analysis, the true bone motion was identified using reference bone data (Lanovaz, et al., 2002) from a same group of horses. Skin marker correction algorithms (Appendix A) were obtained from the reference bone data using the same marker locations for the tibia and metatarsal segments. The tibial segmental coordinate system (Figure 2-13) was constructed from the markers over the proximal tibia at the attachment of the lateral collateral ligament of the femorotibial joint, the lateral malleolus and the medial malleolus. The first axis to be defined was the flexion/extension axis (Y), which was a vector running from lateral malleolus to medial malleolus. The second axis was the abduction/adduction axis (X), which was calculated as a vector perpendicular to both the Y axis and a line from the lateral malleolus to the proximal tibia. This axis was positive in a caudal to cranial direction. The third axis was the internal/external rotation axis (Z),

which was calculated as a vector perpendicular to both X and Y axes, and positive in a distal to proximal direction. The origin of the tibial segmental coordinate system was embedded in the bone midway between lateral and medial malleoli. The metatarsal segmental coordinate system (Figure 3-13) was constructed using markers over the dorsal edge of the heads of the fourth and second metatarsals, and the distal condyle of the third metatarsus on its lateral side. The procedures used to obtain X, Y and Z axes of the metatarsal segmental coordinate system were similar to those for the tibial segmental coordinate system. The flexion/extension (Y) axis was a vector from the fourth to the second metatarsus, which was positive in the medial direction. The abduction/adduction (X) axis was perpendicular to the Y axis and a line from the head of the fourth metatarsus to the distal third metatarsal condyle. The Y axis was positive in the dorsal direction. The internal/external rotation (Z) axis was mutually perpendicular to both X and Y axes, and was positive in a proximal direction. The origin of the metatarsal coordinate system was embedded in the bone midway between the dorsal edge of the heads of the fourth and second metatarsals (Figure 2-13).

Figure 2-13 Segmental coordinate system of tibial and metatarsal segments.

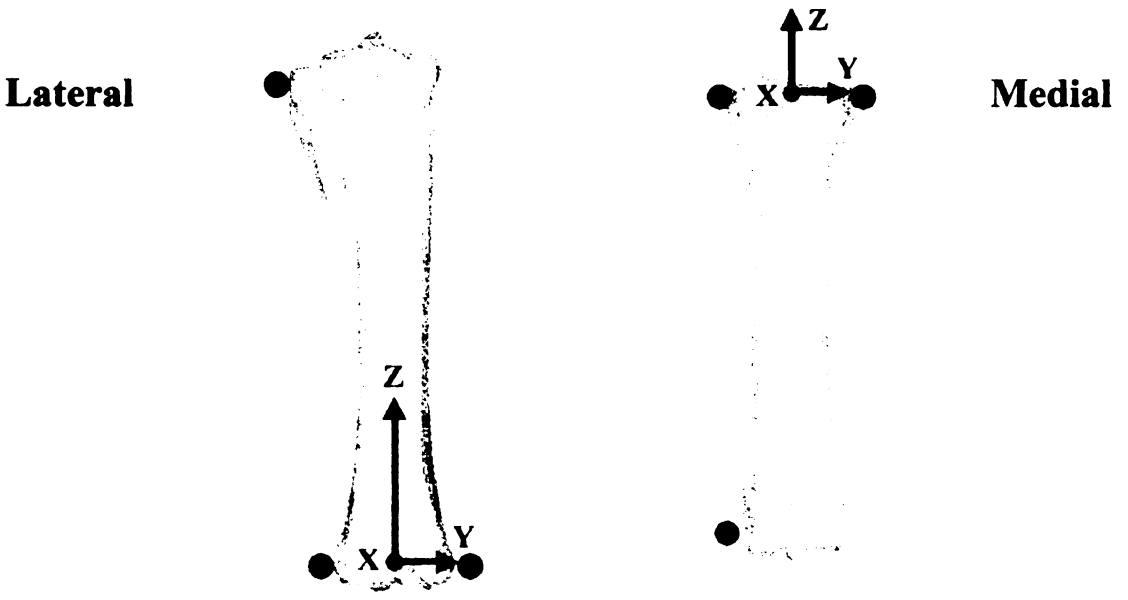

Position of retro-reflective markers (black circles) relative to tibia (left) and third metatarsus (right). Segmental coordinate systems were located at the middle of the distal tibia and at the middle of the proximal third metatarsus. The flexion/extension axis (Y) had a lateral to medial direction. The abduction/adduction axis (X) had a caudal/plantar to cranial/dorsal direction. The internal/external rotation axis (Z) had a distal to proximal direction.

The reference pose was used to relate the location of the skin markers overlying each segment to its segmental coordinate system. A 3D transformation matrix (Winter, 1990) was used to transform the locations of these skin markers from the global coordinate system to their corresponding segmental coordinate system. During the trotting trials, skin markers were tracked and expressed in terms of the global coordinate system. A singular-value decomposition method (Soderkvist and Wedin, 1993) was used to calculate the position and orientation of each segmental coordinate system for every frame during the stride based on the skin markers of each segment.

Complete 3D kinematic analysis of the tarsal joint complex involved the measurement of relative angular and translational motions between the tibial and metatarsal segmental coordinate systems. The relative angular motion between these two coordinate systems was expressed in terms of a spatial attitude vector (Woltring, 1994). This method is based on the finite helical axis representation of relative motion, in which the position and orientation of one body relative to the other can be described as a scalar rotation and translation between two segments (Woltring, et al., 1985). The attitude vector is calculated by multiply the scalar finite helical angle with the component of the unit vector describing the helical axis. The results are three orthogonal angular values that are expressed in term of the coordinate axes of one of the bodies. The magnitude of relative motion of the first segment relative to the second segment was the same as that of the second segment to the first segment, but in the opposite direction.

There were three relative angular motions between the two segments; flexion/extension, abduction/adduction and internal/external rotation. In this study, angular motion was measured as movement of the metatarsus relative to the fixed tibia (Figure 2-14). Flexion/extension was motion around the Y axis; negative values were assigned for flexion, and positive values were assigned for extension. Abduction/adduction was motion around the X axis; negative values were assigned for abduction, and positive values were assigned for adduction. Internal/external rotation was motion around the Z axis; negative values were assigned for external rotation, and positive values were assigned for internal rotation.

Figure 2-14 Three-dimensional angular motion of the metatarsal segment relative to the tibial segment; flexion(-)/extension(+) (left), abduction(-)/adduction(+) (middle) and internal(+)/external(-) rotation (right). Figure illustrates the right hind limb.

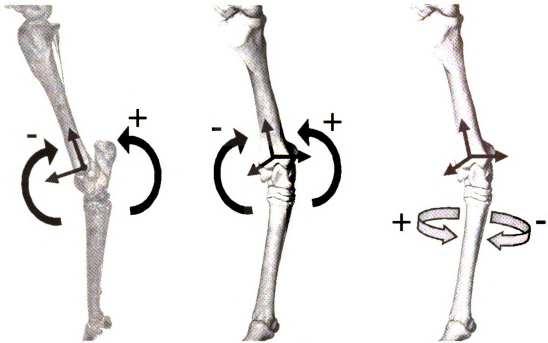

Medial view **Dorsomedial view** **Dorsomedial view**

Translation was measured in three directions; cranial/caudal, medial/lateral and proximal/distal translations. The relative translation was expressed as the metatarsal translation relative to the fixed tibia (Figure 2-15). Cranial/caudal translation was motion along the X axis; negative values were assigned for caudal translation, and positive values were assigned for cranial translation. Medial/lateral translation was motion along the Y axis; negative values were assigned for lateral translation, and positive values were assigned for medial translation. Proximal/distal translation was motion along the Z axis; negative values were assigned for distal translation, and positive values were assigned for proximal translation.

Figure 2-15 Three-dimensional translational motion of the metatarsal segment relative to the tibial segment; cranial(+)/caudal(-) translation (left), medial(+)/lateral(-) translation (middle) and proximal(+)/distal(-) translation (right). Figure illustrates the right hind limb.

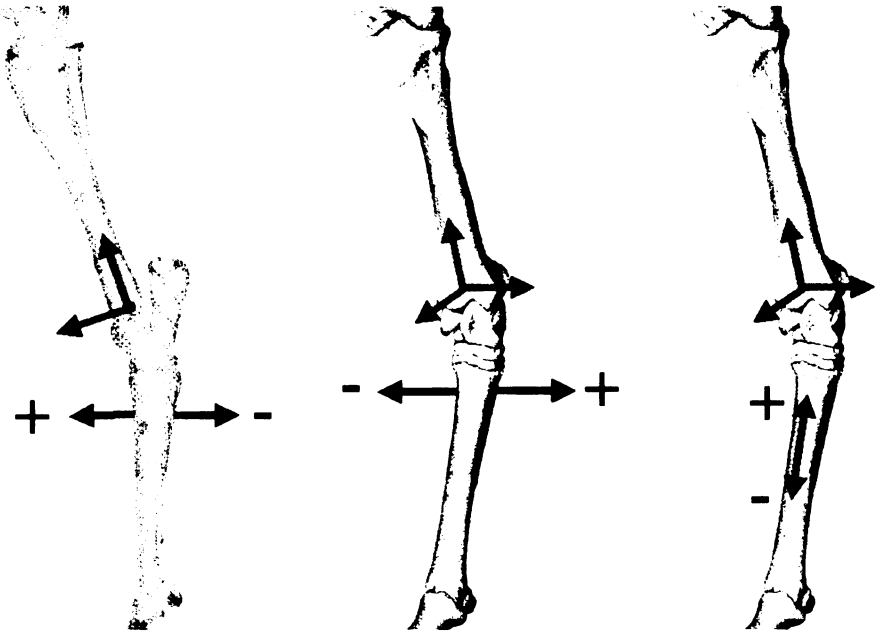

The ranges of 3D angular and translational motion were obtained from every trial during the stance or swing phases for comparison between the sound and lame conditions.

STATISTICAL ANALYSIS

Power analysis is most useful when planning a study to estimate the sample size for the experiment (Thomas, 1997). It was not possible to perform a power analysis during the design phase of this study because there are no comparable data that can be used to estimate power for most of the variables.

Statistical software (SPSS for Windows version 10.1, SPSS Inc., Chicago, IL) was used to analyze the data. Independent t-tests were used to test the difference in velocity between left and right limbs. For two-dimensional variables, kinematic, GRF, net joint moment, net joint power, and net joint energy variables were obtained from 5 trials of each limb. The values of each variable were combined to obtain the mean values that were regarded as being representative values for each limb. The descriptive analysis for the sound condition was performed using the representative values of each variable from left and right hind limbs of all horses to find the mean and standard deviation.

Independent t-tests were used to test whether there was any difference in velocity between sound and lame conditions of each limb. The representative variables of each limb from sound and lame conditions were compared using dependent t-test. Significant differences were obtained when the P value was less than 0.05. A trend toward a significant difference was reported when the P value was less than 0.1 but more than 0.05.

For 3D variables, flexion/extension, adduction/abduction and internal/external rotation, as well as cranial/caudal, medial/lateral and proximal/distal translation were obtained from 5 trials of the right limb of each horse to calculate the representative mean values of each limb. The 3D motion of the tarsal joint from the motion of the tibial and metatarsal bones was obtained (Lanovaz, et al., 2002) to illustrate the true reference kinematics of the bones. The root mean square (RMS) errors of tarsal joint 3D rotation and translation from each individual horse during the whole stance or swing duration were calculated between reference bone data and the kinematic data from both uncorrected and corrected skin markers. The variables that showed reasonable RMS

errors and shape agreement of the motion curves between the reference bone data and corrected skin markers would be analyzed for the ranges of motion during the stance and swing phase. The dependent t-test was used to compare the rotational and translational ranges of motion before and after the synovitis induction. Significant differences were obtained when the P value was less than 0.05.

CHAPTER 3

SAGITTAL PLANE KINEMATICS AND KINETICS OF THE HIND LIMBS IN SOUND TROTTING HORSES: RESULTS AND DISCUSSION

HORSE SELECTION

The lameness examination, radiographic and nuclear scintigraphic results of the four horses used in the study are reported in Table 3-1.

Table 3-1 Examination results from lameness evaluation, radiography and nuclear scintigraphy.

Horse no.	Lameness evaluation	Radiography	Nuclear scintigraphy
1	Grade 1 on the right hind limb before and after flexion test	Mild arthritic change in the right tarsometatarsal joint	Mild increase in radiophamaceutical uptake in the right tarsometatarsal joint
2	Grade 1 on the right hind limb before and after flexion test	Mild arthritic change in the right tarsometatarsal joint	Normal
3	Grade 0 before flexion test and grade 1 after flexion test on the right hind limb	Mild arthritic change on the left distal intertarsal joint	Normal
4	Grade 1 on the right hind limb before and after flexion test	Normal	Mild increase in radiopharmaceutical uptake in the left and right tarsometatarsal joints

TEST FOR DIFFERENCE IN VELOCITY AND SYMMETRY

Data from the left and right sides of the body were collected from different trials with the horses moving in opposite directions. Since most of gait variables vary with velocity, it is important to check for consistency of velocity before proceeding with further analyses. There were no significant differences ($P>0.05$) in limb velocity or velocity in dimensionless units between the left and right forelimbs or left and right hind limbs in the sound condition (Table 3-2). Having established equality of velocity for data collections on the left and right sides, the next step was to assess symmetry between the left and right limbs. Symmetry values calculated according to Merkens (Merkens, et al., 1993) for peak vertical force and vertical impulse were close to 100%, which is indicative of a symmetrical weight-bearing pattern (Table 3-3). The independent t-test of linear variables, indicate no significant differences ($P>0.05$) between left and right hind limbs. Hence the variables could be combined between left and right hind limbs for descriptive analysis of the gait variables.

Table 3-2 Statistical analysis results for testing differences of velocity (m/s) and velocity in dimensionless units between left and right limbs. Values are mean and (SD).

Horse no.	Velocity (m/s)		Velocity in dimensionless units		
	Right fore	Left fore	Right fore	Left fore	P value
1	2.91 (0.09)	2.77 (0.13)	0.77 (0.02)	0.74 (0.04)	0.09
2	2.91 (0.06)	2.85 (0.05)	0.76 (0.02)	0.74 (0.01)	0.82
3	2.83 (0.07)	2.88 (0.07)	0.74 (0.02)	0.75 (0.02)	0.28
4	2.82 (0.06)	2.83 (0.06)	0.75 (0.02)	0.75 (0.02)	0.87
Horse no.	**Velocity (m/s)**		**Velocity in dimensionless units**		
	Right hind	**Left hind**	**Right hind**	**Left hind**	**P value**
1	2.85 (0.09)	2.74 (0.06)	0.76 (0.02)	0.73 (0.02)	0.05
2	2.85 (0.07)	2.87 (0.07)	0.74 (0.02)	0.75 (0.02)	0.74
3	2.82 (0.11)	2.85 (0.08)	0.74 (0.03)	0.75 (0.02)	0.67
4	2.83 (0.04)	2.79 (0.04)	0.76 (0.01)	0.75 (0.01)	0.13

Table 3-3 Symmetry values in sound condition of vertical force peaks (N/kg) and vertical impulses (Ns/kg) between left and right limbs. Standard values represent left-right symmetry of vertical force peaks and vertical impulses expressed as mean and (SD) (Merkens, et al., 1993).

Horse no.	Vertical force peak		Vertical impulse		Standard values
	Forelimbs	Hind limbs	Forelimbs	Hind limbs	
1	94	97	93	98	97 (2)
2	100	99	95	97	97 (2)
3	99	97	96	99	97 (2)
4	98	100	95	98	97 (2)

GROUND REACTION FORCE VARIABLES

The three ground reaction force (GRF) components (vertical, longitudinal and transverse) from both hind limbs in the sound condition are illustrated in Figure 3-1. Vertical GRF was always positive. After a small impact spike, it gradually increased to reach its maximal value around 50% of the stance phase then gradually decreased. Longitudinal GRF had negative and positive phases. The initial negative (braking) impact spike (Min1) was followed by a period of oscillation with peaks Max1, Min2, Max2. After that, there was a more prolonged negative phase with the peak braking force (Min3) that acted to decelerate the horse's forward movement during the first half of stance. It was followed by a positive (propulsive) phase during the second half of stance, with peak Max3 as a peak propulsive force. The longitudinal positive impulse had higher values than longitudinal negative impulse, indicating the important role of the hind limb to propel the body forward. Transverse GRF was least consistent among the three force components. The transverse force was directed laterally during the impact period until around 30% stance, after which the value remained small and quite variable between horses through the end of the stance phase. The means, standard deviations, coefficients

of variation (% CV) of the force peaks and their time of occurrence (% stance duration), together with the corresponding impulses are reported in Table 3-4. Due to the high % CV of the transverse GRF, this variable was not used in the analysis comparing sound and lame conditions.

The center of vertical load distribution between the four limbs could be calculated to observe the pattern of load distribution in each horse. The craniocaudal distribution was obtained from the percent contribution to the load from the front side by dividing vertical impulse of the two forelimbs by total vertical impulse of the four limbs. The distribution between left to right sides was calculated by dividing total left limb vertical impulse by total vertical impulse of the four limbs. A value of 50% on the vertical axis indicates equal contributions to vertical load from the forelimbs and hind limbs, whereas a value of 50% on the horizontal axis indicates equal contributions from the left limbs and right limbs. Table 3-5 reports the vertical impulses in the four horses used in this study. Figure 3-2 illustrates the vertical impulse distribution plotted from the information in Table 3-5.

Figure 3-1 Vertical (above), longitudinal (middle) and transverse (below) components of the ground reaction forces from hind limbs of sound trotting horses. Thick solid line indicates mean values from both hind limb. Thin solid lines indicate one standard deviation above and below the mean.

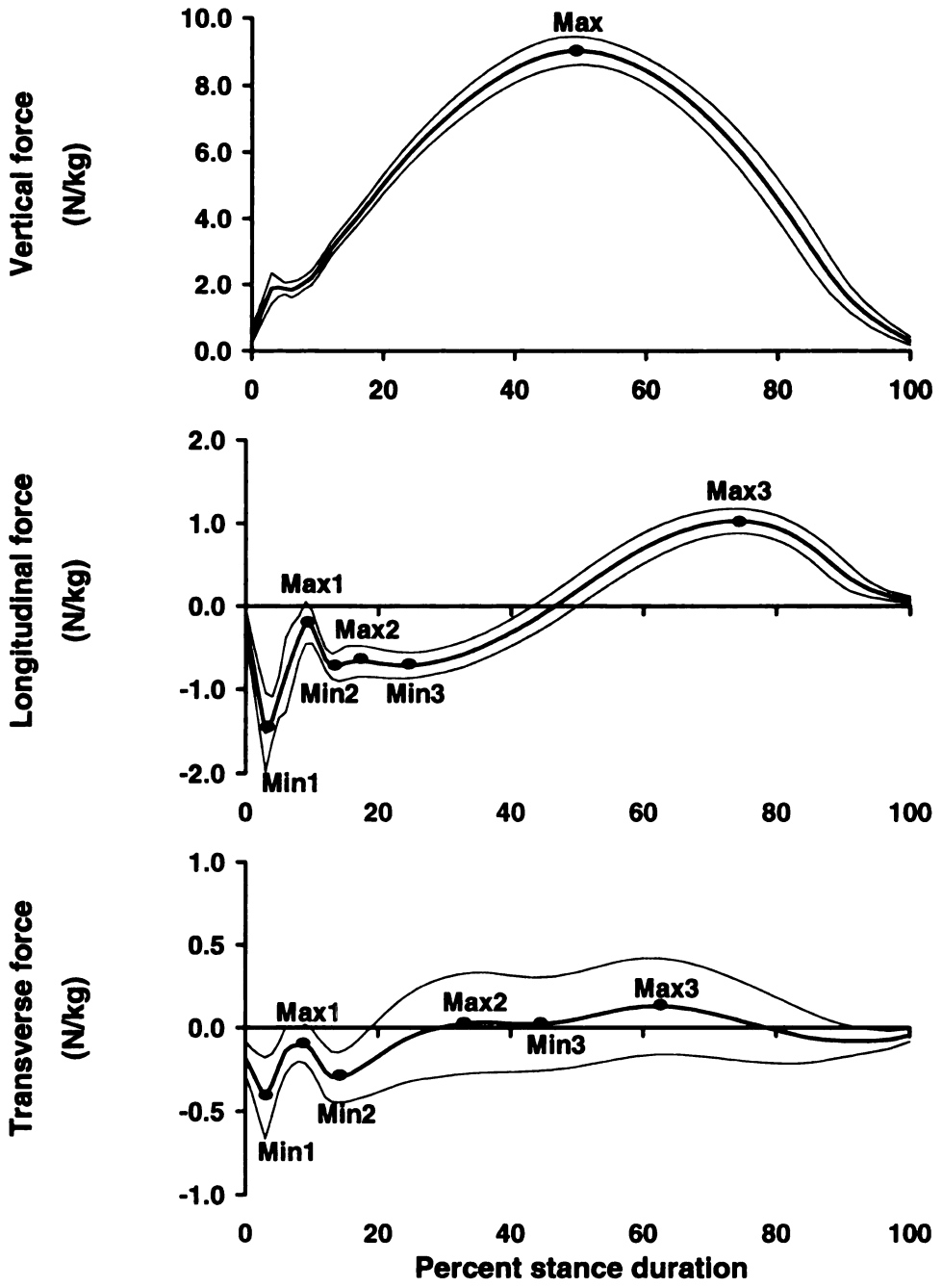

Table 3-4 Ground reaction force (GRF) variables, expressed as mean values for both hind limbs, in sound trotting horses. Values are mean and (SD).

Variables	Mean peak force or impulse	Coefficient of variation (%)	Time of occurrence (% Stance)
Vertical force Max (N/kg)	9.052 (0.402)	4	50.5 (1.6)
Vertical impulse (Ns/kg)	1.453 (0.077)	5	-
Longitudinal force Max1 (N/kg)	-0.134 (0.200)	149	10.0 (0.6)
Longitudinal force Max2 (N/kg)	-0.638 (0.126)	20	17.9 (1.3)
Longitudinal force Max3 (N/kg)	1.037 (0.114)	11	75.1 (1.7)
Longitudinal force Min1 (N/kg)	-1.621 (0.237)	15	4.6 (0.7)
Longitudinal force Min2 (N/kg)	-0.773 (0.108)	14	14.3 (0.9)
Longitudinal force Min3 (N/kg)	-0.717 (0.068)	9	26.4 (1.7)
Longitudinal negative impulse (Ns/kg)	-0.073 (0.008)	11	-
Longitudinal positive impulse (Ns/kg)	0.087 (0.016)	18	-
Transverse force Max1 (N/kg)	-0.040 (0.097)	243	8.9 (1.2)
Transverse force Max2 (N/kg)	0.039 (0.247)	633	32.8 (3.2)
Transverse force Max3 (N/kg)	0.156 (0.238)	153	63.7 (6.0)
Transverse force Min1 (N/kg)	-0.435 (0.212)	49	4.3 (0.5)
Transverse l force Min2 (N/kg)	-0.322 (0.135)	42	15.1 (1.4)
Transverse force Min3 (N/kg)	0.018 (0.271)	1506	46.5 (3.8)
Transverse negative impulse (Ns/kg)	-0.032 (0.032)	100	-
Transverse positive impulse (Ns/kg)	0.022 (0.021)	95	-

Table 3-5 Vertical impulse (Ns/kg) on all four limbs of each horse.

Horse	Left fore	Right fore	Left hind	Right hind	% contribution from the forelimbs	% contribution from the left limbs
1	1.90	1.76	1.32	1.34	57.91	50.89
2	1.97	1.88	1.50	1.47	56.44	50.97
3	1.97	2.05	1.50	1.51	57.22	49.39
4	1.99	1.90	1.48	1.50	56.66	50.47

Figure 3-2 Load distribution of vertical impulse of 4 sound horses. Each dot represents the value from one horse.

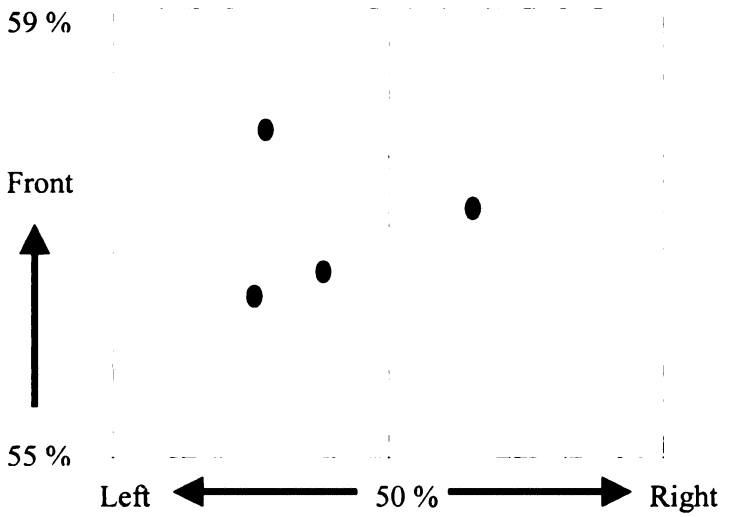

Figure 3-2 shows that all horses had more vertical load on forelimbs than the hind limbs. Three horses had a higher percentage contribution to vertical loading from the left limbs, and only one horse had a higher percentage contribution to vertical loading from the right limbs. This might be an indication of sidedness.

TWO-DIMENSIONAL BIOMECHANICAL PROFILES

Coxofemoral joint. Figures 3-3 and 3-4 illustrate the joint angle, net joint moment and net joint power profiles of coxofemoral joint during stance and swing phases, respectively. The joint gradually extended throughout stance, with the net joint moment on the extensor side of the joint through most of stance, changing to the flexor side during breakover. Two positive power peaks corresponded with bursts of energy generation on the extensor aspect of the coxofemoral joint from 10-40% stance and 45-80% stance. During the swing phase, the joint had a single cycle of flexion and extension, reaching its minimal angle around 60% swing. The net joint moment was on the flexor aspect until 30% swing, then the value remained low until moving to the extensor aspect around 75% swing. There were two peaks of positive net joint power corresponding with a burst of energy generation on the flexor aspect in early swing and a burst of energy generation on the extensor aspect in late swing.

Femorotibial joint. Figures 3-5 and 3-6 illustrate the joint angle, net joint moment and net joint power profiles of the femorotibial joint during stance and swing phases, respectively. During stance, the joint angle reveals fluctuating patterns of flexion and extension with 2 flexion peaks around 20% and 60% stance. After oscillations during impact, the net joint moments were on the flexor aspect of the joint, moving to the extensor aspect during breakover. During the impact period, the femorotibial joint had a large positive net joint power, indicative of energy generation and positive work performed on the flexor aspect of the joint. Between 20% to 60% of stance, the joint extended then flexed against a flexor moment, resulting in negative net joint power and

energy absorption followed by a similar magnitude of positive net joint power and energy generation. This profile is the typical pattern for elastic energy storage and release by tendons and ligaments. After 60% stance, little work was performed around the femorotibial joint.

In the first half of swing, the joint flexed against an extensor moment to reach the minimal flexion around 50% swing. In the second half of swing, the joint extended against a flexor moment. Consequently, net joint power was negative through most of the swing phase, with two distinct negative peaks around 10% and 80% swing. Therefore, flexion and extension of the femorotibial joint during the swing phase were controlled by eccentric activity in the extensor and flexor muscles, respectively.

Tarsal joint. Figures 3-7 and 3-8 illustrate the joint angle, net joint moment and net joint power profiles of the tarsal joint during stance and swing phases, respectively. The tarsal joint extended during the initial 5% stance, after which the joint flexed as the limb accepted the body weight and reached the first flexion peak (Min1) around 20% stance. The joint slightly extended then flexed to reach the second flexion peak (Min2) around 60% stance. The net joint moment had small magnitude oscillations during impact, then remained on the extensor aspect throughout stance. The net joint power profile appeared to show two cycles of elastic energy storage and release. The first cycle, which occupied the initial 30% stance, had a relative large burst of energy absorption followed by a smaller burst of energy generation. The second cycle immediately followed the first cycle. It had a longer duration with a larger burst of energy generation than the first cycle.

During the swing phase, the tarsal joint flexed then extended with a similar pattern to the femorotibial joint, reaching its minimal flexion angle around 50% swing. The net joint moment was on the flexor aspect during the first 50% of swing, then moved to the extensor aspect. The net joint moment and joint angle had the same polarity throughout swing: the joint flexed with a flexor moment in early swing and extended with an extensor moment in late swing. The corresponding positive net joint power peaks occurred around 25% (Max1) and 85% (Max2) swing. Positive work was performed across the tarsal joint to move the joint during the swing phase by two bursts of energy generation, first on the flexor aspect then on the extensor aspect of the joint.

Metatarsophalangeal joint. Figures 3-9 and 3-10 illustrate the joint angle, net joint moment and net joint power profiles of the metatarsophalangeal joint during stance and swing phases, respectively. The metatarsophalangeal joint extended then flexed during the stance phase, with maximal extension around 50% stance. The net joint moment was on the flexor aspect of the joint throughout the stance phase. Net joint power was negative as the joint extended against a flexor moment and positive as the joint flexed with the flexor moment. This resulted in a burst of energy absorption followed by a burst of energy generation, which were of similar magnitude. It was a classic profile of elastic energy storage and release by ligaments and tendons.

During the swing phase, the joint flexed to reach a peak (Min1) around 25% swing. The corresponding net joint moment was on the extensor aspect, resulting in negative net joint power and a burst of energy absorption. From 35% swing, the joint gradually extended against a small flexor moment. Soft tissues around the

metatarsophalangeal joint performed mainly negative work, with the largest burst of energy absorption on the extensor aspect, acting to control flexion in early swing.

Distal interphalangeal joint. Figures 3-11 and 3-12 illustrate the joint angle, net joint moment and net joint power profiles of the distal interphalangeal joint during stance and swing phases, respectively. During the stance phase, the joint flexed to accept body weight with the net moment on the flexor aspect, which resulted in positive net joint power and a small burst of energy generation during 0-40% stance. The joint reached its minimal flexion angle around 40% stance then extended against a flexor moment, which was associated with a large burst of energy absorption. During breakover, the joint reached maximal extension then flexed with the flexor moment, yielding a very small burst of positive work in terminal stance.

During the swing phase, the joint flexed then experienced fluctuating motion like the metatarsophalangeal joint. The net joint moment and net joint power profiles were also similar to those from the metatarsophalangeal joint, but the values were an order of magnitude smaller.

Figure 3-3 Joint angle, net joint moment and net joint power of coxofemoral joint during the stance phase. Thick solid line indicates mean values from both hind limbs of sound trotting horses. Thin solid lines indicate one standard deviation above and below the mean.

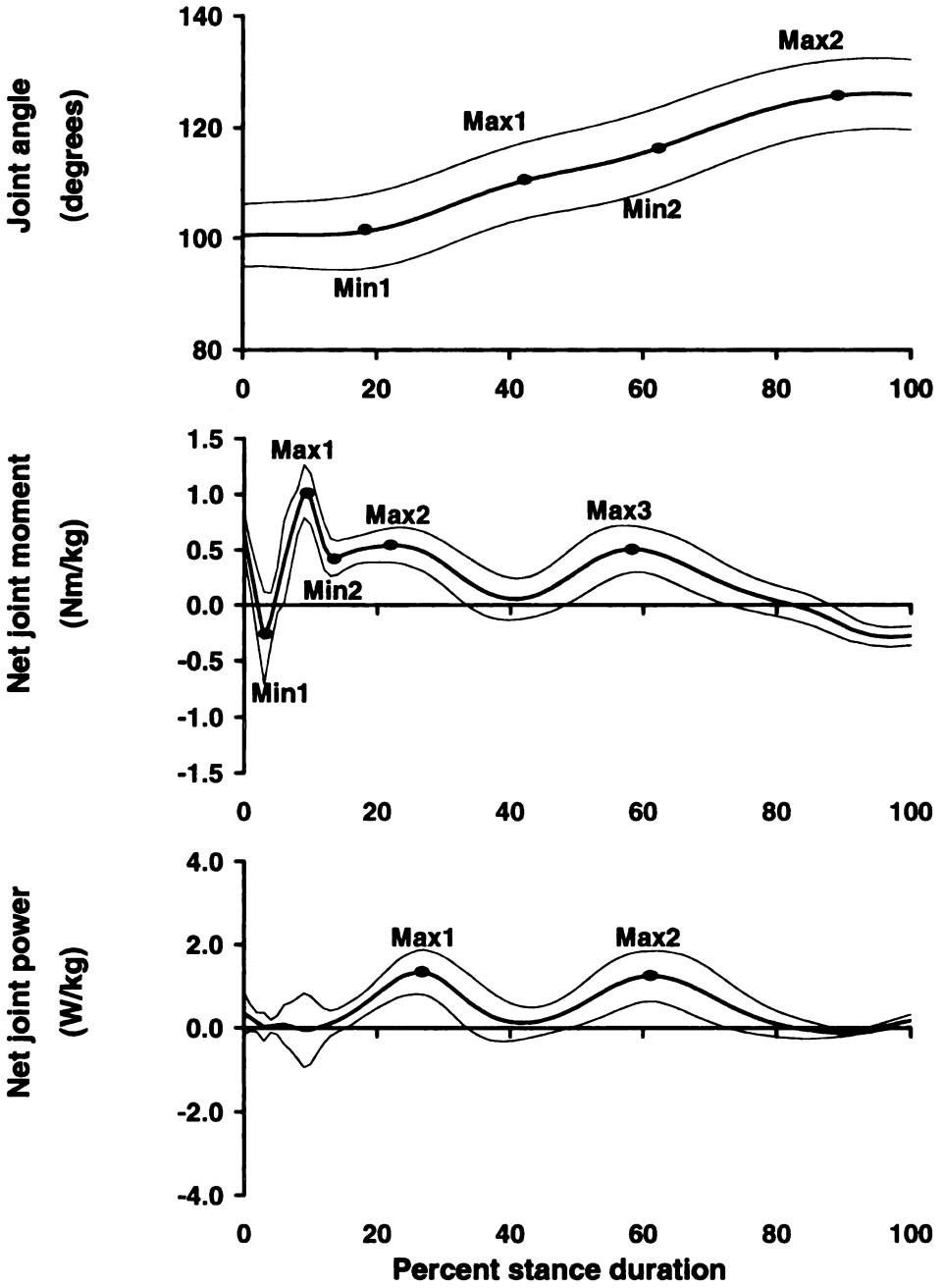

Figure 3-4 Joint angle, net joint moment and net joint power of coxofemoral joint during the swing phase. Thick solid line indicates mean values from both hind limbs of sound trotting horses. Thin solid lines indicate one standard deviation above and below the mean.

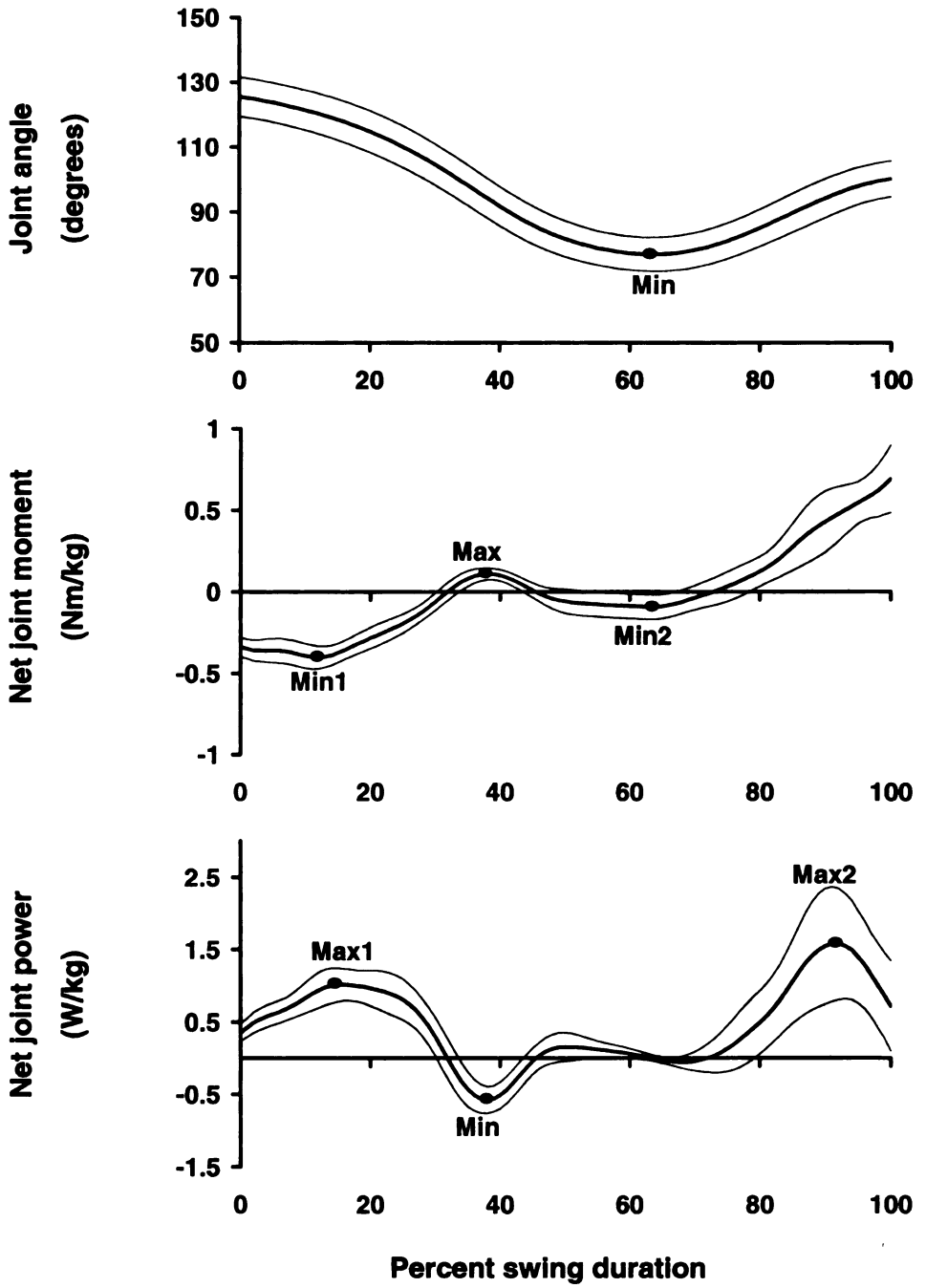

Figure 3-5 Joint angle, net joint moment and net joint power of femorotibial joint during the stance phase. Thick solid line indicates mean values from both hind limbs of sound trotting horses. Thin solid lines indicate one standard deviation above and below the mean.

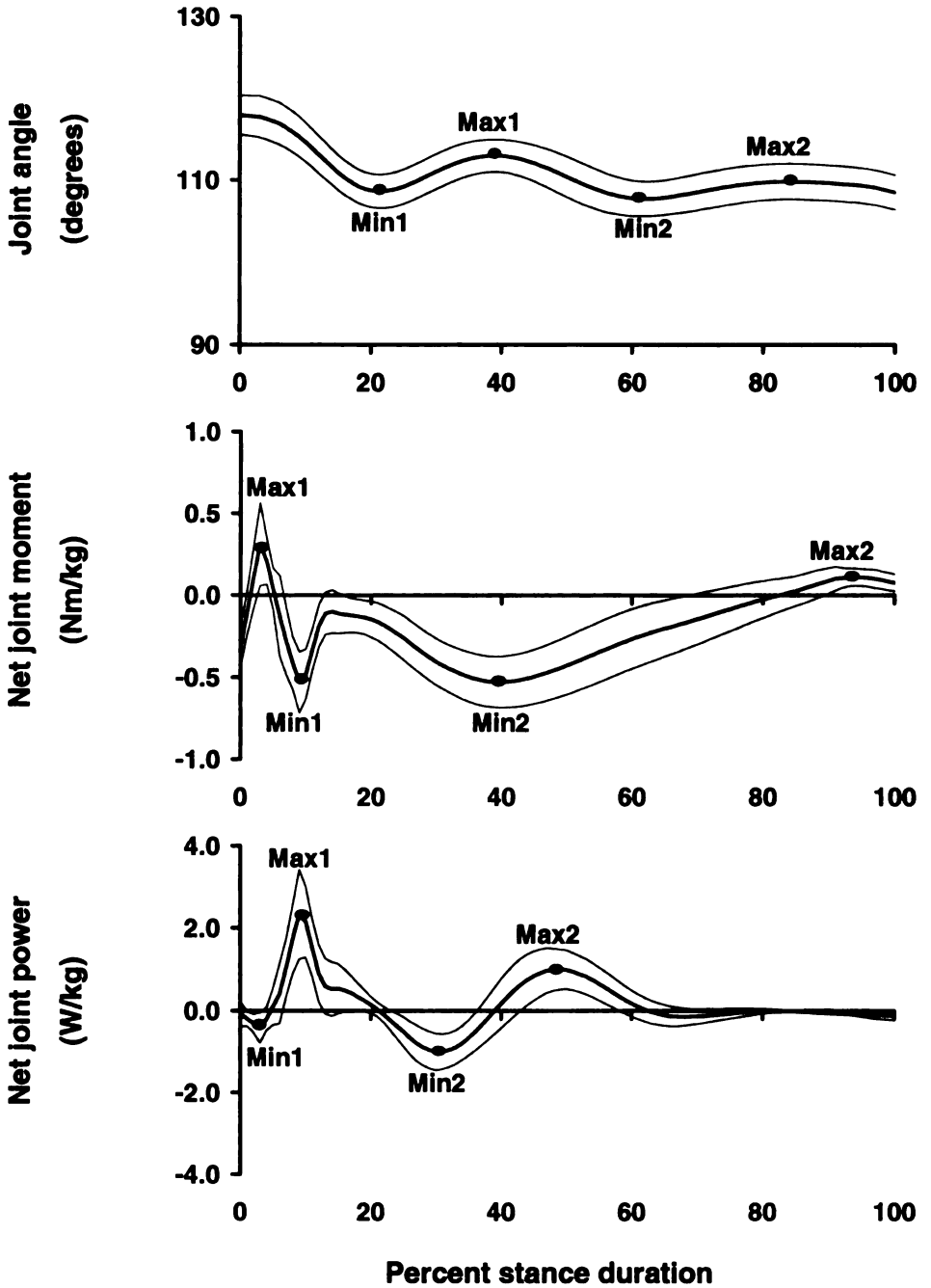

Figure 3-6 Joint angle, net joint moment and net joint power of femorotibial joint during the swing phase. Thick solid line indicates mean values from both hind limbs of sound trotting horses. Thin solid lines indicate one standard deviation above and below the mean.

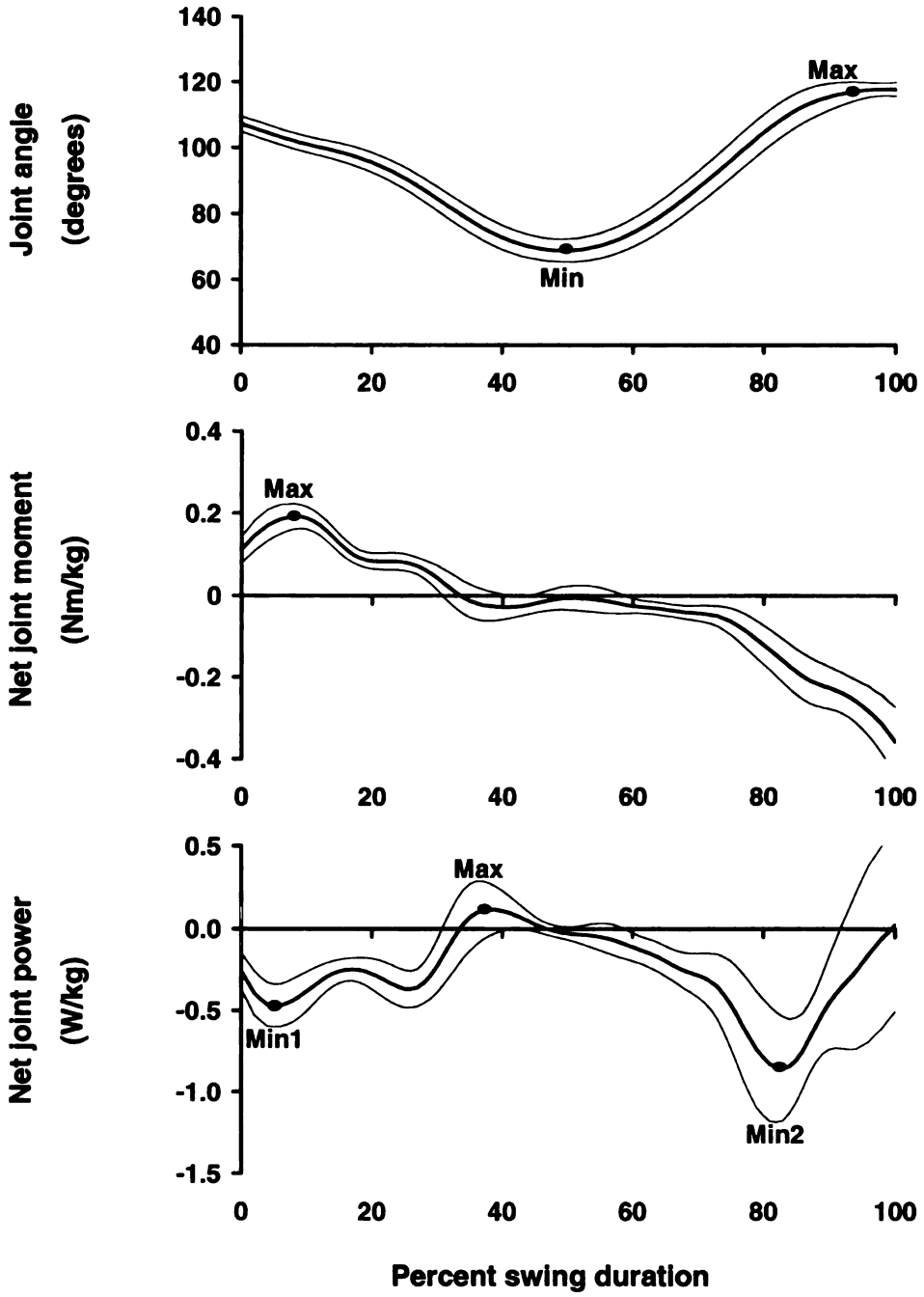

Figure 3-7 Joint angle, net joint moment and net joint power of tarsal joint during the stance phase. Thick solid line indicates mean values from both hind limbs of sound trotting horses. Thin solid lines indicate one standard deviation above and below the mean.

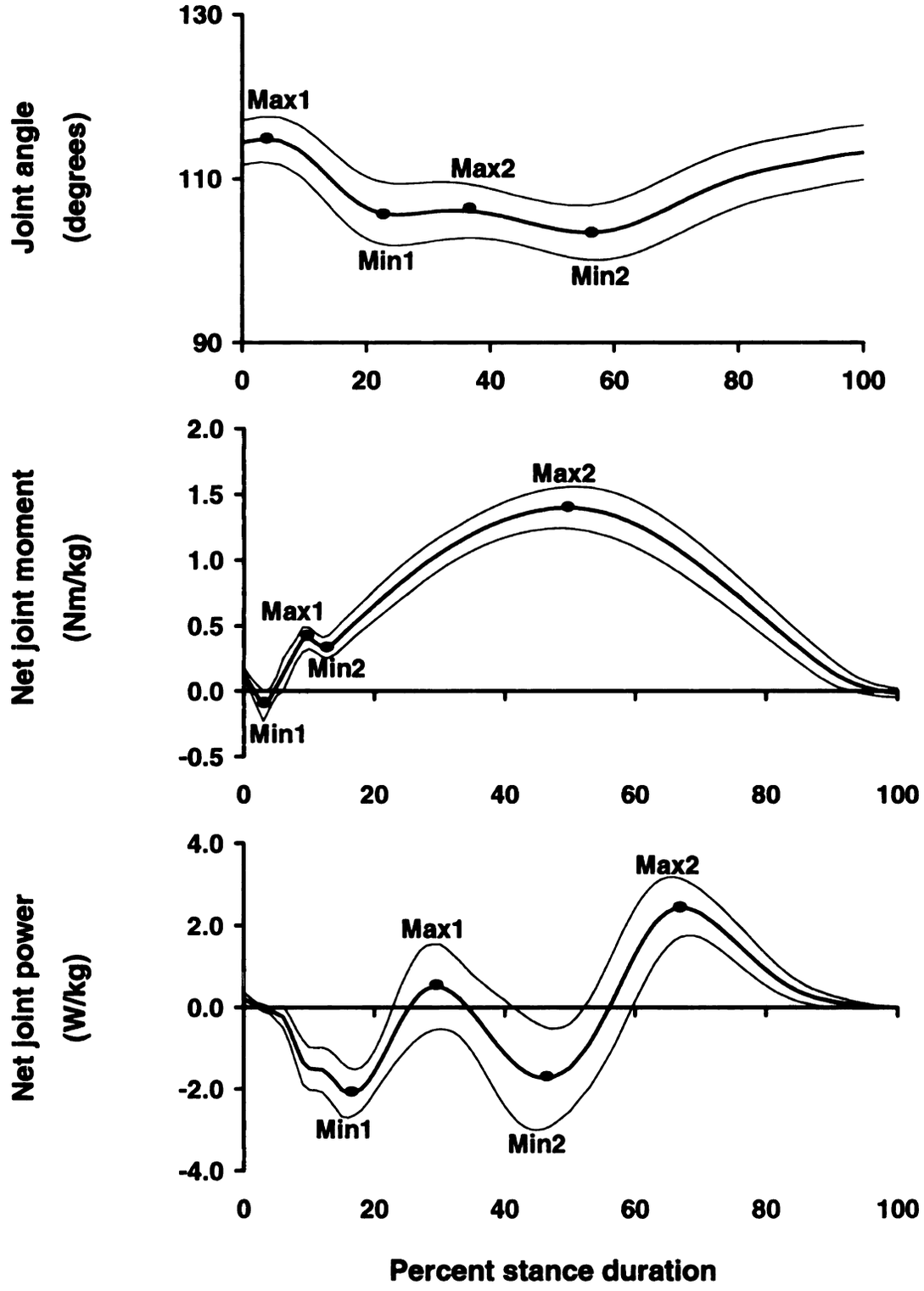

Figure 3-8 Joint angle, net joint moment and net joint power of tarsal joint during the swing phase. Thick solid line indicates mean values from both hind limbs of sound trotting horses. Thin solid lines indicate one standard deviation above and below the mean.

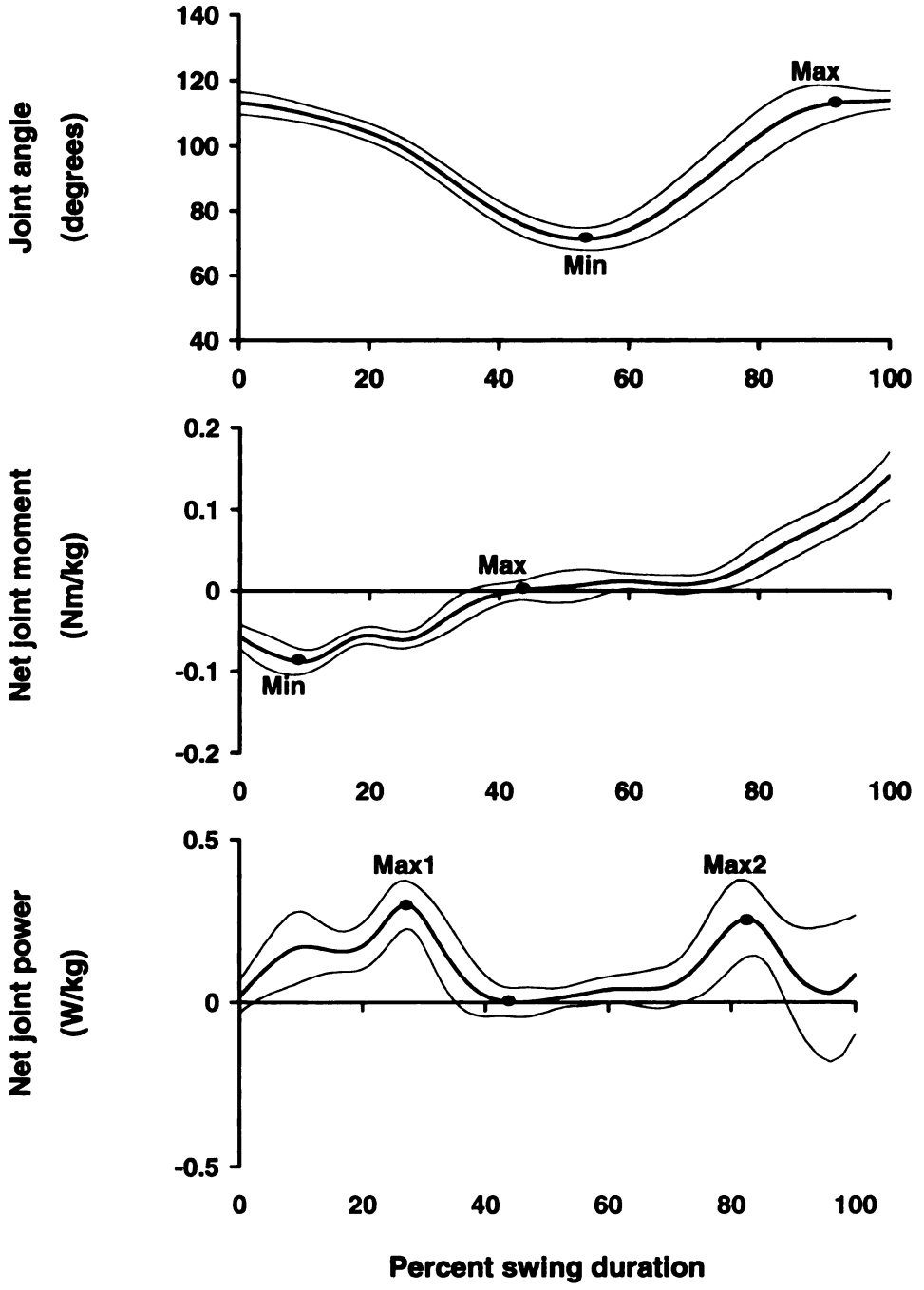

Figure 3-9 Joint angle, net joint moment and net joint power of metatarsophalangeal joint during the stance phase. Thick solid line indicates mean values from both hind limbs of sound trotting horses. Thin solid lines indicate one standard deviation above and below the mean.

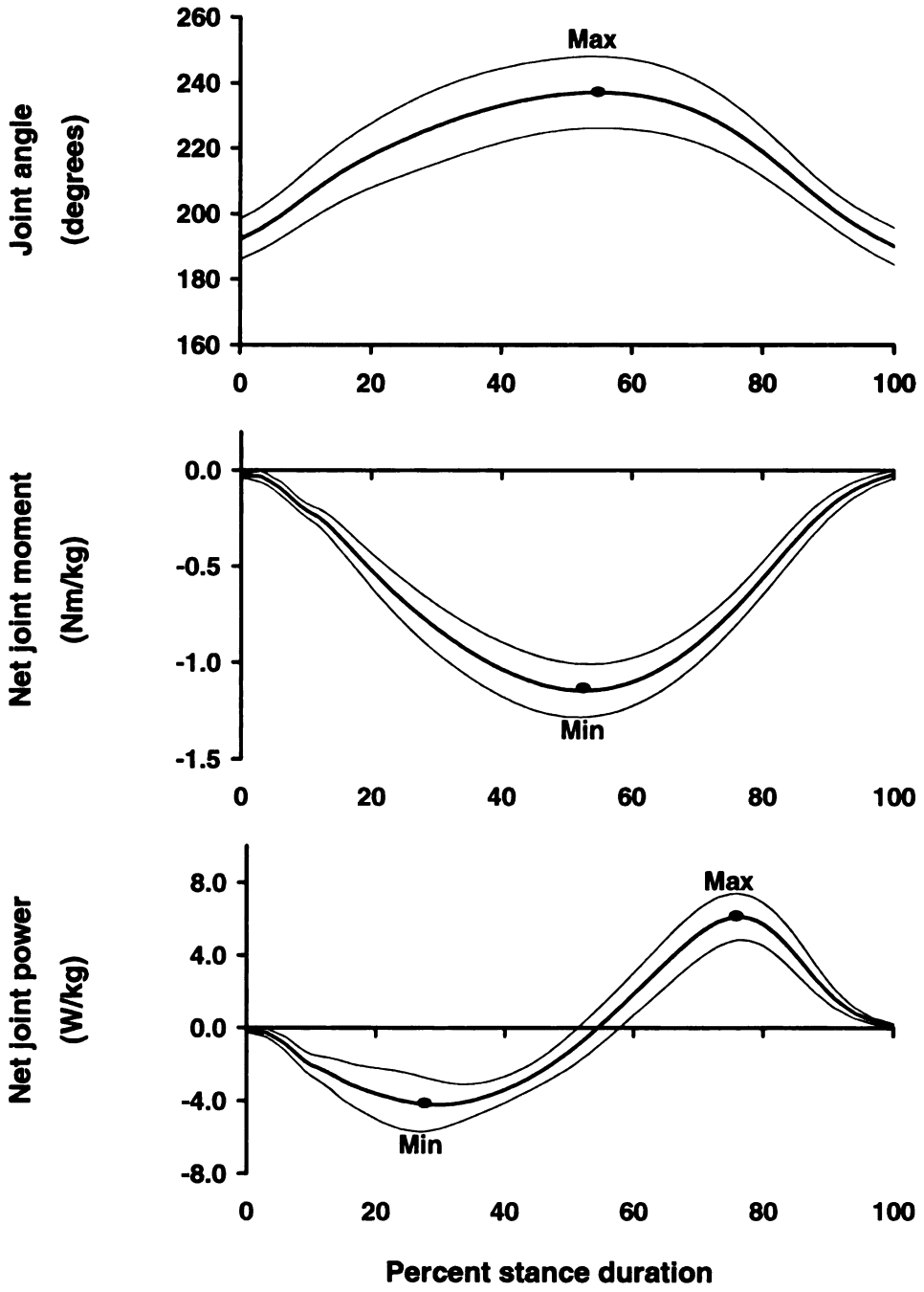

Figure 3-10 Joint angle, net joint moment and net joint power of metatarsophalangeal joint during the swing phase. Thick solid line indicates mean values from both hind limbs of sound trotting horses. Thin solid lines indicate one standard deviation above and below the mean.

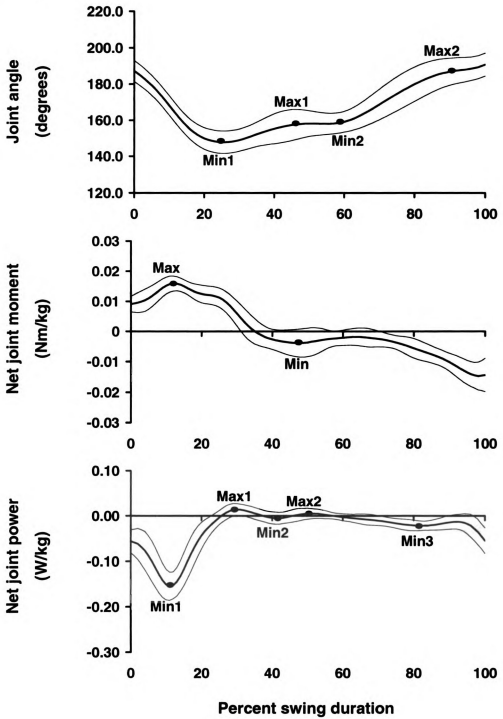

Figure 3-11 Joint angle, net joint moment and net joint power of distal interphalangeal joint during the stance phase. Thick solid line indicates mean values from both hind limbs of sound trotting horses. Thin solid lines indicate one standard deviation above and below the mean.

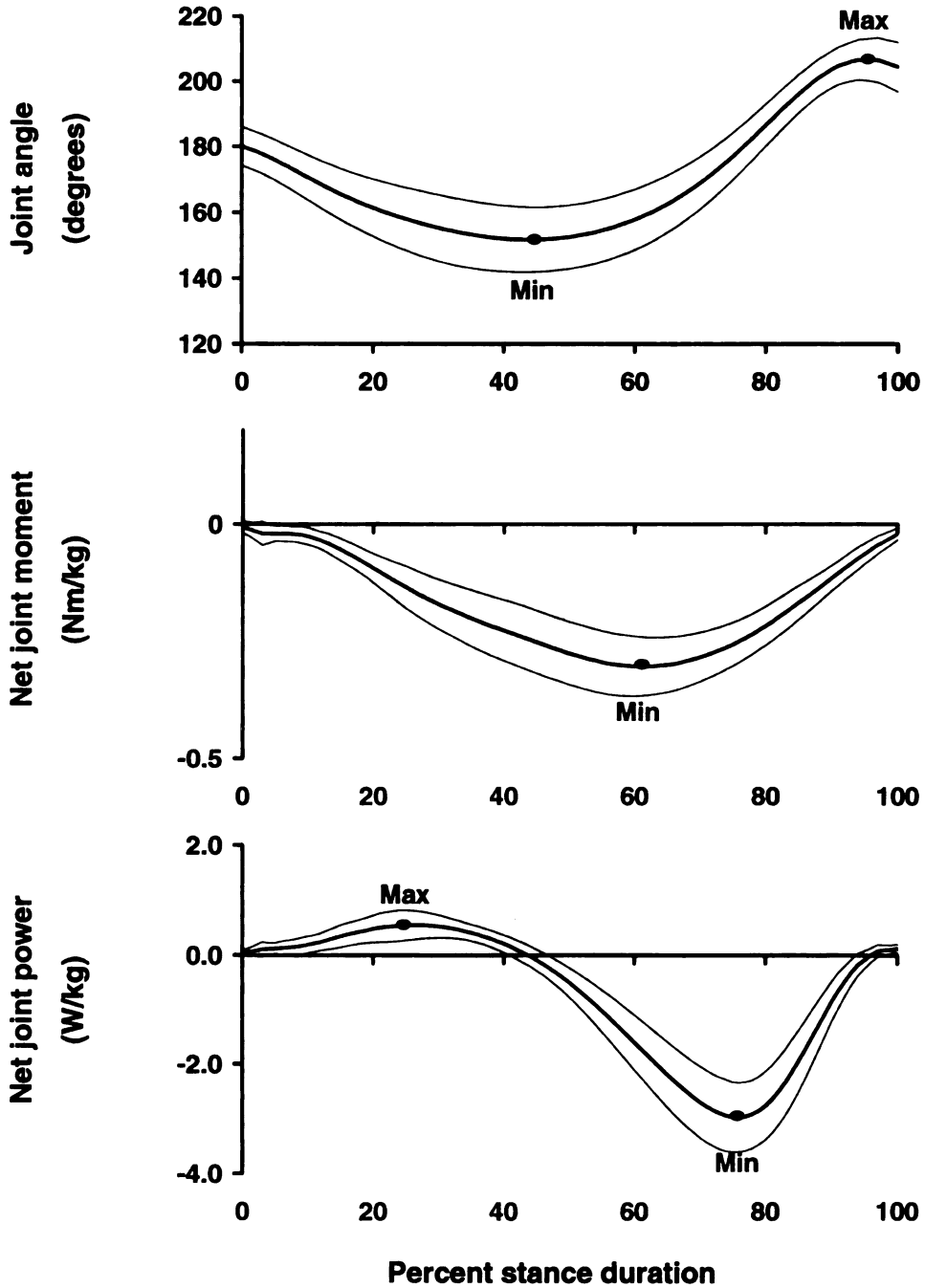

Figure 3-12 Joint angle, net joint moment and net joint power of distal interphalangeal joint during the swing phase. Thick solid line indicates mean values from both hind limbs of sound trotting horses. Thin solid lines indicate one standard deviation above and below the mean.

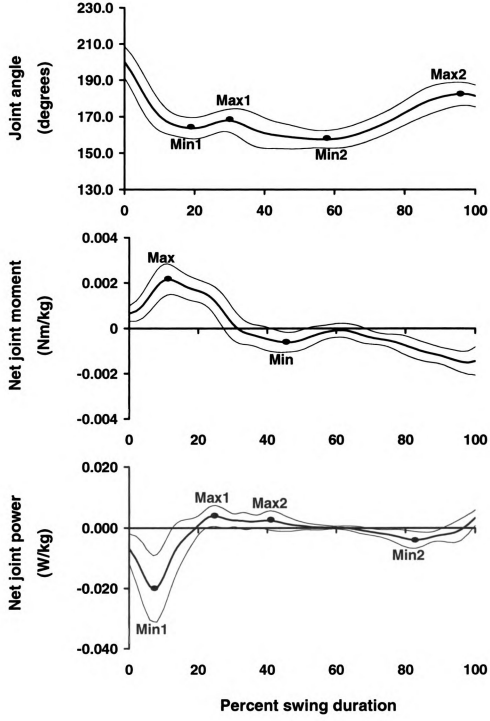

The values of joint angles, net joint moments, net joint powers and net joint energies of all joints are reported in Tables 3-6 to 3-9 for the stance phase and in Tables 3-10 to 3-13 for the swing phase. During the stance phase, the distal interphalangeal joint had the largest range of motion, followed by the metatarsophalangeal joint (Table 3-6). The more proximal joints had a considerably smaller range of motion than the distal joints. The highest net joint moment peaks were the extensor moment at the tarsal joint (Max2), followed by the flexor moment at the metatarsophalangeal joint (Min) and the extensor moment at the coxofemoral joint (Max1) (Table 3-7). The highest positive power peaks were at the metatarsophalangeal joint (Max), followed by the tarsal joint (Max2) and femorotibial joint (Max1). Therefore, these three joints had high rates of performing positive work. The highest negative power peak was on the flexor aspect of the metatarsophalangeal joint (Min), followed by the distal interphalangeal joint (Min) and tarsal joint (Min1) (Table 3-8). Therefore, these three joints had high rates of performing negative work. The femorotibial, tarsal and metatarsophalangeal joints had similar magnitudes of total positive and total negative net joint energies (Table3-9) that reflected the patterns of elastic energy storage and release. The coxofemoral joint performed mostly positive work to protract and retract the limb, while the distal interphalangeal joint performed mostly the negative work.

During the swing phase, all joints had similar ranges of motion (Table 3-10). The magnitude of the net joint moment decreased in a proximal to distal sequence (Table 3-11). The coxofemoral joint had the largest magnitude of net joint moment peak (Min1) on its flexor aspect, and the distal interphalangeal joint had the smallest magnitude net joint moment peak (Min) on its flexor aspect. The absolute values of the net joint power peaks

also decreased from the proximal to distal joints (Table 3-12). The largest net joint power peak was on the extensor aspect of the coxofemoral joint (Max2) during late swing. From the net joint energy profiles (Table 3-13), the coxofemoral joint performed the largest amount of positive work to swing the limb forward, assisted by positive work at the tarsal joint. The femorotibial joint performed the largest amount of negative work to control joint movement. The metatarsophalangeal and distal intertarsal joints showed only small amounts of both energy generation and absorption, which indicated that their motion was driven by inertia and segmental energy transfers from the more proximal joint during swing.

Magnitudes of the mean net energy generation and absorption of the hind limb joints during stance phase, swing phase and total stride are summarized in Table 3-14. The net energy generation and absorption during stance had similar magnitudes, with a small net mechanical energy absorption of -0.018 J/kg. During swing, there was a net mechanical energy generation of 0.1194 J/kg. This resulted in a net mechanical energy generation of 0.1014 J/kg during the whole stride.

Table 3-6 Joint angle peaks (degrees) averaged from both hind limbs in sound trotting horses during the stance phase. Values are mean and (SD).

Joint	Variables	Joint angle	Time of occurrence (% Stance)
Coxofemoral	Max1	109.78 (7.46)	41.0 (3.4)
	Max2	125.20 (6.64)	88.0 (6.6)
	Min1	101.12 (7.18)	17.8 (4.9)
	Min2	114.84 (7.78)	60.2 (4.0)
	Range	26.27 (1.23)	-
Femorotibial	Max1	113.24 (1.90)	40.3 (2.8)
	Max2	109.97 (2.19)	85.6 (5.4)
	Min1	108.46 (2.00)	22.3 (1.2)
	Min2	107.36 (2.08)	63.3 (3.6)
	Range	10.97 (2.67)	-
Tarsal	Max1	114.79 (2.87)	5.2 (0.7)
	Max2	106.45 (3.74)	37.36 (4.30)
	Min1	105.44 (4.20)	25.9 (3.6)
	Min2	103.33 (3.41)	58.2 (2.4)
	Range	12.12 (0.96)	-
Metatarsophalangeal	Max	237.34 (11.49)	55.2 (2.9)
	Range	47.79 (9.16)	-
Distal interphalangeal	Max	206.92 (6.45)	95.8 (1.2)
	Min	151.55 (10.20)	44.9 (2.3)
	Range	55.66 (6.42)	-

Table 3-7 Net joint moment peaks (Nm/kg) averaged from both hind limbs in sound trotting horses during the stance phase. Values are mean and (SD).

Joint	Variables	Joint moment	Time of occurrence (% Stance)
Coxofemoral	Max1	1.101 (0.129)	10.0 (0.5)
	Max2	0.575 (0.126)	23.8 (3.6)
	Max3	0.557 (0.185)	60.0 (3.4)
	Min1	-0.372 (0.248)	4.5 (0.7)
	Min2	0.367 (0.096)	15.2 (2.2)
Femorotibial	Max1	0.365 (0.100)	4.5 (0.7)
	Max2	0.135 (0.055)	94.7 (2.0)
	Min1	-0.59 (0.131)	9.8 (0.6)
	Min2	-0.537 (0.144)	4.07 (2.1)
Tarsal	Max1	0.422 (0.086)	10.3 (0.6)
	Max2	1.406 (0.154)	50.4 (2.1)
	Min1	-0.132 (0.052)	4.4 (0.7)
	Min2	0.325 (0.076)	13.7 (0.5)
Metatarsophalangeal	Min	-1.149 (0.140)	53.8 (1.7)
Distal interphalangeal	Min	-0.304 (0.058)	62.4 (2.3)

Table 3-8 Net joint power peaks (W/kg) averaged from both hind limbs in sound trotting horses during the stance phase. Values are mean and (SD).

Joint	Variables	Joint power	Time of occurrence (% Stance)
Coxofemoral	Max1	1.501 (0.419)	25.3 (5.3)
	Max2	1.473 (0.554)	63.3 (4.0)
Femorotibial	Max1	2.488 (0.875)	10.2 (0.6)
	Max2	1.150 (0.493)	49.9 (3.2)
	Min1	-0.503 (0.188)	4.7 (0.8)
	Min2	-1.085 (0.384)	32.1 (2.0)
Tarsal	Max1	0.862 (0.762)	31.7 (4.1)
	Max2	2.627 (0.565)	68.2 (2.7)
	Min1	-2.219 (0.496)	17.9 (1.9)
	Min2	-2.159 (1.073)	47.5 (4.0)
Metatarsophalangeal	Max	6.237 (1.284)	77.5 (1.4)
	Min	-4.653 (1.316)	31.4 (5.3)
Distal interphalangeal	Max	0.588 (0.258)	28.0 (4.5)
	Min	-3.037 (0.625)	77.1 (1.6)

Table 3-9 Net joint energies (J/kg) calculated by time integration of the corresponding net joint power peaks during the stance phase. Values were averaged from both hind limbs in sound trotting horses. Values are mean and (SD).

Joint	Variables	Joint energy
Coxofemoral	Max1	0.063 (0.023)
	Max2	0.073 (0.034)
	Total positive energy	0.140 (0.140)
	Total negative energy	-0.014 (0.009)
Femorotibial	Max1	0.037 (0.016)
	Max2	0.041 (0.018)
	Min1	-0.004 (0.001)
	Min2	-0.031 (0.011)
	Total positive energy	0.079 (0.027)
	Total negative energy	-0.043 (0.015)
Tarsal	Max1	0.024 (0.014)
	Max2	0.125 (0.023)
	Min1	-0.075 (0.016)
	Min2	-0.076 (0.043)
	Total positive energy	0.147 (0.023)
	Total negative energy	-0.151 (0.038)
Metatarsophalangeal	Max	0.394 (0.094)
	Min	-0.386 (0.108)
	Total positive energy	0.394 (0.094)
	Total negative energy	-0.387 (0.108)
Distal interphalangeal	Max	0.038 (0.018)
	Min	-0.222 (0.049)
	Total positive energy	0.040 (0.017)
	Total negative energy	-0.223 (0.049)

Table 3-10 Joint angle peaks (degrees) averaged from both hind limbs in sound trotting horses during the swing phase. Values are mean and (SD).

Joint	Variables	Joint angle	Time of occurrence (% Swing)
Coxofemoral	Min	76.85 (5.43)	64.7 (1.1)
	Range	48.63 (1.41)	-
Femorotibial	Max	114.97 (4.03)	90.2 (2.6)
	Min	68.35 (3.09)	50.2 (2.9)
	Range	50.44 (2.63)	-
Tarsal	Max	113.38 (4.99)	91.1 (2.6)
	Min	70.77 (3.09)	54.5 (2.7)
	Range	44.67 (1.90)	-
Metatarsophalangeal	Max1	160.54 (6.94)	42.9 (7.8)
	Max2	185.90 (7.63)	88.7 (2.0)
	Min1	147.70 (6.67)	25.3 (2.5)
	Min2	156.61 (6.76)	56.3 (7.2)
	Range	45.31 (3.38)	-
Distal interphalangeal	Max1	170.08 (6.34)	31.9 (4.2)
	Max2	180.41 (8.29)	90.9 (6.7)
	Min1	162.60 (5.69)	19.1 (3.4)
	Min2	155.33 (6.13)	46.1 (6.4)
	Range	45.29 (5.05)	-

Table 3-11 Net joint moment peaks (Nm/kg) averaged from both hind limbs in sound trotting horses during the swing phase. Values are mean and (SD).

Joint	Variables	Joint moment	Time of occurrence (% Swing)
Coxofemoral	Max	0.1190 (0.0299)	39.1 (1.1)
	Min1	-0.4313 (0.0575)	16.8 (12.1)
	Min2	-0.1347 (0.0650)	60.1 (4.5)
Femorotibial	Max	0.1993 (0.0285)	8.9 (1.9)
Tarsal	Max	0.0185 (0.0115)	48.8 (7.3)
	Min	-0.0928 (0.0160)	10.3 (2.2)
Metatarsophalangeal	Max	0.0170 (0.0021)	13.9 (3.0)
	Min	-0.0070 (0.0025)	44.0 (5.8)
Distal interphalangeal	Max	0.0023 (0.0007)	14.7 (4.4)
	Min	-0.0010 (0.0002)	41.7 (6.7)

Table 3-12 Net joint power peaks (W/kg) averaged from both hind limbs in sound trotting horses during the swing phase. Values are mean and (SD).

Joint	Variables	Joint power	Time of occurrence (% Swing)
Coxofemoral	Max1	1.1630 (0.1830)	18.3 (3.4)
	Max2	1.8785 (0.6698)	92.0 (4.7)
	Min	-0.6299 (0.1565)	38.8 (1.0)
Femorotibial	Max	0.1595 (0.1381)	41.0 (3.7)
	Min1	-0.5193 (0.1201)	12.8 (7.4)
	Min2	-0.9414 (0.3216)	86.1 (3.6)
Tarsal	Max1	0.3340 (0.0590)	25.6 (5.0)
	Max2	0.3179 (0.1124)	86.2 (5.8)
Metatarsophalangeal	Max1	0.0187 (0.0121)	30.6 (3.0)
	Max2	0.0150 (0.0057)	48.5 (6.9)
	Min1	-0.1663 (0.0245)	12.3 (1.7)
	Min2	-0.0167 (0.0101)	40.5 (6.4)
	Min3	-0.0315 (0.0086)	80.6 (5.0)
Distal interphalangeal	Max1	0.0056 (0.0028)	25.4 (3.3)
	Max2	0.0059 (0.0017)	39.9 (6.1)
	Min1	-0.0230 (0.0117)	8.6 (1.9)
	Min2	-0.0055 (0.0024)	87.1 (3.8)

Table 3-13 Net joint energies (J/kg) calculated by time integration of the corresponding net joint power peaks during the swing phase. Values were averaged from both hind limbs in sound trotting horses. Values are mean and (SD).

Joint	Variables	Joint energy
Coxofemoral	Max1	0.1041 (0.0095)
	Max2	0.1223 (0.0419)
	Min	-0.0269 (0.0101)
	Total positive energy	0.2291 (0.0365)
	Total negative energy	-0.0277 (0.0100)
Femorotibial	Min1	-0.0485 (0.0103)
	Min2	-0.0786 (0.0131)
	Total positive energy	0.0119 (0.0088)
	Total negative energy	-0.1290 (0.0207)
Tarsal	Max1	0.0291 (0.0075)
	Max2	0.0221 (0.0088)
	Min	-0.0016 (0.0014)
	Total positive energy	0.0520 (0.0129)
	Total negative energy	-0.0040 (0.0029)
Metatarsophalangeal	Max1	0.0006 (0.0004)
	Max2	0.0004 (0.0002)
	Min1	-0.0094 (0.0019)
	Min2	-0.0004 (0.0002)
	Min3	-0.0024 (0.0007)
	Total positive energy	0.0011 (0.0005)
	Total negative energy	-0.0131 (0.0019)
Distal interphalangeal	Max1	0.0002 (0.0001)
	Max2	0.0002 (0.0001)
	Min1	-0.0009 (0.0004)
	Min2	-0.0004 (0.0001)
	Total positive energy	0.0004 (0.0002)
	Total negative energy	-0.0013 (0.0005)

Table 3-14 Summary of means energy generation and absorption (J/kg) at the joints of the hind limb during stance phase, swing phase and the total stride.

Joint	Energy generated stance	Energy absorbed stance	Energy generated swing	Energy absorbed swing	Net energy stride
Coxofemoral	0.140	-0.014	0.2291	-0.0277	0.3274
Femorotibial	0.079	-0.043	0.0119	-0.1290	-0.0811
Tarsal	0.147	-0.151	0.0520	-0.0040	0.044
Metatarsophalangeal	0.394	-0.387	0.0011	-0.0131	-0.005
Distal interphalangeal	0.040	-0.223	0.0004	-0.0013	-0.1839
Total	0.800	-0.818	0.2945	-0.1751	0.1014

DISCUSSION

Kinematic data. The application of skin correction algorithms to the raw kinematic data is very important, especially proximal to the tarsal joint. The coupled motion of the femorotibial and tarsal joints via the function of the reciprocal apparatus could not be identified in data without correction for skin motion (Kobluk, et al., 1989), but could be observed after the movement of skin markers had been corrected (van den Bogert, 1990; van Weeren, et al., 1990). The models for correction of skin displacement may not be able to account for all individual variation. It has been suggested that only 70% of skin displacement at the femorotibial joint center of rotation (femoral condyle) can be predicted correctly (van Weeren, et al., 1992a). Nevertheless, much improvement was found for the reciprocal movement between femorotibial and tarsal joints flexion and extension after the application of skin correction algorithms to the femorotibial joint, including the joint extension during the end of stance and joint flexion/extension during

swing (van den Bogert, et al., 1990; van Weeren, et al., 1992b; Back, et al., 1995b). Even the skin correction algorithm could not eliminate all the errors from skin displacement, but it helps improve the kinematic information. Therefore, the skin correction algorithms should be applied in studies based on data from skin markers, especially in the limb segment proximal to the tarsal joint.

Distal interphalangeal joint angles have the highest variation among hind limb joints (Back, et al., 1995b; Degueurce, et al., 1997; Pourcelot, et al., 1997b). The coefficient of variation for the range of motion of the distal interphalangeal joint in this study was 12% during stance and 11% during swing, which is similar to the value (14%) reported during the whole stride (Back, et al., 1995b). Radiographic identification of the distal interphalangeal joint center of rotation reduced inter-individual variations due to errors in marker placement on the hoof wall.

Trotting velocity affects range of motion at the hind limb joints. An increase in trotting velocity resulted in increases in tarsal joint flexion, tarsal and coxofemoral joint ranges of motion, and range of retraction-protraction of the entire limb (Galisteo, et al., 1998). Velocity also seems to influence the tarsal joint angle profile. In Dutch warmbloods trotting at 4 m/s (Back, et al., 1995b) the angle profile showed two flexion peaks similar to the pattern in this study, whereas Standardbreds trotting at 10.7 to 11.5 m/s (Johnston, et al., 1996) had different profiles with a single flexion peak around 40% stance. At faster trotting velocities, peak tarsal flexion tends to occur earlier than at slower velocities (Clayton, personal communication). Therefore, comparisons of angle-time graphs for the tarsal joint should be performed cautiously and only within a similar range of trotting velocities.

The joint angle diagrams of the hind limb joints in this study were similar to those reported previously (Back, et al., 1994; Back, et al., 1995b). During early stance, the hind limb was compressed by flexion of the femorotibial, tarsal, and distal interphalangeal joints and hyperextension of the metatarsophalangeal joint (Hjerten, et al., 1994) while the coxofemoral joint gradually extend thorough the stance phase. The decrease in total limb length during stance was described as a mechanism to absorb impact shock (Back, et al., 1995b). Movements of the femorotibial and tarsal joints were completely synchronized by the reciprocal apparatus during the swing phase. During the stance phase, small discrepancies of flexion and extension between the femorotibial and tarsal joint could be observed during impact and prior to lift off. In Back, et al. (1995b), the femorotibial and tarsal joint profiles during the early stance before and after skin correction showed the same profile in each joint, therefore, the profiles of these two joints obtained from the study that did not use skin correction could be compared during early stance. During impact, tarsal joint extended while the femorotibial joint slightly flexed, similar to the finding from previous studies (Holmstrom, et al., 1994; Back, et al., 1995b; Holmstrom, et al., 1995b). This discrepancy during early stance was not observed at the walk (Galisteo, et al., 1996; Hodson, et al., 2001). The higher GRFs in the trot compared with the walk might be sufficient to stretch the peroneus tertius, which shows a brief period of increased strain during this time (van Weeren, et al., 1992b). At the end of stance, the femorotibial joint maintained its angle while the tarsal joint extended. Consequently, the peroneus tertius was stretched and reached its maximal strain just prior to lift off. Strain decreased rapidly after lift off, which indicated a release of stored energy (van Weeren, et al., 1992b).

Force plate data. Vertical and longitudinal ground reaction forces (GRFs) and impulses in this study had similar magnitudes but lower % CV than Merkens, et al. (1993). In that study, the velocity ranged from 3.9 to 4.3 m/s. Subject velocity influences peak vertical force and impulse at walk (Khumsap, et al., 2001b) and vertical impulse at trot (McLaughlin, et al., 1996). Due to the velocity dependent effects on GRF, subject velocity was controlled by standardizing the dynamic similarity and consequently the variation between horses was reduced.

The center of load distribution indicated that the forelimbs contributed more than the hind limbs in accepting the total body load. In this study, the horses' forelimb carried 56.44% to 57.91%, which is in accordance with the fact that the center of gravity is located closer to the forelimbs (Sprigings and Leach, 1986). Each horse has a slight asymmetry loading at the trot between the left and right sides in the forelimb or hind limb pairs (Merkens, et al., 1993). Quarter horses showed a lead limb preference (Deuel and Lawrence, 1987), and sidedness may evident in Standardbred trotters as young as 8 months old (Drevemo, et al., 1987). A slight asymmetry in vertical impulse might be an indication of sidedness in each horse that is equivalent to handedness in people. In this study, three of the four horses loaded the left limbs a little more than the right limbs.

Impact oscillations of the GRF ended earlier in the vertical GRF than the braking GRF, which is similar to the results in previous studies (Merkens and Schamhardt, 1994; Schamhardt and Merkens, 1994; Clayton, 2001). The hind limb made heel first contact with the ground just prior to the start of the main loading phase (Merkens and Schamhardt, 1994). The hind hoof had more horizontal velocity than vertical velocity during trotting impact (Back, et al., 1995c). This resulted in a little forward sliding of

hind hoof at impact, which may be a mechanism to reduce the oscillation in the metatarsophalangeal joint. Therefore, the metatarsophalangeal joint angle curve was smoother than that of the metacarpophalangeal joint during early stance (Merkens and Schamhardt, 1994; Back, et al., 1995c).

There have been limited studies reporting GRFs in the hind limb of trotting horses. In contrast, there have been several studies of GRFs in normal trotting dogs and dogs with orthopedic problems. Studies in humans have shown a similar GRF pattern to the equine hind limb, but most of the human clinical studies focus on GRF analysis at the walk. The studies in humans and dogs offer some insight into the role of normal joints on GRF generation and the effect of specific pathologies on those forces. In dogs with degenerative joint disease of the coxofemoral joint, total hip replacement resulted in significant increases in vertical and propulsive impulses in the treated limb (Budsberg, et al., 1996). This suggests that the mechanical role of the coxofemoral joint is to generate a propulsive force and impulse to push the body upward and forward.

In humans, quadriceps action modulates the magnitude of the heel strike transient, and quadriceps paralysis resulted in a large increase in the heel strike transient (Jefferson, et al., 1990). In dogs with induced-synovitis of the femorotibial joint (Cross, et al., 1997), and cats with degeneration of the femorotibial joint (Suter, et al., 1998), GRF analysis indicated decreases in peak vertical and braking GRFs without a significant change in propulsive impulse. These findings suggest that the femorotibial joint plays a role in deceleration during the first half of stance.

Comparison of canine GRFs, before and after temporary impairment of the tibial nerve, revealed a significant decrease in vertical GRF without a change in braking or

propulsive forces (Rumph and Steiss, 1998). The function of the tarsal joint, therefore, seems to be important in generating vertical force, rather than longitudinal forces.

Inverse dynamic analysis. Inverse dynamic analysis is sensitive to the protocol for data collection and the method for data analysis. The fact that the horse is not a set of perfectly rigid body segments, and kinematic data are contaminated by measurement errors and soft tissue deformation, affects the results of inverse dynamic analysis. The results are acceptable, however, as long as the same methodology is used to evaluate and compare locomotion in each horse (van den Bogert, 1998).

The two important forces that the limb joints have to overcome are the GRF and gravitational force. During stance, the main effect of the net joint moments is to resist the collapse of the limb joints under the influence of a large GRF. The forces needed to overcome gravity and to accelerate the limb can be considered negligible. During swing, the only external force acting on the limb is the gravitational force, and the muscular work performed across the proximal joints to accelerate and decelerate the limb causes large inertial forces in the distal limb. Therefore, it is important to apply inertial parameters for inverse dynamic analysis of the limb segments during swing (Schamhardt, 1998; Lanovaz and Clayton, 2001).

The equine hind limb has many muscles that cross two or more joints and have complicated actions. Several coxofemoral extensors also act as femorotibial flexors, while femorotibial extensors also act as coxofemoral flexors. The reciprocal apparatus also has an important role in coordinating movement of the femorotibial and tarsal joints. Some of tarsal extensors, such as the gastrocnemius and deep digital flexor muscle, also

influence femorotibial joint flexion. The same muscle or tendon may perform positive work at one joint and negative work at another joint. Calculation of power flows between segments (Colborne, et al., 1997b) may give more information about these energy transfers, but the technique is beyond the scope of this study. The objective of using inverse dynamic analysis here is to develop a deeper understanding of limb function and to relate these findings to the previous literature.

Coxofemoral joint. Extensor muscles performed positive work to extend the joint throughout stance. Electromyographic (EMG) studies (Wentink, 1978; Tokuriki and Aoki, 1995; Robert, et al., 1998; Robert, et al., 1999) have indicated that gluteus medius, biceps femoris and semitendinosus are active during these bursts of energy generation. EMG activity of tensor fascia latae commenced during the second half of stance, but its activity was initially less than that of the extensor muscles, resulting in a net moment on the extensor aspect. The net moment moved to the flexor aspect during late stance due to either a decrease in extensor activity or an increase in flexor activity or both. Since joint angle did not change during late stance, net muscular work was diminished, probably due to the simultaneous development of tension in the coxofemoral extensors and flexors at this time.

Tensor fascia latae activity continued until the middle of swing, during which time the muscle performed positive work to flex the joint and protract the limb. Semitendinosus also showed activity during early swing that ceased just before the middle of swing, but its activity was probably more important for flexing the femorotibial joint. During the second half of swing, EMG activity was present in semitendinosus,

gluteus medius and biceps femoris (Wentink, 1978; Tokuriki and Aoki, 1995; Robert, et al., 1998), which performed positive work to extend the coxofemoral joint in preparation for impact.

Femorotibial joint. The femorotibial joint plays a role in controlling the braking force (Jefferson, et al., 1990; Cross, et al., 1997; Suter, et al., 1998). In this study, an extensor moment was present with negative power during 0-5% stance, which corresponded with the first negative longitudinal force peak (Min1) that acted to decelerate the forward movement of the hoof. The following oscillation in the longitudinal forces matched the oscillation pattern in the femorotibial net joint moment in early stance. EMG studies in horses reported activity of rectus femoris and vastus lateralis from terminal swing into the stance phase (Wentink, 1978; Robert, et al., 1999). Our findings indicated that the role of these muscles was to perform negative work on the extensor aspect of the femorotibial joint, which had the effect of smoothing the longitudinal impact shock. The biarticular coxofemoral extensors, which also acted as femorotibial flexors, were active during stance. These muscles performed positive muscular work to flex the joint until 20% stance. The joint extended from 20-40% stance, corresponding to the extension of the coxofemoral joint. During this period, the GRF vector passed cranial to both the coxofemoral and femorotibial joints, which tended to flex the former joint and extend the latter joint. The muscles needed to generate forces that counteracted the GRF to control the motion, which resulted in a net extensor moment at the coxofemoral joint and a net flexor moment at the femorotibial joint. The coxofemoral joint was actively extended by positive work of semitendinosus and biceps

femoris. The femorotibial joint passively extended, controlled by a flexor moment produced by the coxofemoral extensors. This resulted in energy absorption at the femorotibial joint during 20-40% stance. During this period, the tarsal joint also extended but to a lesser degree than the femorotibial joint, which caused stretching of superficial digital flexor (SDF) tendon, which shows an increase in load at this time (Riemersma, et al., 1988). Hence, energy absorption on the flexor aspect of the femorotibial joint appeared to correspond with elastic energy storage in the SDF tendon. Elastic energy was released as the tendon recoiled between 40-60% stance as the femorotibial joint flexed. In late stance, EMG activity in the vastus lateralis and tensor fascia latae created a net extensor moment at the femorotibial joint but the joint angle changed only slightly during this period, so very little mechanical work was performed.

Energy was absorbed through most of swing. During the first half of swing, the femorotibial joint flexed against a net extensor moment. That was likely provided by tensor fascia latae, which was actively flexing the coxofemoral joint. This resulted in net extensor moment and net negative work at the femorotibial joint. During the second half of swing, the femorotibial joint extended against a net flexor moment, which was likely due to contraction of the biarticular semitendinosus and biceps femoris that were actively extending the coxofemoral joint during this time. The bursts of energy absorption at the femorotibial joint (Min1, Min2) occurred at approximately the same time as energy generation at the coxofemoral joint (Max1, Max2), which supports the importance of bi-articular muscle activities between coxofemoral and femorotibial joints.

Tarsal joint. The tarsal joint appears to play an important role in vertical force generation. The oscillating pattern of the net joint moment profile during early stance reflected the oscillating pattern found in the vertical GRF. During 0-5% stance, there was a brief period of joint extension which continued from the swing phase until the hoof was flat on the ground, in agreement with a previous kinematic study (Hjerten, et al., 1994). From approximately 5-25% stance, the net joint moment was on the extensor aspect corresponding with EMG activity in the gastrocnemius (Wentink, 1978), deep digital flexor (DDF) muscle (Jansen, et al., 1992) and increasing load in the SDF and DDF tendons (Riemersma, et al., 1988). The negative work came from a combination of energy absorption during eccentric muscular contraction and elastic energy storage in the tendons. Stored elastic energy was released between 20-40% stance, but the amount of energy released was less than the preceding burst of energy absorption, indicating the important role of gastrocnemius in absorbing impact shock. The tarsal flexor tendons continued to store elastic energy, with peak energy storage (Min2) coinciding with the vertical force peak. The tarsus was the only joint in the hind limb that had a negative net joint power peak coinciding with the vertical force peak, which may reflect its role in absorbing peak vertical force from body weight. Peak Min2 in the net joint power profile was highly variable between horses, which may reflect different mechanisms for managing the load. The elastic energy released from 60-90% (Max2) exceeded the amount of energy absorbed (Min2). Therefore, the tarsal extensors performed positive work in addition to the elastic energy release. Gastrocnemius had incidental periodical activity during this time (Wentink, 1978). The DDF muscle, which was active (Jansen, et al., 1992) and its tendon reached maximal load in the second half of stance (Riemersma,

et al., 1988), might have more responsible than gastrocnemius to move the tarsal joint. These two muscles performed positive work to extend the tarsus in terminal stance. Since the femorotibial joint angle did not change during this period, the peroneus tertius tendon was stretched. The strain peaked just prior to lift off, but strain magnitude did not exceed 3% at the walk or the trot (van Weeren, et al., 1992b). The cranial tibial muscle (Wentink, 1978) became active in late stance through early swing.

In early swing, the tarsal joint flexed due to positive work performed by contraction of cranial tibial muscle and elastic energy recoil of the peroneus tertius. Activity of the cranial tibial muscle ceased before the middle of swing, therefore, the continuing flexion of the tarsus came from the action of the reciprocal apparatus. The gastrocnemius muscle became active from the middle of swing through early stance (Wentink, 1978), performing positive work on the extensor aspect to extend the joint from around 60% to the end of swing. The positive work performed by gastrocnemius during this time might contribute to the passive extension of the femorotibial joint thorough the function of reciprocal apparatus, resulting in the femorotibial joint extension against flexor moment and energy absorption during the second half of swing.

Metatarsophalangeal joint. The structures distal to the tarsal joint are mostly tendons and ligaments that can support the distal joints mechanically. During stance the metatarsophalangeal joint had a burst of negative work followed by a burst of positive work, that were typical of elastic energy storage and release. The joint angle, net joint moment and net joint power profiles of the metatarsophalangeal joint were similar to those of the metacarpophalangeal joint (Clayton, et al., 1998; Clayton, et al., 2000c), but

peak power was lower in the hind limbs due to the lower vertical GRF. During the first half of stance, the joint extended to accept body weight, with energy absorption in the SDF and DDF tendons and suspensory ligament (Riemersma, et al., 1988). Later in the stance phase, elastic energy was released as these structures recoiled during the joint flexion, and the net joint power became positive. The transition from negative to positive power occurred a little later in the hind limb than the forelimb, in accordance with differences in the joint angle profiles. The metacarpophalangeal joint extended faster, reached maximal extension earlier (Back, et al., 1995c) and had a shorter period of energy absorption than the metatarsophalangeal joint.

The coupling mechanism of the reciprocal apparatus on the plantar aspect of the limb includes the metatarsophalangeal joint via the SDF tendon (Molenaar, 1983; Back, et al., 1995b). This causes the metatarsophalangeal joint to flex when the femorotibial and tarsal joints flex in early swing. This flexion is controlled by an extensor moment during 0-35% swing, probably from negative work of the long digital extensor tendon (Robert, et al., 1999). In the second half of the swing, the metatarsophalangeal joint was passively extended due to the inertial motion of pastern and hoof segments. The digital flexor muscles, which were active during this time (van den Bogert, 1989), controlled the motion of those two segments to prevent the overextension of the joint and to position the distal segments for impact.

Distal interphalangeal joint. The joint angle, net joint moment and net joint power profiles of the distal interphalangeal joint in the hind limb were similar to those of the forelimb (Clayton, et al., 1998; Clayton, et al., 2000c). During 0-45% stance, the joint

actively flexed due to the positive work of the deep digital flexor muscle (Jansen, et al., 1992). After that, the joint extended under control of the same muscle, which was performing negative work. The change in net joint power from positive to negative occurred a little earlier in the forelimb, around 35% stance, than in the hind limb. Other researchers have shown that the hoof sole angle relative to the ground at contact was greater in the hind limb than the forelimb (Back, et al., 1995c), indicating a more exaggerated heel-first placement in the hind hoof. Consequently, the hind hoof moved into a flat position and the distal interphalangeal joint reached its maximal joint flexion later than the fore hoof. The longer duration of distal interphalangeal joint flexion in the hind limb resulted in a longer period of energy generation.

During swing, the movement and power profiles of the distal interphalangeal joint were similar to those of the metatarsophalangeal joint. The mechanism of joint motion was thought to be similar, involving control of inertial forces. Since the hoof segment has such a small mass, the magnitude of negative work needed to restrain flexion and extension of the distal interphalangeal joint motion was only about one tenth of that required at the metatarsophalangeal joint. The most influential single inertial parameter in net joint moment calculations during swing is the mass of the hoof segment (Lanovaz and Clayton, 2001). Adding heavy shoes or pads to the hoof increases the segmental mass, gravitational force and inertial forces, requiring more negative work to restrain the joint motion.

Hind limb coordination. Muscular work is used to transform joint rotations into forward translation of the entire hind limb. Muscles also transfer energy from one

segment to the other (Winter, 1990). Mechanical energy transfer among proximal and distal limb segments causes an efficient conversion between rotational motions of body segments and translation of the body center of gravity. In human sprinters, the rectus femoris muscle transferred power from coxofemoral to femorotibial joint, while the hamstrings transferred power from femorotibial to coxofemoral joint. Gastrocnemius transferred power from femorotibial to tarsal joint (Jacobs, et al., 1996). In the equine limb, several muscles and tendons cross more than one joint. The tendinous structures connecting the proximal and the distal parts of the limbs also have the capacity to transfer mechanical, muscular energy to other parts of the limbs (Schamhardt, 1998). Muscles and their tendons can transfer energy between segments if the two segments are rotating in the same direction (Winter, 1990). During most of stance, the femoral, tibial and metatarsal segments rotated in the same direction. During terminal stance, only the femoral and metatarsal segments rotated in the same direction (Hodson, et al., 2001). Energy transfers among these three segments could enhance the efficiency of trotting gait.

Trotting horses use elastic energy conservation to minimize energy expenditure (Cavagna, et al., 1977; Minetti, et al., 1999). Net energy during stance in the trot was almost balanced (-0.018 J/kg), while at the walk energy was generated 0.098 J/kg during stance (Clayton, et al., 2001). Elastic energy storage and release in the hind limb contributed two-thirds of overall energy storage (Biewener, 1998). In this study the metatarsophalangeal, tarsal and femorotibial joints contributed to elastic energy storage and release. The elastic energy storage may come from a mechanical energy transfer in a proximal to distal direction when the body center of mass is decelerated downward and

backward until the middle of stance (Buchner, et al., 2000). Energy transfers might occur via the musculotendinous and ligamentous structures that connected the femoral, tibial and metatarsal segments. During the second half of stance, elastic energy release may result in energy transfer in a distal to proximal direction to accelerate the body center of mass upward and forward during the second half of stance. The gait during stance was balanced in net energy generation and absorption due to elastic spring around the metatarsophalangeal, tarsal and femorotibial joints, while energy generation at the coxofemoral joint was balanced by absorption at the distal interphalangeal joint, which acted as an energy damper.

Energy transfers might assist the proximal joints in moving the distal segments. During most of the swing, the femoral, tibial, metatarsal, pastern and hoof segments rotated accordingly (Hodson, et al., 2001). Most of the muscular activities during swing are around the proximal limb joints. During the first half of swing, the tensor fascia latae flexed the coxofemoral joint, while semitendinosus flexed the femorotibial joint. The tarsal joint flexed under the activity of cranial tibial muscle. During the second half of swing, the coxofemoral joint was extended by hamstring muscles, while the tarsal joint was extended by gastrocnemius. There was little activity in the digital flexors and extensors during swing. Therefore, the distal joints moved under the influence of the activity around proximal joints, probably via energy transfer through digital extensor and flexor tendons. In the bouncing gait, such as the trot, the elastic energy release from the end of stance may also contribute to the flexion of the limb during swing. Joint flexions bring the moment of inertia of the hind limb closer to the pivot point in the acetabulum, thus reducing the needed to accelerate and decelerate the entire limb during swing.

Therefore, the internal mechanical work required to move the body segments relative to the body center of mass at the trot is less than that at the walk (Minetti, et al., 1999). The combination of elastic energy storage and release and reduction in moment of inertia might explain the lower net mechanical energy of the limb during the whole stride at the trot (0.1014 J/kg) than that at the walk (0.161 J/kg) (Clayton, et al., 2001).

A proximal to distal temporal sequence of peak positive powers was consistently found in human sprinters, and was thought to be the appropriate sequence to generate high sprinting speed (Jacobs and van Ingen Schenau, 1992; Johnson and Buckley, 2001). In this study, the peak positive powers during the second half of stance were found sequentially in the coxofemoral joint (Max2) followed by the tarsal joint (Max2) and the metatarsophalangeal joint (Max), indicating a proximal to distal sequence of energy generation.

CONCLUSION

The coxofemoral and tarsal joints were the source of energy generation to move the limb throughout the stride. The coxofemoral joint protracts and retracts the entire limb, whereas the tarsal joint is more concerned with proximal and distal movement. The femorotibial joint was an important site of energy absorption during swing. The sources of elastic energy storage and release in the hind limb were the metatarsophalangeal, tarsal and femorotibial joints. The distal joints were driven by inertial forces during swing, following the active motion of the proximal joints.

CHAPTER 4

EFFECT OF UNILATERAL SYNOVITIS OF DISTAL INTERTARSAL AND TARSOMETATARSAL JOINTS ON SAGITTAL PLANE KINEMATICS AND KINETICS OF TROTTING HORSES: RESULTS AND DISCUSSION

LAMENESS AND PHYSICAL EXAMINATION

Before lameness induction, every horse had normal rectal temperature, pulse rate, respiratory rate, mucous membrane color, and capillary refill time, and the tarsal joint had a normal appearance. Rectal temperature increased by 0.6-2.0°F within 6-12 hours after induction, after which the rectal temperature gradually decreased to baseline values within 18 hours. None of the horses became inappetant during the observation period. All horses became lame within 4 hours after injection of endotoxin, but there were minimal changes in joint appearance and no swelling of the periarticular tissues.

Lameness evaluation performed 12 hours after endotoxin injection indicated lameness more severe than grade 3 in 3 horses (Horses no. 2, 3, 4), so 0.5-1 g of phenylbutazone was given orally to those horses. At the lameness evaluation 24 hours after endotoxin injection, three horses (Horses no.1, 2, 3) were lame at grade 2 or less and were ready for gait analysis. Horse no.4 was assessed as grade 2 lame at 30 hours after endotoxin injection. Within one week after synovitis induction, none of the horses was lame at the walk and lameness was minimal at the trot (less than grade 1). At this time the horses were returned to pasture.

EFFECT OF SYNOVITIS ON INTRA-LIMB COORDINATION

Test for differences in velocities. There was no significant difference in velocity between sound and lame conditions (P>0.05) (Table 4-1), therefore the differences in magnitude of the variables were not affected by subject velocities and could be interpreted as effects of synovitis of the distal intertarsal and tarsometatarsal joints.

Table 4-1 Statistical analysis comparing velocity (m/s) and velocity in dimensionless units of each limb between sound and lame conditions. Values are mean and (SD).

Horse no.	Velocity (m/s)		Velocity in dimensionless units		
	RF sound	RF lame	RF sound	RF lame	P value
1	2.91 (0.09)	2.87 (0.09)	0.77 (0.02)	0.76 (0.02)	0.45
2	2.91 (0.06)	2.88 (0.04)	0.76 (0.02)	0.75 (0.01)	0.38
3	2.83 (0.07)	2.87 (0.08)	0.74 (0.02)	0.75 (0.02)	0.31
4	2.82 (0.06)	2.79 (0.05)	0.75 (0.02)	0.74 (0.01)	0.36
Horse no.	**Velocity (m/s)**		**Velocity in dimensionless units**		
	LF sound	**LF lame**	**LF sound**	**LF lame**	**P value**
1	2.77 (0.13)	2.89 (0.18)	0.74 (0.04)	0.77 (0.05)	0.27
2	2.85 (0.05)	2.87 (0.03)	0.74 (0.01)	0.75 (0.01)	0.47
3	2.88 (0.07)	2.91 (0.07)	0.75 (0.02)	0.76 (0.02)	0.47
4	2.83 (0.06)	2.81 (0.07)	0.75 (0.02)	0.75 (0.02)	0.72
Horse no.	**Velocity (m/s)**		**Velocity in dimensionless units**		
	RH sound	**RH lame**	**RH sound**	**RH lame**	**P value**
1	2.85 (0.09)	2.85 (0.10)	0.74 (0.02)	0.76 (0.03)	0.92
2	2.88 (0.06)	2.90 (0.07)	0.74 (0.02)	0.75 (0.02)	0.31
3	2.82 (0.11)	2.83 (0.04)	0.74 (0.03)	0.74 (0.01)	0.89
4	2.83 (0.04)	2.78 (0.07)	0.76 (0.01)	0.74 (0.02)	0.16
Horse no.	**Velocity (m/s)**		**Velocity in dimensionless units**		
	LH sound	**LH lame**	**LH sound**	**LH lame**	**P value**
1	2.74 (0.06)	2.81 (0.05)	0.73 (0.02)	0.75 (0.01)	0.10
2	2.87 (0.07)	2.88 (0.05)	0.75 (0.02)	0.75 (0.01)	0.66
3	2.85 (0.08)	2.86 (0.07)	0.75 (0.02)	0.75 (0.02)	0.83
4	2.79 (0.04)	2.79 (0.06)	0.75 (0.01)	0.74 (0.02)	0.92

Kinematic variables. There were no significant differences (P>0.05) in stride duration, stance duration, swing duration or stride length between sound and lame conditions on the right hind limb. The range of vertical displacement of the talus during the stance phase was significantly smaller in the lame condition, with the mean difference (SD) between sound and lame conditions of 0.32 (0.18) cm. There were also significant decreases in tarsal and distal interphalangeal joint ranges of motion and a trend toward a decrease in coxofemoral joint peak extension (Max1) in the middle of the stance phase (Table 4-2). At the tarsal joint during stance, angular displacement between impact and peak Min1 (tarsal joint range of flexion) and angular displacement between peak Min2 and the angle obtained at the end of stance (tarsal joint range of extension), had trends toward a decrease in range of motion (P=0.06 and P=0.09, respectively), with mean differences (SD) of 2.68 (1.81) and 1.42 (1.12) degrees, respectively. During the swing phase, there was a significant increase in vertical displacement of the tuber coxae and a trend toward a decrease in distal interphalangeal joint vertical displacement (P=0.09), with mean differences (SD) of 0.61 (0.37) and 1.31 (1.10) cm, respectively.

Ground reaction forces. Figure 4-1 illustrates the vertical and longitudinal ground reaction force (GRF) profiles from the right hind limb in sound and lame conditions. Peak vertical force of the right hind limb was significantly lower in the lame condition compared with the sound condition. There were trends toward decreases in vertical impulse (P=0.06) and peak propulsive force (P=0.09) in the right hind limb (Table 4-2).

Net joint moments, net joint powers and net joint energies. Several variables in this category showed significant differences and trends toward differences between sound and lame conditions. During stance (Table 4-2), there was a decrease in positive work (energy Max2) at the femorotibial joint. At the tarsal joint, the main findings were a lower negative power peak (power Min1) with a trend toward decreased energy absorption (energy Min1) during initial stance, and a significant reduction in peak power and energy generation during late stance (power Max2 and energy Max2). The distal interphalangeal joint showed trends toward decreases in energy generation (energy Max) during initial stance and energy absorption (power Min and energy Min) during the second half of stance.

During the swing phase (Table 4-3), the femorotibial joint absorbed less energy as the joint was passively extended during the second half of swing (energy Min2). The tarsal joint showed a decrease in peak flexor moment (Min1) and a trend toward decrease in energy generation (energy Max1) in early swing. In late swing, the tarsal extensors produced a smaller power peak (power Max2) without a decrease in energy generation. Both the metatarsophalangeal and distal interphalangeal joints showed significant reductions in energy absorption (energy Min1, both joints) as the joints flexed during the initial swing phase.

The kinematic and kinetic variables reported in Tables 4.2 and 4.3 are those that showed significant differences ($P<0.05$) and trends toward differences ($0.05<P<0.1$) between sound and lame conditions as shown in Figures 4-1 to 4-11. Tables with complete data for all variables are shown in Appendix B.

Table 4-2 Differences between sound and lame conditions in variables that differed significantly or showed a trend toward a significant difference during the stance phase of the right hind limb.

Joint	Variables	Mean difference	SD
Ground reaction force	Vertical force Max (N/kg)	-0.312 [a]	0.182
	Vertical impulse (Ns/kg)	-0.052 [b]	0.034
	Longitudinal force Max3 (N/kg)	-0.089 [b]	0.073
Coxofemoral	Joint angle Max1 (degrees)	-1.28 [b]	0.97
Femorotibial	Net joint energy Max2 (J/kg)	-0.008 [a]	0.004
Tarsal	Joint range of motion (degrees)	-2.20 [a]	1.28
	Net joint power Max2 (W/kg)	-0.374 [a]	0.060
	Net joint power Min1 (W/kg)	-0.597 [a]	0.306
	Net joint energy Max2 (J/kg)	-0.023 [a]	0.005
	Net joint energy Min1 (J/kg)	-0.022 [b]	0.015
	Total positive energy (J/kg)	-0.028 [a]	0.015
	Total negative energy (J/kg)	-0.033 [a]	0.020
Metatarsophalangeal	Net joint moment Min (Nm/kg)	-0.034 [a]	0.017
Distal interphalangeal	Joint range of motion (degrees)	-5.21 [a]	2.00
	Net joint moment Min (Nm/kg)	-0.058 [b]	0.044
	Net joint power Min (W/kg)	-0.770 [b]	0.620
	Net joint energy Max (J/kg)	-0.012 [b]	0.009
	Net joint energy Min (J/kg)	-0.056 [b]	0.043

Negative mean differences indicate values were higher in the sound condition than in the lame condition. [a] $P<0.05$. [b] $0.05<P<0.1$.

Table 4-3 Differences between sound and lame conditions in variables that differed significantly or showed a trend toward a significant difference during the swing phase of the right hind limb.

Joint	Variables	Mean difference	SD
Femorotibial	Net joint moment Max (Nm/kg)	-0.0142 [b]	0.0094
	Net joint power Min2 (W/kg)	-0.1138 [b]	0.0897
	Net joint energy Min2 (J/kg)	-0.0069 [a]	0.0035
	Total negative energy (J/kg)	-0.0121 [b]	0.0091
Tarsal	Net joint moment Min (Nm/kg)	-0.0065 [a]	0.0036
	Net joint power Max2 (W/kg)	-0.0859 [a]	0.0431
	Net joint energy Max1 (J/kg)	-0.0042 [b]	0.0029
	Total positive energy (J/kg)	-0.0089 [b]	0.0063
Metatarsophalangeal	Net joint power Max1 (W/kg)	-0.0058 [a]	0.0033
	Net joint power Max2 (W/kg)	-0.0047 [b]	0.0040
	Net joint power Min1 (W/kg)	-0.0247 [b]	0.0161
	Net joint energy Max1 (J/kg)	-0.0002 [b]	0.0002
	Net joint energy Max2 (J/kg)	-0.0001 [a]	0.00003
	Net joint energy Min1 (J/kg)	-0.0013 [a]	0.0005
	Total negative energy (J/kg)	-0.0025 [a]	0.0014
Distal interphalangeal	Net joint moment Max (Nm/kg)	-0.0009 [a]	0.0006
	Net joint power Max1 (W/kg)	-0.0021 [a]	0.0010
	Net joint power Max2 (W/kg)	-0.0015 [a]	0.0008
	Net joint power Min1 (W/kg)	-0.0109 [a]	0.0057
	Net joint energy Max1 (J/kg)	-0.0001 [a]	0.00004
	Net joint energy Min1 (J/kg)	-0.0004 [a]	0.0003
	Net joint energy Min2 (J/kg)	-0.0001 [b]	0.0001
	Total positive energy (J/kg)	-0.0002 [b]	0.0001
	Total negative energy (J/kg)	-0.0005 [a]	0.0003

Negative mean differences indicate values were higher in the sound condition than in the lame condition. [a] $P<0.05$. [b] $0.05<P<0.1$.

Figure 4-1 Vertical and longitudinal ground reaction force data from the right hind limb. The thick black line and dashed lines indicate the mean value and one standard deviation above and below the mean of the sound condition. The thick gray line indicates mean of the lame condition. Dot represents variable that differs significantly between sound and lame conditions. [a] $P<0.05$. [b] $0.05<P<0.1$.

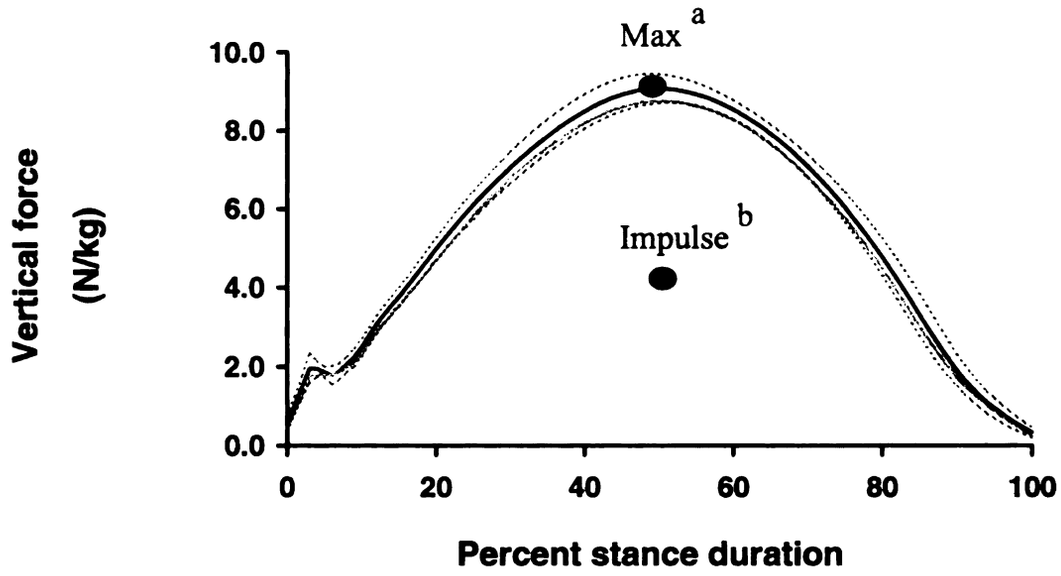

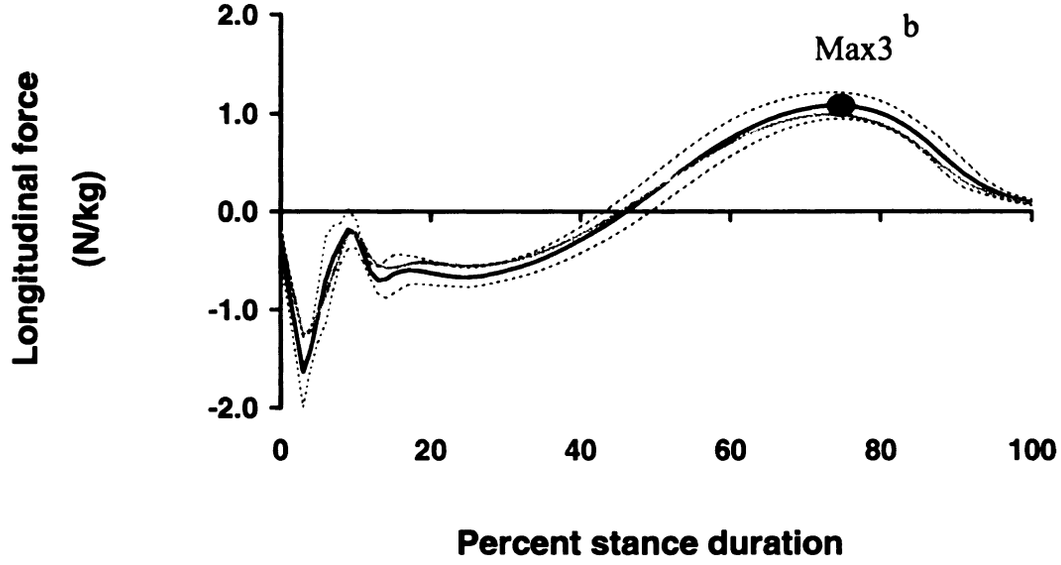

Figure 4-2 Kinematic and kinetic variables of the right coxofemoral joint during stance. The thick black line and dashed lines indicate the mean value and one standard deviation above and below the mean of the sound condition. The thick gray line indicates mean of the lame condition. Dot represents variable that differs significantly between sound and lame conditions. [a] $P<0.05$. [b] $0.05<P<0.1$.

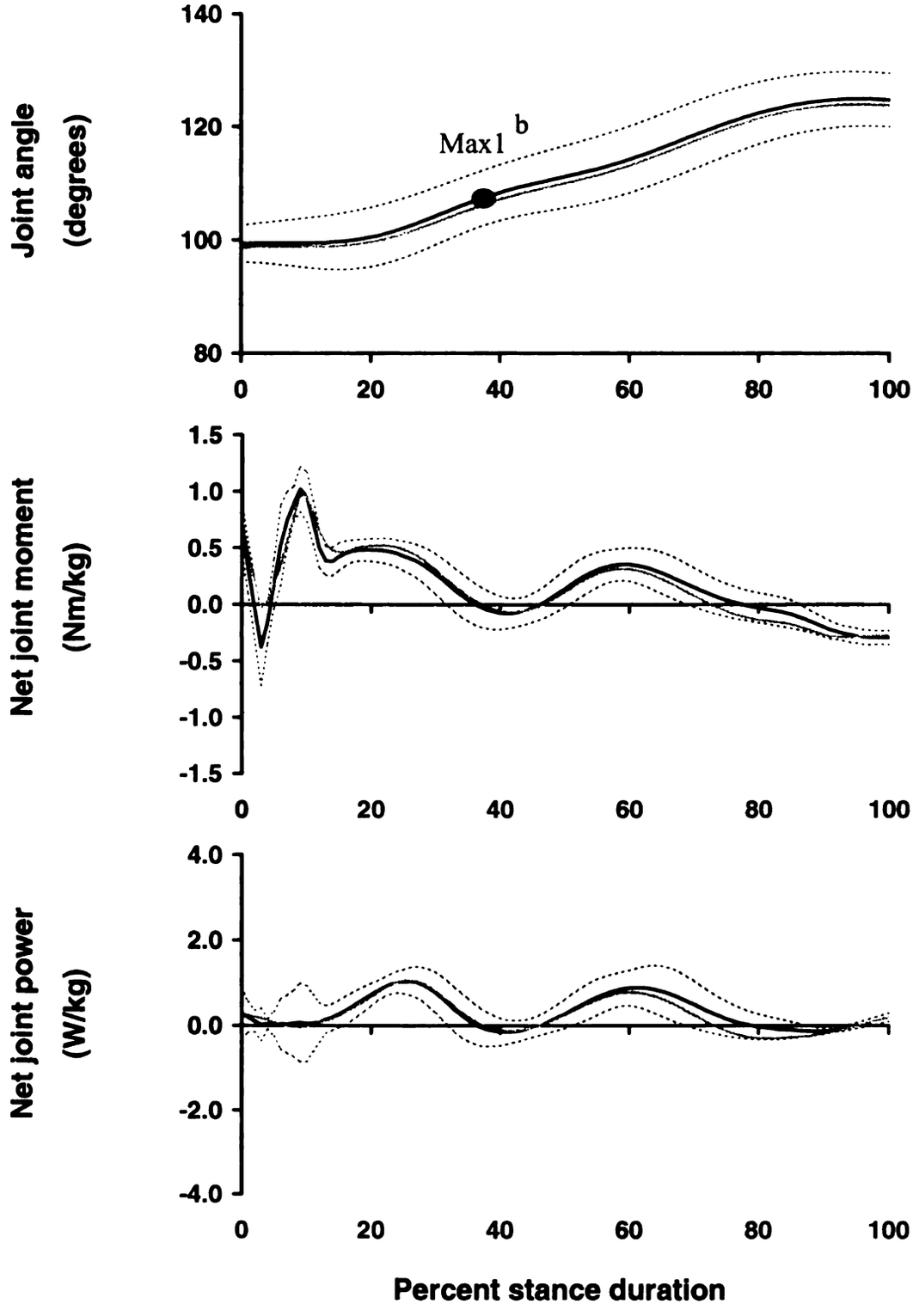

Figure 4-3 Kinematic and kinetic variables of the right coxofemoral joint during swing. The thick black line and dashed lines indicate the mean value and one standard deviation above and below the mean of the sound condition. The thick gray line indicates mean of the lame condition.

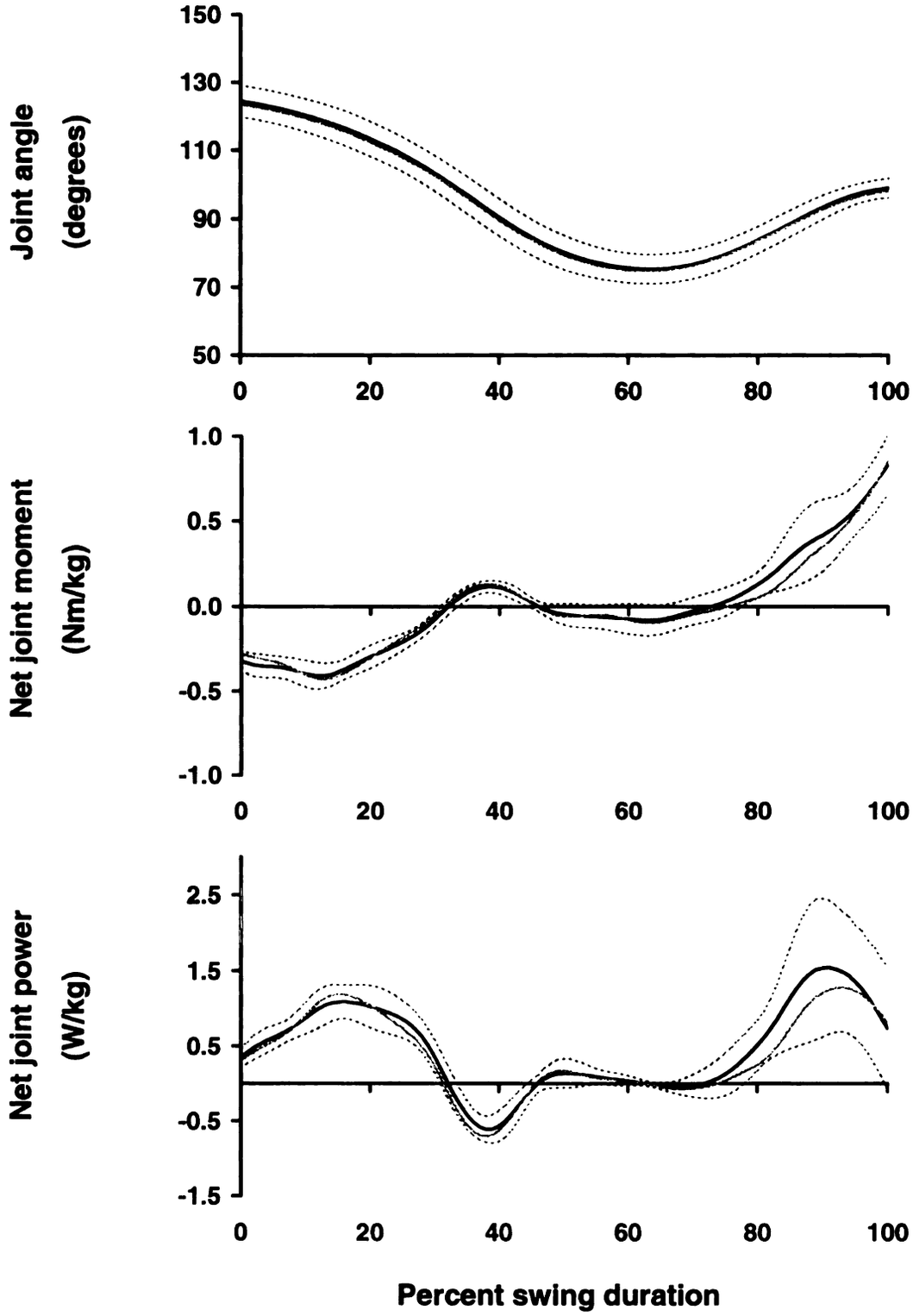

Figure 4-4 Kinematic and kinetic variables of the right femorotibial joint during stance. The thick black line and dashed lines indicate the mean value and one standard deviation above and below the mean of the sound condition. The thick gray line indicates mean of the lame condition. Dot represents variable that differs significantly between sound and lame conditions. [a] $P<0.05$. [b] $0.05<P<0.1$.

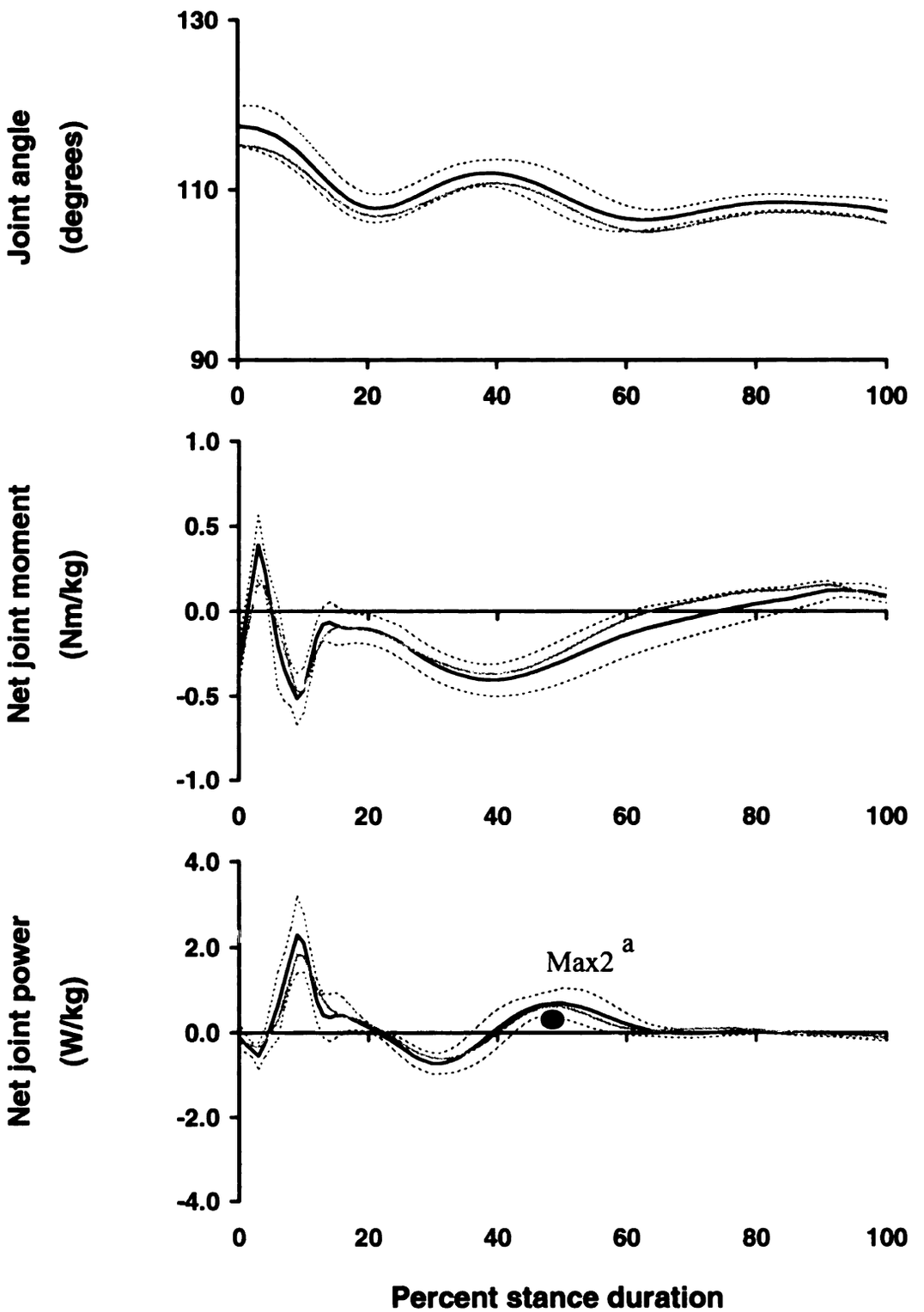

Figure 4-5 Kinematic and kinetic variables of the right femorotibial joint during swing. The thick black line and dashed lines indicate the mean value and one standard deviation above and below the mean of the sound condition. The thick gray line indicates mean of the lame condition. Dot represents variable that differs significantly between sound and lame conditions. [a] $P<0.05$. [b] $0.05<P<0.1$.

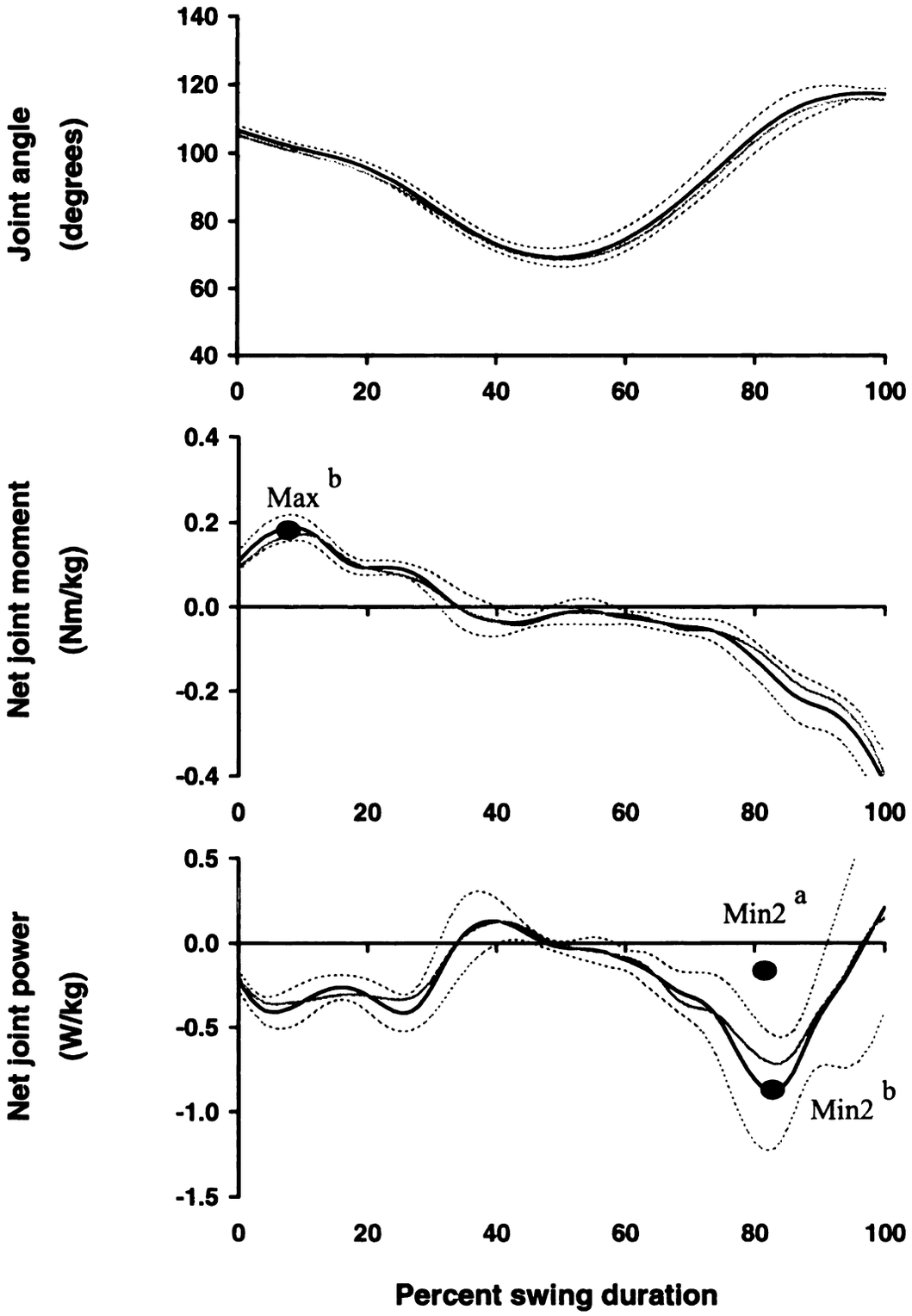

Figure 4-6 Kinematic and kinetic variables of the right tarsal joint during stance. The thick black line and dashed lines indicate the mean value and one standard deviation above and below the mean of the sound condition. The thick gray line indicates mean of the lame condition. Dot represents variable that differs significantly between sound and lame conditions. [a] $P<0.05$. [b] $0.05<P<0.1$.

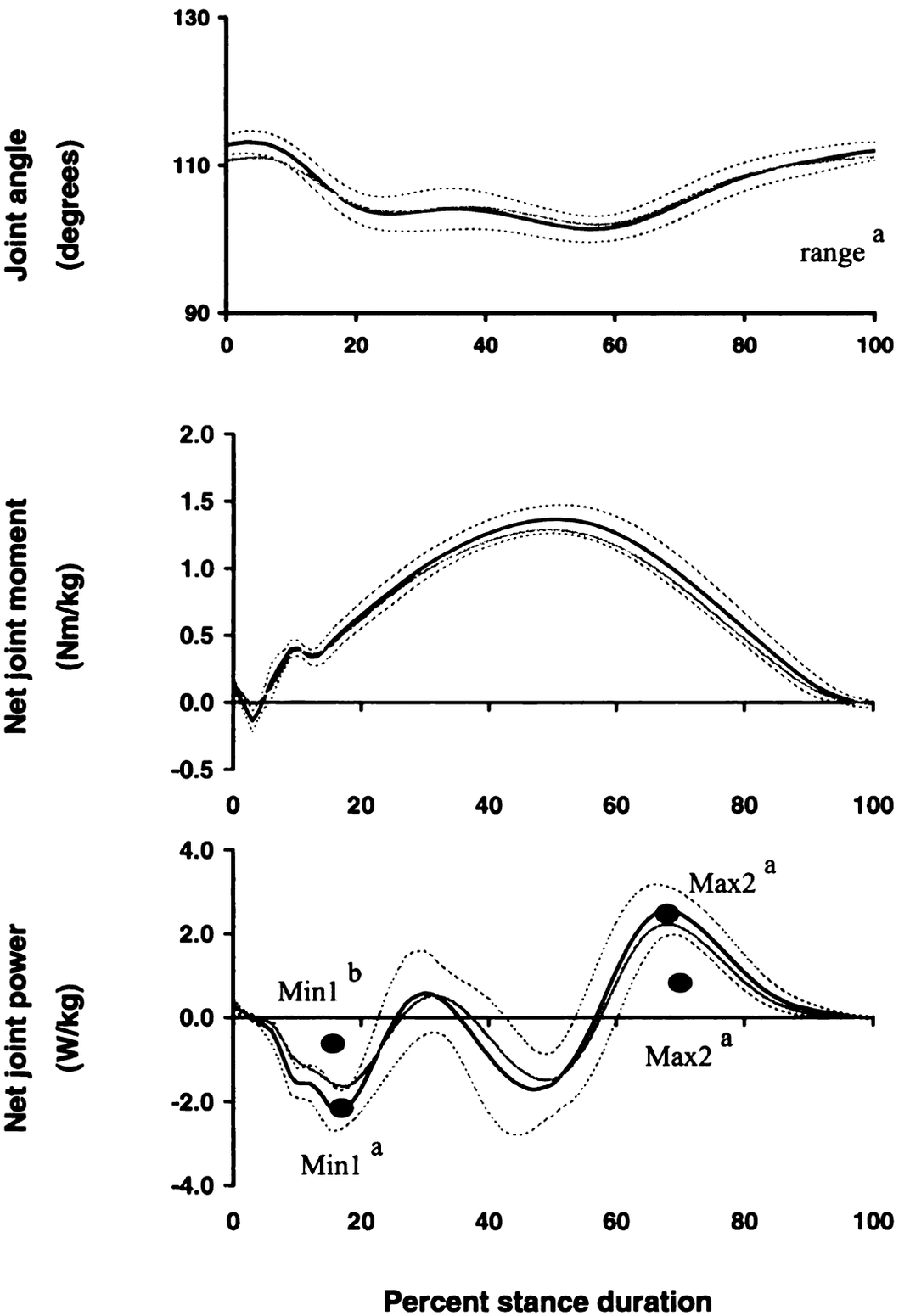

Figure 4-7 Kinematic and kinetic variables of the right tarsal joint during swing. The thick black line and dashed lines indicate the mean value and one standard deviation above and below the mean of the sound condition. The thick gray line indicates mean of the lame condition. Dot represents variable that differs significantly between sound and lame conditions. [a] $P<0.05$. [b] $0.05<P<0.1$.

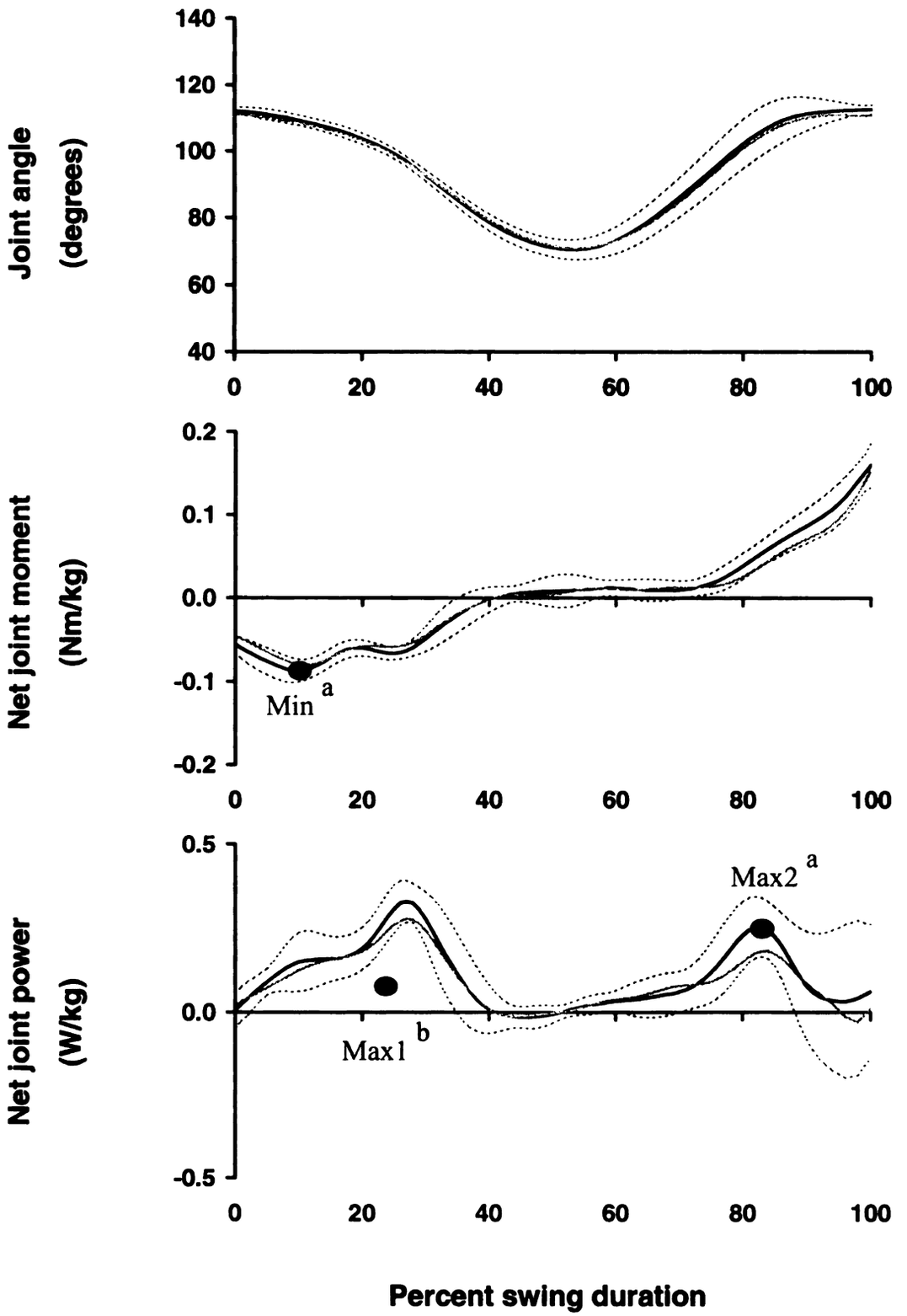

Figure 4-8 Kinematic and kinetic variables of the right metatarsophalangeal joint during stance. The thick black line and dashed lines indicate the mean value and one standard deviation above and below the mean of the sound condition. The thick gray line indicates mean of the lame condition. Dot represents variable that differ significantly between sound and lame conditions. [a] $P<0.05$. [b] $0.05<P<0.1$.

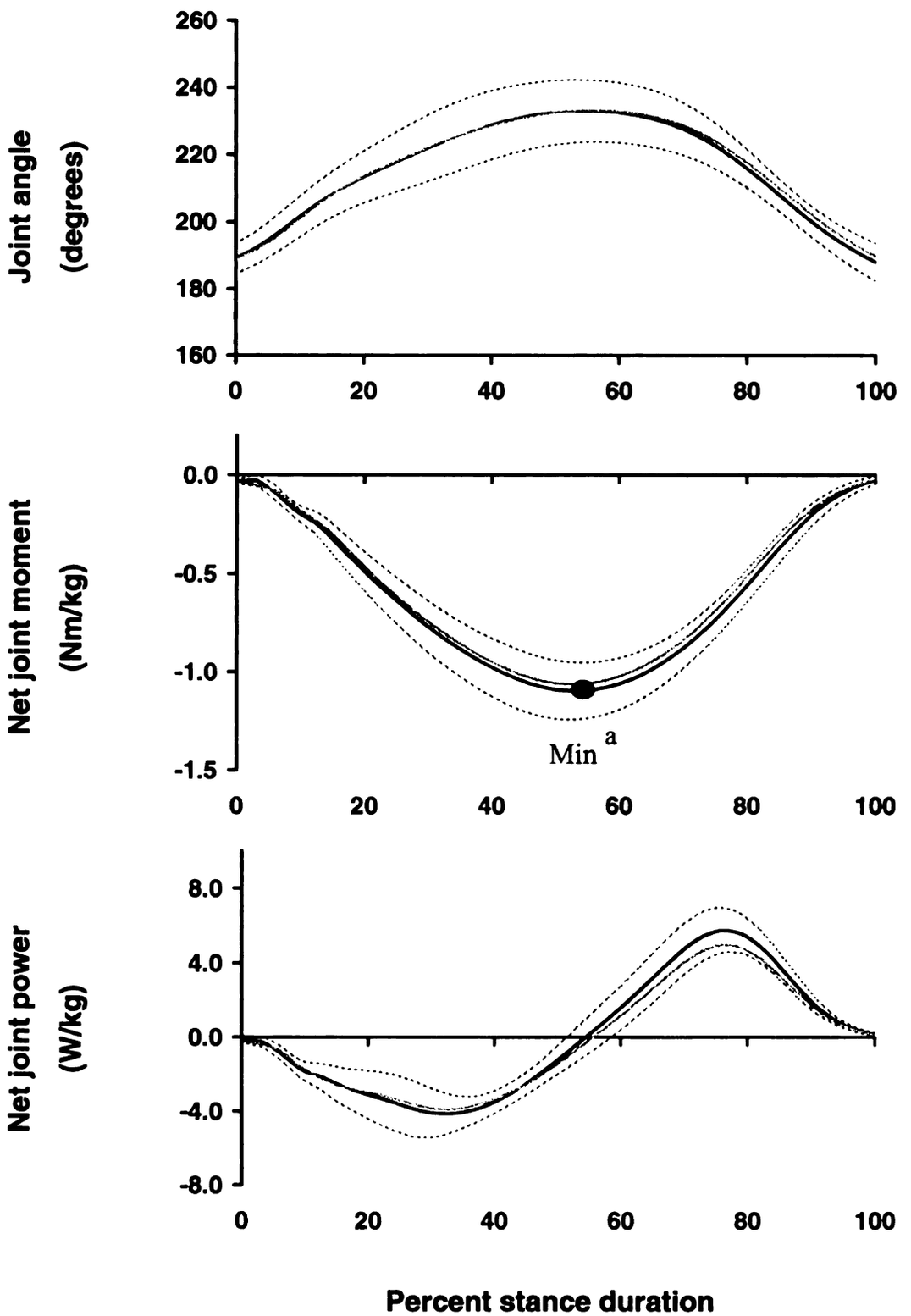

Figure 4-9 Kinematic and kinetic variables of the right metatarsophalangeal joint during swing. The thick black line and dashed lines indicate the mean value and one standard deviation above and below the mean of the sound condition. The thick gray line indicates mean of the lame condition. Dot represents variable that differs significantly between sound and lame conditions. [a] $P<0.05$. [b] $0.05<P<0.1$.

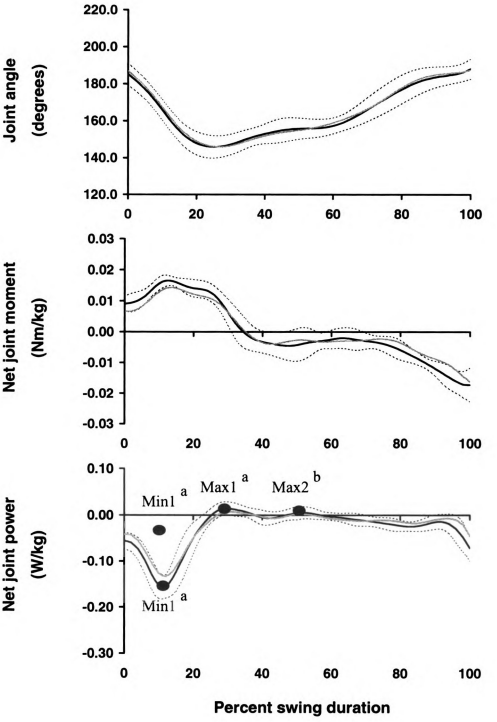

Figure 4-10 Kinematic and kinetic variables of the right distal interphalangeal joint during stance. The thick black line and dashed lines indicate the mean value and one standard deviation above and below the mean of the sound condition. The thick gray line indicates mean of the lame condition. Dot represents variable that differs significantly between sound and lame conditions. [a] $P<0.05$. [b] $0.05<P<0.1$.

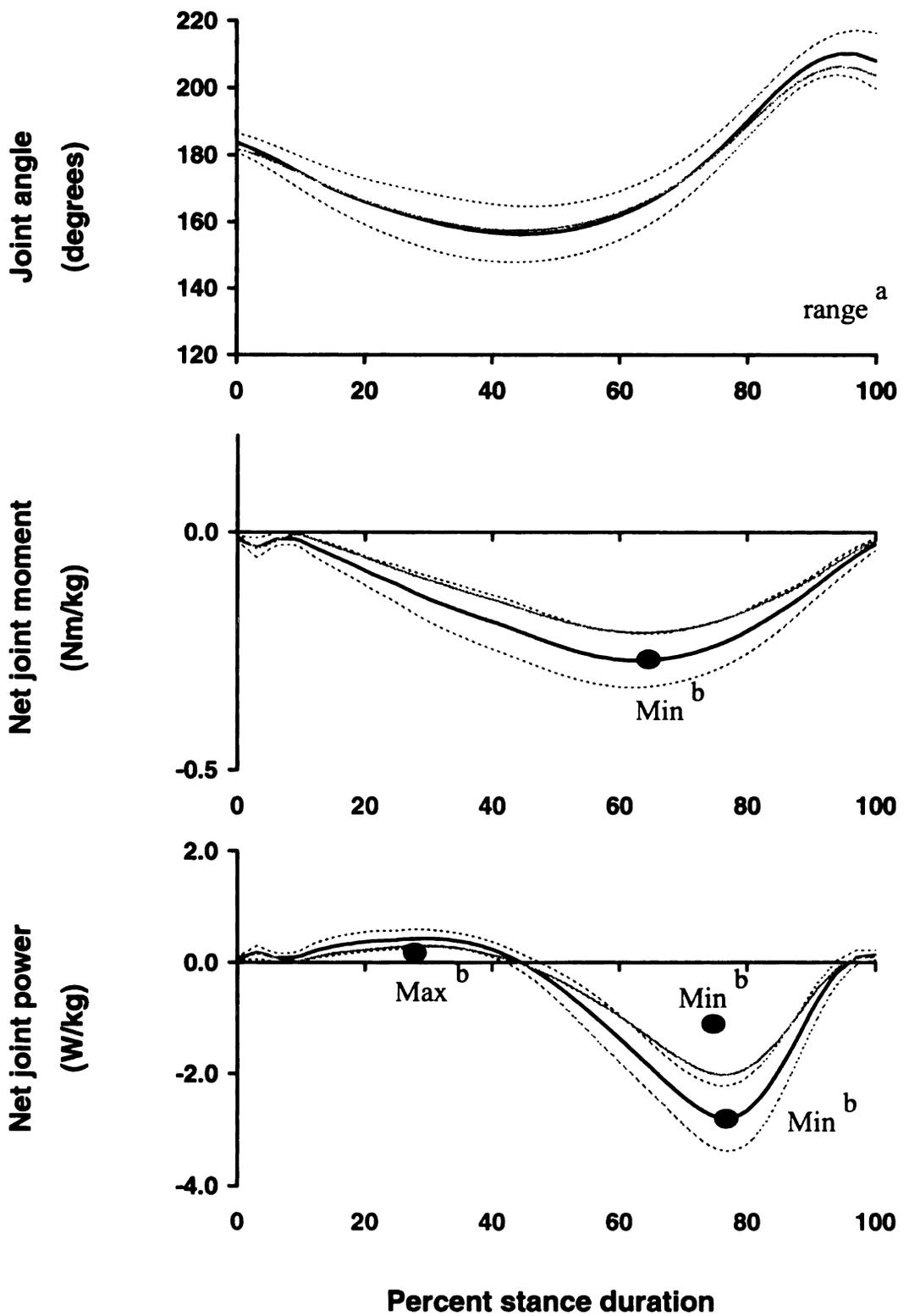

Figure 4-11 Kinematic and kinetic variables of the right distal interphalangeal joint during swing. The thick black line and dashed lines indicate the mean value and one standard deviation above and below the mean of the sound condition. The thick gray line indicates mean of the lame condition. Dot represents variable that differs significantly between sound and lame conditions. [a] $P<0.05$. [b] $0.05<P<0.1$.

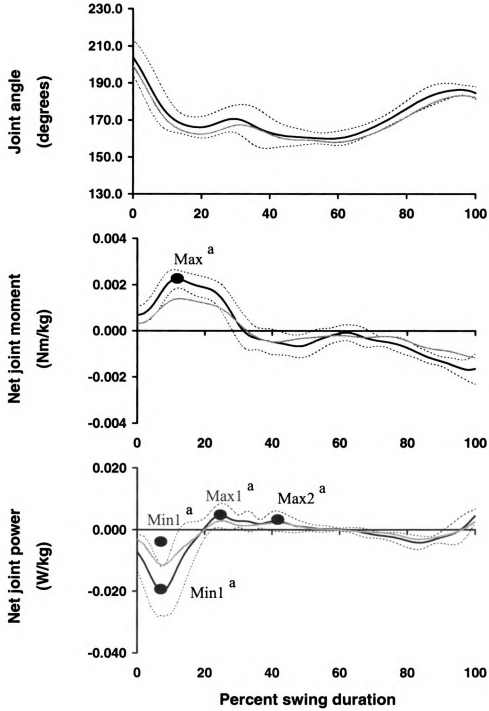

FORELIMB VARIABLES IN THE SOUND CONDITION

Before comparing forelimb variables between the sound and lame conditions, a brief explanation of the biomechanical profiles of the forelimbs in the sound condition will be given. Kinematic, ground reaction force, net joint moment and net joint power patterns from both forelimbs in this study were similar to previous studies (Clayton, et al., 1998a; Lanovaz, et al., 1999; Clayton, et al., 2000c). The peak values of some variables were slightly different, which may be due to breed differences. During the stance phase, the net joint moment was mainly on the cranial side of the scapulohumeral joint, which was the extensor side. The other joints had the net joint moment on the caudal/palmar side, which was the extensor side of the cubital joint and the flexor side of the carpal, metacarpophalangeal and distal interphalangeal joints (Figure 4-12). During limb protraction in the first half of swing, the net joint moment was on the cranial/dorsal side of all joints, which was an extensor moment for all except the cubital joint. When the limb was retracted in the second half of swing, the net joint moment moved to the caudal/palmar side of all joints (Figure 4-13).

Net joint power profiles during the stance phase (Figure 4-14) showed evidence of elastic energy storage and release patterns at the scapulohumeral, cubital, carpal and metacarpophalangeal joints. The distal interphalangeal joint performed mostly negative work. During the swing phase (Figure 4-15), the cubital joint was the only joint that performed positive work, with bursts of energy generation in early swing and late swing. At the other joints, the amount of energy absorption decreased in a proximal to distal sequence.

Figure 4-12 Net joint moment profiles at the scapulohumeral, cubital, carpal, metacarpophalangeal and distal interphalangeal joints averaged from both forelimbs of sound trotting horses during the stance phase. The heavy line is the mean curve and the two lighter lines indicate one standard deviation.

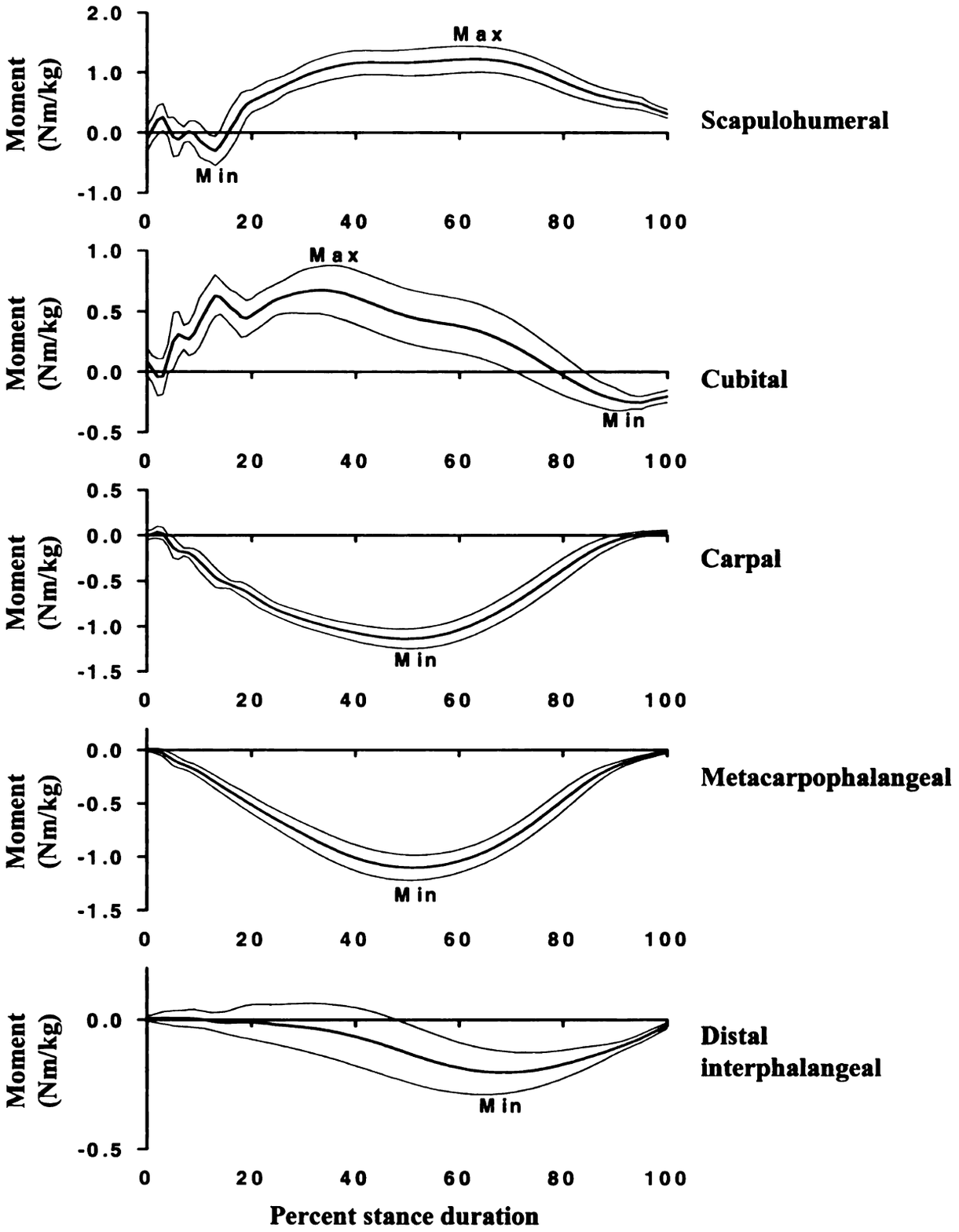

Figure 4-13 Net joint moment profiles at the scapulohumeral, cubital, carpal, metacarpophalangeal and distal interphalangeal joints averaged from both forelimbs of sound trotting horses during the swing phase. The heavy line is the mean curve and the two lighter lines indicate one standard deviation.

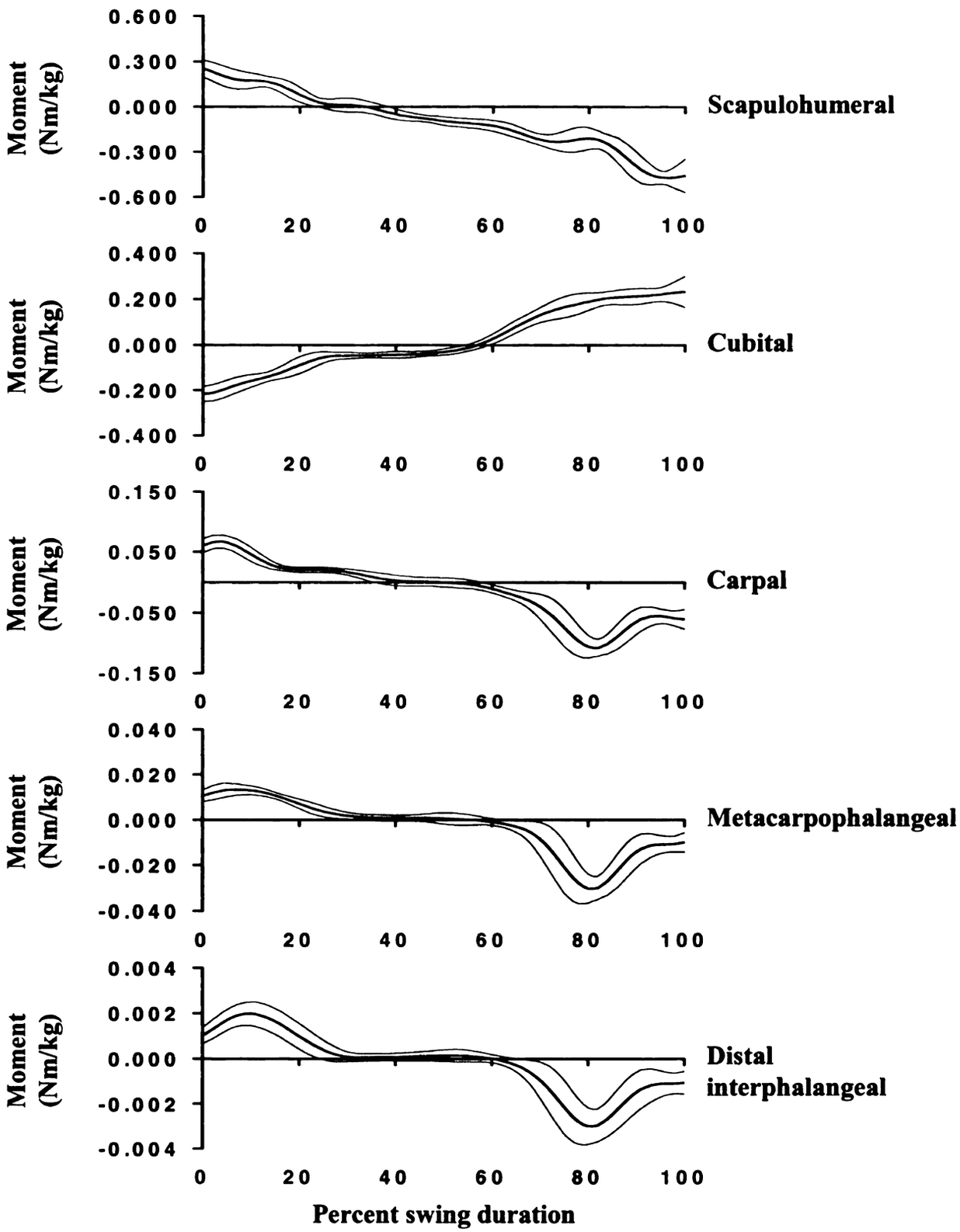

Figure 4-14 Net joint power profiles at the scapulohumeral, cubital, carpal, metacarpophalangeal and distal interphalangeal joints averaged from both forelimbs of sound trotting horses during the stance phase. The heavy line is the mean curve and the two lighter lines indicate one standard deviation.

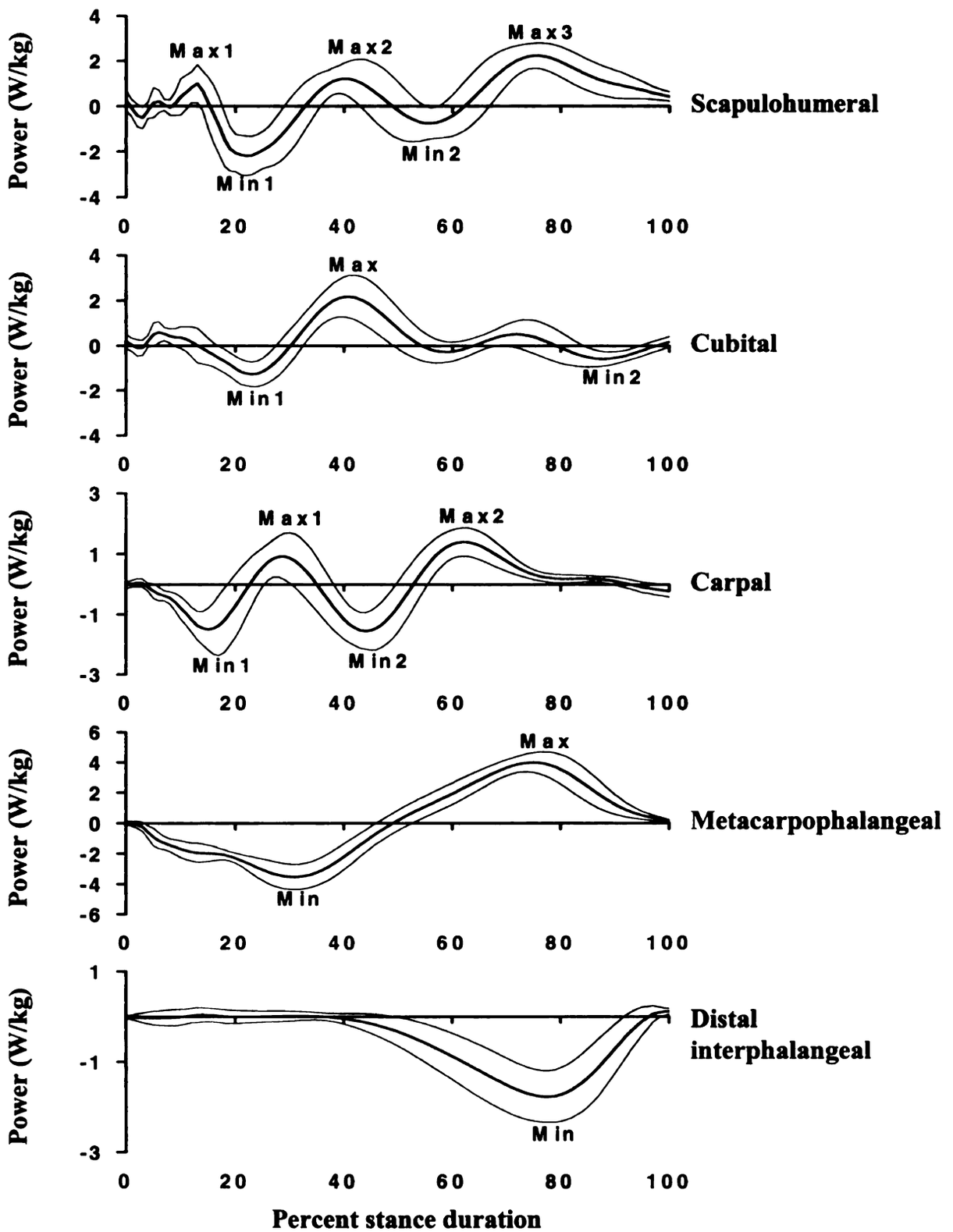

Figure 4-15 Net joint power profiles at the scapulohumeral, cubital, carpal, metacarpophalangeal and distal interphalangeal joints averaged from both forelimbs of sound trotting horses during the swing phase. The heavy line is the mean curve and the two lighter lines indicate one standard deviation.

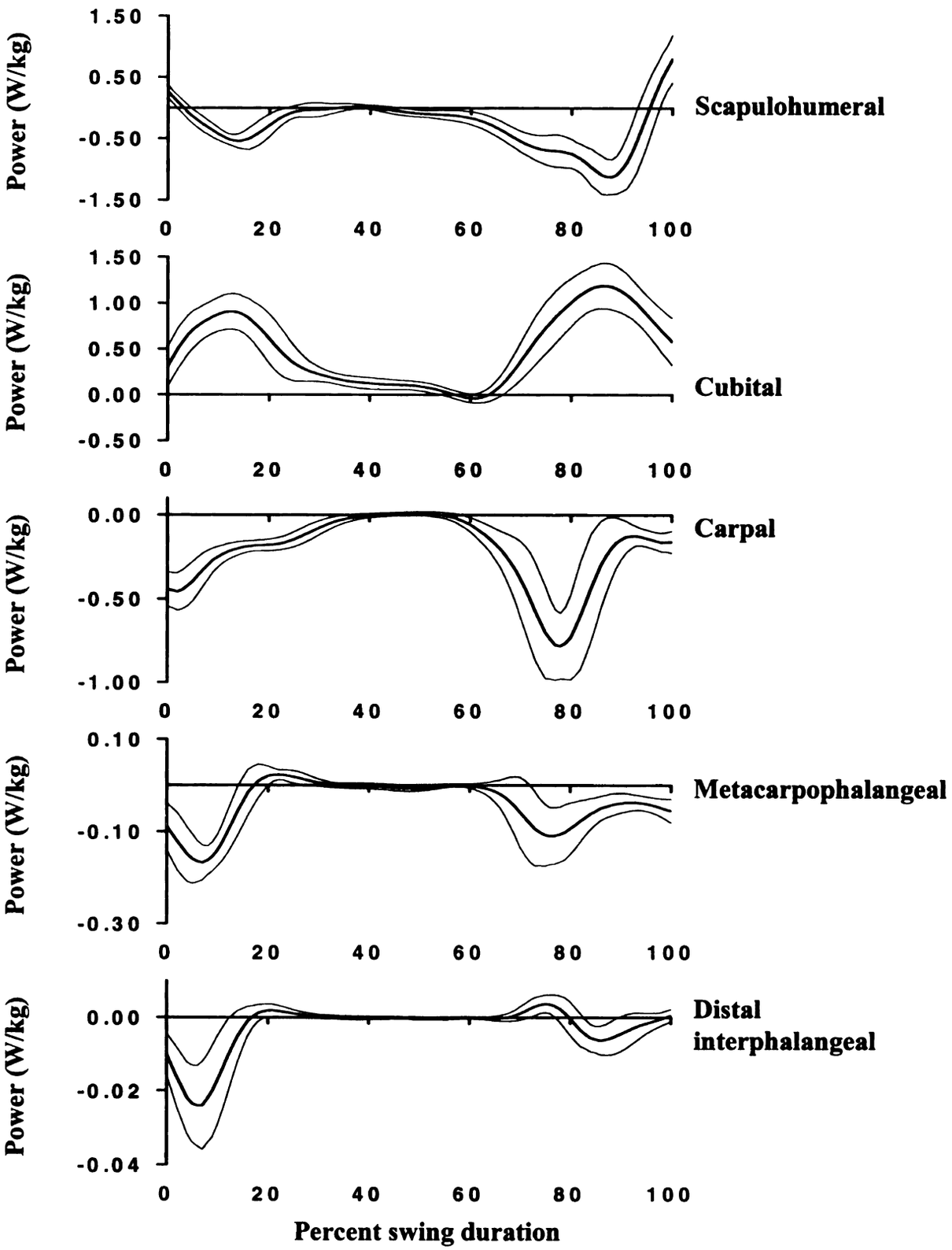

INTER-LIMB COMPENSATION FOR LAMENESS OF THE RIGHT HIND LIMB

Kinematic variables. Data were collected at the similar velocity in the sound and lame conditions. There were no significant differences ($P>0.05$) in stride, stance and swing duration, or stride length in the compensating left hind limb, left forelimb or right forelimb. To assess the asymmetrical motion of the tuber coxae in the lame condition, the quotient of tuber coxae range of vertical displacement between the right and left hind limbs during stance of each horse was calculated (Buchner, et al., 1996c). In the sound condition, all horses had a slightly bigger range of tuber coxae displacement on the right side than on the left side as shown by the quotient values greater than one (Table 4.4). In the lame condition, three of the four horses had smaller quotient than in the sound condition, indicating a relative increase in displacement of the left tuber coxae. Further evaluation showed a significant increase in vertical displacement of the left tuber coxae during the stance phase with a mean difference (SD) of 0.23 (0.13) cm. There was also a trend toward an increase in distal hoof wall vertical displacement ($P=0.09$) during the swing phase of the left hind limb, with a mean difference of 0.5 (0.4) cm.

Ground reaction forces. There were changes in GRF in the left (contralateral) fore and hind limbs. In the left hind limb, there was a trend toward an increase in peak vertical force ($P=0.08$) and a significant decrease in braking impulse ($P<0.05$), with mean differences (SD) of 0.170 (0.133) N/kg and 0.007 (0.004) Ns/kg, respectively. The left forelimb showed a significant decrease in vertical impulse ($P<0.05$) in the lame condition, with a mean difference of 0.050 (0.023) Ns/kg.

To assess the compensating pattern of load distribution, the center of vertical load distribution between the four limbs in the lame condition was calculated in each horse and plotted with the values from the sound condition (Figure 4-16). In three horses, the load distribution was shifted to the left in the lame condition, while Horse no.2 had different pattern by shifting the load to the right side of the body.

The symmetry index expressed as a percent quotient between the hind limb pair (Weishaupt, et al., 2001) was applied to the vertical impulse in this study. The symmetry index (Table 4-5) of Horses no.1 and 4 indicated a smaller vertical impulse in the right hind limb in the lame condition, whereas the symmetry index in Horses no.2 and 3 did not change. A similar calculation was applied within the same limb to determine a quotient for the vertical impulse (Table 4-6). All horses, except Horse no.2, showed a decrease in vertical impulse in the lame condition of the right hind limb, but only Horses no.1 and 4 showed a compensatory increase in vertical impulse in the left hind limb.

Net joint moments, net joint powers and net joint energies. Significant differences or trends toward differences were found in limbs that showed significant differences in kinematic and GRF variables. During stance, the only significant change in the left hind limb (Table 4-7) was an increase in the metatarsophalangeal joint peak flexor moment (Min). During swing, there was an increase in magnitude of peak flexor moment at the coxofemoral joint (moment Min1) and an increase in peak positive power (power Max1) in early swing. In terminal swing, the coxofemoral joint generated less energy (energy Max2) and the femorotibial joint had smaller peak negative power (power Min1).

In the left forelimb stance phase (Table 4-8), there were significant decreases in peak flexor moments at the carpal and metacarpophalangeal joints. The metacarpophalangeal joint also showed a trend toward a decrease in peak negative power (power Min1) and elastic energy storage (energy Min1) in early stance. The only joint that showed a significant decrease in energy generation was the carpal joint (energy Max2).

Figure 4-16 Load distribution of vertical impulse of 4 horses. The black dot represents the value in the sound condition. The gray dot represents the value in the lame condition. Arrow represents the direction of load distribution changes in each horse.

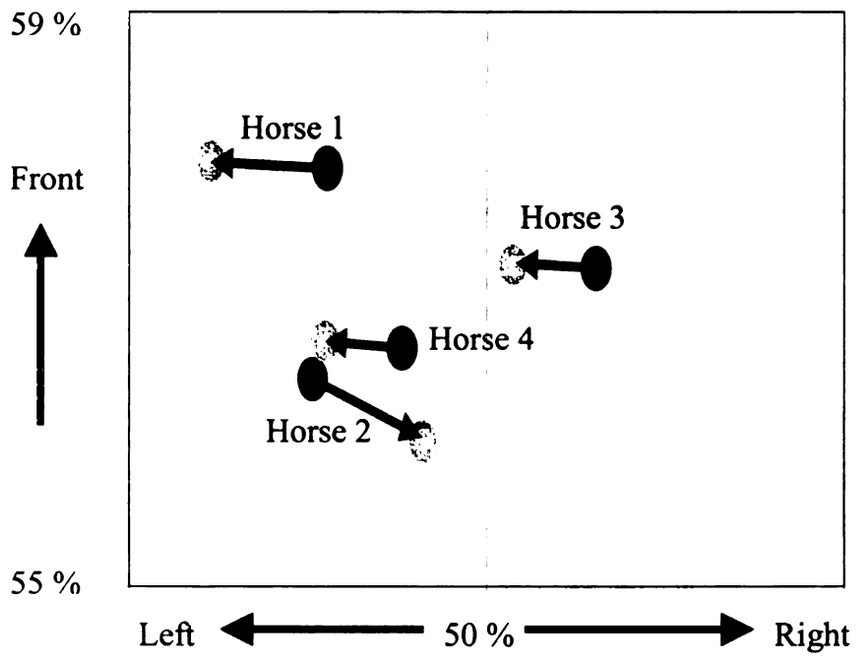

Table 4-4 Symmetry index as a quotient value of difference of tuber coxae displacement between the hind limb pair from the sound and lame conditions. Values greater than one mean the displacement range is greater in the right hind limb than the left hind limb.

	Horse 1	Horse 2	Horse 3	Horse 4
Sound condition	1.00	1.11	1.03	1.08
Lame condition	0.98	1.13	1.00	0.97

Table 4-5 Symmetry index as a percent quotient of difference of vertical impulses between the hind limb pair from the sound and lame conditions. Negative values mean the impulse is greater in the left hind limb than the right hind limb.

	Horse 1	Horse 2	Horse 3	Horse 4
Sound condition	1%	-1%	0%	-1%
Lame condition	-2%	-1%	0%	-4%

Table 4-6 Symmetry index as a percent quotient of difference of vertical impulses between the sound and lame conditions in the same hind limb. Negative values mean the impulse is greater in the sound condition than the lame condition.

	Horse 1	Horse 2	Horse 3	Horse 4
Right hind limb	-3%	0%	-2%	-3%
Left hind limb	1%	-1%	-1%	2%

Table 4-7 Differences between sound and lame conditions in variables that differed significantly or showed a trend toward a significant difference during stance and swing phases of the left hind limb.

Joint (Stance or Swing)	Variables	Mean difference	SD
Coxofemoral (Swing)	Net joint moment Min1 (Nm/kg)	0.047 [a]	0.021
	Net joint moment Min2 (Nm/kg)	-0.023 [b]	0.018
	Net joint power Max1 (Nm/kg)	0.139 [a]	0.073
	Net joint energy Max2 (J/kg)	-0.020 [b]	0.017
Femorotibial (Swing)	Net joint power Min1 (W/kg)	-0.115 [a]	0.029
Metatarsophalangeal (Stance)	Net joint power Min (W/kg)	0.291 [a]	0.128
Metatarsophalangeal (Swing)	Net joint power Max1 (W/kg)	-0.0035 [b]	0.0029
	Total positive energy (J/kg)	-0.0003 [a]	0.0001
Distal interphalangeal (Swing)	Net joint energy Max2 (J/kg)	-0.0001 [b]	0.00004

Negative mean differences indicate values were higher in the sound condition than in the lame condition. [a] $P<0.05$. [b] $0.05<P<0.1$.

Table 4-8 Differences between sound and lame conditions in variables that differed significantly or showed a trend toward a significant difference during stance phases of the left fore limb.

Joint	Variables	Mean difference	SD
Carpus	Net joint moment Min (Nm/kg)	-0.104 [a]	0.049
	Net joint energy Max2 (J/kg)	-0.013 [a]	0.005
Metacarpophalangeal	Net joint moment Min (Nm/kg)	-0.051 [a]	0.028
	Net joint power Min (W/kg)	-0.468 [b]	0.327
	Net joint energy Min (J/kg)	-0.019 [b]	0.015

Negative mean differences indicate values were higher in the sound condition than in the lame condition. [a] $P<0.05$. [b] $0.05<P<0.1$.

DISCUSSION

Lameness model. The ability to induce a transient lameness in sound horses offers an important and reliable method to study the locomotor pattern in horses with a specific, well-defined lameness in a controlled manner that minimizes individual variations (Buchner, 2001b). The lameness model used in this study has been used previously to study the effect of pain in the distal tarsal joints on two-dimensional hind limb kinematics (Kramer, et al., 2000). In that study, the induction procedures were slightly different from those reported here; phosphate buffered saline was used to dilute the endotoxin and there was an injection of contrast solution into the distal tarsal joints before endotoxin injection. Soft tissue swelling extended distally to the proximal or mid metatarsus in all horses in that study, which may be for two reasons. Firstly, the use of phosphate buffered saline could cause irritation to the joint. Secondly, the distal intertarsal joint is narrow, and if the volume of fluid injected into the joint exceeded the total volume of the joint space, there might be some leakage into periarticular tissue during withdrawal of the needle. The non-steroidal anti-inflammatory medication administered in this study helped to reduce inflammation and decreased the time between induction and gait analysis.

Endotoxin induced synovial membrane inflammation. The lameness model used in this study induced pain in the distal tarsal joints, which are the most common site of tarsal osteoarthritis. The painful sensation may be slightly different from that of naturally occurring osteoarthritis. Degeneration of high-load low motion joints is likely due to trauma to the periarticular soft tissues (Pool, 1996), leading to degeneration of

cartilage and subchondral bone sclerosis. Furthermore, in the natural disease pain may be associated with different events in the stride cycle, and horses may learn to accommodate over a period of time. The effects of the tarsal synovitis model represent a general response to pain in the distal tarsal joints, but the effects may not be identical to the natural disease.

Effects of synovitis on symmetry of motion and vertical impulse of hind limbs. Clinical evaluation in the equine hind limb is based on symmetry of left and right gluteal rises. But it is recognized that, in mild lameness, the gluteal rise may be symmetrical, which makes it difficult to identify the lame limb (Stashak, 1987). Several kinematic studies have assessed asymmetrical motion in hind limb lameness (Buchner, et al., 1993; Buchner, et al., 1996c; Pourcelot, et al., 1997a). Comparison between vertical displacement of the left and right tuber coxae or tuber sacrale is simple and corresponds to the usual method of subjective assessment by clinicians. In this study, comparison of the height of the tuber coxae and vertical impulse of the left and right hind limbs in the lame condition did not yield significant differences ($P>0.05$) in the whole group of horses. The time that elapsed between subjectively grading the lameness and data collection allowed further improvement of clinical signs. Therefore, lameness was less than grade 2 at the time of data collection. When the horses were analyzed individually, it was found on the basis of tuber coxae displacement (Table 4-4) and analysis of vertical impulses (Table 4-6) that Horse no.2 was only slightly lame when the data were collected for the lame condition. The tuber coxae displacement quotient in Horses no.1, 3 and 4 decreased in the lame condition, while Horse no.2 had a slight increase. In a previous

study (Buchner, et al., 1996c) found that the mean differences in the tuber coxae displacement quotient between sound and grade 1 lame, and between sound and grade 2 lame were 0.25 and 0.34, respectively. This was much larger than the difference seen in three horses (0.02-0.11) in this study. The previous study used the lameness grading system of Stashak (1987) in which the definition of grade 1 lame implies a more marked lameness than grade 1 lame in the AAEP grading system (American Association of Equine Practitioners, 1991) used in this study. Certainly, the lameness observed in this study was very mild in all horses.

Criteria for grading the degree of lameness by vertical impulse have been proposed based on the mean difference between the two hind limbs: 0-2% mean difference for grade 1, 2-4% mean difference for grade 2, and more than 4% mean difference for grade 3 (Weishaupt, et al., 2001). The clinical grading system in that study was similar to the one used in this study, so the criteria might be applied as an objective evaluation in the present study. The mean difference of vertical impulse between the left and right hind limbs in the lame condition (Table 4-5) indicated that Horses no.1 and 4 would be assessed as grade 2 lame, while Horses no.2 and 3 would be assessed as grade 1 lame.

The analysis of the center of vertical loading distribution indicated that, even in the sound condition, the vertical loading of the left and right limbs was not symmetrical, which is probably a reflection of sidedness. In sound horses, asymmetry in tuber coxae displacement (Buchner, et al., 1996c; Pourcelot, et al., 1997a; Pourcelot, et al., 1997b), in peak vertical force (Williams, et al., 1999) and in vertical impulse (Merkens, et al., 1993) have been reported at the trot. Sidedness is known to exist in horses (Deuel and

Lawrence, 1987; Drevemo, et al., 1987), and trainers are well aware of the fact that horses naturally have a slightly asymmetrical movement pattern, preferring to carry more weight on one hind limb, usually the left hind limb (Ljungquist, 1976). The effect of slight sidedness on gait variables and the evaluation of asymmetry in mild lameness have not been investigated. In this study, Horse no.3 had its center of vertical loading on the right side in the sound condition. Although the center of vertical loading moved toward the left when the horse was lame in the right hind limb, the effect was to produce a more symmetrical loading pattern. If the lameness had been more severe, it is anticipated that the center of loading would have shifted further to the left. The shift in load distribution in Horse no.2 also brought the center of vertical loading closer to the midline of the body, but it is not known why the loading shifted toward the lame limb. In mild lameness, it is possible that certain gait variables actually became more symmetrical, though a more severe lameness would be expected to produce the more typical patterns of asymmetry.

When evaluating very mild lameness, it is important to take account of the fact that even sound horses may show asymmetrical motion and weight-bearing patterns. It can be difficult to determine whether these asymmetries are simply individual variation due to sidedness or the effect of a real pathology. There is a gray zone between sidedness and slight lameness (Buchner, 2001a). When comparing mean difference of vertical impulse in the right hind limb (Table 4-6), three horses were assessed as grade 2 lame, and one horse was assessed as grade 1 lame. By making direct comparisons within the same limb between sound and lame conditions, the effects of sidedness in the individual horses were reduced. Therefore, comparisons between conditions in the same limb might

be more suitable in evaluating mild lameness than the asymmetry indices that have been used in more severe lameness.

Due to the small sample size in this study, there was a risk of Type II statistical errors (Vincent, 1999). Therefore, variables that showed a trend ($P<0.10$) toward differences between sound and lame conditions are reported in addition to those showing significant differences ($P<0.05$). If a larger number of subjects had been available, the increase in statistical power might reveal additional differences between sound and lame conditions.

Intra-limb coordination. During the stance phase, the main functions of the tarsal joint are to absorb energy during the impact phase and to generate energy during push off. The effects of distal tarsal joint pain were apparent in the tarsal joint mechanical profiles during stance. The mean decrease in tarsal joint range of motion during stance was 2.2 degrees. Since there was no significant difference in peak flexion or extension, it seems likely that the decrease in range of motion was due to small decreases in both peak flexion and peak extension, as shown by a trend toward a decrease in tarsal joint range of flexion during the first half of stance, and a trend toward a decrease in tarsal joint range of extension during the second half of stance.

Most of the significant changes in tarsal joint function occurred in early and late stance. During early stance, the decreased rate of performing negative work (tarsal power Min1) on the extensor aspect of the tarsus could be due to reduced activity of the gastrocnemius. The SDF tendon, assisted by the DDF tendon, might be responsible for the trend toward a decrease in energy absorption during this time by absorbing a little less

elastic energy as the joint accepted load. During terminal stance, there was a trend toward a decrease in tarsal joint range of extension. A kinematic study of distal tarsal joint lameness (Kramer, et al., 2000) also reported a decrease in maximum tarsal joint extension at the end of stance. The decrease in rate of performing positive work during late stance was probably also an attempt to reduce peak power on the extensor aspect. The DDF muscle is active to provide propulsion at this time (Jansen, et al., 1992) and the decrease in energy generation in late stance was most likely due to a decrease in muscular work from this muscle. The DDF muscle also affected the energy profile at the distal interphalangeal joint, causing a trend toward decreases in peak negative power and energy absorption. Changes in the tarsal joint due to synovitis during early and late stance corresponded with the occurrence of peak braking and propulsive forces. The propulsive force showed a trend toward a decrease in peak magnitude. This might be an attempt to adjust the limb function to reduce shear force acting on the tarsal joint complex.

The main function of the tarsal joint during swing is to raise and lower the distal limb, so that the hoof swings clear of the ground. The mechanical events in late stance affected the subsequent swing phase. The decrease in positive work of the tarsal extensor muscles during late stance led to a more gradual increase in joint extension with less stretching of peroneus tertius. The elastic energy storage in this tendon decreased, with a corresponding decrease in the amount of elastic energy released during early swing. This explains the significant decrease in peak net flexor moment (Min1) at the tarsal joint around 10% of swing. During early swing, the rate of performing positive work (power Max1) on the flexor aspect did not change, which might indicate a constant rate of performing positive work by the cranial tibial muscle during this period. Therefore, the

trend toward decreased energy generation in early swing was thought to be due to a decrease in elastic energy release from peroneus tertius.

In the second half of swing, tarsal extensors, most likely gastrocnemius muscle, reduced the rate of performing positive work without a decrease in energy generation. This again suggests an attempt to reduce the peak power. The reduction in rate of work performed continued into early stance as described previously.

In the present study, there was a significant decrease in tarsal joint range of motion and a trend toward a decrease in tarsal joint range of flexion during stance. On the contrary, lameness located in the hind hoof was associated with an increase in peak tarsal joint flexion during mid stance (Buchner, et al., 1996b). This suggests a different mechanism of compensation for lameness at different sites within the limb. In the hind hoof lameness, increased flexion of the tarsal joint was thought to reflect a greater role in shock absorption by using the tarsal extensor muscles to adjust limb loading (Buchner, et al., 1996b). This implies an increase in negative work performed by the tarsal extensor muscles, though this was not confirmed by inverse dynamic analysis. As a result, the loading increased more gradually during mid stance and the peak force on the hoof was reduced. In the distal tarsal joint lameness in this study, there were no compensatory increases in shock absorbing duty from other joints within the lame limb. Instead, there was a reduction of loading of the entire limb.

Kinematic characteristics of distal tarsal osteoarthritis (bone spavin) are a reduction in tarsal joint flexion during swing and a lower height of the foot flight arc (Gough and Munroe, 1998). Synovitis induction in this study was associated with a trend

toward a decrease in vertical displacement of distal interphalangeal joint during swing, but there was no change in tarsal range of motion during swing.

One of the surgical procedures for treating bone spavin is cunean tenectomy (Cottage, et al., 1997; Bohanon, 1999), the objective of which is to relieve tension from this tendon during contraction of the cranial tibial muscle. Reports on the efficacy of this procedure are limited. Since the rate of performing work by the cranial tibial muscle and the range of joint flexion during early swing in the present study did not change in the lame condition, cunean tenectomy might not give a good response in mild lameness due to synovitis. In horses affected with natural bone spavin, assessment of the owner's satisfaction with the outcome of the cunean tenectomy appeared to be good (Eastman, et al., 1997), but that study did not report the level of lameness in the affected hind limb before surgery. If lameness were more severe, it might have reduced the activity of the cranial tibial muscle and relieved tension on the cunean tendon, so that cunean tenectomy allowed an improvement in function. This could be investigated using inverse dynamic analysis before and after surgery. Changes in net joint power and energy generation during early swing might be a suitable quantitative indicator to assess the outcome and might even be used as a prognostic tool.

The ability of a horse to advance to a high level in equestrian sports may be limited by subtle lameness in the distal tarsal joints. In its early stages, osteoarthritis of low-motion joints tends to cause performance-related problems rather than obvious lameness. Most of these problems are subtle and slowly progressive (Moyer, et al., 1993). Since the medial branch of cranial tibial tendon comes under tension during tarsal flexion (Molenaar, 1983), the distal tarsal joints experience compression on their medial side

during joint flexion. When the horse performs collected work, especially piaffe and passage, the femorotibial and tarsal joints are more flexed during early and mid stance (Holmstrom, et al., 1995a). In the study reported here, peak joint flexion occurred closely in time with peak negative power at the tarsal joint. Repetitive loading on the medial side of the joint may lead to synovitis. In an experimental study of repetitive impulsive loading in rabbit femorotibial joints, synovial inflammation was apparent after eight weeks of loading. Cartilage breakdown was focal and limited to the weight-bearing area (Lukoschek, et al., 1986). Low impact produced acute tissue stresses below the injury threshold, while high-intensity impacts produced stresses that exceeded the threshold of joint degeneration (Newberry, et al., 1998). In cartilage regions subjected to high contact stress, synthesis of large aggregating proteoglycans was decreased and synthesis of decorin was increased (Little, et al., 1997). Moreover, articular cartilage from aged horses has markedly less overall metabolic activity, compared with cartilage from young horses (Morris and Treadwell, 1994). In contrast to the catabolic effects of exercise, synovial fluid from ponies that had been exercised for a week had anabolic effects on explanted cartilage by enhancing glycosaminoglycan synthesis (Hoogen, et al., 1998). Ideally, the training regimen of athletic horses should be adjusted to balance the catabolic and anabolic effects. If the training regimen exceeds the physiological limit, joint inflammation commences. The resulting pain may lead to a reluctance to perform collected movements, which require a lot of tarsal joint flexion.

Inter-limb compensation. Quadrupeds show complex interactions and patterns of compensation between the four limbs. This study showed a trend toward an increase in

vertical peak force and a significant increase in peak net joint moment on the flexor aspect of metatarsophalangeal joint of the contralateral hind limb. Kinematic adaptations suggestive of a compensatory increase in loading of the contralateral hind limb have been reported in horses in which lameness was induced by pressure on the sole of the hoof (Buchner, et al., 1996b), with the observed changes including an increase in maximal flexion of the tarsal joint during stance. An increase in peak vertical force in the compensating hind limb was also reported in dogs with anterior cruciate ligament transection (Rumph, et al, 1995). If horses that are mildly lame due to inflammation of the distal intertarsal and tarsometatarsal joints continue to work, the increase in vertical force on the contralateral hind limb may be sufficient to cause inflammation in the distal tarsal joints, which may explain the fact that osteoarthritis in the distal tarsal joints (bone spavin) often occurs bilaterally.

Lameness due to unilateral hind limb lameness may give the appearance of lameness in the ipsilateral forelimb, when assessed by head acceleration asymmetry (Uhlir, et al., 1997). In sound horses at trot, the head accelerates downward during the first half of stance, then accelerates upward during the second half of stance. In unilateral hind limb lameness, the vertical head acceleration during the contralateral forelimb stance was more than that during the ipsilateral forelimb (Uhlir, et al., 1997). An increase in head vertical acceleration amplitude has been reported on the diagonal of the lame hind limb in horses with hoof lameness (Buchner, et al., 1996c), but the finding was not statistically significant among lameness grade 0, 1 and 2. Therefore, compensating head movements are not a consistent finding in mild hind limb lamenesses.

In the present study, the lame condition showed a decrease in vertical impulse in the contralateral forelimb, which is indicative of unloading of the diagonal lame limb pair. There was a similar finding of decreased vertical force peaks in both forelimbs in a dog with unilateral acute synovitis of the femorotibial joint (Rumph, et al., 1993), though the exact mechanism of redistribution could not be identified. In induced carpal joint lameness in horses, there also appeared to be a tendency toward overall reduction in vertical forces. It might be that the horse maintained forward velocity with less vertical displacement of the body center of mass, resulting in a less bouncy gait with lameness (Morris and Seeherman, 1987). In induced fore hoof lameness, the vertical acceleration of the body center of mass, which represents the total vertical force, reduced significantly during the diagonal lame limb stance (Buchner, et al., 2001). In the synovitis condition, the metacarpophalangeal and carpal joints of the contralateral forelimb, which are crossed by several tendinous structures on their flexor aspect, showed decreases in peak flexor moment in both joints, a trend toward a decrease in elastic energy absorption at the metacarpophalangeal joint and a decrease in energy generation at the carpal joint (energy Max2). This might reflect decreased bouncing of the body mass during lameness.

Horses affected with osteoarthritis of the distal tarsal joints often present with back pain (Dyson, 1995; Cottage, et al., 1997; Gough and Munroe, 1998), which may develop over a period of time in association with chronic pain in the distal tarsal joints. This might indicate adaptation of back motion with this kind of lameness. There is an interaction between movement of the limbs and movement of the vertebral column at the trot (Faber, et al., 2001a). At the trot, the vertebral column can rotate in three dimensions: flexion/extension, lateral bending and axial rotation. During the first half of hind limb

stance at the trot, which corresponds with the first half of the contralateral hind limb swing, the inter-vertebral joints show extension, lateral bending toward the supporting hind limb and axial rotation toward the swinging hind limb. During the second half of stance, which corresponds with the second half of swing of the contralateral hind limb, inter-vertebral motion involves flexion, lateral bending toward the swinging hind limb and axial rotation toward the supporting hind limb (Faber, et al., 2001a). The skin marker set in our study was not designed for direct analysis of back motion, but movements of the sacrum might be inferred from the relative displacements of the left and right tubera coxarum. During a complete stride, each tuber coxae had two cycles of down and up motion. The highest position occurred during the suspension period and the lowest position around mid stance of the ipsilateral and contralateral hind limbs. Vertical displacement of the tuber coxae could be a result of either rotational motion of the sacrum or adjustment of hind limb joints to accept load. In the lame condition in this study, there was an increase in vertical displacement of the left tuber coxae during left hind stance but, at the same time there was an increase in vertical displacement of the right tuber coxae during swing of the right hind limb. Because the joint range of motion in the left hind limb did not change, this is probably an indication of more lumbosacral extension during the first half of stance of the left hind limb. After mid stance, a propulsive force from the hind limb flexed the vertebral column by providing a forward and upward force. The back flexion is thought to restrain by longissimus dorsi (Faber, et al., 2001a), which is active twice around the period of back flexion during the complete stride (Robert, et al., 1998). This muscle provides physiological rigidity of the vertebral column, thus enhancing the forward propulsive thrust (Rooney, 1977). A trend toward an

increase in peak vertical force during stance might tend to increase flexion of the vertebral column, which would require more activity from the longissimus dorsi to resist the flexion. An increase in peak positive power at the left coxofemoral joint during early swing, probably from tensor fascia latae, might increase the momentum of the limb as it swings forward, thus helping to propel the body forward, and maintain the body's forward velocity.

During the second half of stance in sound trotting horses, the coxofemoral joint extends and the pelvis rotates axially toward the supporting hind limb, which facilitates ground clearance of the contralateral hind limb as it is protracted (Faber, et al., 2001a). In the lame right hind limb in this study, there was a decrease in the coxofemoral joint peak extension (Max1) during stance, which would make it more difficult for the left hind limb to be protracted clear of the ground during the second half of swing. Gluteus medius works primarily as a coxofemoral extensor and secondarily as a coxofemoral abductor (Dyce, et al., 1987). A trend toward a decrease in coxofemoral energy generation (energy Max2) during swing of the left hind limb might indicate a transition of gluteus medius from performing positive work in the sagittal plane to performing more abduction. This adjustment might help the protracting left hind limb to clear the ground but, at the same time, might change the pattern of back motion. Possible increase in back extension during stance, in combination with the possible changes in back motion during swing of the left coxofemoral joint, may lead to fatigue of the back muscles over a period of time.

CONCLUSION

Differences in kinetic variables between sound and lame conditions were identified using inverse dynamic analysis. In mild lameness, comparison of variables in the same limb between conditions was more suitable than comparison of asymmetrical variables between hind limbs. The energetic variables calculated from inverse dynamic analysis gave more informative changes in the lame tarsal joint than kinematics or GRF alone. Important characteristics of lameness due to synovitis in the distal intertarsal and tarsometatarsal joints were a decrease in impact energy absorption during early stance and a decrease in energy generation during push off at the tarsal joint in the lame hind limb. These changes, in combination with a decrease in vertical impulse in the contralateral forelimb, indicated unloading of the diagonal lame limb pair. Compensatory changes were found in the contralateral hind limb, which showed a trend toward an increase in peak vertical force and an increase in positive power at the coxofemoral joint during early swing. A possible mechanism for causing back pain secondarily to lameness in the distal tarsal joints was described.

CHAPTER 5

THREE-DIMENSIONAL KINEMATICS OF THE EQUINE TARSAL JOINT: RESULTS AND DISCUSSION

REFERENCE BONE DATA

The true rotational and translational motion of the tarsal joint complex was obtained from retro-reflective markers attached to bone pins inserted on the lateral side of the tibia and metatarsus (Lanovaz, et al., 2002). Motion of the metatarsal segment was described relative to the fixed tibial segment in terms of three rotational motions: flexion/extension, abduction/adduction and internal/external rotation, and three translational motions: cranial/caudal, medial/lateral and proximal/distal.

The three-dimensional (3D) motions are illustrated as means and standard deviations of rotational (Figure 5-1) and translational (Figure 5-2) motions of the tarsal joint from reference bone data during stance from 4 horses. The values were expressed relative to the impact value. During stance, the tarsal joint flexed, then extended, similar to the motion found in the two-dimensional (2D) analysis. The distal part of the metatarsal segment moved away from the mid line of the body relative to the tibia, resulting in abduction during the first half of stance, after which the angle returned to the impact value. Flexion peaked around 40% stance, which corresponded with the peaks in abduction, cranial translation and proximal translation. The joint gradually extended, adducted and caudally translated passing through the impact angle around 80% stance, then continued these movements until the end of stance. The metatarsal segment was

internally rotated relative to the tibial segment throughout stance (Figure 5-1). The medial and lateral translation patterns differed between horses, resulting in wide standard deviations. The mean curve indicated that the metatarsal segment translated laterally relative to the tibial segment throughout stance.

During swing, the rotational (Figure 5-3) and translational (Figure 5-4) motions of the tarsal joint from reference bone data are illustrated and expressed relative to the impact values in the previous stance phase. During swing, the joint flexed, abducted and externally rotated with the peaks of these motions occurring at the same time around the middle of swing, after which the joint moved back to the impact values. The cranial/caudal and proximal/distal translational motion had similar patterns. The metatarsal segment translated cranially and proximally, reaching peaks around the same time as the rotational motion, then returned to impact values. The medial/lateral translations, however, were quite varied among horses. During early and late swing, the metatarsal segment translated laterally showing a large variation in the amount of lateral translation in the middle of swing.

Figure 5-1 Three-dimensional rotation of the tarsal joint from reference bone data during stance: flexion(-)/extension(+) angle (top), abduction(-)/adduction angle (middle) and internal(+)/external(-) rotation angle (bottom). The thick black line indicates mean value from 4 horses. Thin lines indicate one standard deviation above and below the mean. Zero indicates the impact value.

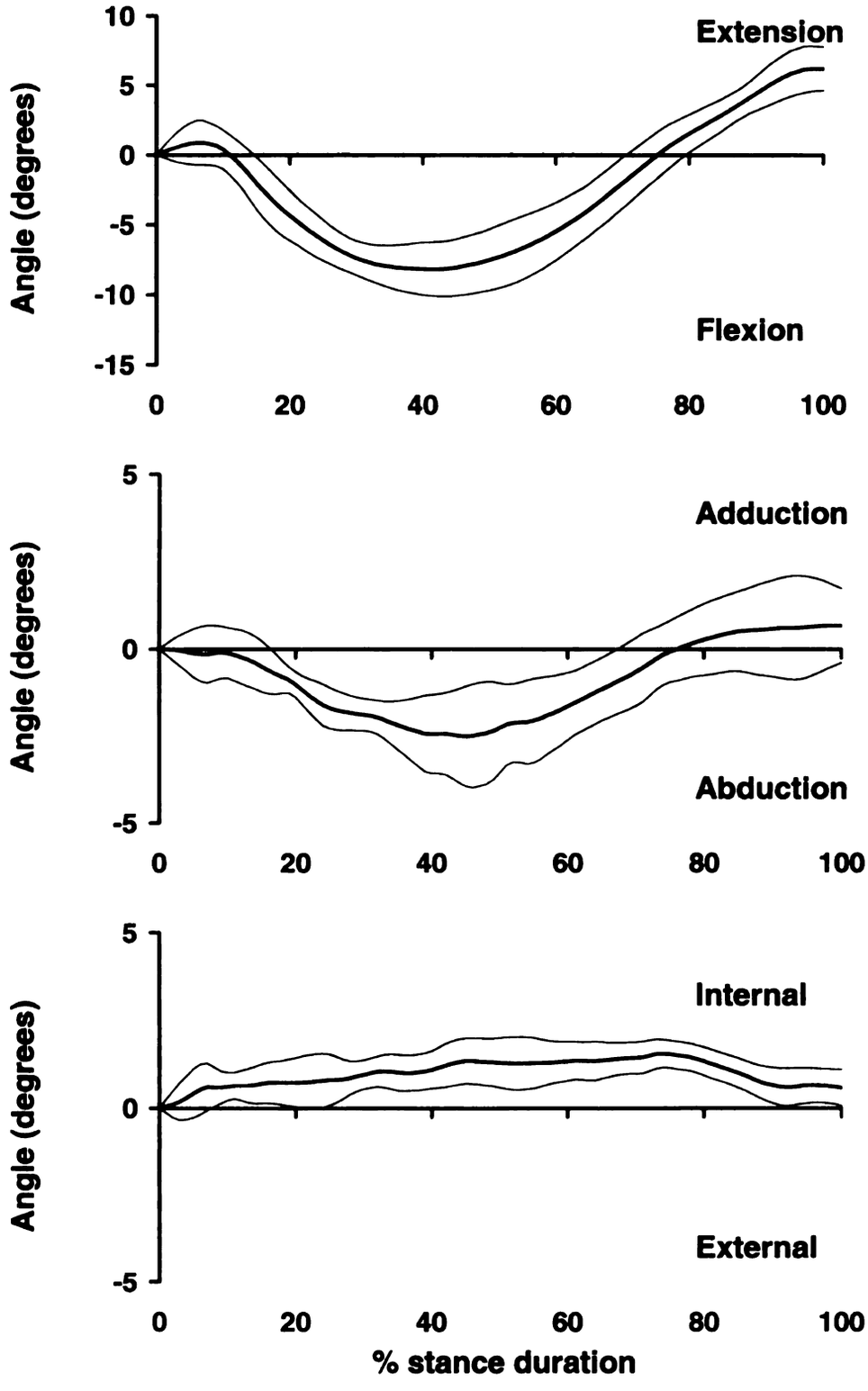

Figure 5-2 Three-dimensional translation of the tarsal joint from reference bone data during stance: cranial(+)/caudal(-) translation (top), medial(+)/lateral(-) translation (middle) and proximal(+)/distal(-) translation (bottom). The thick black line indicates mean value from 4 horses. Thin lines indicate one standard deviation above and below the mean. Zero indicates the impact value.

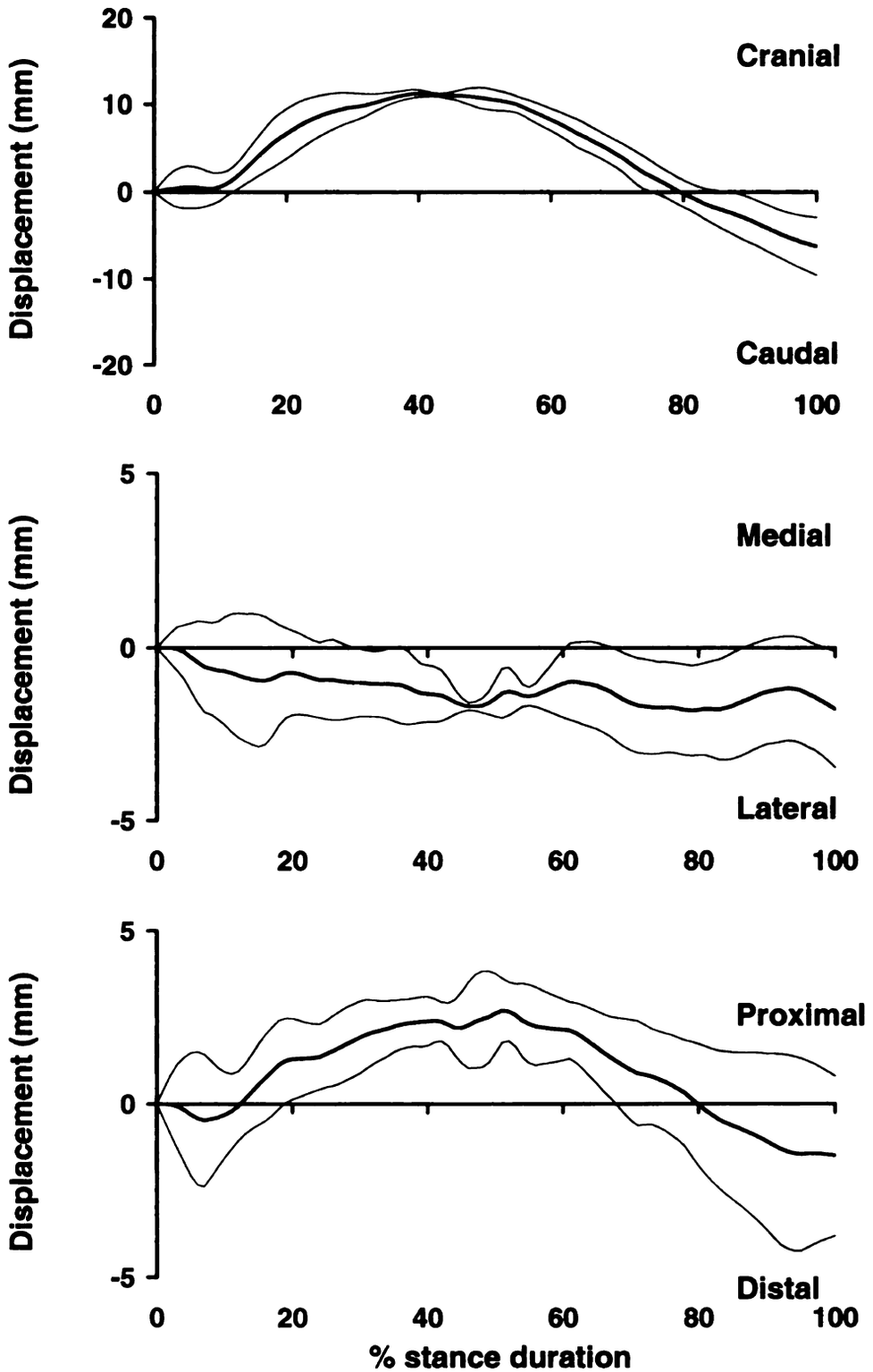

Figure 5-3 Three-dimensional rotation of the tarsal joint from reference bone data during swing: flexion(-)/extension(+) angle (top), abduction(-)/adduction angle (middle) and internal(+)/external(-) rotation angle (bottom). The thick black line indicates mean value from 4 horses. Thin lines indicate one standard deviation above and below the mean. Zero indicates the impact value.

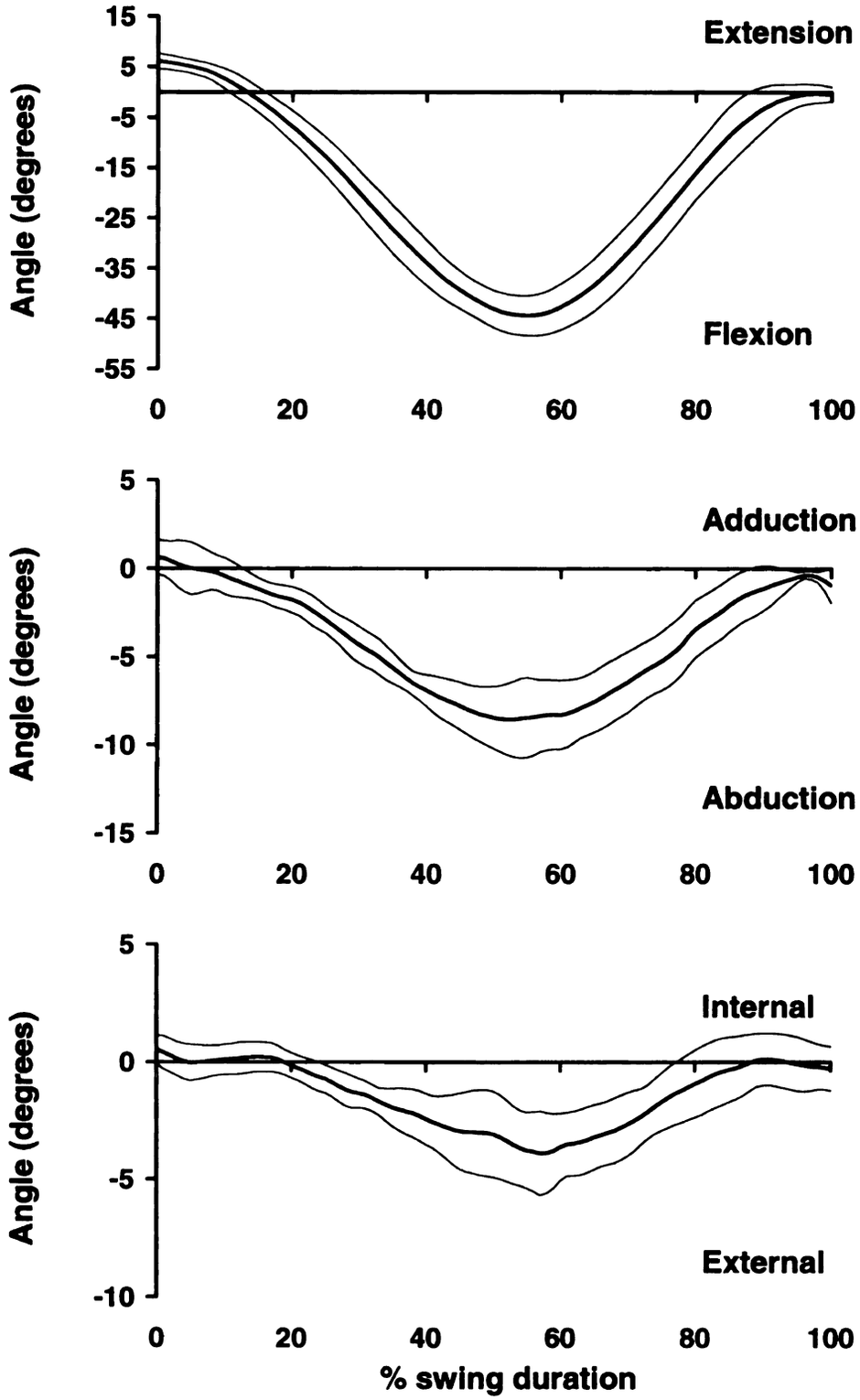

Figure 5-4 Three-dimensional translation of the tarsal joint from reference bone data during swing: cranial(+)/caudal(-) translation (top), medial(+)/lateral(-) translation (middle) and proximal(+)/distal(-) translation (bottom). The thick black line indicates mean value from 4 horses. Thin lines indicate one standard deviation above and below the mean. Zero indicates the impact value.

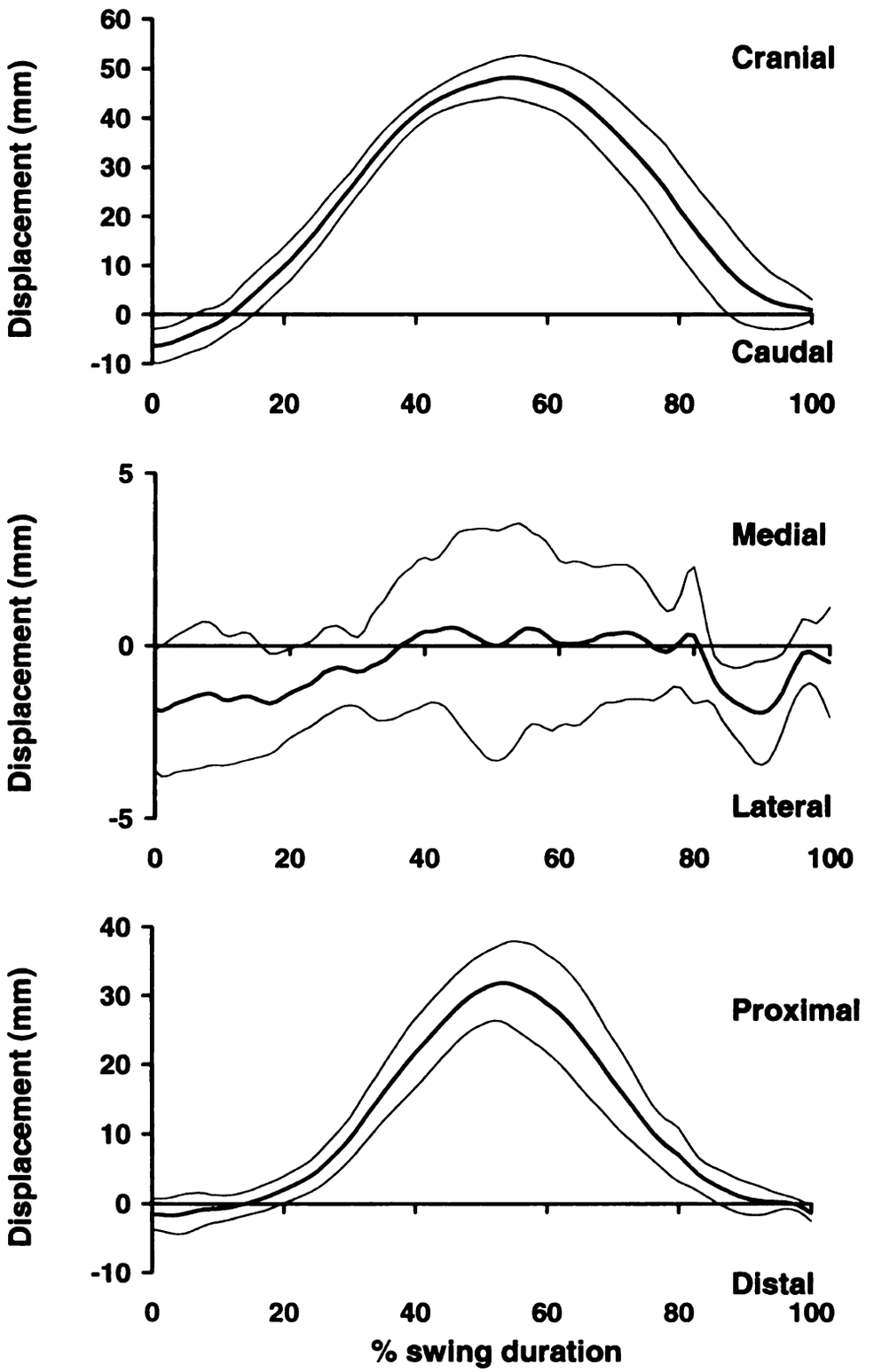

COMPARISON BETWEEN REFERENCE BONE DATA AND SKIN MARKER DATA

Root mean square (RMS) errors were calculated as an indication of the amount of deviation between the shapes of the two curves from reference bone data and skin marker data. The values were calculated during stance for the three joint angles (Table 5-1) and the three joint displacements (Table 5-2), and during swing for the three joint angles (Table 5-3) and the three joint displacements (Table 5-4). In addition, RMS errors between the reference bone data and skin data corrected for flexion/extension angle using 2D skin correction algorithms from the literature (van Weeren, 1989) were also calculated during stance and swing phases. RMS errors between the reference bone data and corrected skin data were smaller than those between reference bone data and uncorrected skin data, indicating an improvement of the data after the application of skin correction algorithms. Uncorrected skin data for flexion/extension obtained using 6 skin markers per segment had smaller RMS errors than data from 2 markers per segment corrected using algorithms published for 2D data.

The RMS errors only identified the magnitude of the errors. To explore similarities and differences in the shape of the curves, the reference bone data and corrected skin data from individual horses were plotted and evaluated qualitatively. Agreement between curves was assessed as 'good' when the shape and direction of the curves were similar for the two sets of data; 'fair' when the shape and direction of the curves were less similar; and 'poor' when neither the shape nor direction of the curves were similar. During stance, the shape agreement in individual horses for three rotational motions (Figures 5-5 to 5-7) and three translational motions (Figures 5-8 to 5-10), and the

mean shape from all horses (Figures 5-11 and 5-12) were evaluated and reported in Tables 5-1 and 5-2. During swing, the shape agreement from individual horses for three rotational motions (Figures 5-13 to 5-15) and three translational motions (Figures 5-16 to 5-18), and the mean shape from all horses (Figures 5-19 and 5-20) were evaluated and reported in Tables 5-3 and 5-4.

The curves showed better agreement in shape during the swing phase than during the stance phase. Three motions were assessed as having fair shape agreement. In abduction/adduction (Figure 5-1) and proximal/distal translation (Figures 5-2 and 5-4), the reference bone data showed relatively wide standard deviations, indicating a considerable amount of variation among the horses. The directions of motion were the same but there was some disagreement between reference bone data and skin corrected data (Figures 5-11, 5-12 and 5-20) in the magnitude of the movement. The fair agreement for cranial/caudal displacement (Figure 5-12) during stance was mainly from the shape difference during early stance, while the information around the middle of stance was quite similar. Therefore, comparisons between conditions for these ranges of motion in the same horse should be acceptable and, based on these findings, further analyses were performed on the range of joint rotational and translational motions in the sound and lame conditions. Due to poor agreement in shape of the curves for medial/lateral translation and internal/external rotation, they were not used for further analysis.

Table 5-1 Root mean square (RMS) errors of three rotational motions during stance between reference bone data and corrected and uncorrected skin data. Shape agreement is the assessment between reference bone data and 3D corrected skin data.

Flexion/extension (degrees)

Horse	Bone data and 3D corrected skin	Shape agreement	Bone data and uncorrected skin	Bone data and 2D corrected skin
1	2.61	Good	2.65	4.23
2	3.31	Good	4.61	6.17
3	2.24	Good	3.28	5.21
4	1.34	Good	1.65	3.22
Mean	2.38	Good	3.05	4.71

Abduction/adduction (degrees)

Horse	Bone data and 3D corrected skin	Shape agreement	Bone data and uncorrected skin
1	0.37	Good	0.96
2	0.97	Fair	1.06
3	0.75	Fair	1.37
4	2.67	Fair	2.42
Mean	1.19	Fair	1.45

Internal/external rotation (degrees)

Horse	Bone data and 3D corrected skin	Shape agreement	Bone data and uncorrected skin
1	0.98	Fair	8.67
2	2.77	Poor	8.86
3	3.29	Poor	9.44
4	2.10	Poor	7.51
Mean	2.29	Poor	8.62

Table 5-2 Root mean square (RMS) errors of three translational motions during stance between reference bone data and corrected and uncorrected skin data. Shape agreement is the assessment between reference bone data and 3D corrected skin data.

Cranial/caudal translation (mm)

Horse	Bone data and 3D corrected skin	Shape agreement	Bone data and uncorrected skin
1	3.29	Fair	4.41
2	3.87	Fair	5.15
3	5.08	Fair	5.80
4	8.01	Fair	8.22
Mean	5.06	Fair	5.89

Medial/lateral translation (mm)

Horse	Bone data and 3D corrected skin	Shape agreement	Bone data and uncorrected skin
1	1.86	Fair	3.08
2	1.60	Poor	4.47
3	1.52	Fair	4.46
4	2.34	Poor	5.42
Mean	1.83	Poor	4.36

Proximal/distal translation (mm)

Horse	Bone data and 3D corrected skin	Shape agreement	Bone data and uncorrected skin
1	2.65	Fair	5.74
2	2.72	Fair	7.00
3	2.03	Fair	6.09
4	2.65	Fair	5.89
Mean	2.51	Fair	6.18

Table 5-3 Root mean square (RMS) errors of three rotational motions during swing between reference bone data and corrected and uncorrected skin data. Shape agreement is the assessment between reference bone data and 3D corrected skin data.

Flexion/extension (degrees)

Horse	Bone data and 3D corrected skin	Shape agreement	Bone data and uncorrected skin	Bone data and 2D corrected skin
1	1.74	Good	2.00	6.10
2	2.73	Good	2.21	4.82
3	3.68	Good	4.98	8.29
4	3.15	Good	5.02	6.41
Mean	2.83	Good	3.55	6.41

Abduction/adduction (degrees)

Horse	Bone data and 3D corrected skin	Shape agreement	Bone data and uncorrected skin
1	2.35	Fair	6.73
2	0.69	Good	5.28
3	1.57	Good	6.01
4	1.89	Good	5.71
Mean	1.63	Good	5.93

Internal/external rotation (degrees)

Horse	Bone data and 3D corrected skin	Shape agreement	Bone data and uncorrected skin
1	3.41	Poor	8.40
2	1.68	Poor	8.68
3	1.34	Fair	8.96
4	4.50	Poor	11.34
Mean	2.73	Poor	9.35

Table 5-4 Root mean square (RMS) errors of three translational motions during swing between reference bone data and corrected and uncorrected skin data. Shape agreement is the assessment between reference bone data and 3D corrected skin data.

Cranial/caudal translation (mm)

Horse	Bone data and 3D corrected skin	Shape agreement	Bone data and uncorrected skin
1	9.78	Fair	10.46
2	2.60	Good	6.58
3	5.27	Good	11.71
4	8.59	Good	13.58
Mean	6.56	Good	10.58

Medial/lateral translation (mm)

Horse	Bone data and 3D corrected skin	Shape agreement	Bone data and uncorrected skin
1	2.87	Poor	3.56
2	1.98	Poor	10.23
3	1.59	Fair	9.31
4	5.14	Poor	7.04
Mean	2.89	Poor	7.54

Proximal/distal translation (mm)

Horse	Bone data and 3D corrected skin	Shape agreement	Bone data and uncorrected skin
1	6.33	Fair	10.80
2	1.43	Good	12.06
3	8.12	Fair	18.50
4	4.89	Good	7.78
Mean	5.19	Fair	12.29

Figure 5-5 Flexion (-)/extension (+) angle of horses 1-4 (top to bottom) during stance. The gray line indicates angle obtained from skin markers. The black line indicates angle obtained after application of 3D skin correction algorithm. The dotted line indicates angle obtained from bone pins. Zero indicates the impact value.

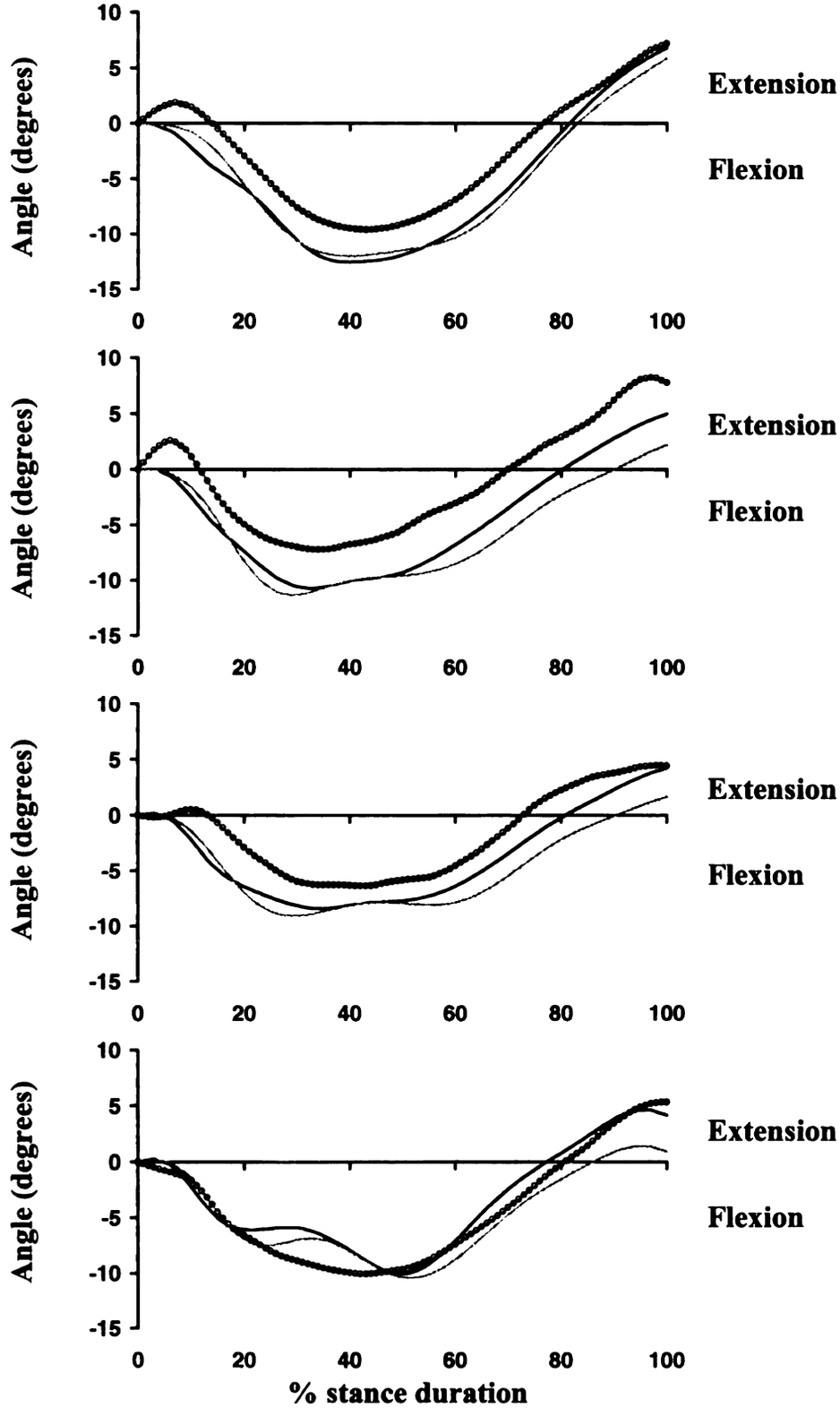

Figure 5-6 Abduction (-)/adduction (+) angle of horses 1-4 (top to bottom) during stance. The gray line indicates angle obtained from skin markers. The black line indicates angle obtained after application of 3D skin correction algorithm. The dotted line indicates angle obtained from bone pins. Zero indicates the impact value.

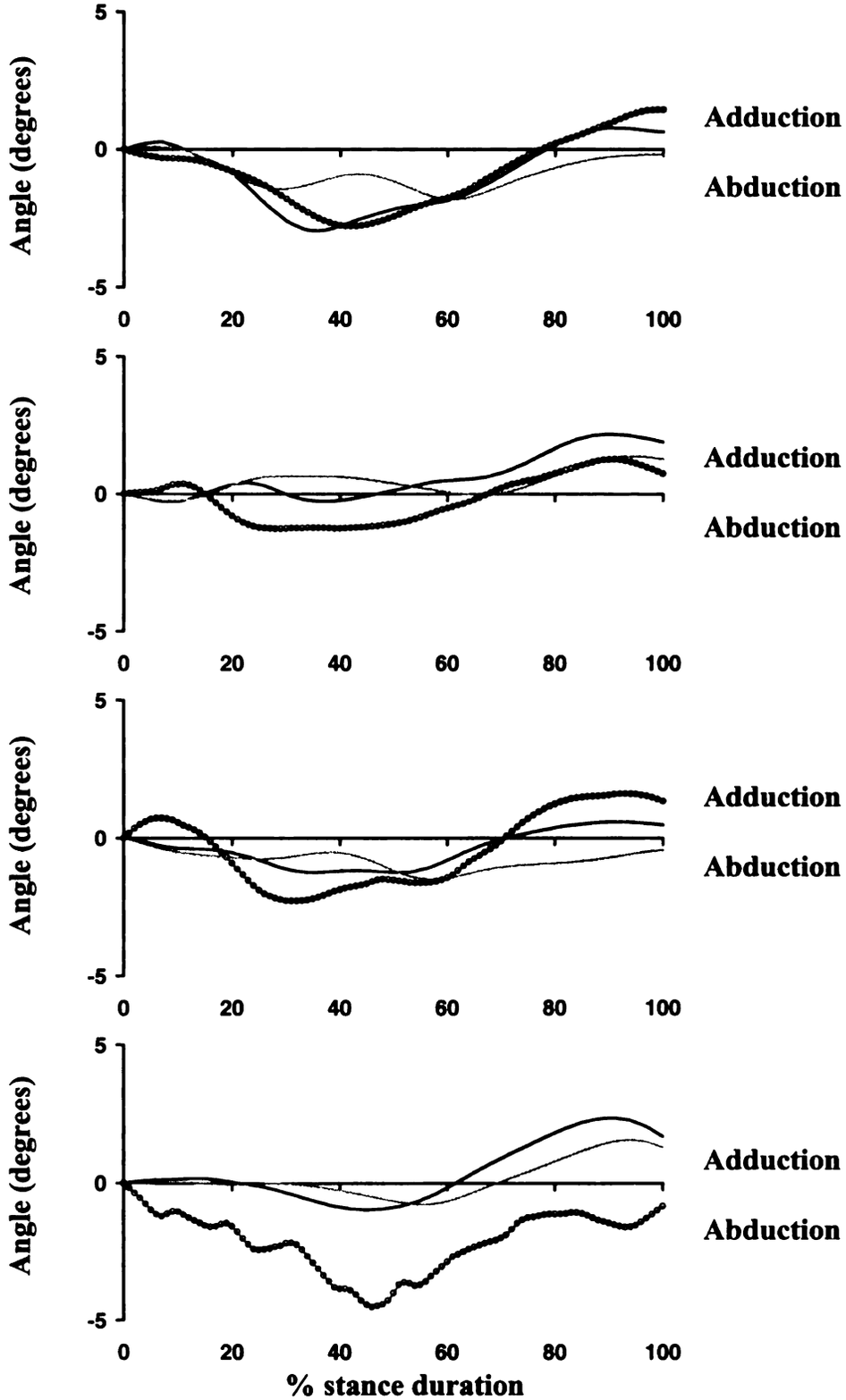

Figure 5-7 Internal (+)/external (-) rotation angle of horses 1-4 (top to bottom) during stance. The gray line indicates angle obtained from skin markers. The black line indicates angle obtained after application of 3D skin correction algorithm. The dotted line indicates angle obtained from bone pins. Zero indicates the impact value.

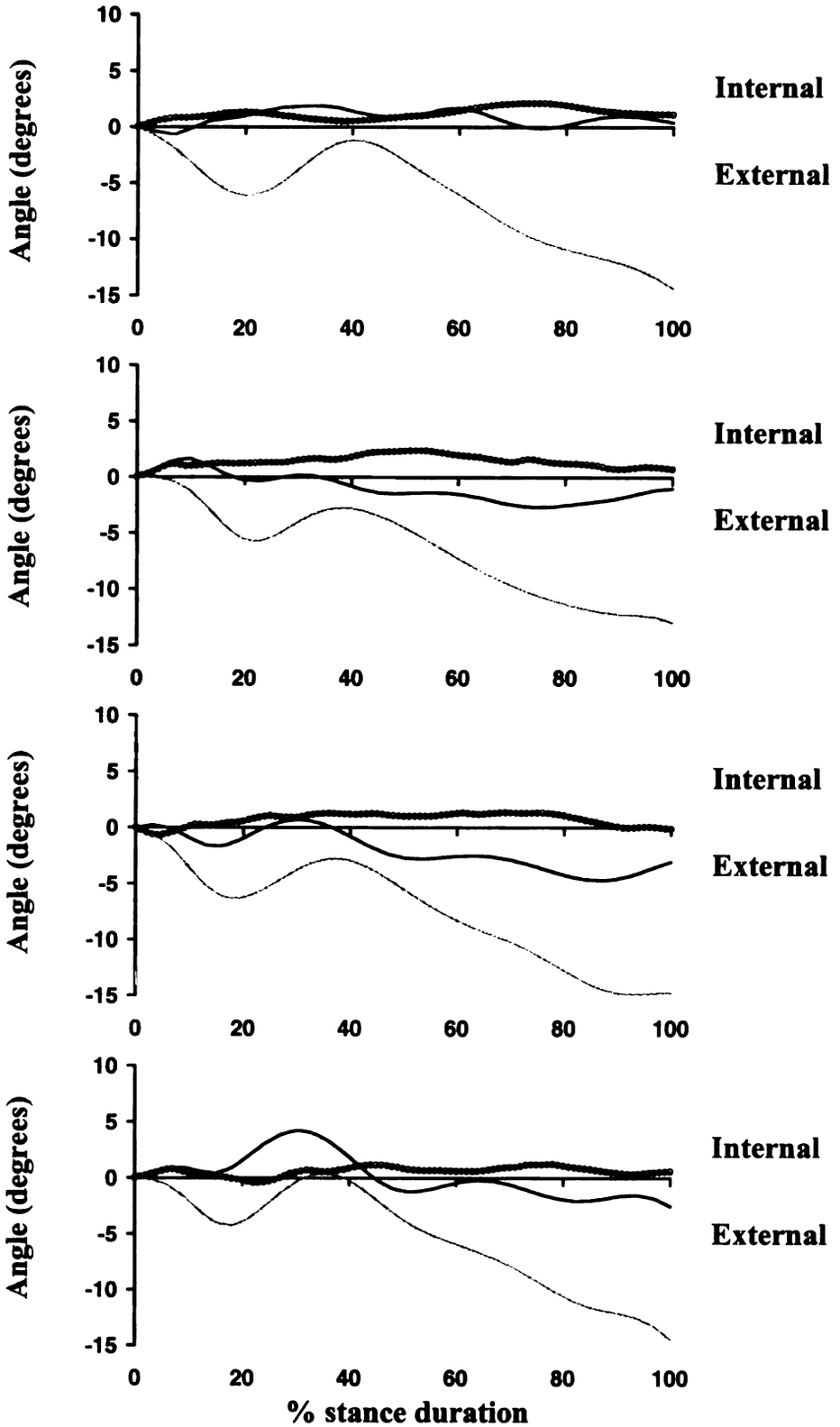

Figure 5-8 Cranial (+)/caudal (-) translation of horses 1-4 (top to bottom) during stance. The gray line indicates angle obtained from skin markers. The black line indicates angle obtained after application of 3D skin correction algorithm. The dotted line indicates angle obtained from bone pins. Zero indicates the impact value.

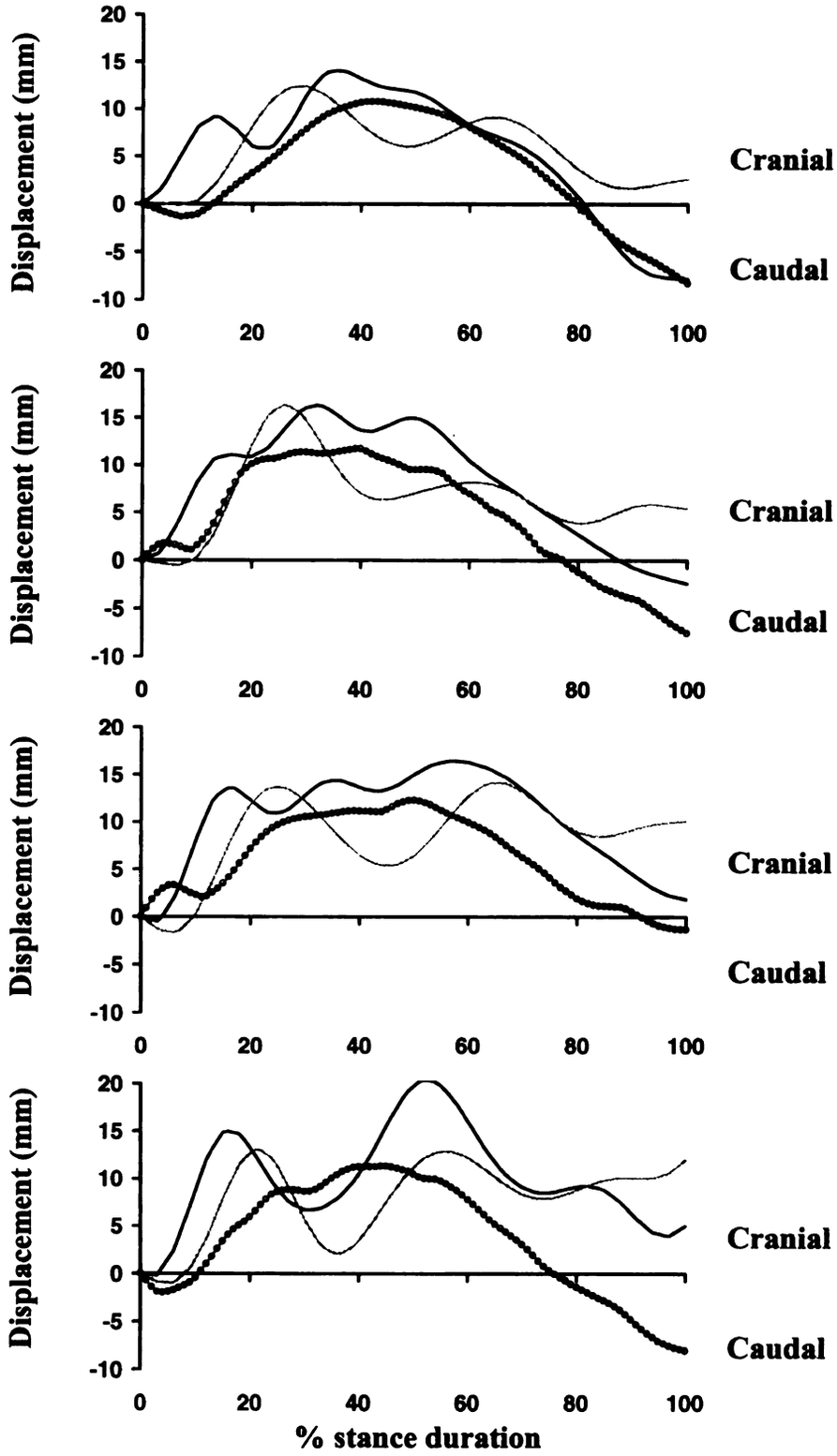

Figure 5-9 Medial (+)/lateral (-) translation of horses 1-4 (top to bottom) during stance. The gray line indicates angle obtained from skin markers. The black line indicates angle obtained after application of 3D skin correction algorithm. The dotted line indicates angle obtained from bone pins. Zero indicates the impact value.

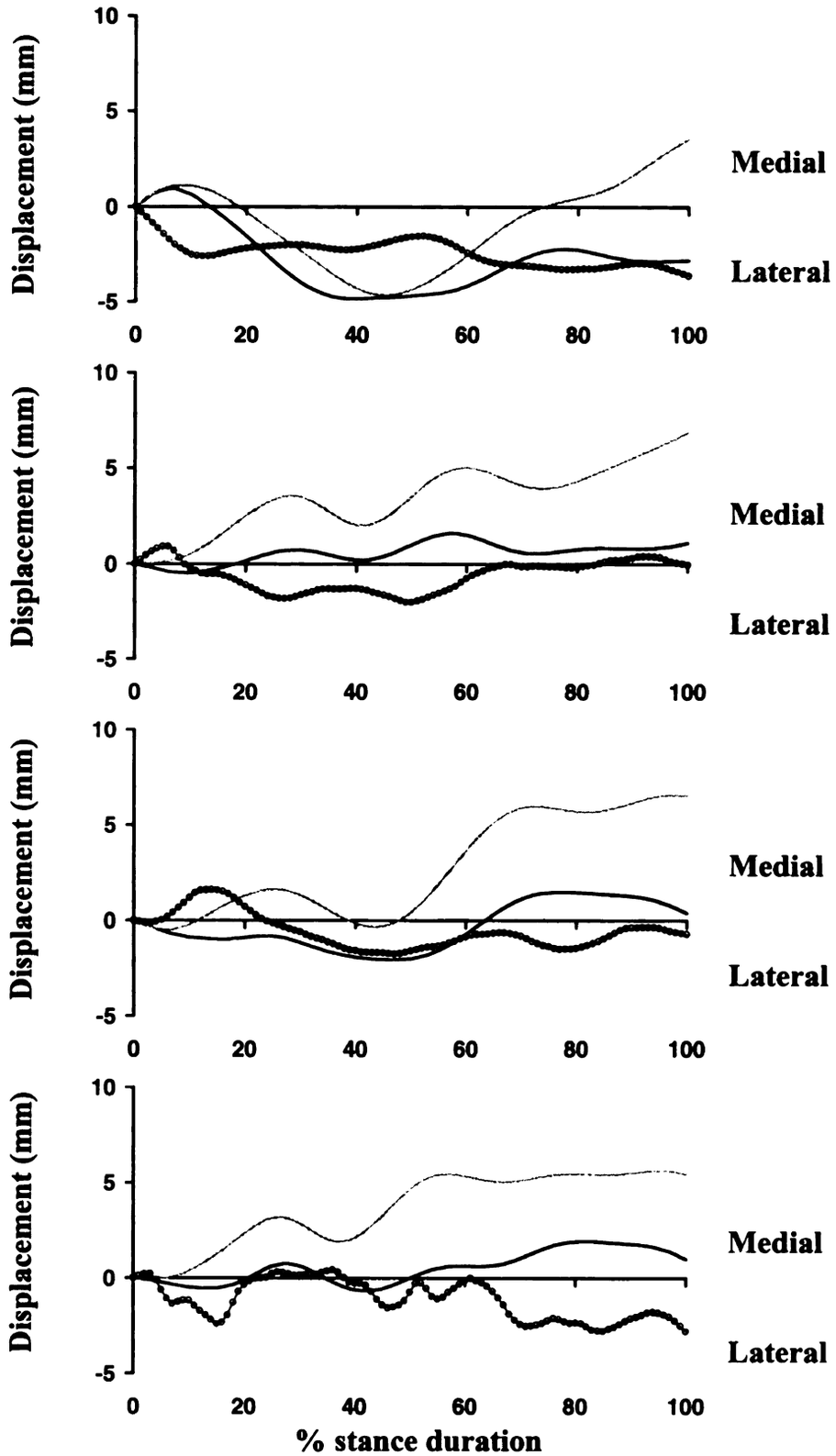

Figure 5-10 Proximal (+)/distal (-) translation of horses 1-4 (top to bottom) during stance. The gray line indicates angle obtained from skin markers. The black line indicates angle obtained after application of 3D skin correction algorithm. The dotted line indicates angle obtained from bone pins. Zero indicates the impact value.

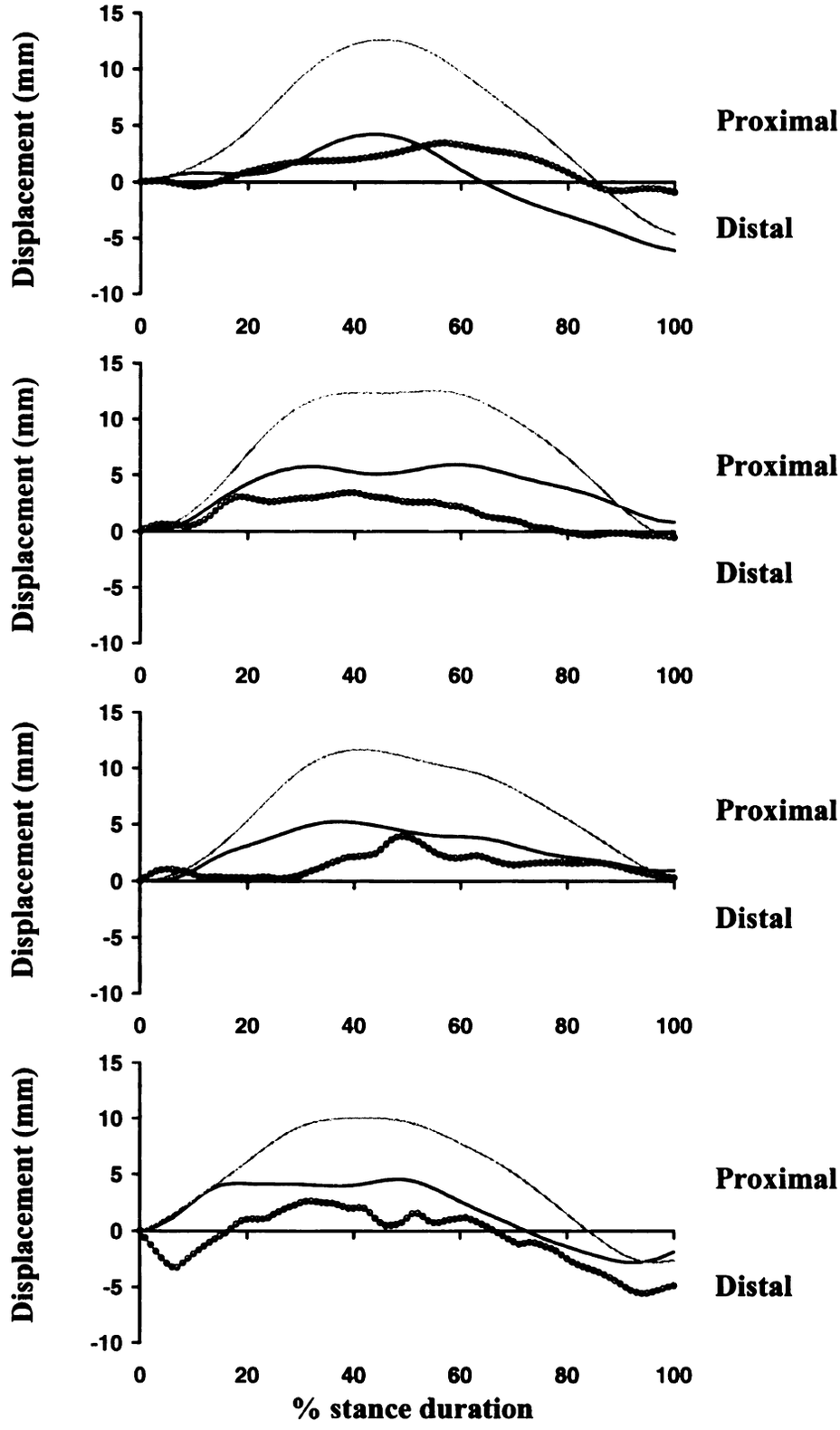

Figure 5-11 Three-dimensional rotation of the tarsal joint obtained from all horses during stance: flexion(-)/extension(+) angle (top), abduction(-)/adduction angle (middle) and internal(+)/external(-) rotation angle (bottom). The black line indicates mean value from corrected skin data. The dotted line indicates mean value from reference bone data. Zero indicates the impact value.

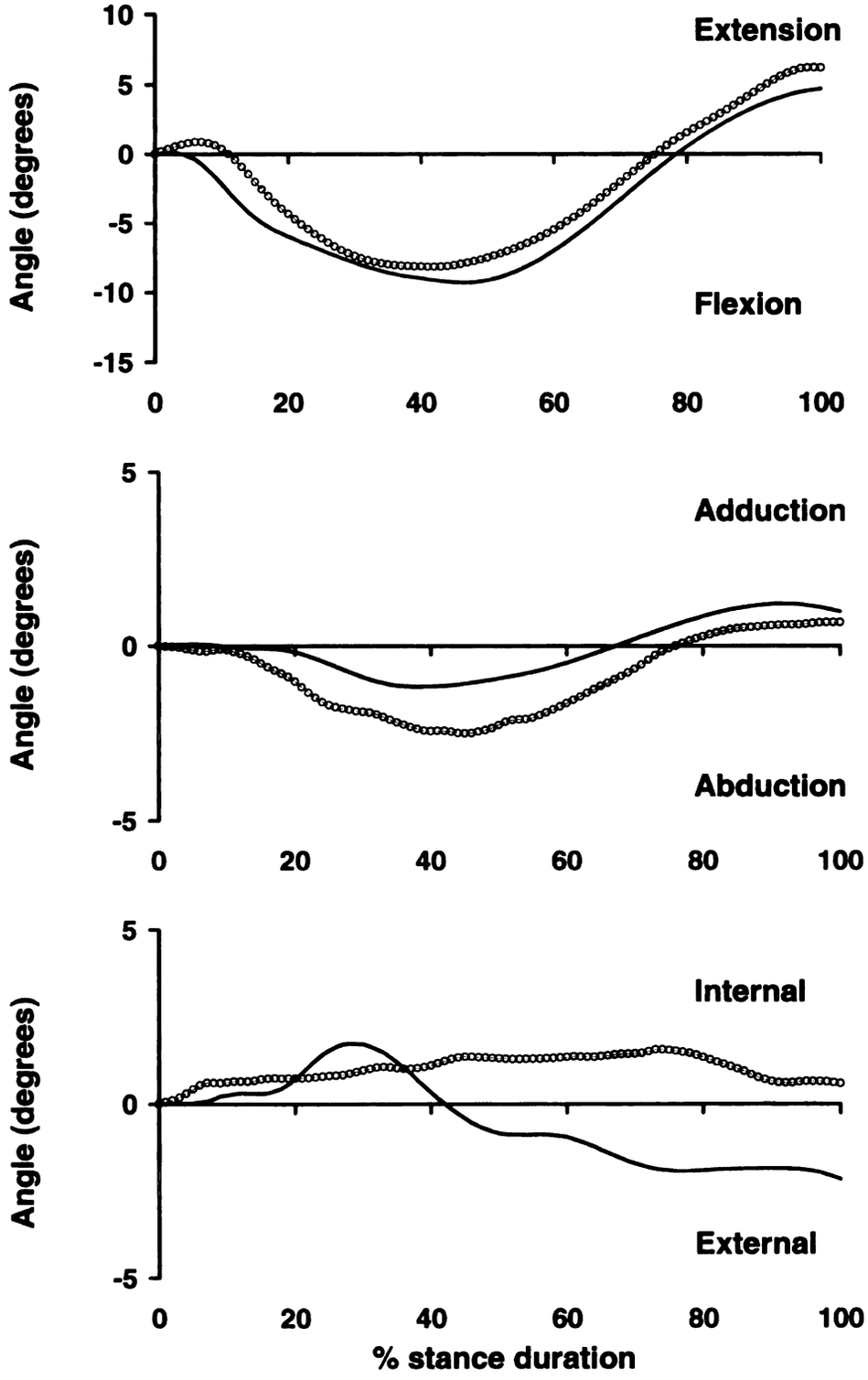

Figure 5-12 Three-dimensional translation of the tarsal joint obtained from all horses during stance: cranial(+)/caudal(-) translation (top), medial(+)/lateral(-) translation (middle) and proximal(+)/distal(-) translation (bottom). The black line indicates mean value from corrected skin data. The dotted line indicates mean value from reference bone data. Zero indicates the impact value.

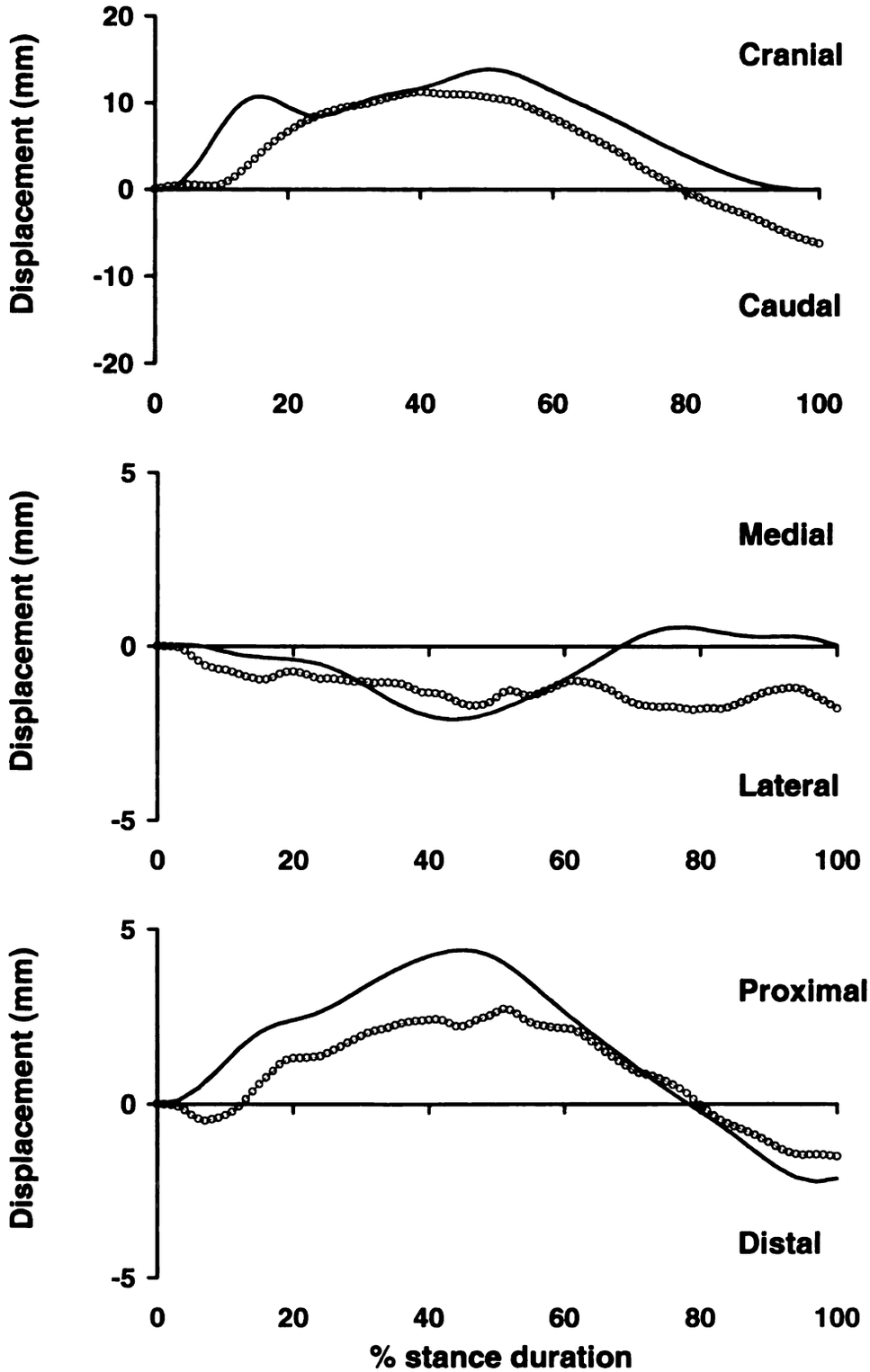

Figure 5-13 Flexion (-)/extension (+) angle of horses 1-4 (top to bottom) during swing. The gray line indicates angle obtained from skin markers. The black line indicates angle obtained after application of 3D skin correction algorithm. The dotted line indicates angle obtained from bone pins. Zero indicates the impact value.

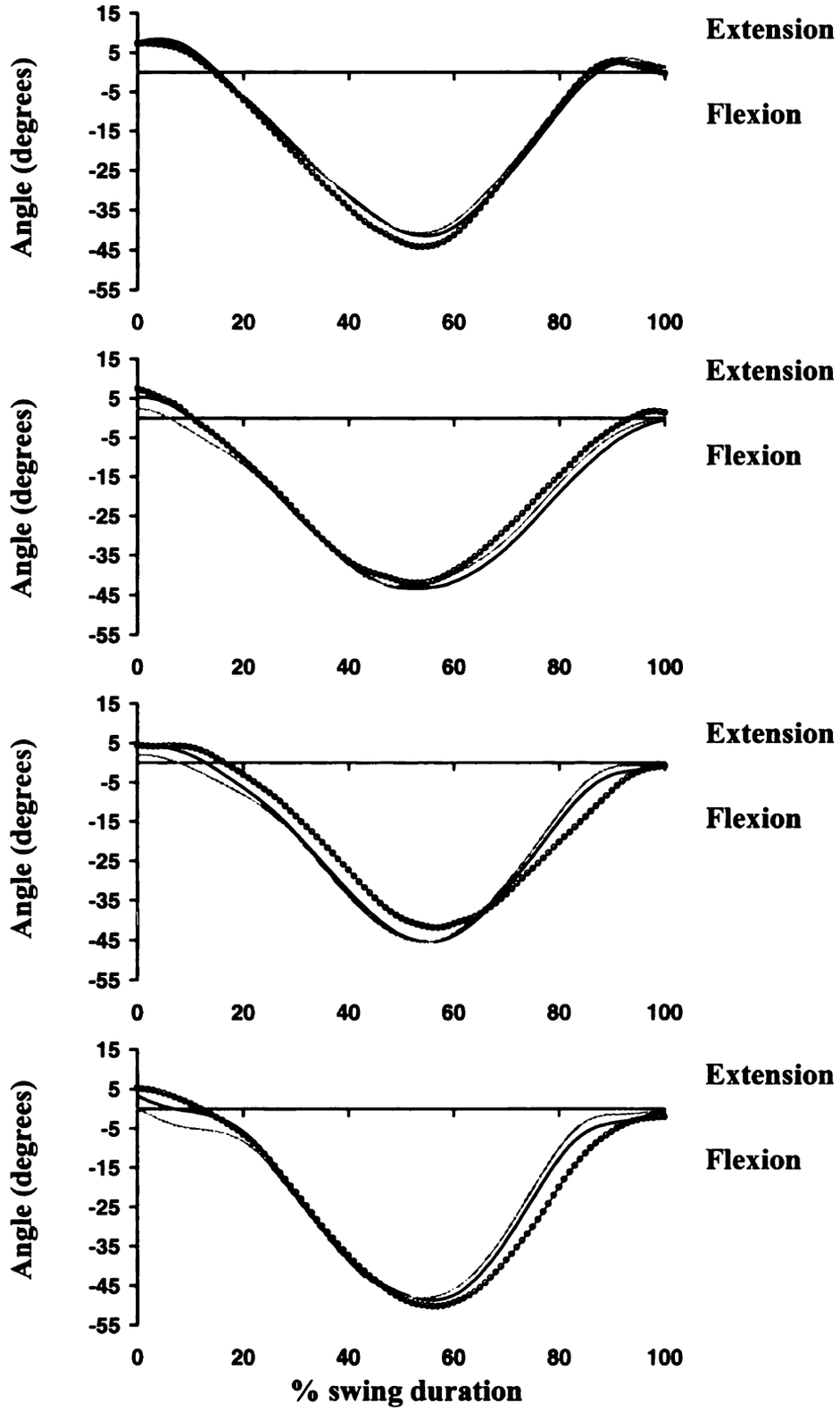

Figure 5-14 Abduction (-)/adduction (+) angle of horses 1-4 (top to bottom) during swing. The gray line indicates angle obtained from skin markers. The black line indicates angle obtained after application of 3D skin correction algorithm. The dotted line indicates angle obtained from bone pins. Zero indicates the impact value.

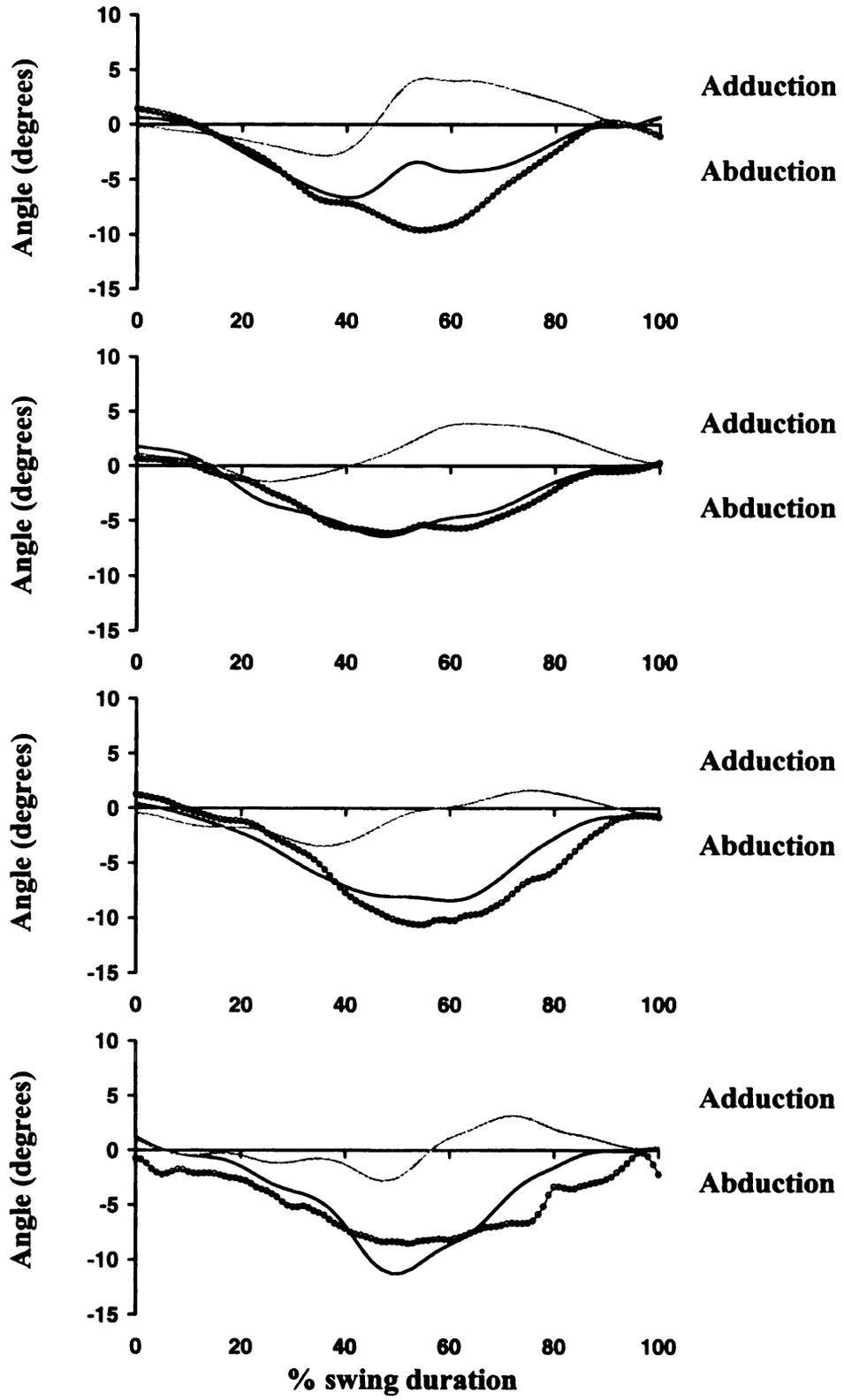

Figure 5-15 Internal (+)/external (-) rotation angle of horses 1-4 (top to bottom) during swing. The gray line indicates angle obtained from skin markers. The black line indicates angle obtained after application of 3D skin correction algorithm. The dotted line indicates angle obtained from bone pins. Zero indicates the impact value.

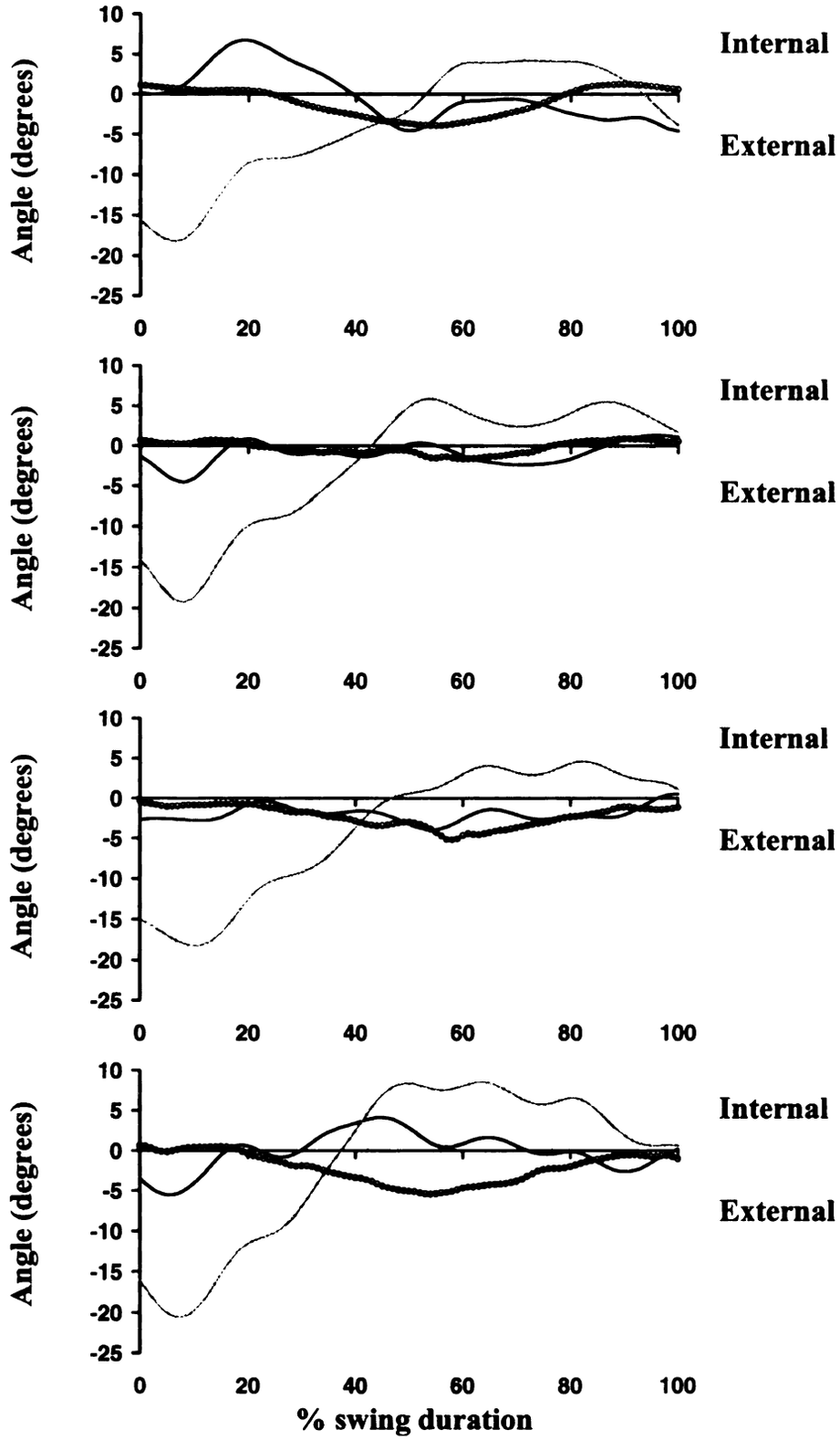

Figure 5-16 Cranial (+)/caudal (-) translation of horses 1-4 (top to bottom) during swing. The gray line indicates angle obtained from skin markers. The black line indicates angle obtained after application of 3D skin correction algorithm. The dotted line indicates angle obtained from bone pins. Zero indicates the impact value.

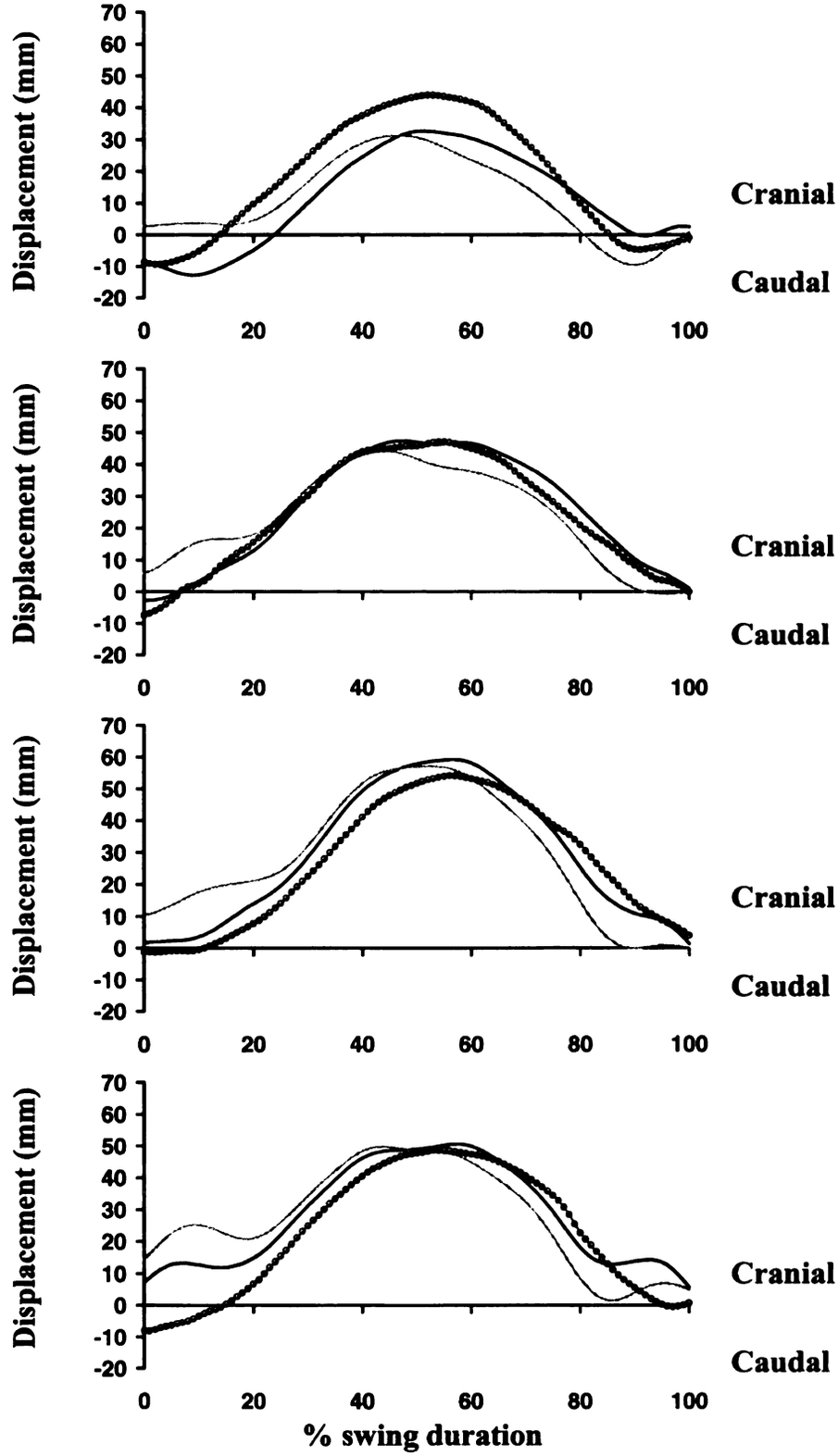

Figure 5-17 Medial (+)/lateral (-) translation of horses 1-4 (top to bottom) during swing. The gray line indicates angle obtained from skin markers. The black line indicates angle obtained after application of 3D skin correction algorithm. The dotted line indicates angle obtained from bone pins. Zero indicates the impact value.

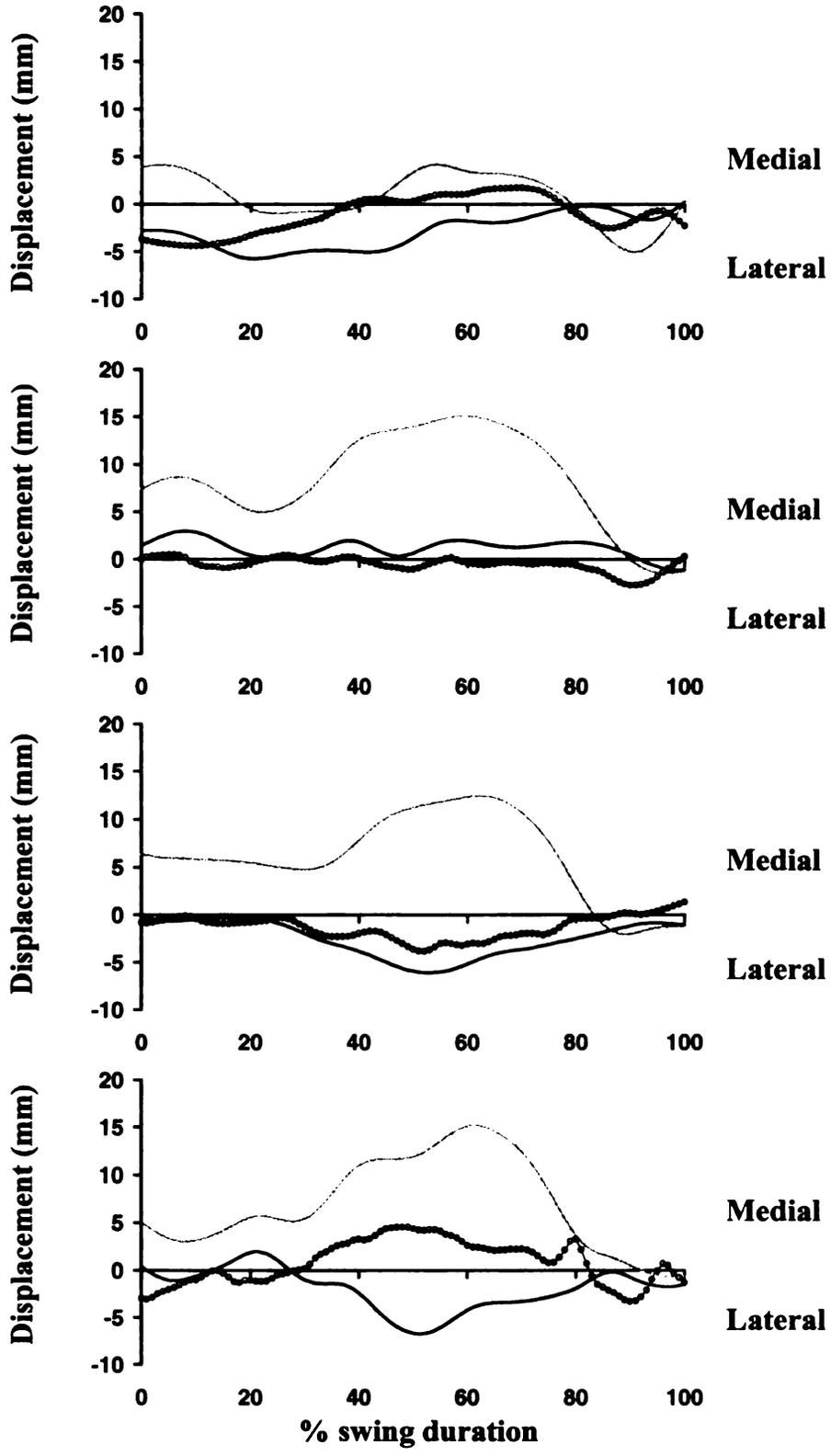

Figure 5-18 Proximal (+)/distal (-) translation of horses 1-4 (top to bottom) during swing. The gray line indicates angle obtained from skin markers. The black line indicates angle obtained after application of 3D skin correction algorithm. The dotted line indicates angle obtained from bone pins. Zero indicates the impact value.

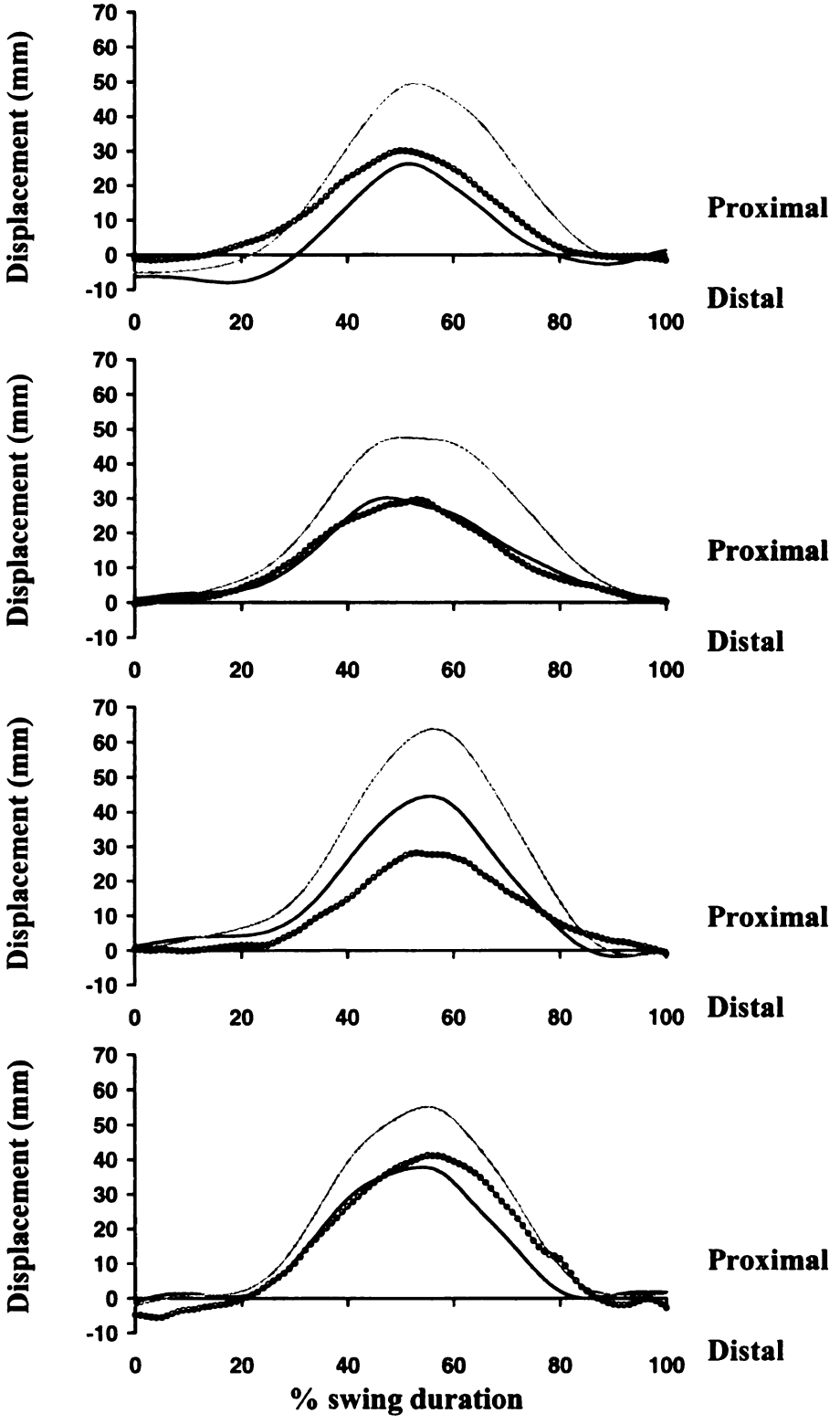

Figure 5-19 Three-dimensional rotation of the tarsal joint obtained from all horses during swing: flexion(-)/extension(+) angle (top), abduction(-)/adduction angle (middle) and internal(+)/external(-) rotation angle (bottom). The black line indicates mean value from corrected skin data. The dotted line indicates mean value from reference bone data. Zero indicates the impact value.

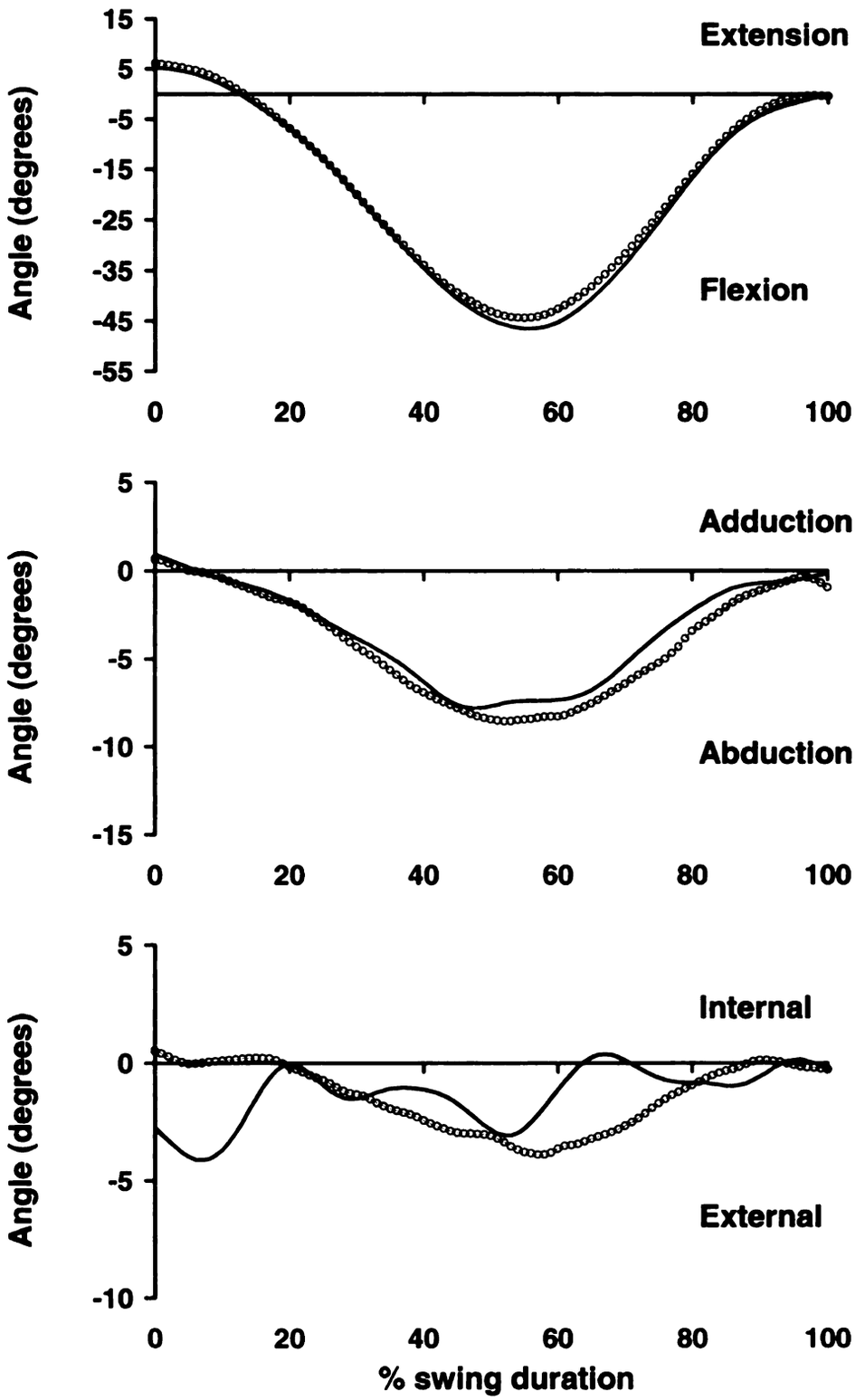

Figure 5-20 Three-dimensional translation of the tarsal joint obtained from all horses during swing: cranial(+)/caudal(-) translation (top), medial(+)/lateral(-) translation (middle) and proximal(+)/distal(-) translation (bottom). The black line indicates mean value from corrected skin data. The dotted line indicates mean value from reference bone data. Zero indicates the impact value.

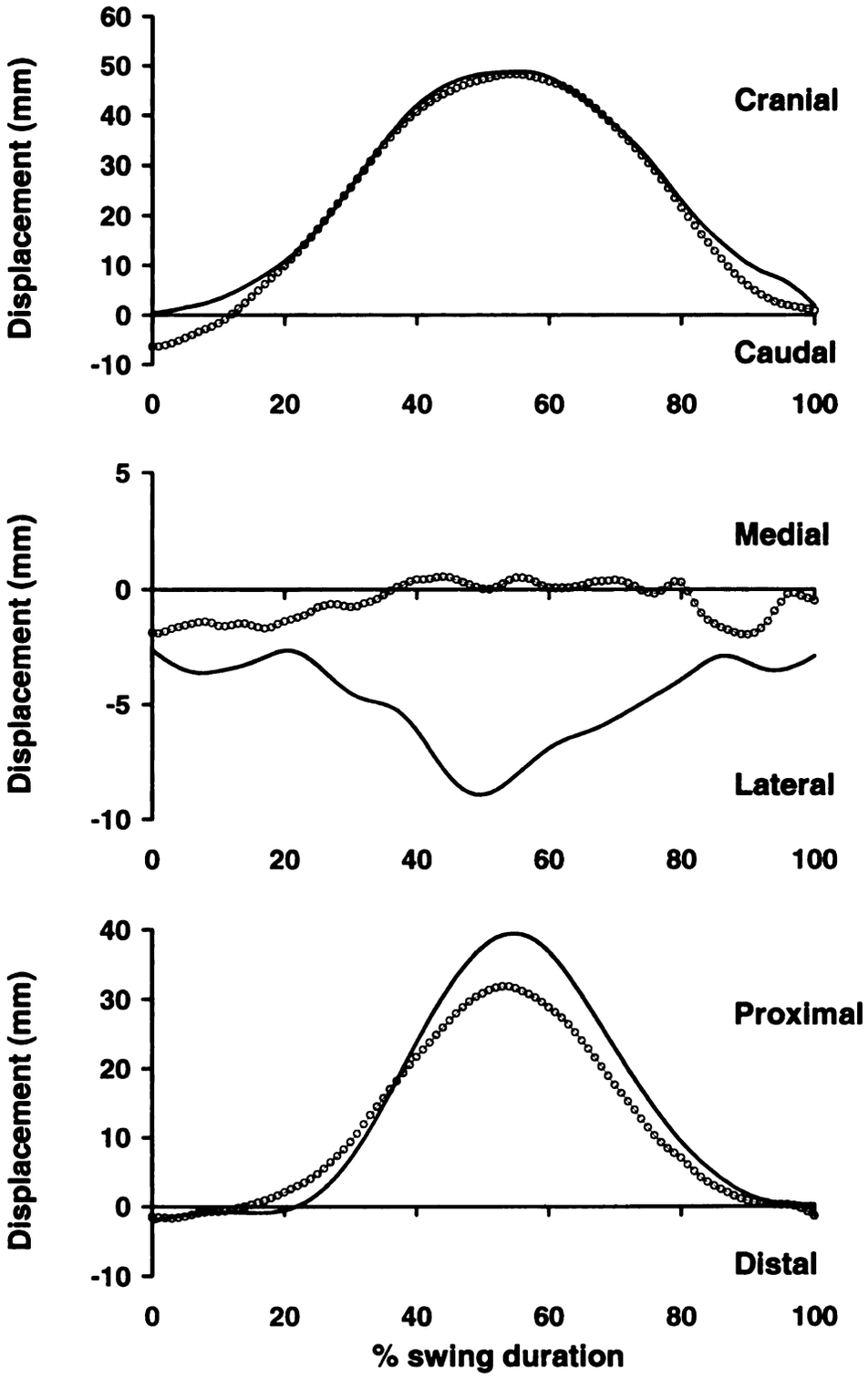

EFFECTS OF TARSAL LAMENESS ON 3D MOTION

Several values were measured during stance and swing to represent each type of rotational or translational motion. The curve obtained from cranial/caudal translation during stance indicated that the second peak from skin corrected data had the closest value to the peak cranial translation from the reference bone data, and this peak was used to represent peak cranial translation during stance. Angular and linear displacements during stance were obtained from the impact value to peak flexion, to peak abduction, to the second peak of cranial translation and to peak proximal translation. The ranges of motion were calculated as the differences between the minimal and maximal values during stance. During swing, the angular and linear displacements were obtained from the impact value to peak flexion, to peak abduction, to peak cranial translation and to peak proximal translation. The total ranges of motion during swing were calculated as described for the stance phase. Dependent t-tests were used to compare the measured variables in the sound and lame conditions (Table 5-5). The corresponding ranges of motion from impact to peak flexion from 2D analysis of the right hind limb in the sound condition (Chapter 3) were 9.77 (1.49) and 41.95 (2.65) degrees during stance and during swing, respectively. The total ranges of joint flexion/extension (Chapter 3) were 12.44 (1.14) and 44.05 (1.78) degrees during stance and swing, respectively.

From Table 5-5, the significant decrease in range of flexion during the first half of stance corresponded with the significant decrease in range of cranial translation and a trend toward a decrease in proximal translation of the metatarsal segment relative to the fixed tibia. In the normal tarsal joint, the rotational and translational motions occur synchronously. Due to the shape of the talus, rotation is coupled with translation. To

quantify the magnitude of coupling between the other motions with the joint flexion/extension, reference bone data were used to determine the ratios of the joint rotation and translation relative to changes in flexion (Table 5-6). These ratios were selected corresponding to the variables that differed significantly between sound and lame conditions in Table 5-5.

Table 5-5 Differences of three-dimensional variables between sound and lame conditions of the right hind limb. Values are mean and (SD).

Stance phase

Variables	Sound condition	Lame condition	Mean difference
Impact to peak flexion (degrees)	10.6 (1.7)	8.1 (0.6)	-2.5 (1.4) [a]
Total range of flexion/extension (degrees)	15.9 (2.8)	14.5 (1.9)	-1.4 (1.3)
Impact to peak abduction (degrees)	1.6 (1.0)	1.6 (1.5)	0.0 (0.7)
Total range of abduction/adduction (degrees)	3.1 (0.8)	3.2 (1.8)	0.1 (1.1)
Impact to peak cranial translation (mm)	17.1 (3.0)	12.9 (2.1)	-4.2 (2.5) [a]
Total range of cranial/caudal translation (mm)	20.4 (1.9)	16.9 (2.6)	-3.5 (1.8) [a]
Impact to peak proximal translation (mm)	5.1 (1.0)	3.8 (0.9)	-1.3 (1.1) [b]
Total range of proximal/distal translation (mm)	8.2 (2.0)	7.1 (1.4)	-1.1 (1.6)

Swing phase

Variables	Sound condition	Lame condition	Mean difference
Impact to peak flexion (degrees)	46.8 (4.0)	44.0 (3.4)	-2.8 (3.4)
Total range of flexion/extension (degrees)	52.2 (3.0)	50.4 (1.7)	-1.9 (3.4)
Impact to peak abduction (degrees)	9.4 (2.1)	9.1 (1.5)	-0.3 (2.8)
Total range of abduction/adduction (degrees)	10.5 (2.4)	10.1 (2.1)	-0.3 (3.4)
Impact to peak cranial translation (mm)	49.7 (11.9)	43.2 (8.5)	-6.5 (5.9)
Total range of cranial/caudal translation (mm)	52.1 (7.4)	46.7 (5.5)	-5.4 (6.2)
Impact to peak proximal translation (mm)	39.5 (9.3)	37.1 (8.7)	-2.4 (1.4) [a]
Total range of proximal/distal translation (mm)	44.2 (8.4)	40.3 (7.7)	-4.0 (3.1) [b]

Negative mean differences indicated values from sound condition were higher than values from lame condition. [a] indicated $P<0.05$. [b] indicated $0.05<P<0.1$.

Table 5-6 Range of motion obtained from reference bone data during stance and swing phases.

Variables	Mean (SD)	Magnitude change *
Impact to peak flexion, stance (degrees)	6.23 (1.5)	1.00
Impact to peak cranial translation, stance (mm)	7.71 (0.62)	1.24
Impact to peak proximal translation, stance (mm)	1.87 (0.95)	0.30
Impact to peak flexion, swing (mm)	33.43 (3.22)	1.00
Impact to peak proximal translation, swing (mm)	23.47 (5.19)	0.70

* Magnitude change means the change in a variable with 1-degree change in flexion/extension angle.

DISCUSSION

The tarsal joint complex consists of four joints. The major motion is the flexion/extension at the tarsocrural joint. The motions at the other 3 joints, proximal intertarsal, distal intertarsal and tarsometatarsal joints, are considered to be small. Due to the oblique orientation of the talar ridges, flexion/extension of the tarsocrural joint is accompanied by translational motion, which is characteristic of helical motion (Badoux, 1987). The largest force loading the distal tibia is a torsional force (Schneider, et al., 1982; Hartman, et al., 1984). The combination of torsional loading from the tibia and the oblique orientation of the talus may lead to motion at the other three low-motion joints in the tarsal joint complex. The objective of this study was to develop a non-invasive method of measuring 3D motion of the tarsal joint complex. Since the segments between the three distal tarsal joints are extremely short, it is not possible to attach skin markers to represent each segment of the tarsal joint complex, though some assumptions could be made regarding the motion of these joints. The tarsocrural joint has a screw motion

(Badoux, 1987; Lanovaz, et al., 2002), which implies that rotational and translational motions of the tarsocrural joint in any direction are highly coupled with flexion/extension of this joint. Loss of coupling between flexion/extension and the other motions suggests movement at tarsal joints outside the tarsocrural joint (Lanovaz, et al., 2002).

The flexion/extension angle obtained from skin markers using 2D skin correction algorithms (van Weeren, 1989) had higher RMS errors compared to the flexion/extension angle obtained from uncorrected 3D skin data (Tables 5-1 and 5-3). This was because the number of markers per segment in 3D skin marker set was higher and the markers were more widely distributed over the segment than in the 2D skin marker set. The tarsal joint motion from the 2D marker set was constructed from 3 markers connected by two straight lines representing the tibial and metatarsal segments. Tarsal joint motion from the 3D marker set was constructed from 12 markers distributed over the two segments. The motions of all 12 markers were taken into account for calculating the segmental motion. Therefore, even uncorrected, the 3D skin marker set could represent the motion of the segment better than the straight line in the 2D marker set. The tibial markers underwent much larger displacements than those on the third metatarsus (Appendix A). The 3D skin correction algorithm reduced errors due to skin displacement, resulting in lower RMS errors in joint flexion/extension compared with the reference bone data. It was shown in this study that the skin corrected 2D marker set might underestimate the flexion/extension ranges of motion during both stance and swing phases.

The correction algorithms for skin displacement are important for obtaining accurate kinematic data from skin-based markers. In order to study 3D kinematics of the tarsal joints using skin-based markers, it was necessary to develop 3D skin correction

algorithms based on knowledge of the motion of the underlying bones. The advantage of this study was that the same horses were used for two data collection sessions. Approximately one month after recovery from synovitis, the same horses were used in the bone pin study of tibial and third metatarsal kinematics (Lanovaz, et al., 2002), the data from which were used to construct skin correction algorithms (Appendix A). By using the same horses for both studies, it enhanced the ability to test how closely the skin correction algorithms could correct the skin marker data to the real bone motion in the individual horse.

Data from the reference bone motion indicated that some variation among horses existed in rotational and translational motions. Therefore, the skin correction algorithms, which were calculated as the best fit for a group of horses, might not be able to account for individual variation in all motions. Even though the RMS errors for internal/external rotation and medial/lateral translation were small, their ranges of motion were also small. In addition, the shape agreement between the reference bone data and skin corrected data were poor. Therefore, it is not suggested that this 3D marker set be used for testing any changes in these two motions. During stance, abduction/adduction, proximal/distal translation and cranial/caudal translation were evaluated as having fair shape agreement. As described previously, the shape disagreement for those first two motions were due to different in the magnitude of the movement, but the directions of motion were correct. The fair agreement for cranial/caudal displacement was mainly from different shapes in early stance, while the information around the middle of stance was quite similar. Therefore, the comparisons between conditions for these ranges of motion in the same

horse should be acceptable, but direct comparison between different horses should be avoided due to underestimation or overestimation of joint motion from skin-based data.

During swing, the shape agreements for internal/external rotation and medial/lateral translation were also poor as described during stance. Therefore, it is not suggested to use this 3D skin marker set to obtain information describing these two motions during swing. Proximal/distal translation showed good agreement in shape, although proximal displacement in mid swing was overestimated (Figure 5-20), the value still fell within one standard deviation of the reference bone data. Therefore, swing phase flexion/extension, abduction/adduction, cranial/caudal translation and proximal/distal translation ranges of motion can be estimated with acceptable accuracy from corrected skin data.

Since the placements of 3D skin markers in the same horse were similar between sound and lame conditions, the skin correction algorithms should correct for skin displacement in a similar way. Therefore, changes in the 3D range of motion should represent the effect of synovitis in the distal intertarsal and tarsometatarsal joints on the 3D tarsal joint motion. The 2.5 degrees decrease in joint flexion when pain existed in the distal intertarsal and tarsometatarsal joints was similar to the 2.2 degrees decrease in the tarsal joint range of motion during stance obtained from 2D analysis. From reference bone data, the cranial/caudal translation was not completely proportional to the flexion/extension angles during stance. The additional cranial translation of the metatarsus relative to tibia might come from superposition of motion outside the tarsocrural joint (Lanovaz, et al., 2002). According to Table 5-6, the 2.5 degrees decrease in flexion angle during stance should be coupled with 3.1 mm decrease in cranial

translation. The significant decrease of 4.2 mm in cranial translation exceeded the calculated values accompanying the decrease in flexion angle, which suggests a decrease in cranial translation outside the tarsocrural joint of around 1.1 mm.

During stance when the tarsal joint flexes, the medial branch (cunean tendon) of the cranial tibial tendon comes under tension (Molenaar, 1983). The insertion of the tendon might pull the fused first and second tarsal bone forward, consequently, compressing and pushing the central and third tarsal bones forward. On the right hind limb in the lame condition, the gastrocnemius adjusted by reducing the high peak negative power during the first half of stance (Chapter 4). This corresponded to the time when tarsal joint range of motion decreased from impact to peak flexion. This might reduce compression on the central tarsal bone in an attempt to reduce the motion due to pain from synovitis, leading to reduction of cranial translation in the lame limb.

In the normal joint, motion is essential for maintaining healthy cartilage. The movement of nutrients, water and waste within the cartilage matrix is facilitated when the articular cartilage is cyclically loaded during locomotion (Pool, 1996). Due to the flat shape of the central tarsal and third tarsal bones, motion of the distal intertarsal and tarsometatarsal joints is likely restricted to translation and axial rotation. Information obtained from the reference bone data (Lanovaz et al, 2002) indicated the presence of axial rotation and cranial/caudal translation of the metatarsal segment relative to the fixed tibial segment during stance that was not coupled with flexion/extension of the tarsocrural joint. Although synovitis might be associated with changes in internal/external rotation, the correction algorithm for estimating internal/external rotation from the skin markers was shown not to be sufficiently accurate for general use. The decrease in cranial

translation that occurred in horses with synovitis could not be separated among the joints in the tarsal joint complex, but the change between the sound and lame conditions was assumed to be the effect of synovitis on the motion of the distal intertarsal and tarsometatarsal joints. This small, but significant, decrease in cranial translation might represent a stage in pathogenesis of distal tarsal osteoarthritis. Examination of specimens in different stages in development of bone spavin strongly suggests that the cause is probably trauma to the periarticular soft tissues (Pool, 1996). The resulting pain and inflammation reduces the joint movement and gliding motion ceases. Formation of enthesophytes and periosteal new bone formation at the joint capsule insertion line strengthens the traumatized tissues, and also restricts the gliding motion of the distal tarsal joints. Repetitive forces of weight bearing are transmitted through the stationary distal tarsal joints, resulting in full-thickness necrosis of articular cartilage and focal subchondral bone remodeling at the area of force transmission through the joints.

Strain gauges mounted on the third metatarsus of walking ponies showed that the point of force application at the tarsometatarsal joint was located in the dorsomedial portion of the joint surface during the first peak of vertical GRF, and was located in the dorsolateral portion during the second peak of vertical GRF (Schamhardt, et al., 1989). At trot and canter, the third metatarsus was loaded with a higher compressive force than at walk and the third metatarsus was closely aligned with the ground reaction force throughout most of the stance (Biewener, et al., 1988). Unfortunately, the latter study did not indicate the point of force application at the tarsometatarsal joint. The radiographic changes in horses affected with bone spavin are mostly found on the dorsomedial side of the distal tarsal joints (Cottage, et al., 1997). This area of the joint surfaces was examined

histologically in studies designed to assess early pathological changes in the distal tarsal joints (Laverty, et al., 1991; Barneveld and van Weeren, 1999), which might be the area through which the load is transmitted across the distal tarsal joints. The reduction in cranial translation in horses with synovitis of the distal tarsal joints would lead to stationary joint surfaces in this area. If the horses are subjected to high intensity work, the load transmitted through this area might exceed the physiological limit and lead to necrosis of articular cartilage. If this hypothesis is correct, it could support the pathogenesis of bone spavin proposed by Pool (1996).

During swing, there was a significant decrease of 2.4 mm in the range of proximal translation at the tarsal joint complex without a change in the range of joint flexion. This decrease might be related to the snapping motion of the tarsal joint that is due to the eccentric attachment of the collateral ligaments relative to the center of rotation of the tarsal joint. The collateral ligaments are stretched when the joint is fully extended at the end of stance, thus storing elastic energy. As the joint flexes, the tibia moves around the talar groove until it passes the critical point at which there is no tension on the ligament. At that point, the collateral ligament recoils and elastic energy is released (Rooney, 1990), resulting in a snapping motion of the tarsal joint. Because the collateral ligaments attach with a proximal/distal orientation, some of the elastic energy release might contribute to the proximal/distal translation of the tarsal joint complex. None of the other tested variables changed in association with the decrease in proximal translation found in this study. In the reference bone data (Figures 5-1 and 5-2), joint extension at the end of stance was accompanied by internal rotation and lateral translation. Since the skin corrections were inadequate to assess these two motions, information between sound and

lame conditions could not be compared. It is theorized that when lameness occurs in the distal intertarsal and tarsometatarsal joints, it limits joint motion by decreasing internal rotation and lateral translation, which might decrease the distance between proximal and distal attachments of the lateral collateral ligament when the joint was fully extended. Therefore, elastic energy storage decreases, with a consequent decrease in elastic energy release to generate the proximal displacement.

The range of motion from impact to peak flexion during stance decreased by 2.5 degrees when synovitis was present, corresponding to a decrease in tarsal joint range of flexion/extension of 2.2 degrees as determined by 2D skin markers. The 2D kinematic analysis offers a relatively quick and easy marker setup and appears to provide reasonable information to assess the effect of different conditions on flexion and extension of the joint. In horses affected with natural bone spavin, the point of force application to the hoof, assessed by a force plate analysis, was more caudal and lateral than in normal horses, which was believed to be an adaptation to reduce loading in the painful medial aspect of the tarsal joint (Boswell, et al., 2000). Even though the 3D skin marker set in this study provided fair assessment of magnitude of 3D motion during stance, it might be interesting to apply the 3D marker set to observe the pattern of tarsal joint motion which might correspond to the more caudal and lateral loading in Boswell, et al. (2000). Conservative treatment of bone spavin includes balancing and trimming the foot and the application of special shoes, such as the rolled toe shoe with a lateral extension or lateral trailers (Dyson, 1995), raised heel/rolled toe shoe (Cottage, et al., 1997) or lateral extension shoe (Gough and Munroe, 1998). The 3D kinematics, in combination with the analysis of 2D tarsal net joint energy profiles might enhance the

quantification of biomechanical changes after the application of special shoes, as a method of testing the usefulness of each type of orthopedic shoes. The relatively good 3D information obtained from the 3D skin marker set during swing allows analysis and comparison of information between horses. It may be useful for assessing motion other than flexion/extension, such as the extreme motion in the athlete during performance, or the stabbing motion of the tarsal joint during swing (Dyson, 1995; Gough and Munroe, 1998).

CONCLUSION

The tarsal joint complex has motion outside the sagittal plane. The motions during stance include flexion, abduction, internal rotation, cranial translation, lateral translation and proximal translation of the metatarsus relative to the tibia. The motions during swing were similar to those during stance, except for external rotation of the metatarsus relative to the tibia. The skin marker set in this study could be used to assess the motion during swing fairly accurately. During stance, it is acceptable to compare the motion within horses. The ranges of motion during swing were larger than those during stance. Distal tarsal synovitis resulted in decreases in ranges of tarsal joint flexion, cranial translation during stance and a decrease in proximal translation during swing. The findings might support the hypothesis that synovitis is the primary event in the development of osteoarthritis in distal tarsal joints.

CONCLUSIONS

Gait analysis techniques, including kinematic and force plate analysis, have been successfully applied to study normal and pathological gaits in horses. In the present study, inverse dynamic analysis was used to study the two-dimensional net joint mechanical work of the equine hind limb at the trot. Net joint moment, net joint power and net joint energy profiles of the coxofemoral, femorotibial, tarsal, metatarsophalangeal and distal interphalangeal joints in sound trotting horses have been identified. The biomechanical profiles of the hind limb joints were similar between horses after adjustment for the effect of subject velocity and body mass, which supports Hypothesis 1. During stance, the coxofemoral and tarsal joints were the main sources of energy generation to propel the body forward. During trotting, energy expenditure reduced by elastic energy conservation, especially at the metatarsophalangeal joint, assisted by the tarsal and femorotibial joints. The distal interphalangeal joint absorbed energy and acted as an energy damper. During swing, the main sources of energy generation were the coxofemoral and tarsal joints. The femorotibial joint performed mostly negative work to control the limb motion, while the distal interphalangeal and metatarsophalangeal joints were driven by the inertia, following the motion of the proximal joints.

Induction of synovitis by injecting lipopolysaccharide endotoxin in the distal intertarsal and tarsometatarsal joints was performed to study the effect of tarsal lameness on equine locomotion at the trot. The lameness in this study appeared to be mild, which made it difficult to identify asymmetrical motion between the left and right hind limbs. Comparisons between lame and sound conditions in the same limb proved more suitable

for evaluating mild lameness than the asymmetry indices that have been used in more severe lameness. There were several kinematic and kinetic changes within the lame limb and between different limbs when compared between the sound and lame conditions, which supports Hypothesis 2. In the lame tarsal joint during stance, there were decreases in peak vertical force, tarsal joint range of motion, peak negative net joint power during early stance, peak positive power and positive energy during push off. Mechanical energy deficits were found in the lame tarsal joint by decrease in total positive and negative net joint energy. During swing, there were decreases in peak flexor moment during early swing and peak positive net joint power during late swing. There was a trend toward a decrease in total positive net joint energy at the tarsal joint during swing. There was no compensatory increase in energy generation from other joints within the lame limb. Instead, the load was redistributed between the limbs, so that the lame diagonal pair was unloaded, with a reduction of the diagonal forelimb vertical impulse in the lame condition. The contralateral hind limb compensated by showing a trend toward an increase in peak vertical force. During early swing, there was an increase in positive power at the left (compensating) coxofemoral joint, which increases the momentum of the limb as it swings forward, thus helping to propel the body forward, and maintain the body's forward velocity.

Three-dimensional (3D) kinematics of the right tarsal joint was studied using an array of skin-based markers to study rotational and translational motions of the third metatarsus relative to the tibia. Six markers were attached on each bone segment. Comparison between reference bone data and skin-based marker data indicated that tarsal joint complex has the motion outside the sagittal plane and the motion can be identified

using skin markers, which supports Hypothesis 3. Flexion/extension and abduction/adduction rotational motions and proximal/distal and cranial/caudal translational motions could be measured fairly accurately during swing, and the motions during stance were acceptable for comparison within horses. Internal/external rotational and medial/lateral translational motions during stance and swing were not successfully obtained from this skin marker set. Tarsal synovitis in the distal intertarsal and tarsometatarsal joints resulted in a reduction of the joint flexion and cranial translation during stance, and a decrease in proximal translation of the third metatarsus relative to the tibia during swing.

From this study, it can be stated that tarsal joint is an important source of positive work to move the limb throughout the stride. Energy generation at the tarsal joint came from both muscular work and elastic energy conservation. Elastic energy storage and release occurs mainly during stance. When mild lameness occurs in the distal tarsal joints, adjustments in the locomotion pattern were identified using the inverse dynamic analysis. The horse maintained its forward velocity with minimal changes in kinematics making visual detection of lameness difficult in the early stage of synovitis. The availability of data describing the horse's locomotor characteristics when sound might be worthwhile for monitoring that horse through time. The technique could be applied objectively to evaluate the outcome of treatment regimes in horses affected with pain in the distal intertarsal and tarsometatarsal joints.

APPENDIX A

THE DEVELOPMENT OF CORRECTIONS FOR SKIN DISPLACEMENT ARTIFACTS AT THE EQUINE TARSAL JOINT AND APPLICATION TO 3D JOINT KINEMATICS

Joel L. Lanovaz, Siriporn Khumsap, Hilary M. Clayton

ABSTRACT

In horses, the tarsus is arguably the most critical hind limb joint with respect to both performance and injury. Previous kinematic investigations have focused on 2D planar motion. Routine study of 3D tarsal kinematics is hampered by errors due to the displacement of skin surface tracking markers relative to the underlying bones. Reliable kinematics can be obtained with bone-fixed markers, but an accurate, non-invasive method would have more applications.

Simultaneous kinematic data from skin-based and bone-fixed markers attached to the tibia and third metatarsus were collected from three trotting subjects. The 3D skin displacement patterns for the skin-based markers were parameterized using a truncated Fourier series model. These displacements were expressed in terms of the local coordinate systems for each bone. The 3D kinematics of the segments for any stride could then be calculated by relating the motion of the skin-based markers in global coordinates and the local skin displacements using an SVD based algorithm. The results showed that the displacement model could reduce the RMS error in the joint kinematics 35 to 65% over uncorrected skin-based data. When the models were applied to two additional independent subjects, the shapes of the resulting traces matched well with the

bone-fixed kinematics. The errors in tarsal internal/external rotation estimation and translation with respect to the mediolateral axis of the tibia from the corrected data were still too high to accurately reproduce those degrees of freedom. However, the remaining rotations and translations were estimated with sufficient accuracy to be used in general analysis.

INTRODUCTION

The tarsal joint is one of the primary sites of lameness in the equine hind limb (Gabel, 1983; Winter et al., 1996; Gough and Munroe, 1998) and its basic kinematic parameters have been correlated with sport horse performance (Holmström et al., 1995). Several studies have reported planar 2D equine tarsal joint motion (Kobluk et al., 1989; Holmström et al., 1994; Back et al., 1995; Hodson et al., 2001), but only a few studies have examined 3D equine tarsal kinematics either in vitro (Schamhardt et al., 1984) or in vivo (Lanovaz et al., 2002).

When skin surface markers are used to track segmental motion, 3D kinematics calculated from these markers are especially sensitive to skin motion artifacts. Relative displacements between skin and bone at some sites over the equine tibia have a range of motion of over 80 mm during a stride at the trot (van Weeren et al., 1992). Marker cluster design and placement can reduce some errors (Cappozzo et al., 1997), but actual underlying bone motion is still difficult to reproduce (Cappozzo et al., 1996). This is true even when utilizing a redundant marker set and a least-squares estimator of the transformation data (Reinschmidt et al., 1997a).

Kinematic data collected using bone-fixed markers have been used to describe the true underlying in vivo kinematics of joints in human subjects (Lafortune et al., 1992; Cappozzo et al., 1996; Reinschmidt et al., 1997b) and in horses (van Weeren et al., 1992; Lanovaz et al., 2002). The use of bone-fixed markers is invasive and it is desirable to develop procedures that avoid the need for surgical intervention but still produce an acceptable degree of accuracy.

Skin displacement artifact correction algorithms have been successfully developed for 2D kinematics in horses (van Weeren et al., 1992) and this procedure has been shown to improve joint angular data over non-corrected kinematics. The feasibility of using 3D correction algorithms has not been investigated in equine subjects.

Alexander and Andriacchi (2001) suggested a 3D skin correction procedure based on the point cluster technique (Andriacchi et al., 1998) that utilized information about skin displacement in the local bone coordinate system. The current study employs a similar but more direct approach using a singular value decomposition (SVD) algorithm (Söderkvist and Wedin, 1993). In this study, simultaneous kinematic data collected from skin surface and bone-fixed markers from the tibia and third metatarsus of equine subjects are used to parameterize the general motion of skin marker sites relative to the underlying bone. Models of the skin motion are developed and these displacement models are then used in the SVD procedure to calculate 3D kinematics from skin surface markers.

METHODS

Subjects. The subjects were 5 sound Quarter Horses of similar mass and size. The horses were judged to be free of obvious lameness during a clinical examination prior to the study. The protocol used for this investigation was approved by the university's ethical use committee.

Bone based markers. Subjects 1-3 were utilized for the following bone-fixed kinematic protocol. A detailed explanation of the bone-fixed procedure has been presented elsewhere (Lanovaz et al., 2002). In summary, 4.75 mm diameter Steinmann pins were inserted percutaneously under general anesthesia into the tibia and third metatarsus of the right hind limb of each of the three subjects. A marker triad with 25 mm diameter reflective spherical markers was rigidly attached to each pin during data collection session. Analgesics were administered systemically and locally, and all subjects appeared pain free and moved normally during data collection.

Skin-based markers. For all 5 subjects, a set of six 25 mm diameter, spherical reflective markers were attached at predetermined locations on the surface of the skin over the right tibia and the right metatarsus of each subject (Fig 1). This was in addition to the bone-fixed marker triads for subjects 1-3. The distance between markers TIB-A and TIB-B served as the reference length for the tibia and the distance between markers MET-A and MET-B served as the reference length for the third metatarsus. The skin-based markers were distributed over the lateral aspect of each segment, since most studies

track kinematic data from the lateral side. The tibial markers were concentrated proximally in order to minimize visual merging with the bone pin marker triads.

Bone coordinate systems. In order to define local bone-based coordinate systems (BCS), all subjects were placed in a normal standing position and an additional reflective marker was placed over the medial malleolus of the tibia (TIB-C) and the dorsal edge of the head of second metatarsal bone (MET-C). These markers were removed for data collection.

A right-handed coordinate system was developed for the tibia by first defining the flexion/extension axis as the vector running from TIB-B to TIB-C. The adduction/abduction axis of the tibia was defined as a vector pointing cranially and perpendicular to the plane formed by the flexion/extension axis and the vector running from TIB-B to TIB-A. Finally, the internal/external rotation axis of the tibia was defined as a vector pointing proximally along the long axis of the bone perpendicular to the plane formed by the flexion/extension and adduction/abduction axes. The origin of the tibial BCS was embedded in the bone midway between TIB-B and TIB-C.

The third metatarsal BCS was defined in a similar manner to the tibial system with the flexion/extension axis defined as a vector running from MET-B to MET-C. The adduction/abduction axis was defined as a vector pointing cranially and perpendicular to the plane formed by the flexion/extension axis and the vector running from MET-B to MET-A. The internal/external rotation axis was defined as pointing proximally and perpendicular to the other two axes, forming a right-handed coordinate system. The origin of the third metatarsal BCS was embedded in the bone midway between MET-B

and MET-C. For both the tibia and third metatarsus, the adduction/abduction, flexion/extension and internal/external rotation axes are also referred to as the x, y and z axes respectively.

Data Collection. All subjects were led in hand at the trot along a 40 m rubber covered, concrete runway. Three dimensional kinematic data were collected using a 6 camera analysis system (ExpertVision RealTime, Motion Analysis Corporation, Santa Rosa, CA) recording at 120 frames per second. A volume measuring 5 m by 2 m by 3 m was calibrated and the mean error in measuring a known length within the volume was 0.88 mm. Each successful trial consisted of a single stride of the right hind limb, starting with stance. Data collected from a force platform (LG6-4-8000, AMTI, Watertown, MA) embedded in the runway were used to detect the onset and termination of the right hind stance. Termination of a right hind stride was determined by an automatic algorithm that matched terminal swing phase kinematics to the kinematic pattern at the beginning of the previous stance phase. The kinematic data from the trot trials were optimally filtered using a Generalized Cross Validation (GCV) spline routine (Woltring, 1986). For subjects 1-3, the bone-fixed triads and the skin-based markers were tracked simultaneously for each trial. Four strides from each horse were selected in order to closely match forward velocity between subjects.

Reference Kinematics. The 3D kinematics of the tibia and third metatarsus, as calculated by the motion of the bone-fixed triads, were defined as the "true" reference kinematics of the bones. The orientation matrices and displacement vectors for the reference kinematics were calculated by relating the locations of the triads in their

corresponding BCS with their global locations during each frame of motion data using an SVD method (Söderkvist and Wedin, 1993). The 3D attitudes of the segments and tarsal joint were expressed in terms of a spatial attitude vector (Woltring, 1994). The attitude vector components are referred to as θ_X, θ_Y and θ_Z and correspond generally to the abduction/adduction, flexion/extension, and internal/external rotation angles respectively.

The segment attitude vectors were expressed with respect to the global coordinate system. The joint angular motion of the tarsal joint complex was calculated as the motion of the third metatarsus with respect to the tibia (Lanovaz et al., 2002). Translations of the tarsal joint were calculated as the motion of the origin of the third metatarsal BCS with respect to the origin of the tibial BCS, expressed in terms of the tibial BCS. The three components of translation along the x, y and z-axes of the tibia are referred to as DX, DY and DZ respectively.

Quantification of Skin Displacement. The 3D movement of the skin-based markers in the global coordinate system were collected for the motion data. For subjects 1-3, the data from each frame were transformed using the orientation matrices and displacement vectors calculated from the bone-fixed triads and expressed in terms of their corresponding BCS. The skin-based data from each subject were normalized to a percentage of the segment reference length calculated from the standing pose.

The data from the skin-based markers were parameterized by representing the data from each coordinate of each marker as a truncated Fourier series (Capozzo et al., 1975; van Weeren et al., 1992) given by

$$C(t) = p_O + \sum_{k=1}^{n} p_k \cos\left(\frac{2\pi kt}{100}\right) + \sum_{k=1}^{n} q_k \sin\left(\frac{2\pi kt}{100}\right) \qquad (1)$$

where *C(t)* is an x, y or z coordinate of a marker, *t* is expressed as a percentage of cycle time, p_O is the constant offset, p_k and q_k are Fourier series parameters and *n* is the number of harmonics used to describe the data.

In order to determine *n* for each coordinate, the pooled data from all 12 trials from subjects 1-3 were fit to Eq. (1) using a standard least-squares method, with *n* ranging from 1 to 30. A GCV criterion method (Woltring, 1990) was used to find the statistically optimal *n* for each coordinate of each marker and the Fourier parameters p_o, p_k, and q_k were then calculated. Model parameters were also calculated for each subject, using the optimum number of harmonics derived from the fit to the complete pool of trials (van Weeren et al., 1992).

In order to minimize the effects of any marker placement variation between subjects, the standing pose value of the coordinate (expressed as a percentage of segment length) was subtracted from the skin displacement prior to fitting the data to the Fourier series. The p_O value in the model then became a mean offset from the standing pose. The standing pose value for the subject was added to the results from the Fourier model to obtain a final value.

As an estimate of the goodness of fit for the pooled data Fourier parameters, the RMS fit error between the model and the actual data was calculated for each coordinate of each marker. The RMS and peak to peak amplitudes of the skin displacement for each coordinate of each marker were calculated from the fitted Fourier parameters.

For comparison, skin displacements for the x-axis and z-axis of TIB-A, TIB-B, MET-B and MET-A were calculated based on published 2D models (van Weeren et al., 1992) using mean kinematics from the 12 trials from subjects 1-3 of the current study. The axes from van Weeren et al. (1992) were transformed to correspond with the conventions used in this investigation.

Three dimensional skin correction. The Fourier models of the skin displacement were used to estimate the actual three dimensional orientation and position of the tibia and third metatarsus from the skin-based marker data alone. It is assumed that the reference standing pose does not contain any skin displacement artifacts. The marker positions in the reference pose, expressed in the local BCS, are used as the base position for the SVD method (Söderkvist and Wedin, 1993). It can be shown that, using the SVD method, the orientation matrix R_O and the displacement vector d_O describing the three-dimensional position of a segment in global coordinates can be found by solving

$$\min_{R\in\Omega,d} \sum_{i=1}^{m} \left\| R_O x_i + d_O - y_i \right\|^2 \qquad (2)$$

where m is the number of markers on the segment, x_i are the three-dimensional reference pose locations of the markers, expressed in the local BCS, and y_i are the three-dimensional locations of the markers at some point in time during the movement, expressed in the global coordinate system.

When skin displacement artifacts are present, the solution of R_O and d_O from Eq. (2) contains errors since the skin artifacts are incorrectly interpreted as changes in position of the segment. Although these errors are minimized in the least-squares sense, they can still result in large discrepancies when calculating kinematic variables (Reinschmidt et al., 1997a). However, if the nature of the skin artifact is known in relation to the local BCS, the values of x_i can be adjusted for the skin displacement and then used in Eq. (2) to recover the true orientation and position of the segment.

The Fourier parameters obtained from the skin displacement quantification procedures described above were used to generate the positions of the markers in their local BCS for each frame of data. The SVD algorithm was used to calculate orientation matrices and position vectors for each segment using the generated local BCS marker positions containing the skin displacement as x_i and the measured global coordinate skin marker locations as y_i in Eq. (2).

The orientation matrices derived from the corrected skin data for the tibia and third metatarsal segments were expressed as spatial attitude vectors with respect to the global coordinate system. The three-dimensional kinematics of the tarsal joint were also calculated from the corrected skin data and expressed in the same manner as those calculated from the bone-fixed kinematics. The kinematics of the tibia and third metatarsal segment were calculated from the uncorrected skin-based markers. Using all of the trials from subjects 1-3, the RMS error was calculated between the bone-fixed kinematic data and both the uncorrected and corrected skin-based data for all six degrees of freedom.

Application. The data from subjects 4 and 5 were used to test the general applicability of the skin correction model. Corrected tibial and third metatarsal kinematics calculated from the skin-based marker data of subjects 4 and 5 were compared to the mean bone-fixed kinematics from subjects 1-3.

RESULTS

Descriptive data from the subjects and the kinematic trials are given in Table A-1.

The reconstructions of the skin displacements from the Fourier model are shown in Figures A-22 and A-3. The skin displacement based on the pooled data and on the data for each of the three subjects are given on the same graph in order to visualize any variation between horses. The data from the model are plotted without adding the standing pose value so that they can be compared at similar scales. The mean values for the standing pose locations of the markers are given in Table A-2. The skin displacement patterns for the x-axis and z-axis of the tibial markers showed similar patterns with higher amplitudes at the proximal locations. The y-axis of the tibial markers showed little movement except for TIB-1 and TIB-2, which were located furthest from the reference line of the segment. On the third metatarsus, the displacement patterns for the x-axis and z-axis of the markers had similar amplitudes and patterns during the swing phase, but during the stance phase the displacement at the proximal end of the segment was in the opposite direction to that of the distal end. The y-axis displacements of the third metatarsal segment markers had small amplitudes and higher variability between sites and subjects. Overall, the tibial markers underwent much larger displacements than those on the third metatarsus.

The optimal number of harmonics, the p_O value, the RMS fit error of the pooled model to the actual skin displacement, and the RMS and peak to peak amplitudes of the skin displacement models are given in Table 3. The RMS amplitude of the skin displacement for the tibial markers ranged from 0.1% to 7.1% of the segment length, with most ranging from 2 to 5 % of segment length. This corresponds to approximate displacements of 7 to 17 mm. The largest peak to peak amplitude of skin displacement in the tibial markers was for the z-axis of marker TIB-A which showed a range of motion of 15.9% of segment length or approximately 55 mm. The tibial p_o values averaged 2 to 3% of segment length (approximately 8 mm). For the third metatarsal segment, the RMS skin displacement amplitudes ranged from 0.4 % to 2.6% with most values in the 1.5 to 2 % range corresponding to approximate values of 4 to 5 mm. The largest peak to peak amplitude of skin displacement in the third metatarsal markers was 5.7% of the segment length (approximately 14 mm), seen in the z-axis of marker MET-4. The p_O values for the third metatarsus were relatively low.

The average number of harmonics required to model the skin displacements was between 7 and 8 for the tibia and between 4 and 5 for the third metatarsus. The pooled trial Fourier model showed a good fit to the actual skin data, with most values for the RMS fit error being well below the peak to peak amplitude of the displacement itself (Table A-3).

The skin displacements for the x-axis and z-axis of TIB-A, TIB-B, MET-B and MET-A calculated from 2D models given by van Weeren (van Weeren, et al (1992) are

plotted against the current data (Figure A-4). In general, the 2D study tended to estimate a larger range of skin displacement than the current study.

The segmental kinematics were calculated with respect to the global coordinate system. The average RMS difference between the bone-fixed segment angles and the corrected skin segment angles was 1.7 ° (Table A-4), with the best fit in the θ_y angle of the third metatarsus (0.8 °) and the largest RMS difference in the third metatarsus θ_z angle (3.4 °). The average RMS difference in segment displacements was 2.9 mm. Angular kinematics calculated from the bone-fixed data are compared to those calculated from the skin marker data corrected using the Fourier displacement models (Figure A-5). The mean trace of all 12 trials is presented for each data set.

The mean kinematics of the tarsal joint from bone-fixed data, corrected skin marker data and uncorrected skin marker data are shown in Figure A-6. There is good agreement between the bone-fixed data and the corrected skin data, and there is a significant improvement between corrected and uncorrected skin data. The uncorrected skin data underestimates the θ_x range of motion and overestimates the DY and DZ ranges of motion. Some of the largest errors in the uncorrected skin data occur in the θ_z angle, where the average range of motion is 4 times larger than the bone-fixed or corrected skin values.

Kinematics derived from uncorrected and corrected skin marker data in subjects 4 and 5 are compared with the bone-fixed data from subjects 1-3 in Figure A-7. The corrected skin kinematics show some offsets relative to the bone-fixed data, but there is

good shape agreement for θ_x, θ_y, DX and DZ. The θ_z angle and the DY translation have an overall poor shape agreement. To account for the inter-individual offsets, the data were also expressed relative to their values at the start of stride (Figure A-7). The RMS differences between the corrected kinematic data from subjects 4 and 5 and the mean bone-fixed data are given in Table A-6 and are expressed both in terms of absolute data and data referenced to the start of the stride.

DISCUSSION

The periodic nature of the skin displacement lends itself to being modeled with a truncated Fourier series. The general displacement patterns were reproducible within and between subjects and this was reflected in the low fit errors.

The only previous equine skin displacement investigation (van Weeren et al. 1992) developed regression equations for 4 of the sites looked at in this study. Despite differences between that study and the current one in terms of the nature of the data (i.e. 2D vs 3D) and differences in subject breeds and sizes, the data are quite comparable. Although van Weeren (van Weeren, et al., 1992) gave models for the x-axis displacements of both ends of the third metatarsus, their original data were within the systematic error range of their study and they deemed the models not useful for correction. This may explain the differences in those axes compared with the results presented here. The other difference between the two studies is an offset seen in the x-axis displacement data of the proximal tibia. Van Weeren (van Weeren, et al., 1992) assumed that the skin oscillates around the original marker position and therefore the p_o

value of their Fourier model was set to zero before fitting the data. The current study found that this assumption is probably valid for the third metatarsus and distal tibia, but is not true for the proximal tibia.

In all cases, the θ_Z value showed the highest RMS error when skin marker data were compared to bone-fixed data. The skin-based markers were distributed as widely as possible on each segment, given the requirement of visibility from the lateral aspect and the physical limitations of segment size. However, on the third metatarsus, the skin markers tended to be clustered around the segmental z-axes. This type of marker configuration results in an increased sensitivity to marker location error (Söderkvist and Wedin, 1993; Cappozzo et al., 1997), especially in the calculation of θ_Z which is generally the most sensitive to errors (Cappozzo et al., 1996). In the case of the θ_Z value for the tarsal joint kinematics, the RMS error of the corrected skin data is as high as the average range of motion. This indicates that a generalized skin correction model based on a pool of horses for the current marker configuration still contains too much error to accurately reproduce θ_Z values for the tarsal joint. This was apparent when the skin correction model was applied to subjects 4 and 5.

The θ_X value calculated from the corrected skin markers, however, shows both a drastic improvement over the uncorrected skin data and a low RMS error when compared with the bone-fixed data. The application of the model on the last two subjects also showed a good shape agreement. The θ_Y values showed a low RMS error for the

corrected skin markers and the correction model gave good results when applied to the independent subjects. The RMS error for the θ_y values from the uncorrected skin markers was also low. This is an indication of the general robustness of the SVD algorithm and shows that, with a suitable redundant marker set, the flexion/extension angles of the tarsal joint can be calculated fairly accurately without correction for skin artifacts.

The structure of the equine tarsal joint, with the tibia moving along the grooves of a circular talus roughly 80 mm in diameter (Badoux, 1987), dictates that most joint rotations have corresponding coupled translations. The translation errors in the uncorrected skin-based data are largely due to the errors in the estimation of the θ_x and θ_z values. The skin correction model significantly reduced the RMS error in all translations, with the greatest RMS error improvement in the DX value and the best shape improvement in the DY translation. When the correction model was applied to the independent subjects, the DZ translation matched well with the bone-fixed data. There was an offset in the DX and DY curves but a good shape agreement in the DX curve. Even though the DY translation estimation is improved with the correction model, it still had a relatively poor shape agreement, especially during swing which can be attributed to errors in estimating the θ_z rotation and possibly to an overestimation of the θ_x rotation at mid-swing (Figure A-7).

In general, inter-subject differences were reduced when the data were expressed relative to a reference pose. For example, when the data were expressed with respect to the start of the stride, the RMS error for the DX translation was reduced by an average of

70% in the independent subjects. The unguligrade stance of horses raises the phalanges and metatarsal bones off the ground and allows a range of limb segment lengths and angulations, even within uniform populations. The use of the start of the stride as a normalization point to account for between subject conformational effects is one approach and has been shown to be fairly consistent for the equine tarsal joint (Lanovaz et al., 2002).

The use of the SVD algorithm to adjust for skin displacement artifacts is straight forward and easy to implement. The 3D motion of the tibia and third metatarsus was reproduced well and the relative joint motion of the tarsus calculated using the corrected skin-based markers showed a marked improvement over the uncorrected skin markers. The θ_X, θ_Y, DX and DZ estimations are suitable for use in general analysis. It is suggested that for between-subject comparisons, the skin corrected kinematics should be expressed relative to a reference orientation such as the start of the stride.

ACKNOWLEDGEMENTS

This work was supported by the McPhail Endowment, College of Veterinary Medicine, Michigan State University. The authors would like to thank Drs. John Stick and Jennifer Brown for performing the surgical procedures and Carissa Wickens and Sarah Fox for assistance during data collection. The authors would also like to thank Dr. Ton van den Bogert for providing additional information regarding the 2D correction procedures.

REFERENCES

Alexander, E.J., Andriacchi, T.P., 2001. Correcting for deformation in skin-based marker systems. Journal of Biomechanics 34, 355-361.

Andriacchi, T.P., Alexander, E.J., Toney, M.K., Dyrby, C.O., Sum, J., 1998. A point cluster method for in vivo motion analysis: applied to a study of knee kinematics. Journal of Biomechanical Engineering 120, 743-749.

Badoux, D.M., 1987. Some biomechanical aspects of the structure of the equine tarsus. Anatomischer Anzeiger 164, 53-61.

Cappozzo, A., Leo, T., Pedotti, A., 1975. A general computing method for the analysis of human locomotion. Journal of Biomechanics 8, 307-320.

Cappozzo, A., Catani, F., Leardini, A., Benedetti, M.G., Della Croce, U., 1996. Position and orientation in space of bones during movement: experimental artifacts. Clinical Biomechanics 11, 90-100.

Cappozzo, A., Cappello, A., Della Croce, U., Pensalfini, F., 1997. Surface-marker cluster design criteria for 3-D bone movement reconstruction. IEEE Transactions on Biomedical Engineering 44, 1165-1174.

Back, W., Schamhardt, H.C., Savelberg, H.H.C.M., van den Bogert, A.J., Bruin, G., Hartman, W., Barneveld, A., 1995. How the horse moves: 2. Significance of graphical representations of equine hind limb kinematics. Equine Veterinary Journal 27, 39-45.

Gabel, A.A., 1983. Prevention, diagnosis and treatment of inflammation of the distal hock. In Proceedings of the 28th Annual Convention of the American Association of Equine Practitioners. Manhattan, NY, pp 287-298.

Gough, M., Munroe, G., 1998. Decision making in the diagnosis and management of bone spavin in horses. In Practice 20, 252-259.

Hodson E.F., Clayton, H.M., Lanovaz, J.L., 2001. The hind limb in walking horses: 1. Kinematics and ground reaction forces. Equine Veterinary Journal 33, 38-43.

Holmström, M., Fredricson, I., Drevemo, S., 1994. Biokinematic analysis of the Swedish Warmblood riding horse at trot. Equine Veterinary Journal 26, 235-240.

Holmström, M., Fredricson, I., Drevemo, S., 1995. Biokinematic effects of collection on the trotting gaits in the elite dressage horse. Equine Veterinary Journal 27, 281-287.

Kobluk, C.N., Schnurr, D., Horney, F.D., Hearn, T.C., Summer-Smith, G., Willoughby, R.A., DeKleer, V.S., 1989. Use of high speed cinematography and computer generated gait diagrams for the study of equine hind limb kinematics. Equine Veterinary Journal 21, 48-58.

Lafortune, M.A., Cavanagh, P.R., Sommer III, H.J., Kalenak, A. 1992. Three-dimensional kinematics of the human knee during walking. Journal of Biomechanics 25, 347-357.

Lanovaz, J.L., Khumsap, S., Clayton, H.M., Stick, J.A., Brown, J., 2002. Three dimensional kinematics of the tarsal joint at the trot. Equine Veterinary Journal Supplement 34, 308-313.

Reinschmidt, C., van den Bogert, A.J., Nigg, B.M., Lundberg, A., Murphy, N., 1997a. Effect of skin movement on the analysis of skeletal knee joint motion during running. Journal of Biomechanics 30, 729-732.

Reinschmidt, C., van den Bogert, A.J., Murphy, N., Lundberg, A., Nigg, B.M., 1997b. Tibiocalcaneal motion during running – measured with external and bone markers. Clinical Biomechanics 12, 8-16.

Schamhardt, H.C., Hartman, W. , De Lange, A., 1984. Kinematics of the equine tarsus. Abstracts of the XV Congress of the European Association of Veterinary Anatomists, Utrecht, The Netherlands, 178-179.

Söderkvist, I., Wedin, P., 1993. Determining the movements of the skeleton using well-configured markers. Journal of Biomechanics 26, 1473-1477.

van Weeren, P.R., van den Bogert, A.J., Barneveld, A., 1992. Correction models for skin displacement in equine kinematic gait analysis. Journal of Equine Veterinary Science 12, 178-192.

Winter, D., Bruns, E., Glodek, P., Hertsch, B., 1996. Genetic disposition of bone diseases in sport horses. Zuchtungskunde 68, 92-108.

Woltring, H.J., Huiskes, R., De Lange, A., Veldpaus, F., 1985. Finite centroid and helical axis estimation from noisy landmark measurements in the study of human joint kinematics. Journal of Biomechanics 18, 379-389.

Woltring, H.J., 1986. A FORTRAN package for generalized, cross-validatory spline smoothing and differentiation. Advances in Engineering Software 8 (2), 104-113.

Woltring, H.J., 1990. Model and measurement error influences in data processing. In: Biomechanics of human movement: applications in rehabilitation, sports and ergonomics. Bertec Corporation, Worthington, Ohio, pp. 203-237.

Woltring, H.J., 1994. 3D attitude representation of human joints: a standardization proposal. Journal of Biomechanics 27, 1399-1414.

Table A-1 Descriptive data from the subjects and the mean descriptive data from the kinematic trials

Subject	Height at Withers (m)	Mass (kg)	Tibia Length (mm)	3rd Metatarsus Length (mm)	Velocity (m/s)	Stride Time (ms)	Stance Percentage
1	1.44	323	357	259	2.68	688	36.8 %
2	1.41	361	329	230	2.66	702	40.2 %
3	1.47	375	360	262	2.63	742	39.7 %
4	1.48	375	332	272	2.77	763	36.1%
5	1.43	339	319	224	2.81	706	39.5%
Mean(SD)	1.45 (0.03)	355 (23)	339 (18)	249 (21)	2.71 (0.08)	720 (31)	38.5 % (1.9 %)

Table A-2 Mean (SD) of marker locations from the standing poses of subjects 1-3. Data are expressed with respect to the local bone coordinate systems and are given in percentage of segment length.

Marker	X	Y	Z
TIB-A	0% (0%)	-21% (2%)	100% (0%)
TIB-1	14% (3%)	-6% (3%)	87% (3%)
TIB-2	-14% (2%)	-23% (2%)	72% (4%)
TIB-3	-2% (2%)	-22% (1%)	52% (2%)
TIB-4	12% (3%)	-12% (0%)	36% (6%)
TIB-B	0% (0%)	-17% (1%)	0% (0%)
MET-B	0% (0%)	-18% (1%)	0% (0%)
MET-1	16% (2%)	-9% (2%)	-13% (1%)
MET-2	-3% (2%)	-13% (2%)	-28% (2%)
MET-3	-2% (2%)	-13% (2%)	-74% (2%)
MET-4	14% (0%)	-7% (4%)	-88% (4%)
MET-A	0% (0%)	-19% (1%)	-100% (0%)

Table A-3 Descriptive statistics from the modeled skin displacements for the X, Y and Z coordinate for each skin surface marker.

The order indicates the optimal number of harmonics in the Fourier model and the p_o value is the mean offset from the standing pose location. The RMS error is the difference between the actual displacement and the model. The RMS amp and Peak amp are the RMS and Peak to Peak amplitudes of the skin displacement calculated using the model. All percent values refer to percent of the tibia or third metatarsus segment length.

	X					Y					Z				
Marker	Order (n)	p_o	RMS error	RMS amp	Peak amp	Order (n)	p_o	RMS error	RMS amp	Peak amp	Order (n)	p_o	RMS error	RMS amp	Peak amp
TIB-A	10	-7.4%	2.1%	5.5%	12.9%	9	-2.2%	0.9%	1.4%	3.2%	9	-2.0%	1.0%	7.1%	15.9%
TIB-1	5	-3.1%	1.6%	1.9%	4.8%	7	-4.3%	1.8%	3.2%	7.4%	6	-0.4%	1.0%	4.1%	10.2%
TIB-2	9	-5.3%	1.2%	4.2%	9.8%	8	1.9%	1.4%	2.2%	5.0%	4	-3.0%	1.3%	7.1%	15.9%
TIB-3	11	-4.0%	0.8%	2.7%	6.2%	5	0.8%	0.6%	0.8%	2.2%	4	-1.4%	1.0%	4.7%	11.1%
TIB-4	2	-3.0%	0.7%	2.0%	4.5%	9	-1.5%	0.7%	0.8%	2.1%	8	0.1%	0.7%	2.6%	6.1%
TIB-B	16	-0.5%	0.9%	1.2%	4.0%	2	0.2%	0.7%	0.1%	0.2%	12	-0.5%	0.5%	1.8%	3.9%
MET-B	6	-0.3%	1.1%	1.3%	3.4%	5	-0.1%	1.0%	0.7%	1.8%	7	-0.6%	0.7%	1.8%	3.6%
MET-1	2	-0.6%	1.5%	0.8%	2.0%	4	-0.5%	2.1%	0.7%	1.7%	7	-1.1%	0.9%	1.9%	3.9%
MET-2	5	0.0%	1.4%	0.8%	2.4%	4	1.3%	1.9%	0.4%	1.1%	5	-1.3%	1.3%	1.6%	4.0%
MET-3	25	1.0%	0.9%	1.2%	4.1%	4	0.0%	0.9%	0.3%	0.7%	6	-0.9%	1.0%	0.8%	1.7%
MET-4	4	0.7%	0.9%	0.4%	1.0%	1	0.7%	1.3%	0.8%	1.7%	4	-2.2%	1.0%	2.6%	5.7%
MET-A	4	-0.3%	1.1%	1.4%	3.3%	5	0.6%	0.7%	0.4%	1.1%	6	-1.0%	0.7%	1.5%	3.6%

Table A-4 RMS differences between bone-fixed and skin-based kinematics

	Angles (deg)			Displacements (mm)		
	θ_x	θ_y	θ_z	DX	DY	DZ
Tibia Bone-fixed vs Corrected Skin[a]	0.9	1.6	2.3	2.9	1.7	2.7
Third Metatarsus Bone-fixed vs Corrected Skin[a]	1.3	0.8	3.4	3.5	4.1	2.7
Tarsal Joint Bone-fixed vs Corrected Skin	2.1	1.8	4.6	4.8	4.0	5.0
Tarsal Joint Bone-fixed vs Uncorrected Skin	5.5	3.5	12.2	13.7	6.1	8.6
Subject 4: Absolute Bone-fixed vs Corrected Skin[b]	1.9	3.2	13.8	17.4	18.3	5.7
Subject 5: Absolute Bone-fixed vs Corrected Skin[b]	3.6	5.5	10.8	23.9	7.8	11.4
Subject 4: Relative Bone-fixed vs Corrected Skin[b]	1.3	3.9	3.3	7.0	2.5	4.5
Subject 5: Relative Bone-fixed vs Corrected Skin[b]	1.0	6.0	4.4	5.3	3.3	11.6

[a]Tibia and third metatarsal segmental kinematics are with respect to the global coordinate system

[b]Data for subjects 4 and 5 are tarsal joint kinematics

Figure A-1 Lateral view of the tibia (left) and third metatarsus (right) of a right limb showing the locations of the skin surface markers relative to the underlying bones.

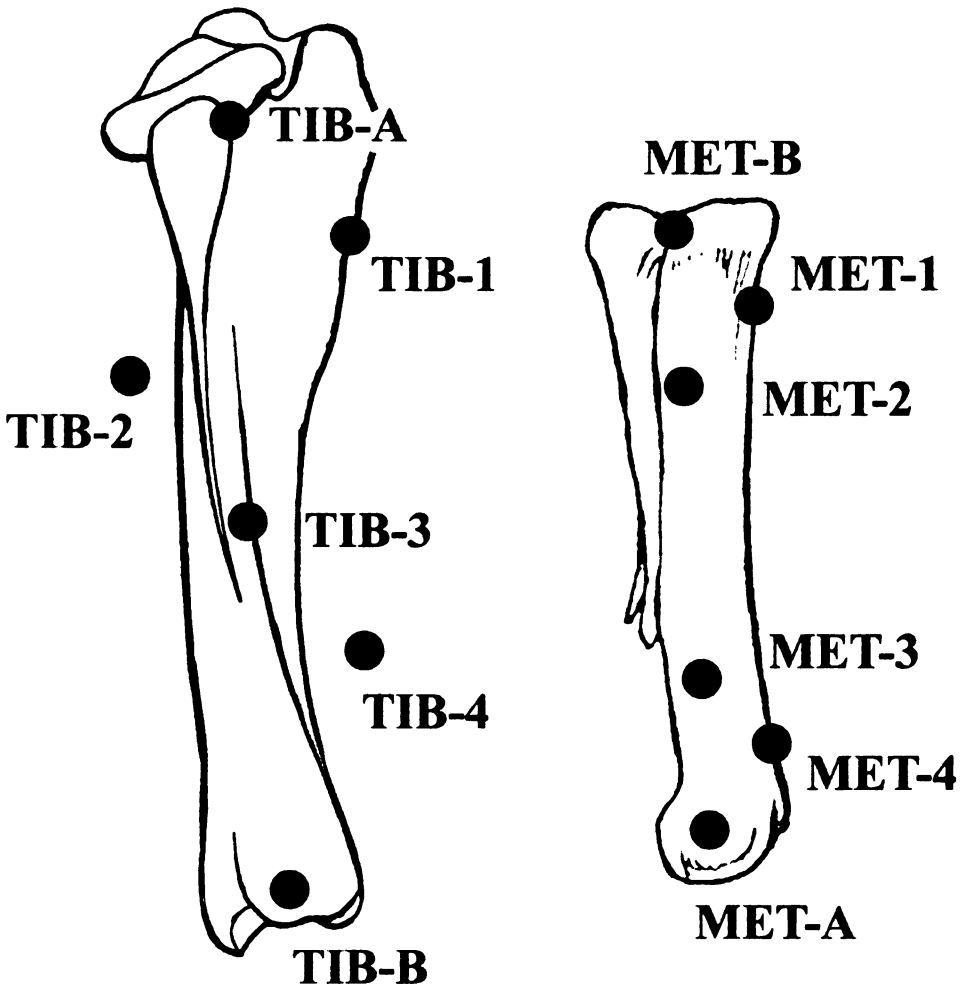

TIB-A: distal site of attachment of the lateral collateral femoro-tibial ligament, TIB-1: 1/6 of the segment length distal to TIB-A and over the tibial crest, TIB-2: 1/6 of the segment length proximally from TIB-3 and approximately 1/6 of the segment length caudal to the TIB-A/TIB-B line, TIB-3: mid-way along the line between TIB-A and TIB-B, TIB-4: 1/6 of the segment length distally from TIB-3 and about 1/6 of the segment length cranial to the line between TIB-A and TIB-B, TIB-B: over the lateral malleolus of the tibia, MET-B: dorsal edge of the head of the fourth metatarsal bone, MET-1: dorsal aspect of the bone mid-way between MET-B and MET-2, MET-2: 1/4 of the segment length distally from MET-B, MET-3: 1/4 of the segment length proximally from MET-A, MET-4: dorsal aspect of the bone mid-way between MET-A and MET-3, MET-A: metatarsal attachment of the lateral collateral ligament of the metatarsophalangeal joint. Not shown are the markers TIB-C and MET-C which are used during the standing reference pose and are placed on the medial side of the limb, opposite to TIB-B and MET-B respectively.

Figure A-2 Skin displacements for each coordinate of each tibial marker. The data are generated from the truncated Fourier series models. The dashed and dotted lines are from models fit to the three individual horses, while the thick solid line is from the model based on the pool of 12 trials from subjects 1-3. The columns represent the x, y and z coordinates respectively. Each row represents a marker with the top row being TIB-A and bottom row being TIB-B.

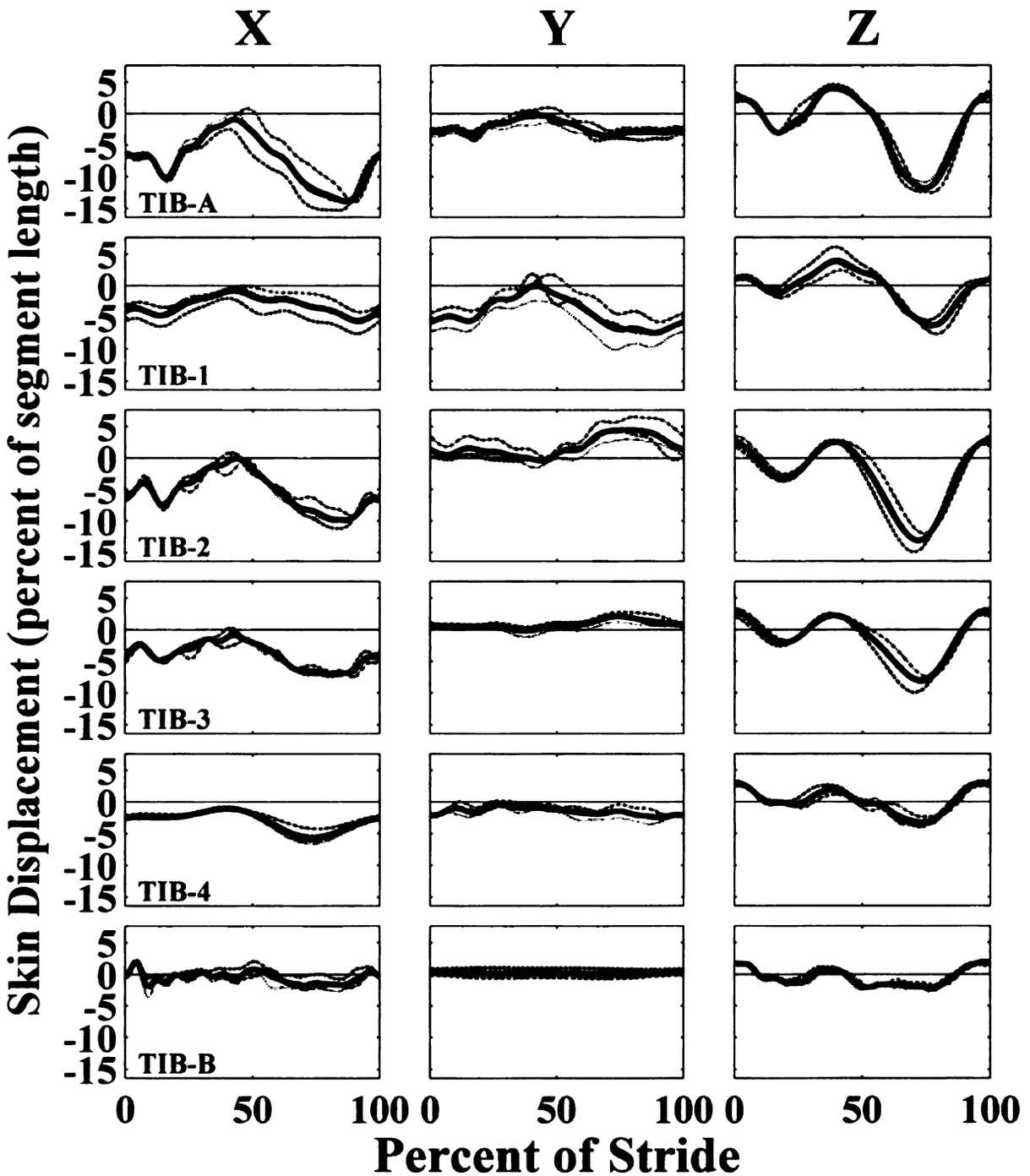

Figure A-3 Skin displacements for each coordinate of each third metatarsal marker. The data are generated from the truncated Fourier series models. The dashed and dotted lines are from models fit to the three individual horses, while the thick solid line is from the model based on the pool of 12 trials from subjects 1-3. The columns represent the x, y and z coordinates respectively. Each row represents a marker with the top row being MET-B and bottom row being MET-A.

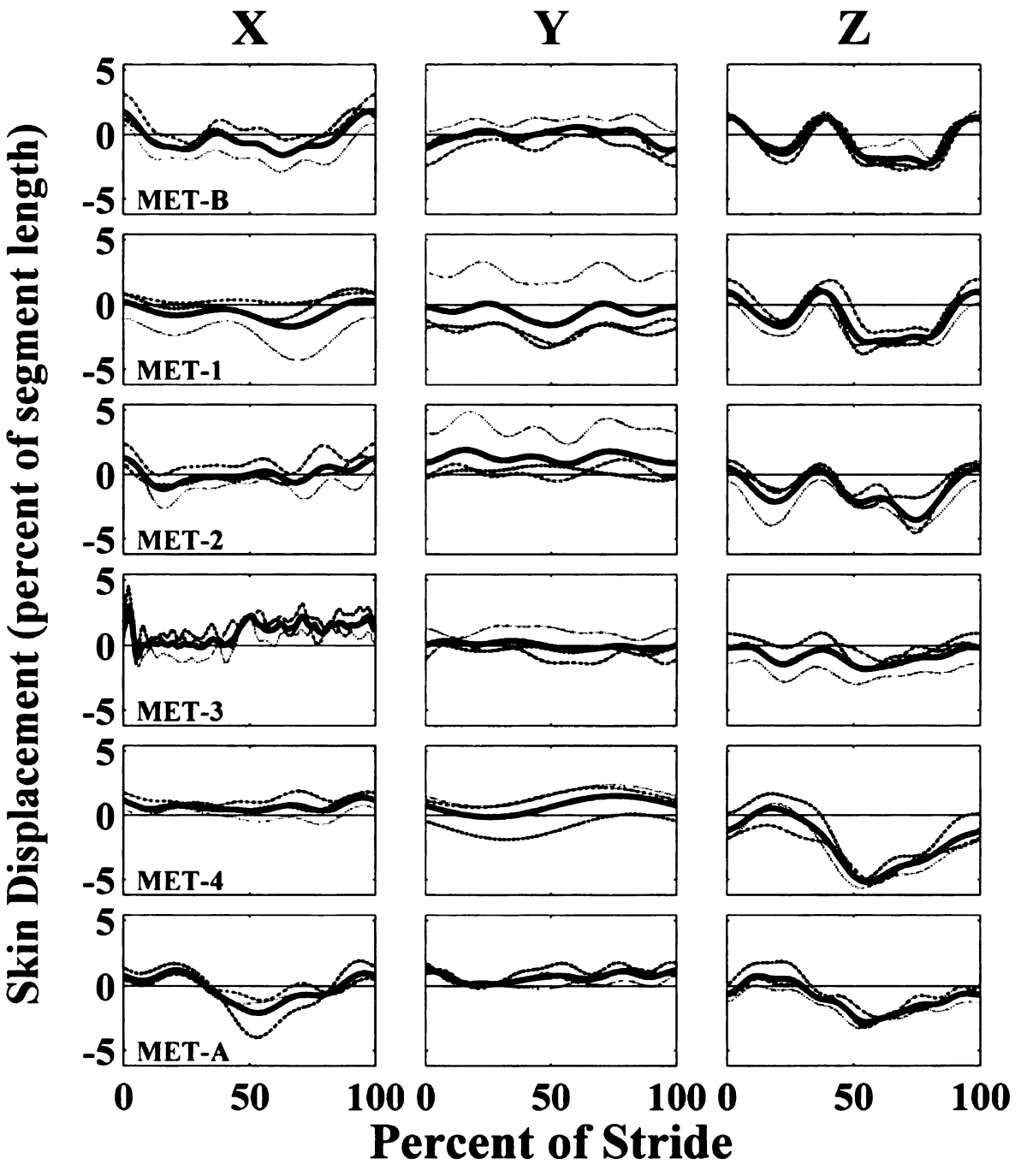

Figure A-4 Comparison of skin displacement models for the proximal and distal ends of the tibia and third metatarsus. The solid lines are from the models for the TIB-A, TIB-B, MET-A and MET-B markers from the current study. The open dotted lines are from the models given in van Weeren (van Weeren, et al., 1992) for the corresponding locations. The first column is the displacement data for the x-axis and the second column is the displacement data for the z-axis. The data are given as a percentage of segment length.

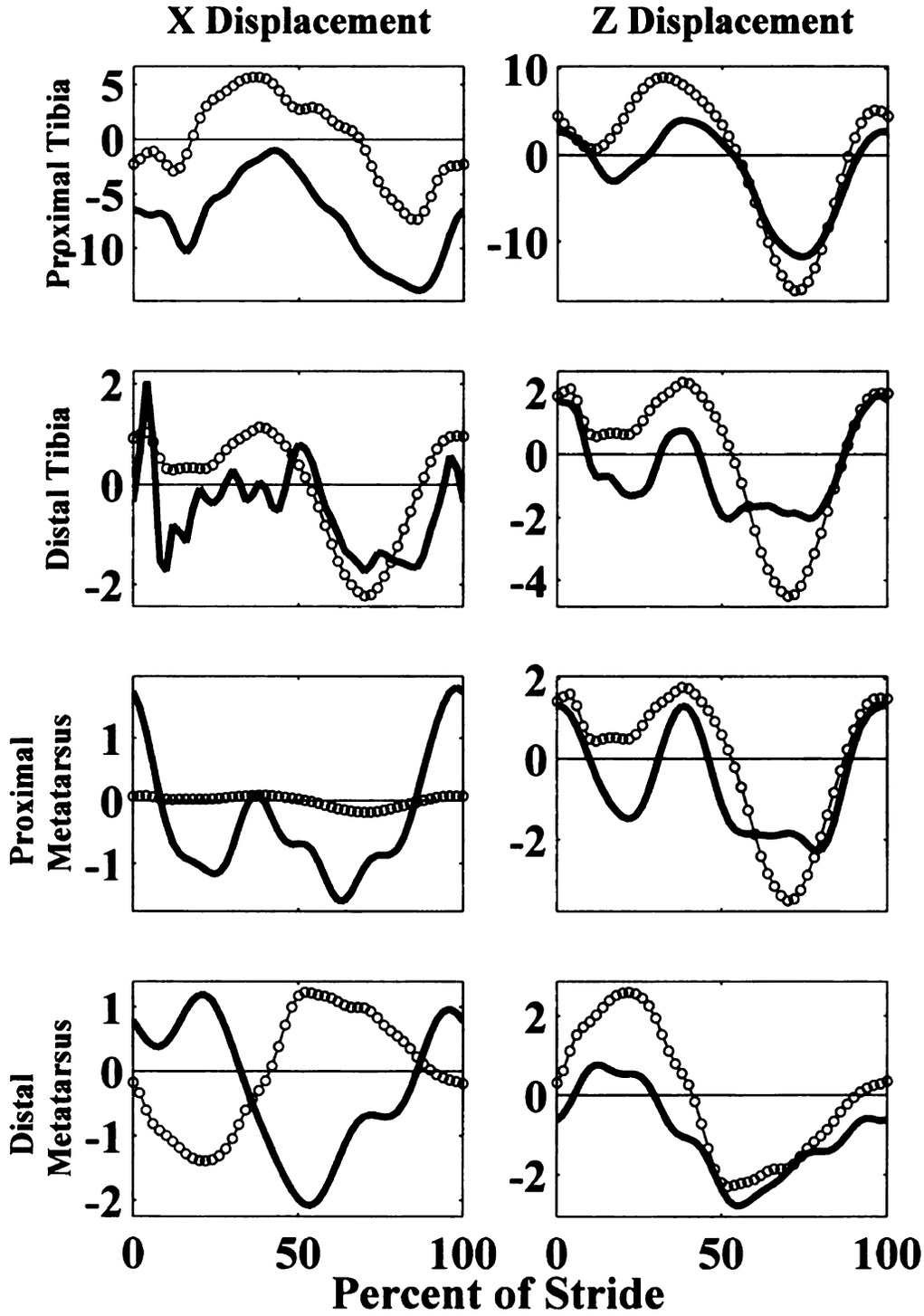

Figure A-5 Angular kinematics of the tibia and third metatarsus with respect to the global coordinate system. The solid lines are from the bone-fixed kinematics and the dotted lines are from corrected skin kinematics. Data are a mean of the 12 trials from subjects 1-3, normalized to percent of stride.

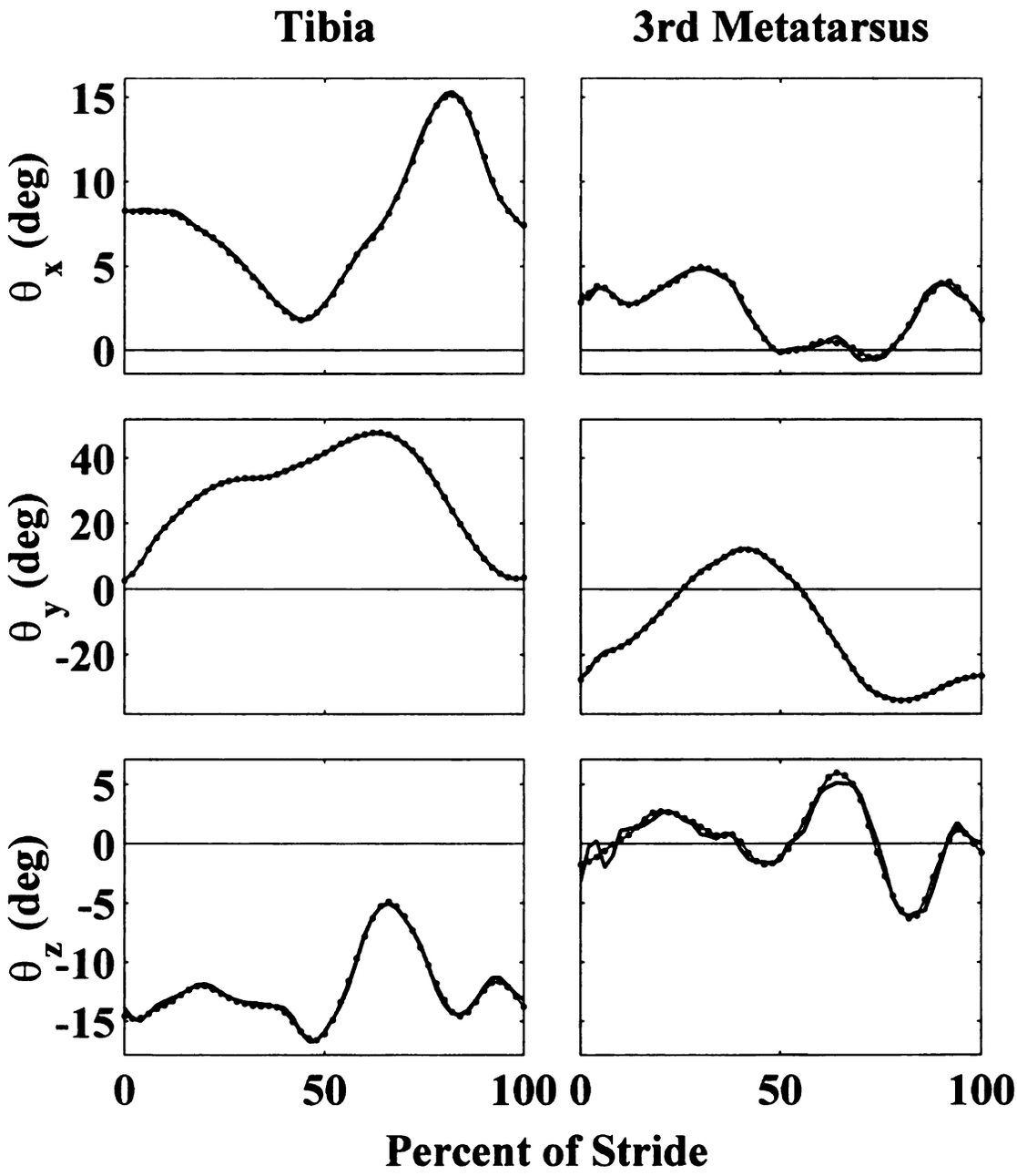

Figure A-6 Kinematics of the tarsal joint (motion of the third metatarsus relative to the tibia). The right hand column is the angular data (in degrees) and the left hand column is the displacements (in mm). The solid lines represents bone-fixed kinematics, the filled dotted lines represents corrected skin kinematics, and the open dotted lines are kinematics from uncorrected skin markers. Data are a mean of the 12 trials from subjects 1-3.

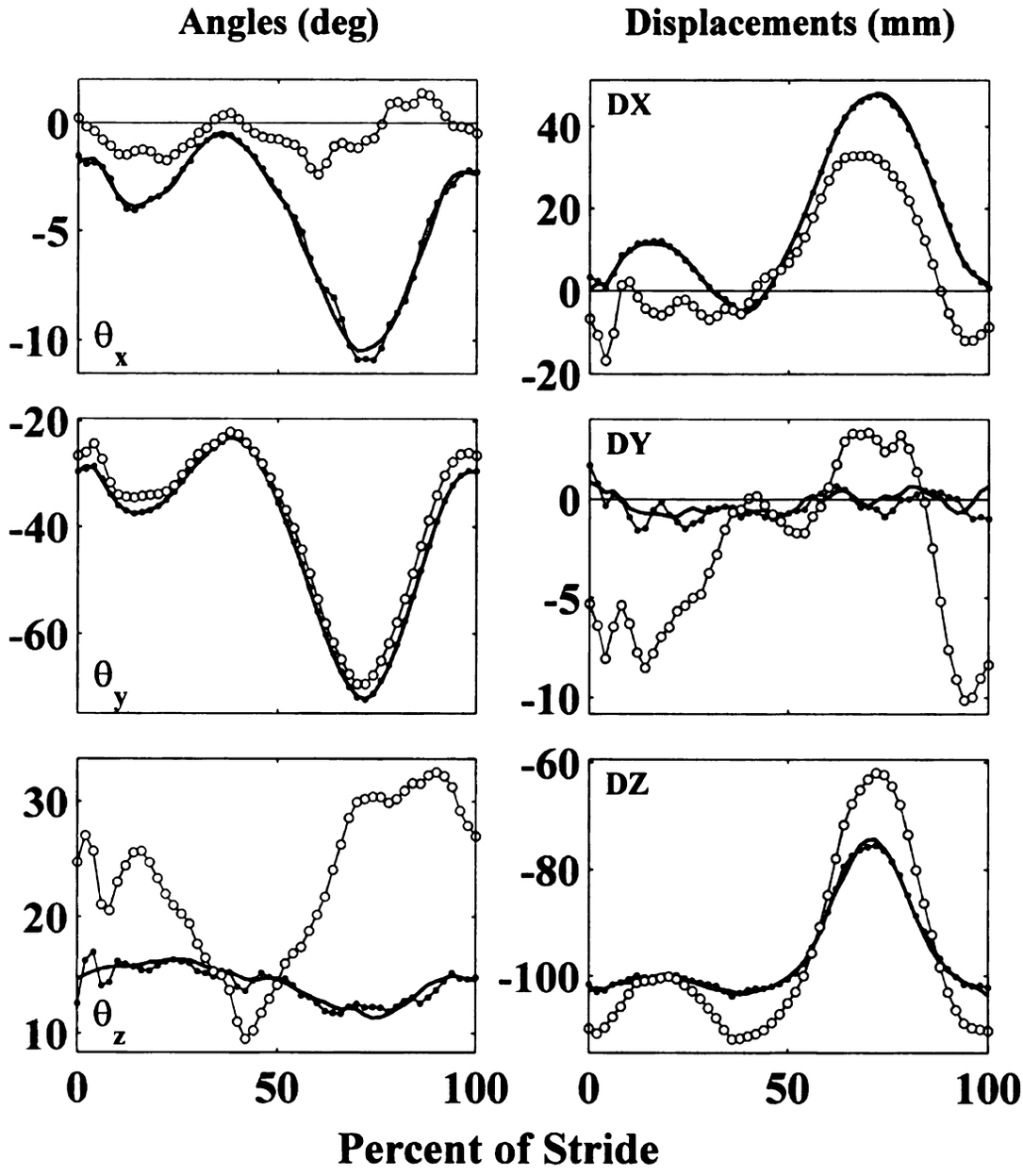

Figure A-7 Application of correction models to kinematics of the tarsal joint (motion of the third metatarsus relative to the tibia) in absolute values and referenced to the start of the stride. The right hand columns are the angular data (in degrees) and the left hand columns are the displacements (in mm). The solid lines represents bone-fixed kinematics from subjects 1-3, the filled dotted lines represents corrected skin kinematics from subject 4, and the open dotted lines are kinematics from corrected skin markers of subject 5.

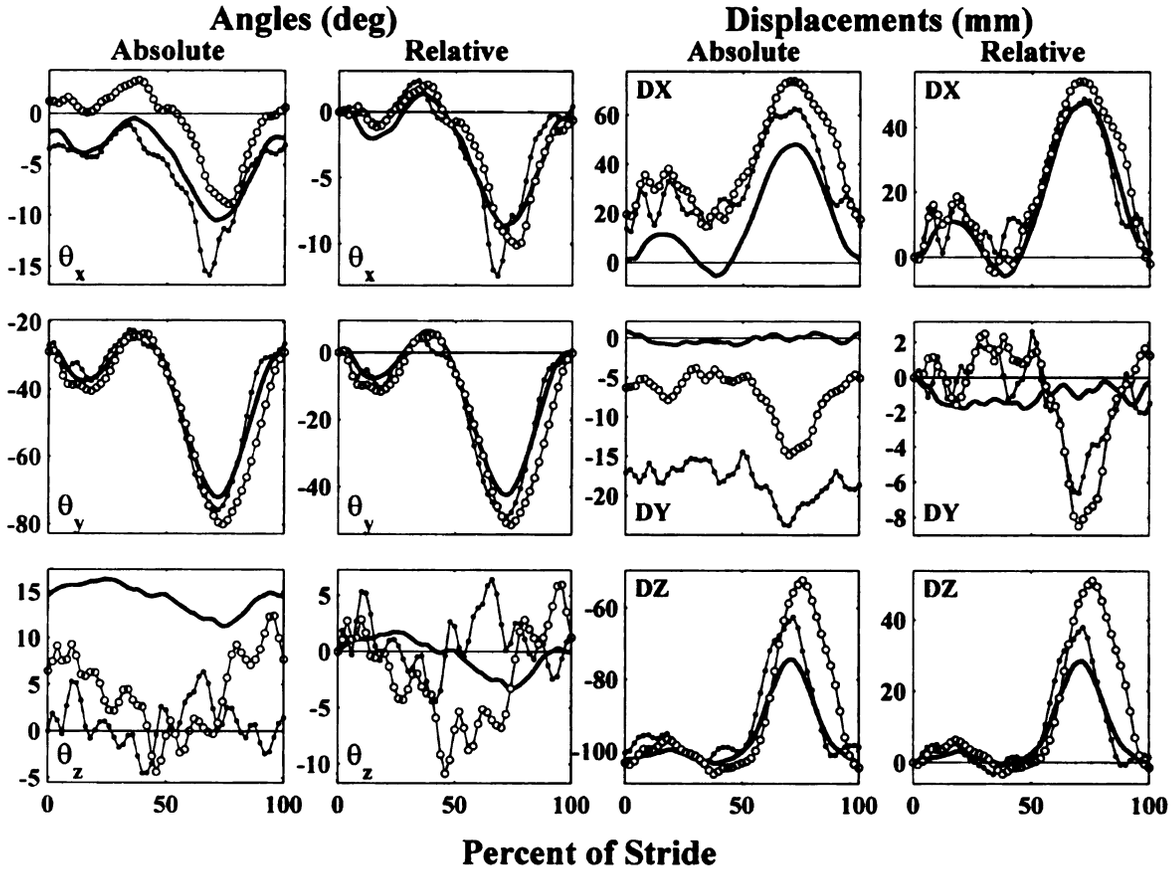

APPENDIX B

BIOMECHANICAL VARIABLES IN SOUND AND LAME CONDITIONS

Table B-1 Ground reaction force (GRF) variables in the hind limbs. Values from sound condition are averaged from both hind limbs. Lame RH is the limb in which synovitis was induced. Compensating LH is the contralateral hind limb. Values are mean and (SD). [a] $P<0.05$. [b] $0.05<P<0.1$.

Variables	Sound	Lame RH	Compensating LH
Vertical force Max (N/kg)	9.052 (0.402)	8.780 (0.558) [a]	9.183 (0.455) [b]
Vertical impulse (Ns/kg)	1.453 (0.077)	1.404 (0.089) [b]	1.459 (0.087)
Longitudinal force Max1 (N/kg)	-0.134 (0.200)	-0.128 (0.144)	-0.190 (0.262)
Longitudinal force Max2 (N/kg)	-0.638 (0.126)	-0.511 (0.115)	-0.645 (0.126)
Longitudinal force Max3 (N/kg)	1.037 (0.114)	1.001 (0.094) [b]	1.086 (0.032)
Longitudinal force Min1 (N/kg)	-1.621 (0.237)	-1.481 (0.320)	-1.580 (0.542)
Longitudinal force Min2 (N/kg)	-0.773 (0.108)	-0.640 (0.149)	-0.783 (0.117)
Longitudinal force Min3 (N/kg)	-0.717 (0.068)	-0.566 (0.112)	-0.722 (0.040)
Longitudinal negative impulse (Ns/kg)	-0.073 (0.008)	-0.069 (0.007)	-0.071 (0.008) [a]
Longitudinal positive impulse (Ns/kg)	0.087 (0.016)	0.086 (0.016)	0.091 (0.002)

Table B-2 Joint angle (degrees) during stance in the hind limbs. Values from sound condition are averaged from both hind limbs. Lame RH is the limb in which synovitis was induced. Compensating LH is the contralateral hind limb. Values are mean and (SD). [a] $P<0.05$. [b] $0.05<P<0.1$.

Joint	Variables	Sound	Lame RH	Compensating LH
Coxofemoral	Max1	109.78 (7.46)	107.22 (5.19) [b]	111.35 (9.57)
	Max2	125.20 (6.64)	123.95 (4.39)	127.89 (8.36)
	Min1	101.12 (7.18)	99.06 (4.34)	102.73 (8.13)
	Min2	114.84 (7.78)	112.77 (5.33)	116.84 (9.01)
	Range	26.27 (1.23)	25.64 (1.23)	26.38 (0.91)
Femorotibial	Max1	113.24 (1.90)	110.96 (3.03)	114.04 (1.78)
	Max2	109.97 (2.19)	107.46 (1.96)	111.13 (2.29)
	Min1	108.46 (2.00)	106.72 (3.17)	108.94 (1.19)
	Min2	107.36 (2.08)	104.87 (2.19)	108.59 (1.64)
	Range	10.97 (2.67)	10.69 (2.74)	10.34 (2.85)
Tarsus	Max1	114.79 (2.87)	111.07 (3.89)	116.08 (3.20)
	Max2	106.45 (3.74)	104. 60 (3.74)	107.89 (2.87)
	Min1	105.44 (4.20)	103.53 (3.34)	107.86 (4.02)
	Min2	103.33 (3.41)	101.80 (2.94)	104.98 (4.83)
	Range	12.12 (0.96)	10.24 (0.99) [a]	11.72 (1.86)
Metatarsophalangeal	Max	237.34 (11.49)	233.25 (9.87)	240.65 (11.04)
	Range	47.79 (9.16)	45.86 (8.56)	48.98 (10.41)
Distal interphalangeal	Max	206.92 (6.45)	206.64 (5.30)	202.53 (5.39)
	Min	151.55 (10.20)	157.25 (8.86)	146.77 (9.21)
	Range	55.66 (6.42)	54.60 (5.41) [a]	56.27 (7.97)

Table B-3 Net joint moment peaks (Nm/kg) during stance in the hind limbs. Values from sound condition are averaged from both hind limbs. Lame RH is the limb in which synovitis was induced. Compensating LH is the contralateral hind limb. Values are mean and (SD). [a] $P<0.05$. [b] $0.05<P<0.1$.

Joint	Variables	Sound	Lame RH	Compensating LH
Coxofemoral	Max1	1.101 (0.129)	1.055 (0.078)	1.044 (0.108)
	Max2	0.575 (0.126)	0.542 (0.134)	0.644 (0.059)
	Max3	0.557 (0.185)	0.353 (0.062)	0.689 (0.160)
	Min1	-0.372 (0.248)	-0.219 (0.396)	-0.313 (0.563)
	Min2	0.367 (0.096)	0.391 (0.167)	0.378 (0.087)
Femorotibial	Max1	0.365 (0.100)	0.293 (0.186)	0.329 (0.330)
	Max2	0.135 (0.055)	0.176 (0.032)	0.105 (0.058)
	Min1	-0.59 (0.131)	-0.529 (0.125)	-0.553 (0.138)
	Min2	-0.537 (0.144)	-0.416 (0.078)	-0.676 (0.082)
Tarsus	Max1	0.422 (0.086)	0.410 (0.059)	0.413 (0.089)
	Max2	1.406 (0.154)	1.293 (0.128)	1.471 (0.204)
	Min1	-0.132 (0.052)	-0.065 (0.089)	-0.114 (0.163)
	Min2	0.325 (0.076)	0.351 (0.107)	0.347 (0.139)
Metatarsophalangeal	Min	-1.149 (0.140)	-1.064 (0.167)[a]	-1.199 (1.143)
Distal interphalangeal	Min	-0.304 (0.058)	-0.214 (0.046)[b]	-0.321 (0.072)

Table B-4 Net joint power peaks (W/kg) during stance in the hind limbs. Values from sound condition are averaged from both hind limbs. Lame RH is the limb in which synovitis was induced. Compensating LH is the contralateral hind limb. Values are mean and (SD). [a] $P<0.05$. [b] $0.05<P<0.1$.

Joint	Variables	Sound	Lame RH	Compensating LH
Coxofemoral	Max1	1.501 (0.419)	1.150 (0.301)	1.698 (0.425)
	Max2	1.473 (0.554)	0.917 (0.101)	1.827 (0.497)
Femorotibial	Max1	2.488 (0.875)	2.058 (0.768)	2.325 (0.996)
	Max2	1.150 (0.493)	0.690 (0.258)	1.461 (0.462)
	Min1	-0.503 (0.188)	-0.415 (0.313)	-0.396 (0.434)
	Min2	-1.085 (0.384)	-0.661 (0.165)	-1.402 (0.210)
Tarsus	Max1	0.862 (0.762)	0.812 (0.374)	0.727 (0.815)
	Max2	2.627 (0.565)	2.377 (0.348) [a]	2.648 (0.670)
	Min1	-2.219 (0.496)	-1.758 (0.316) [a]	-2.119 (0.608)
	Min2	-2.159 (1.073)	-1.820 (0.681)	-2.281 (1.476)
Metatarsophalangeal	Max	6.237 (1.284)	5.113 (0.614)	6.566 (1.076)
	Min	-4.653 (1.316)	-4.230 (1.046)	-5.095 (1.615) [a]
Distal interphalangeal	Max	0.588 (0.258)	0.379 (0.030)	0.796 (0.441)
	Min	-3.037 (0.625)	-2.049 (0.323) [b]	-3.137 (0.746)

Table B-5 Net joint energies (J/kg) during stance in the hind limbs. Values from sound condition are averaged from both hind limbs. Lame RH is the limb in which synovitis was induced. Compensating LH is the contralateral hind limb. Values are mean and (SD). [a] $P<0.05$. [b] $0.05<P<0.1$.

Joint	Variables	Sound	Lame RH	Compensating LH
Coxofemoral	Max1	0.063 (0.023)	0.048 (0.030)	0.077 (0.024)
	Max2	0.073 (0.034)	0.038 (0.014)	0.099 (0.018)
	Total +E	0.140 (0.140)	0.090 (0.044)	0.182 (0.032)
	Total -E	-0.014 (0.009)	-0.026 (0.016)	-0.005 (0.003)
Femorotibial	Max1	0.037 (0.016)	0.034 (0.017)	0.040 (0.024)
	Max2	0.041 (0.018)	0.022 (0.017) [a]	0.051 (0.015)
	Min1	-0.004 (0.001)	-0.004 (0.001)	-0.003 (0.001)
	Min2	-0.031 (0.011)	-0.020 (0.006)	-0.042 (0.010)
	Total +E	0.079 (0.027)	0.061 (0.022)	0.092 (0.027)
	Total -E	-0.043 (0.015)	-0.027 (0.009)	-0.055 (0.016)
Tarsus	Max1	0.024 (0.014)	0.018 (0.009)	0.022 (0.005)
	Max2	0.125 (0.023)	0.107 (0.018) [a]	0.125 (0.026)
	Min1	-0.075 (0.016)	-0.059 (0.011) [b]	-0.074 (0.013)
	Min2	-0.076 (0.043)	-0.060 (0.026)	-0.080 (0.058)
	Total +E	0.147 (0.023)	0.126 (0.008) [a]	0.142 (0.033)
	Total -E	-0.151 (0.038)	-0.119 (0.035) [a]	-0.155 (0.068)
Metatarsophalangeal	Max	0.394 (0.094)	0.311 (0.053)	0.408 (0.069)
	Min	-0.386 (0.108)	-0.359 (0.100)	-0.422 (0.129)
	Total +E	0.394 (0.094)	0.311 (0.053)	0.408 (0.069)
	Total -E	-0.387 (0.108)	-0.359 (0.100)	-0.422 (0.129)
Distal interphalangeal	Max	0.038 (0.018)	0.020 (0.007) [b]	0.052 (0.033)
	Min	-0.222 (0.049)	-0.146 (0.021) [b]	-0.229 (0.059)
	Total +E	0.040 (0.017)	0.022 (0.006)	0.053 (0.033)
	Total -E	-0.223 (0.049)	-0.146 (0.021)	-0.229 (0.059)

Table B-6 Joint angle (degrees) during swing in the hind limbs. Values from sound condition are averaged from both hind limbs. Lame RH is the limb in which synovitis was induced. Compensating LH is the contralateral hind limb. Values are mean and (SD). [a] $P<0.05$. [b] $0.05<P<0.1$.

Joint	Variables	Sound	Lame RH	Compensating LH
Coxofemoral	Min	76.85 (5.43)	74.83 (4.68)	78.73 (6.00)
	Range	48.63 (1.41)	48.49 (1.20)	48.49 (2.77)
Femorotibial	Max	114.97 (4.03)	114.29 (4.05)	115.07 (3.98)
	Min	68.35 (3.09)	68.07 (2.82)	68.38 (3.48)
	Range	50.44 (2.63)	49.08 (1.39)	50.87 (2.06)
Tarsus	Max	113.38 (4.99)	110.85 (4.96)	114.35 (5.17)
	Min	70.77 (3.09)	70.48 (3.16)	72.32 (3.30)
	Range	44.67 (1.90)	41.66 (1.47)	44.21 (1.35)
Metatarsophalangeal	Max1	160.54 (6.94)	157.89 (1.02)	161.79 (4.74)
	Max2	185.90 (7.63)	183.48 (4.60)	186.74 (7.20)
	Min1	147.70 (6.67)	144.88 (6.59)	149.94 (5.99)
	Min2	156.61 (6.76)	154.67 (1.49)	158.51 (7.17)
	Range	45.31 (3.38)	44.20 (2.43)	43.90 (5.02)
Distal interphalangeal	Max1	170.08 (6.34)	169.07 (4.67)	167.77 (4.99)
	Max2	180.41 (8.29)	183.20 (7.36)	181.96 (7.39)
	Min1	162.60 (5.69)	160.89 (3.10)	161.57 (6.07)
	Min2	155.33 (6.13)	155.70 (3.41)	154.38 (6.42)
	Range	45.29 (5.05)	43.64 (6.77)	43.24 (3.17)

Table B-7 Net joint moment peaks (Nm/kg) during swing in the hind limbs. Values from sound condition are averaged from both hind limbs. Lame RH is the limb in which synovitis was induced. Compensating LH is the contralateral hind limb. Values are mean and (SD). [a] $P<0.05$. [b] $0.05<P<0.1$.

Joint	Variables	Sound	Lame RH	Compensating LH
Coxofemoral	Max	0.119 (0.030)	0.138 (0.035)	0.118 (0.016)
	Min1	-0.431 (0.058)	-0.445 (0.067)	-0.463 (0.064)[a]
	Min2	-0.135 (0.065)	-0.117 (0.072)	-0.120 (0.059)[b]
Femorotibial	Max	0.199 (0.029)	0.180 (0.033)[b]	0.200 (0.026)
Tarsus	Max	0.019 (0.012)	0.018 (0.010)	0.017 (0.013)
	Min	-0.093 (0.016)	-0.085 (0.014)[a]	-0.093 (0.016)
Metatarsophalangeal	Max	0.017 (0.002)	0.016 (0.003)	0.016 (0.003)
	Min	-0.007 (0.003)	-0.006 (0.001)	-0.007 (0.003)
Distal interphalangeal	Max	0.002 (0.001)	0.002 (0.001)[a]	0.002 (0.001)
	Min	-0.001 (0.000)	-0.001 (0.000)	-0.001 (0.001)

Table B-8 Net joint power peaks (W/kg) during swing in the hind limbs. Values from sound condition are averaged from both hind limbs. Lame RH is the limb in which synovitis was induced. Compensating LH is the contralateral hind limb. Values are mean and (SD). [a] $P<0.05$. [b] $0.05<P<0.1$.

Joint	Variables	Sound	Lame RH	Compensating LH
Coxofemoral	Max1	1.163 (0.183)	1.275 (0.177)	1.243 (0.253) [a]
	Max2	1.879 (0.670)	1.645 (0.532)	1.539 (0.567)
	Min	-0.630 (0.157)	-0.735 (0.174)	-0.616 (0.116)
Femorotibial	Max	0.160 (0.138)	0.144 (0.104)	0.141 (0.128)
	Min1	-0.519 (0.120)	-0.428 (0.137)	-0.457 (0.129) [a]
	Min2	-0.941 (0.322)	-0.843 (0.316) [b]	-0.801 (0.132)
Tarsus	Max1	0.334 (0.059)	0.296 (0.064)	0.316 (0.068)
	Max2	0.318 (0.112)	0.225 (0.091) [a]	0.244 (0.047)
Metatarsophalangeal	Max1	0.019 (0.012)	0.014 (0.011) [a]	0.014 (0.011) [b]
	Max2	0.015 (0.006)	0.011 (0.006) [b]	0.012 (0.009)
	Min1	-0.166 (0.025)	-0.142 (0.034) [b]	-0.159 (0.038)
	Min2	-0.017 (0.010)	-0.016 (0.008)	-0.014 (0.014)
	Min3	-0.032 (0.009)	-0.027 (0.004)	-0.022 (0.003)
Distal interphalangeal	Max1	0.006 (0.003)	0.004 (0.003) [a]	0.004 (0.002)
	Max2	0.006 (0.002)	0.005 (0.001) [a]	0.005 (0.005)
	Min1	-0.023 (0.012)	-0.013 (0.006) [a]	-0.015 (0.007)
	Min2	-0.006 (0.002)	-0.004 (0.003)	-0.004 (0.002)

Table B-9 Net joint energies (J/kg) during swing in the hind limbs. Values from sound condition are averaged from both hind limbs. Lame RH is the limb in which synovitis was induced. Compensating LH is the contralateral hind limb. Values are mean and (SD). [a] $P<0.05$. [b] $0.05<P<0.1$.

Joint	Variables	Sound	Lame RH	Compensating LH
Coxo-femoral	Max1	0.104 (0.010)	0.106 (0.010)	0.106 (0.017)
	Max2	0.122 (0.042)	0.125 (0.052)	0.100 (0.040) [b]
	Min	-0.025 (0.010)	-0.029 (0.019)	-0.022 (0.005)
	Total +E	0.229 (0.037)	0.236 (0.047)	0.210 (0.037)
	Total -E	-0.028 (0.010)	-0.035 (0.012)	-0.026 (0.008)
Femoro-tibial	Min1	-0.049 (0.010)	-0.044 (0.013)	-0.049 (0.013)
	Min2	-0.079 (0.013)	-0.074 (0.014) [a]	-0.75 (0.004)
	Total +E	0.012 (0.009)	0.016 (0.012)	0.011 (0.008)
	Total -E	-0.129 (0.021)	-0.118 (0.027) [b]	-0.124 (0.013)
Tarsus	Max1	0.029 (0.008)	0.026 (0.008) [b]	0.027 (0.009)
	Max2	0.022 (0.009)	0.017 (0.006)	0.019 (0.004)
	Min	-0.002 (0.001)	-0.001 (0.001)	-0.002 (0.001)
	Total +E	0.052 (0.013)	0.043 (0.013) [b]	0.046 (0.011)
	Total -E	-0.004 (0.003)	-0.004 (0.003)	-0.003 (0.003)
Metatarso-phalangeal	Max1	0.001 (0.000)	0.0004 (0.0003) [b]	0.0004 (0.0003)
	Max2	0.0004 (0.0002)	0.0003 (0.0002) [a]	0.0004 (0.0003)
	Min1	-0.009 (0.002)	-0.008 (0.002) [a]	-0.009 (0.003)
	Min2	-0.0004 (0.0002)	-0.0004 (0.0003)	-0.0004 (0.0003)
	Min3	-0.002 (0.001)	-0.002 (0.001)	-0.002 (0.000)
	Total +E	0.0011 (0.0005)	0.0008 (0.0005)	0.0008 (0.0004) [a]
	Total -E	-0.013 (0.002)	-0.012 (0.002) [a]	-0.012 (0.003)
Distal inter-phalangeal	Max1	0.0002 (0.0001)	0.0001 (0.0001) [a]	0.0001 (0.0001)
	Max2	0.0002 (0.0001)	0.0001 (0.0001)	0.0001 (0.0001) [b]
	Min1	-0.001 (0.000)	-0.001 (0.000) [a]	-0.001 (0.000)
	Min2	-0.0004 (0.0001)	-0.0003 (0.0001) [b]	-0.0003 (0.0001)
	Total +E	0.0004 (0.0002)	0.0003 (0.0002) [b]	0.0003 (0.0002)
	Total -E	-0.001 (0.001)	-0.001 (0.000) [a]	-0.001 (0.000)

Table B-10 Ground reaction force (GRF) variables in the forelimbs. Values from sound condition are averaged from both forelimbs. Lame RF and Lame LF are the compensating limb. Values are mean and (SD). [a] $P<0.05$. [b] $0.05<P<0.1$.

Variables	Sound	Lame RF	Lame LF
Vertical force Max (N/kg)	10.385 (0.492)	10.195 (0.547)	10.249 (0.754)
Vertical impulse (Ns/kg)	1.929 (0.088)	1.879 (0.105)	1.910 (0.039) [a]
Longitudinal force Max1 (N/kg)	-0.206 (0.091)	-0.256 (0.116)	-0.249 (0.163)
Longitudinal force Max2 (N/kg)	-1.010 (0.134)	-1.040 (0.201)	-1.012 (0.207)
Longitudinal force Max3 (N/kg)	0.872 (0.146)	0.810 (0.140)	0.845 (0.207)
Longitudinal force Min1 (N/kg)	-1.206 (0.146)	-1.200 (0.043)	-1.328 (0.123)
Longitudinal force Min2 (N/kg)	-1.197 (0.157)	-1.188 (0.210)	-1.150 (0.185)
Longitudinal force Min3 (N/kg)	-1.162 (0.162)	-1.175 (0.212)	-1.168 (0.119)
Longitudinal negative impulse (Ns/kg)	-0.134 (0.022)	0.134 (0.025)	-0.134 (0.014)
Longitudinal positive impulse (Ns/kg)	0.074 (0.019)	0.067 (0.017)	0.073 (0.019)

REFERENCES

Anonymous. 1991. Definition and classification of lameness, p. 19. In American Association of Equine Practitioners Guide for Judging of Equestrian Events, 4 ed.

Audigie, F., Pourcelot, P., Degueurce, C., Geiger, D. and Denoix, J. M. 2001. Kinematic analysis of the symmetry of limb movements in lame trotting horses. Equine Veterinary Journal. 33(supplement):128-134.

Axelsson, M., Eksell, P., Roneus, B., Brostrom, H., Haggstrom, J. and Carlsten, J. 1998. Relationship between hind limb lameness and radiographic signs of bone spavin in Icelandic horses in Sweden. Acta Veterinary Scandinavia. 39:349-357.

Back, W., Barneveld, A., van Weeren, P. R. and van den Bogert, A. J. 1993. Kinematic gait analysis in equine carpal lameness. Acta Anatomica. 146(2-3):86-89.

Back, W., Barneveld, A., Bruin, G., Schamhardt, H. and Hartman, W. 1994. Kinematic detection of superior gait quality in young trotting warmbloods. The Veterinary Quarterly. 16(suppl 2):S91-S96.

Back, W., Schamhardt, H., Savelberg, H., van den Bogert, A., Bruin, G., Hartman, W. and Barneveld, A. 1995a. How the horse moves: 1. significance of graphical representations of equine forelimb kinematics. Equine Veterinary Journal. 27(1):31-38.

Back, W., Schamhardt, H., Savelberg, H., van den Bogert, A., Bruin, G., Hartman, W. and Barneveld, A. 1995b. How the horse moves: 2. significance of graphical representations of equine hind limb kinematics. Equine Veterinary Journal. 27(1):39-45.

Back, W., Schamhardt, H., Hartman, W. and Barneveld, A. 1995c. Kinematic differences between the distal portions of the forelimbs and hind limbs of horses at the trot. American Journal of Veterinary Research. 56(11):1522-1528.

Badoux, D. 1987. Some biomechanical aspects of the structure of the equine tarsus. Anatomischer Anzeiger. 164:53-61.

Barneveld, B. and van Weeren, P. 1999. Early changes in the distal intertarsal joint of Dutch Warmblood foals and the influence of exercise on bone density in the third tarsal bone. Equine Veterinary Journal. 31(supplement):67-73.

Barr, A., Dow, S. and Goodship, A. 1995. Parameter of forelimb ground reaction force in 48 normal ponies. Veterinary Record. 136:283-286.

Becker, C. K., Savelberg, H. H., Buchner, H. H. and Barneveld, A. 1998. Long-term consequences of experimental desmotomy of the accessory ligament of the deep digital flexor tendon in adult horses. American Journal of Veterinary Research. 59(3):347-351.

Biewener, A. 1998. Muscle-tendon stresses and elastic energy storage during locomotion in the horse. Comparative Biochemistry and Physiology Part B. 120:73-87.

Biewener, A., Thomason, J. and Lanyon, L. 1988. Mechanics of locomotion and jumping in the horse (Equus): in vivo stress in the tibia and metatarsus. Journal of Zoology London. 214:547-565.

Bjornsdottir, S., Axelsson, M., Eksell, P., Sigurdsson, H. and Carlsten, J. 2000. Radiographic and clinical survey of degenerative joint disease in the distal tarsal joints in Icelandic horses. Equine Veterinary Journal. 32(3):268-272.

van den Bogert, A. 1989. Computer stimulation of locomotion in the horse. Thesis. University of Utrecht. Utretch.

van den Bogert, A. 1998. Computer-assisted gait analysis in equine orthopedic practice: the case for inverse dynamic analysis. Equine Veterinary Journal. 30(5):362-363.

van den Bogert, A., van Weeran, P. and Schamhardt, H. 1990. Correction for skin displacement errors in movement analysis of the horse. Journal of Biomechanics. 23(1):97-101.

Bohanon, T. C. 1999. The tarsus, p. 848-862. In J. A. Auer and J. A. Stick (ed.), Equine surgery, 2nd ed. W. B. Saunders Company, London.

Boswell, J. C., McGuigan, M. P., Schramme, M., Newman, S. and Wilson, A. M. 2000. The position of the point of zero moment relative to the foot in normal horses and horses suffering from osteoarthritis of the small tarsal joints (bone spavin), 67. In Proceeding of the Fourth International Workshop on Animal Locomotion.

Buchner, H. H. F. 2001a. The advance of clinical biomechanics. Equine Veterinary Journal. 33(5):430-432.

Buchner, H. H. F. 2001b. Gait adaptation in lameness, p. 251-279. In W. Back and H. Clayton (ed.), Equine locomotion. W.B. Saunders, London.

Buchner, F., Kastner, J., Girtler, D. and Knezevic, P. 1993. Quantification of hind limb lameness in the horse. Acta Anatomica. 146:196-199.

Buchner, H. H. F., Savelberg, H. H. C. M. and Becker, C. K. 1996a. Load redistribution after desmotomy of the accessory ligament of the deep digital flexor tendon in adult horses. Veterinary Quarterly. 18(suppl 2):S70-S4.

Buchner, H., Savelberg, H., Schamhardt, H. and Barneveld, A. 1996b. Limb movement adaptations in horses with experimentally induced fore- or hindlimb lameness. Equine Veterinary Journal. 28(1):63-70.

Buchner, H., Savelberg, H., Schamhardt, H. and Barneveld, A. 1996c. Head and trunk movement adaptations in horses with experimentally induced fore- or hindlimb lameness. Equine Veterinary Journal. 28(1):71-76.

Buchner, H., Savelberg, H., Schamhardt, H. and Barneveld, A. 1997. Inertial properties of Dutch Warmblood horses. Journal of Biomechanics. 30(6):653-658.

Buchner, H. H. F., Obermuller, S. and Scheidl, M. 2000. Body centre of mass movement in the sound horse. Veterinary Journal. 160:225-234.

Buchner, H. H. F., Obermuller, S. and Scheidl, M. 2001. Body centre of mass movement in the lame horse. Equine Veterinary Journal. 33(supplement):122-127.

Budsberg, S. C., Chambers, J. N., van lue Stephen, L., Foutz, T. L. and Reece, L. 1996. Prosepctive evaluation of ground reaction forces in dogs undergoing unilateral total hip replacement. American Journal of Veterinary Research. 57(12):1781-1785.

Cavagna, G. A., Heglund, N. C. and Taylor, C. R. 1977. Mechanical work in terrestrial locomotion: two basic mechanisms for minimizing energy expenditure. American Journal of Physiology. 233(5):R243-R261.

Chateau, H., Degueurce, C., Jerbi, H., Crevier-Denoix, N., Pourcelot, P., Audigie, F., Pasqui-Boutard, V. and Denoix, J. M. 2001. Normal three-dimensional behavior of the metacarpophalangeal joint and the effect of uneven foot bearing. Equine Veterinary Journal. 33(supplement):84-88.

Clayton, H. 1990. The effect of an acute angulation of the hind hooves on diagonal synchrony of trotting horses. Equine Veterinary Journal. 9(supplement):91-94.

Clayton, H. 1996. Instrumentation and techniques in locomotion and lameness. Veterinary Clinics of North America: Equine practice. 12(2):337-350.

Clayton, H. M. 2001. Performance in Equestrian Sports, p. 193-226. In W. Back and H. Clayton (ed.), Equine locomotion. W.B. Saunders, London.

Clayton, H., Lanovaz, J., Schamhardt, H., Willemen, M. and Colborne, G. 1998a. Net joint moments and powers in the equine forelimb during the stance phase of the trot. Equine Veterinary Journal. 30(5):384-389.

Clayton, H., Theoret, C., Barber, S. and Curle, R. 1998b. Effects of carpal synovectomy on stride kinematics of trotting horses. Veterinary and Comparative Orthopedic & Traumatology. 11:80-84.

Clayton, H., Hodson, E. and Lanovaz, J. 2000a. The forelimb in walking horses: 2. net joint moments and joint powers. Equine Veterinary Journal. 32(4):295-299.

Clayton, H., Schamhardt, H., Willemen, M., Lanovaz, J. and Colborne, G. 2000b. Kinematics and ground reaction forces in horses with superficial digital flexor tendinitis. American Journal of Veterinary Research. 61(2):191-196.

Clayton, H., Schamhardt, H., Willemen, M., Lanovaz, J. and Colborne, G. 2000c. Net joint moments and joint powers in horses with superficial digital flexor tendinitis. American Journal of Veterinary Research. 61(2):197-201.

Clayton, H., Willemen, M., Lanovaz, J. and Schamhardt, H. 2000d. Effects of heel wedge in horses with superficial digital flexor tendinitis. Veterinary and Comparative Orthopedic & Traumatology. 13:1-8.

Clayton, H. M., Hodson, E., Lanovaz, J. L. and Colborne, G. R. 2001. The hindlimb of walking horses: 2. net joint moments and joint powers. Equine Veterinary Journal. 33(1):44-48.

Colborne, G., Lanovaz, J., Sprigings, E., Schamhardt, H. and Clayton, H. 1997a. Joint moments and power in equine gait: a preliminary study. Equine Veterinary Journal. 23(supplement):33-36.

Colborne, G., Lanovaz, J., Sprigings, E., Schamhardt, H. and Clayton, H. 1997b. Power flow in the equine forelimb. Equine Veterinary Journal. 23(supplement):37-40.

Colborne, G., Lanovaz, J., Sprigings, E., Schamhardt, H. and Clayton, H. 1998. Forelimb joint moments and power during the walking stance phase of horses. American Journal of Veterinary Research. 59(5):609-614.

Cottage, I., Lane, M. and Ferrars, W. 1997. Review of current methods available for the treatment of bone spavin. Equine Veterinary Education. 9(5):258-264.

Cross, A. R., Budsberg, S. C. and Keefe, T. J. 1997. Kinetic gait analysis assessment of meloxicam efficiency in a sodium urate-induced synovitis model in dogs. American Journal of Veterinary Research. 58(6):626-631.

Dalin, G. and Jeffcott, L. 1985. Locomotion and gait analysis. Veterinary Clinics of North America: Equine practice. 1(3):549-572.

Degueurce, C., Pourcelot, P., Audigie, F., Denoix, J. and Geiger, D. 1997. Variability of the limb joint patterns of sound horses at trot. Equine Veterinary Journal. 23(supplement):89-92.

Degueurce, C., Charteau, H., Pasqui-Boutard, V., Pourcelot, P., Audigie, F., Crevier-Denoix, N., Jerbi, H., Geiger, D. and Denoix, J. 2000. Concrete use of the joint coordinate system for the quantification of articular rotations in the digital joints of the horse. Veterinary Research. 31:297-311.

Degueurce, C., Charteau, H., Jerbi, H., Crevier-Denoix, N., Pourcelot, P., Pasqui-Boutard, V., Geiger, D. and Denoix, J. 2001. Three-dimensional kinematics of the proximal interpahalangeal joint: effects of raising the heels or the toe. Equine Veterinary Journal. 33(supplement):79-83.

Deuel, N. R. and Lawrence, L. M. 1987. Laterality in the gallop gait of horses. Journal of Biomechanics. 20:645-649.

Dow, S., Leendertz, J., Silver, I. and Goodship, A. 1991. Identification of subclinical tendon injury from ground reaction force analysis. Equine Veterinary Journal. 23(4):266-272.

Drevemo, S., Fredricson, I., Hjerten, G. and McMiken, D. 1987. Early development of gait asymmetries in trotting Standardbred colts. Equine Veterinary Journal. 19:189-191.

Dyce, K. M., Sack, W. O. and Wensing, C. J. G. 1987. The hind limb of the horse, p. 576-595. In D. Pedersen (ed.), Textbook of veterinary anatomy. W. B. Saunders Company, Philadelphia.

Dyson, S. 1995. Distal hock joint pain: diagnosis and management. Ippologia. 6(3):7-23.

Eastman, T. G., Bohanon, T. C., Beeman, G. M. and Swanson, T. D. 1997. Owner survey on cunean tenectomy as a treatment for bone spavin in performance horses, p. 121-122. In 43th Proceedings of the American Association of Equine Practitioners.

Eksell, P., Axelsson, M., Brostrom, H., Roneus, B., Haggstrom, J. and Carlten, J. 1998. Prevalence and risk factors fo bone spavin in Icelandic horses in Sweden: a radiographic field study. Acta Veterinary Scandinavia. 39:339-348.

Faber, M., Schamhardt, H., van Weeren, R., Johnston, C., Roepstorff, L. and Barneveld, A. 2000. Basic three-dimensional kinematics of the vertebral column of horses walking on a treadmill. American Journal of Veterinary Research. 61(4):399-406.

Faber, M., Johnston, C., Schamhardt, H., van Weeren, R., Roepstorff, L. and Barneveld, A. 2001a. Basic three-dimensional kinematics of the vertebral column of horses trotting on a treadmill. American Journal of Veterinary Research. 62(5):757-764.

Faber, M., Johnston, C., Schamhardt, H., van Weeren, R., Roepstorff, L. and Barneveld, A. 2001b. Three-dimensional kinematics of the equine spine during canter. Equine Veterinary Journal. 33(supplement):145-149.

Gabel, A. 1983. Prevention, diagnosis and treatment of inflammation of the distal hock, p. 287-298. In 28th Proceedings of the American Association of Equine Practitioners.

Galisteo, A., Cano, M., Miro, F., Vivo, J., Morales, J. and Aguera, E. 1996. Angular joint parameters in the Andalusian horse at walk, obtained by normal videography. Journal of Equine Veterinary Science. 16(2):73-77.

Galisteo, A., Cano, M., Morales, J., Miro, F., Vivo, J. and Aguera, E. 1997. Kinematics in horses at the trot before and after an induced forelimb supporting lameness. Equine Veterinary Journal. 23(supplement):97-101.

Galisteo, A., Cano, M., Morales, J., Vivo, J. and Miro, F. 1998. The influence of speed and height at the withers on the kinematics of sound horses at the hand-led trot. Veterinary Research Communications. 22(6):415-423.

Goodship, A., Brown, P., MacFIE, H., Lanyon, L. and Silver, I. 1987. A quantitative force plate assessment of equine locomotor performance, p. 236-270. In J. R. Gillespie and N. E. Robinson (ed.) Proceedings of the Second International Conference on Equine Exercise Physiology. ICEEP Publications, Davis.

Gough, M. and Munroe, G. 1998. Decision making in the diagnosis and management of bone spavin in horses. In Practice. 20:252-259.

van Harreveld, P. D., Lillich, J. D., Kawcak, C. E., Gaughan, E. M., McLaughlin, R. M. and DeBowes, R. M. 2002. Clinical evaluation of the effects of immobilization followed by reimmobilization and exercise on the metacarpophalangeal joint in horses. American Journal of Veterinary Research. 63(2):282-288.

Hartman, W., Schamhardt, H., Lammertink, J. and Badoux, D. 1984. Bone strain in the equine tibia: an in vivo strain gauge analysis. American Journal of Veterinary Research. 45(5):880-884.

Hjerten, G. and Drevemo, S. 1993. Shortening of the forelimb in the horse during the stance phase. Acta Anatomica. 146(2-3):193-195.

Hjerten, G., Drevemo, S. and Eriksson, L. 1994. Shortening of the hind limb in the horse during the stance phase. Equine Veterinary Journal. 17(supplement):48-50.

Hodson, E., Clayton, H. M. and Lanovaz, J. L. 2001. The hindlimb in walking horses: 1. kinematics and ground reaction forces. Equine Veterinary Journal. 33(1):38-43.

Hof, A. 2001. Scaled energetics of locomotion, p. 351-363. In W. Back and H. Clayton (ed.), Equine locomotion. W.B. Saunders, London.

Holmstrom, M. 1990. Variation in conformation of Swedish Warmblood horses and conformational characteristics of elite sport horses. Equine Veterinary Journal. 22(3):186-193.

Holmstrom, M., Fredricson, I. and Drevemo, S. 1994. Biokinematic analysis of the swedish warmblood riding horse at trot. Equine Veterinary Journal. 26(3):235-240.

Holmstrom, M., Fredricson, I. and Drevemo, S. 1995a. Biokinematic effects of collection on the trotting gaits in the elite dressage horse. Equine Veterinary Journal. 27(4):281-287.

Holmstrom, M., Fredricson, I. and Drevemo, S. 1995b. Variation in angular pattern adaptation from trot in hand to passage and piaffe in the Grand Prix dressage horse. Equine Veterinary Journal. 18(supplement):132-137.

van den Hoogen, B. M., van de Lest, C. H., van Weeren, P. R., Lafeber, F. P., Lopes-Cardozo, M., van Golde, L. M. and Barneveld, A. 1998. Loading-induced changes in synovial fluid affect cartilage metabolism. British Journal of Rheumatology. 37(6):671-676.

Jacobs, R. and van Ingen Schenau, G. J. 1992. Intermuscular coordination in a sprint push-off. Journal of Biomechanics. 25(9):953-965.

Jacobs, R., Bobbert, M. F. and van Ingen Schenau, G. J. 1996. Mechanical output from individual muscles during explosive leg extensions: the role of biarticular muscles. Journal of Biomechanics. 29(4):513-523.

Jansen, M., van Raaij, J., van den Bogert, A., Schamhardt, H. and Hartman, W. 1992. Quantitative analysis of computer-averaged electromyographic profiles of intrinsic limb muscles in ponies at the walk. American Journal of Veterinary Research. 53(2):2343-2349.

Jefferson, R. J., Collins, J. J., Whittle, M. W., Radin, E. L. and O'Connor, J. J. 1990. The role of the quadriceps in controlling impulsive forces around heel strike. Journal of Engineering in Medicine. 204(1):21-28.

Johnson, M. D. and Buckley, J G. 2001. Muscle power patterns in the mid-acceleration phase of sprinting. Journal of Sports Sciences. 19:263-272.

Johnston, C., Roepstorff, L., Drevemo, S. and Kallings, P. 1996. Kinematic of the distal hindlimb during stance phase in the fast trotting Standardbred. Equine Veterinary Journal. 28(4):263-268.

Keegan, K. G., Wilson, D. J., Wilson, D. A., Barnett, C. D. and Smith, B. 1998a. Effects of balancing and shoeing of the forelimb feet on kinematic gait analysis in five horses with navicular disease. Journal of Equine Veterinary Science. 18(8):522-527.

Keegan, K. G., Wilson, D. A., Wilson, D. J., Smith, B., Gaughan, E .M., Pleasant, R. S., Kramer, J., Howard, R. D., Bacon-Miller, C., Davis, E. G., May, K. A., Valentino, W. L. and van Harreveld, P. D. 1998b. Evaluation of mild lameness in horses trotting on a treadmill by clinicians and interns or residents and correlation of their assessments with kinematic gait analysis. American Journal of Veterinary Research. 59(11):1370-1377.

Keegan, K., Wilson, D., Smith, B. and Wilson, D. 2000. Changes in kinematic variables observed during pressure-induced forelimb lameness in adult horses trotting on a treadmill. American Journal of Veterinary Research. 61(6):612-619.

Keg, P. R., Barneveld, A., Schamhardt, H. C. and van den Belt, A. J. 1994. Clinical and force plate evaluation of the effect of a high plantar nerve block in lameness caused by induced mid-metatarsal tendinitis. Veterinary Quarterly. 16(suppl 2):S70-S75.

Keg, P. R., Schamhardt, H. C. van Weeren, P. R. and Barneveld, A. 1996. The effect of diagnostic regional nerve blocks in the fore limb on the locomotion of clinically sound horses. Veterinary Quarterly. 18(suppl 2):S106-S109.

Khumsap, S., Clayton, H. M. and Lanovaz, J. L. 2001a. Effect of walking velocity on hindlimb kinetics during stance in normal horses. Equine Veterinary Journal. 33(supplement):21-26.

Khumsap, S., Clayton, H. M., and Lanovaz, J. L. 2001b. Effect of walking velocity on ground reaction force variables in the hind limb of clinically normal horses. American Journal of Veterinary Research. 62(6):901-906.

Khumsap, S., Clayton, H. M., Lanovaz, J. L. and Bouchey, M. 2002. Effect of walking velocity on forelimb kinematics and kinetics. Equine Veterinary Journal. 34(supplement):in press.

Kirker-Head, C. A., Fackelman, G. E., Hoogasian, J. J. and Doyle, E. M. 1993. Studies on propentofylline for the treatment of navicular diasease. Journal of Equine Veterinary Science. 13(2):106-113.

Kobluk, C., Schnurr, D., Horney, F., Summer-Smith, G., Willoughby, R., Dekleer, V. and Hearn, T. 1989. Use of high-speed cinematography and computer generated gait diagrams for the study of equine hindlimb kinematics. Equine Veterinary Journal. 21(1):48-58.

Kramer, J., Keegan, K. G., Wilson, D. A., Smith, B. K. and Wilson, D. J. 2000. Kinematic of the hind limb in trotting horses after induced lameness of the distal intertarsal and tarsometatarsal joints and intra-articular administration of anesthetic. American Journal of Veterinary Research. 61(9):1031-1036.

Lanovaz, J. L. and Clayton, H. M. 2001. Sensitivity of forelimb swing phase inverse dynamics to inertial parameter errors. Equine Veterinary Journal. 33(supplement):27-31.

Lanovaz, J., Clayton, H., Colborne, G. and Schamhardt, H. 1999. Forelimb kinematics and net joint moments during the swing phase of the trot. Equine Veterinary Journal. 30(supplement):235-239.

Lanovaz, J. L., Khumsap, S., Clayton, H. M., Stick, J. A. and Brown, J. 2002. Three dimensional kinematics of the tarsal joint at the trot. Equine Veternary Journal. 34(supplement):308-313.

Laverty, S., Stover, S., Belanger, D., O'Brien, T., Pool, R., Pascoe, J., Taylor, K. and Harrington, T. 1991. Radiographic, high detail radiographic, microangiographic and histological findings of the distal portion of the tarsus in weanling, young and adult horses. Equine Veterinary Journal. 23(6):413-421.

Leach, D. 1987. Locomotion analysis technology for evaluation of lameness in horses. Equine Veterinary Journal. 19(2):97-99.

Leach, D. 1993. Recommended terminology for researchers in locomotion and biomechanics of quadrupedal animals. Acta Anatomica. 146:130-136.

Leach, D. and Crawford, W. 1983. Guideline for the future of equine locomotion research. Equine Veterinary Journal. 15(2):103-110.

Leach, D. and Dagg, A. 1983. A review of research on equine locomotion and biomechanics. Equine Veterinary Journal. 15(2):93-102.

Leach, D., Ormrod, K. and Clayton, H. 1984. Standardized terminology for the description and analysis of equine locomotion. Equine Veterinary Journal. 16(6):522-528.

Little, C. B., Ghosh, P. and Rose, R. 1997. The effect of strenuous versus moderate exercise on the metabolism of proteoglycans in articular cartilage from different weight-bearing regions of the equine third carpal bone. Osteoarthritis Cartilage. 5(3):161-172.

Ljungquist, B. 1976. Training of the young or untrained horse, p. 50-78. In Practical dressage manual. Whittet & Shepperson, Richmond, Virginia.

Lukoschek, M., Boyd, R. D., Schaffler, M. B., Burr, D. B. and Radin, E. L. 1986. Comparison of joint degeneration models. Surgical instability and repetitive impulsive loading. Acta Orthopedic Scandinavia. 57(4):349-353.

May, S. A. and Wyn-Jones, G. 1987. Identification of hindlimb lameness. Equine Veterinary Journal. 19(3):185-188.

McLaughlin, R., Gaughan, E., Roush, J. and Skaggs, C. 1996. Effects of subject velocity on ground reaction force measurements and stance times in clinically normal horses at the walk and trot. American Journal of Veterinary Research. 57(1):7-11.

Meershoek, L. S., Schamhardt, H. C., Roepstorff, L. and Johnston, C. 2001. Forelimb tendon loading during jump landings and the influence of fence height. Equine Veterinary Journal. 33(supplement):6-10.

Merkens, H. and Schamhardt, H. 1988. Distribution of ground reaction forces of the concurrently loaded limbs of the Dutch Warmblood horse at the normal walk. Equine Veterinary Journal. 20(3):209-213.

Merkens, H. W. and Schamhardt, H. C. 1994. Relationships between ground reaction force patterns and kinematics in the walking and trotting horse. Equine Veterinary Journal. 17(supplement):67-70.

Merkens, H. W., Schamhardt, H. C., Hartman, W. and Kersjes, A. W. 1985. Ground reaction force patterns of Dutch warmblood horses at normal walk. Equine Veterinary Journal. 18(3):207-214.

Merkens, H., Schamhardt, H., Hartman, W. and Kersjes, A. 1988. The use of H(orse) index: a method of analysing the ground reaction force patterns of lame and normal gaited horses at the walk. Equine Veterinary Journal. 20(1):29-36.

Merkens, H., Schamhardt, H., van Osch, G. and van den Bogert, A. 1993. Ground reaction force patterns of Dutch Warmblood horses at normal trot. Equine Veterinary Journal. 25(2):134-137.

Minetti, A., Ardigo, L., Reinach, E. and Saibene, F. 1999. The relationship between mechanical work and energy expenditure of locomotion in horses. Journal of Experimental Biology. 202:2329-2338.

Molenaar, G. J. 1983. Kinematics of the reciprocal apparatus in the horse. Anatomia Histologia Embryologia. 12(3):278-287.

Morales, J., Manchado, M., Vivo, J., Galisteo, A., Aguera, E. and Miro, F. 1998. Angular kinematic patterns of limbs in elite and riding horses at trot. Equine Veterinary Journal. 30(6):528-533.

Morris, E. A. and Seeherman, H. J. 1987. Redistribution of ground reaction forces in experimentally induced equine carpal lameness, p. 553-563. In J. R. Gillespie and N. E. Robinson (ed.) Proceedings of the Second International Conference on Equine Exercise Physiology. ICEEP Publications, Davis.

Morris, E. A. and Treadwell, B. V. 1994. Effect of interleukin 1 on articular cartilage from young and aged horses and comparison with metabolism of osteoarthritic cartilage. American Journal of Veterinary Research. 55(1):138-146.

Moyer, W., Brokken, T. and Raker, C. 1983. Bone spavin in thoroughbred race horses, p. 81-92. In 29th Proceedings of the American Association of Equine Practitioners.

Moyer, W., Genovese, R. and Corley, J. 1993. Diagnosing subtle lameness problems by employing specific therapy, p. 203-205. In 39th Annual Convention Proceedings of American Association of Equine Practitioners.

Newberry, W. N., Garcia, J. J., Mackenzie, C. D., DeCamp, C. E. and Haut, R. C. 1998. Analysis of acute mechanical insult in an animal model of post-traumatic osteoarthrosis. Journal of Biomechanical Engineer. 120(6):704-709.

Nicodemus, M. C. 2000. Quantification of the locomotion of gaited horses. Thesis. Michigan State University, East Lansing.

Peham, C., Licka, T., Scheidl, M. and Girtler, D. 1998. Speed dependency of motion pattern consistency. Journal of Biomechanics. 31(9):769-772.

Peham, C., Licka, T., Girtler, D. and Scheidl, M. 1999a. Supporting forelimb lameness: clinical judgement vs computerised symmetry measurement. Equine Veterinary Journal. 31(5):417-421.

Peham, C., Scheidl, M. and Licka, T. 1999b. Limb locomotion - speed distribution analysis as a new method for stance phase detection. Journal of Biomechanics. 32:1119-1124.

Peham, C., Licka, T., Mayr, A. and Scheidl, M. 2000. Individual speed dependency of forelimb lameness in trotting horses. Veterinary Journal. 160:135-138.

Peloso, J. G., Stick, J. A., Caron, J. C., Peloso, P. M. and Soutas-Little, R. W. 1993a. Effects of hylan on amphotericin-induced carpal lameness in equids. American Journal of Veterinary Research. 54(9):1527-1534.

Peloso, J. G., Stick, J. A., Soutas-Little, R. W., Caron, J. C., DeCamp, C. E. and Leach, D. H. 1993b. Computer-assisted three-dimensional gait analysis of amphotericin-induced carpal lameness in horses. American Journal of Veterinary Research. 54(9):1535-1543.

Pool, R. R. 1996. Pathologic manifestations of joint disease in the athletic horse, p. 87-104. In C. W. McIlwraith and G. W. Trotter (ed.) Joint disease in the horse. W. B. Saunders Company, London.

Pourcelot, P., Audigie, F., Degueurce, C., Denoix, J. and Geiger, D. 1997a. Kinematic symmetry index: a method for quantifying the horse locomotion symmetry using kinematic data. Veterinary Research. 28:525-538.

Pourcelot, P., Degueurce, C., Audigie, F., Denoix, J. and Geiger, D. 1997b. Kinematic analysis of the locomotion symmetry of sound horses at a slow trot. Equine Veterinary Journal. 23(supplement):93-96.

Riemersma, D., Schamhardt, H., Hartman, W. and Lammertink, L. 1988. Kinetics and kinematics of the equine hind limb: in vivo tendon loads and force plate measurements in ponies. American Journal of Veterinary Research. 49(8):1344-1352.

Robert, C., Valette, J. and Denoix, J. 1998. Surface electromyographic analysis of the normal horse locomotion: a preliminary report, p. 80-85. In Conference on Equine Sports Medicine and Science. Wageningen Pers, Wageningen.

Robert, C., Valette, J. P., Degueurce, C. and Denoix, J. M. 1999. Correlation between surface electromyography and kinematics of the hindlimb of horses at trot on a treadmill. Cells Tissues Organs. 165(2):113-122.

Rooney, J. 1977. The vertebral column, p. 90-95. In Biomechanics of lameness in horses. Williams & Wilkins, Baltimore.

Rooney, J. 1990. The jumping behavior of the humeroradial and tarsocrural joints of the horse. Journal of Equine Veterinary Science. 10(4):311-314.

Rooney, J. R., Thompson, K. N. and Shapiro, R. 1991. A contribution to the study of velocity, stride length, and frequency in the horse. Journal of Equine Veterinary Science. 11(4):208-209.

Rumph, P. F. and Steiss, J. E. 1998. Ground reaction forces in Greyhounds with tibial nerve injury. American Journal of Veterinary Research. 59(4):375-378.

Rumph, P. F., Kincaid, S. A., Baird, D. K., Kammermann, J. R., Visco, D. M. and Goetze, L F. 1993. Vertical ground reaction force distribution during experimentally induced acute synovitis in dogs. American Journal of Veterinary Research. 54(3):365-369.

Rumph, P. F., Kincaid, S. A., Visco, D. M., Baird, D. K., Kammermann, J. R. and West, M. S. 1995. Redistribution of vertical ground reaction force in dogs with experimentally induced chronic hindlimb lameness. Veterinary Surgery. 24(5):384-389.

Savelberg, H., Buchner, H. and Becker, C. 1997. Recovery of equine forelimb function after desmotomy of the accessory ligament of the deep digital flexor tendon. Equine Veterinary Journal. 23(supplement):27-29.

Schamhardt, H. C. 1998. The mechanics of quadrupedal locomotion. How is the body propelled by muscles? European Journal of Morphology. 36(4-5):272-279.

Schamhardt, H. and Merkens, H. 1994. Objective determination of ground contact of equine limbs at the walk and trot: comparison between ground reaction forces, accelerometer data and kinematics. Equine Veterinary Journal. 17(supplement):75-79.

Schamhardt, H., Hartman, W. and Lammertink, J. 1989. Forces loading the tarsal joint in the hind limb of the horse, determined from in vivo strain measurements of the third metatarsal bone. American Journal of Veterinary Research. 50(5):728-733.

Schneider, R., Milne, D., Gabel, A., Groom, J. and Bramlage, L. 1982. Multidirectional in vivo strain analysis of the equine radius and tibia during dynamic loading with and without a cast. American Journal of Veterinary Research. 43(9):1541-1550.

Seeherman, H. J., Morris, E. A. and Fackelman, G. E. 1987. Computerized force plate determination of equine weight-bearing profiles, p. 536-552. In J. R. Gillespie and N. E. Robinson (ed.) Proceedings of the Second International Conference on Equine Exercise Physiology. ICEEP Publications, Davis.

Soderkvist, I. and Wedin, P. 1993. Determining the movements of the skeleton using well-configured markers. Journal of Biomechanics. 26:1473-1477.

Sprigings, E. and Leach, D. 1986. Standardized technique for determining the centre of gravity of body and limb segments of horses. Equine Veterinary Journal. 18(1):43-49.

Stashak, T. S. 1987. Diagnosis of lameness, p. 840-877. In T. S. Stashak (ed.), Adam's lameness in horses, 4th ed. Lea & Febiger, Philadelphia.

Steiss, J. E., White, N. A. and Bowen, J. M. 1989. Electroacupuncture in the treatment of chronic lameness in horses and ponies: a controlled clinical trial. Canadian Journal of Veterinary Research. 53(2):239-243.

Suter, E., Herzog, W., Leonard, T. R. and Nguyen, H. 1998. One-year changes in hind limb kinematics, ground reaction forces and knee stability in an experimental model of osteoarthritis. Journal of Biomechanics. 31(6):511-517.

Thomas, L. 1997. A review of statistical power analysis software. Bulletin of the Ecological Society of America. 78(2):126-139.

Tokuriki, M. and Aoki, O. 1995. Electromyographic activity of the hindlimb muscles during the walk, trot and canter. Equine Veterinary Journal. 18(supplement):152-155.

Uhlir, C., Licka, T., Kubber, P., Peham, C., Scheidl, M. and Girtler, D. 1997. Compensatory movements of horses with a stance phase lameness. Equine Veterinary Journal. 23(supplement):102-105.

Vincent, W. J. 1999. The t test: comparing means from two sets of data, p. 117-148. In Statistics in kinesiology, 2nd ed. Human Kinetics, Champaign.

Vorstenbosch, M. A., Buchner, H. H., Savelberg, H. H., Schamhardt, H. C. and Barneveld, A. 1997. Modeling study of compensatory head movements in lame horses. American Journal of Veterinary Research. 58(7):713-718.

van Weeren, P. 1989. Skin displacement in equine kinematic gait analysis. Thesis. University of Utretch. N.V. SDU, Utretch.

van Weeren, P. 2001. History of locomotion research, p. 1-35. In W. Back and H. Clayton (ed.), Equine locomotion. W.B. Saunders, London.

van Weeren, P., van den Bogert, A., Barneveld, A., Hartman, W. and Kersjes, A. 1990. The role of the reciprocal apparatus in the hind limb of the horse investigated by a modified CODA-3 opto-electronic kinematic analysis system. Equine Veterinary Journal. 9(supplement):95-100.

van Weeren, P. R., van den Bogert, A. J. and Barneveld, A. 1992a. Correction models for skin displacement in equine kinematic gait analysis. Journal of Equine Veterinary Sciences. 12(3):178-192.

van Weeren, P., Jansen, M., van den Bogert, A. and Barneveld, A. 1992b. A kinematic and strain gauge study of the reciprocal apparatus in the equine hind limb. Journal of Biomechanics. 25(11):1291-1301.

Weishaupt, M. A., Wiestner, T., Hogg, H. P., Jordan, P., Auer, J. A. and Barrey, E. 2001. Assessment of gait irregularities in the horse: eye vs. gait analysis. Equine Veterinary Journal. 33(supplement):135-140.

Wentink, G. 1978. Biokinetical analysis of the movements of the pelvic limb of the horse and the role of the muscles in the walk and the trot. Anatomy and Embryology. 152:261-272.

Willemen, M .A., Savelberg, H. H. C. M., Jacobs, M. W. H. and Barneveld, A. 1996. Biomechanical effects of rocker-toe shoes in sound horses. Veterinary Quarterly. 18(suppl 2):S75-S78.

Willemen, M .A., Savelberg, H. H. C. M. and Barneveld, A. 1997. The improvement of the gait quality of sound trotting warmblood horses by normal shoeing and its effect on the load on the lower forelimb. Livestock Production Science. 52(2):145-153.

Willemen, M .A., Savelberg, H. H. C. M. and Barneveld, A. 1999. The effect of orthopedic shoeing on the force exerted by the deep digital flexor tendon on the navicular bone in horses. Equine Veterinary Journal. 31(1):25-30.

Williams, G. E. 2001. Locomotor characteristics of horses with navicular disease. American Journal of Veterinary Research. 62(2):206-210.

Williams, G., Silverman, B., Wilson, A. and Goodship, A. 1999. Disease-specific changes in equine ground reaction force data documented by use of principal component analysis. American Journal of Veterinary Research. 60(5):549-555.

Willms, F., Rohe, R. and Kalm, E. 1996. Significance of genetic aspects of bone diseases in horses. Pferdeheilkunde. 12:345-346.

Wilson, A. M., Seelig, T. J., Shield, R. A. and Silverman, B. W. 1998. The effect of foot imbalance on point of force application in the horse. Equine Veterinary Journal. 30(6):540-545.

Winter, D. A. 1990. Biomechanics and motor control of human movement. John Wiley & Sons, Inc., New York.

Woltring, H. J. 1994. 3D attitude representation of human joints: a standardization proposal. Journal of Biomechanics. 27:1399-1414.

Woltring, H. J., Huiskes, R., De Lange, A. and Veldpaus, F. 1985. Finite centroid and helical axis estimation from noisy landmark measurements in the study of human joint kinematics. Journal of Biomechanics. 18:379-389.

Wu, G. and Ladin, Z. 1996. Limitations of quasi-static estimation of human joint loading during locomotion. Medical and Biological Engineering and Computing. 34(6):472-476.

Zatsiorky, V., Werner, S. and Kaimin, M. 1994. Basic kinematics of walking: step length and step frequency, a review. Journal of Sports Medicine and Physical Fitness. 34(2):109-134.